Automated Glycan Assembly of Oligomannose Glycans for Sensing Applications

Inaugural-Dissertation

to obtain the academic degree

Doctor rerum naturalium (Dr. rer. nat.)

submitted to the Department of Biology, Chemistry, and Pharmacy

of Freie Universität Berlin

by

Priya Mohanrao Bharate

2017

This work was performed between November 2013 and February 2017 under the guidance of Prof. Dr. Peter H. Seeberger in the Department of Biomolecular Systems, Max Planck Institute of Colloids and Interfaces Potsdam, and the Institute of Chemistry and Biochemistry, Freie Universität Berlin.

1st reviewer: Prof. Dr. Peter H. Seeberger

2nd reviewer: Prof. Dr. Rainer Haag

Date of oral defense: 22.11.2017

Declaration

This is to certify that the entire work in this thesis has been carried out by Ms. Priya Bharate. The assistance and help received during the course of investigation have been fully acknowledged.

---------- ----------

(Date, Place) (Signature)

Acknowledgements

I dedicate my special thanks to

- Prof. Dr. Peter H. Seeberger for providing me the opportunity and support in realizing this thesis.
- Prof. Dr. Rainer Haag for generously agreeing to review this thesis.
- My colleagues from the Carbohydrate Materials group especially Ms. Silvia Varela-Aramburu and Dr. Martina Delbianco for proof reading this thesis, Dr. Chian-Hui Lai, Ms. Zhou Ye and Dr. Guillermo Orts-Gil for friendly atmosphere.
- Dr. Claney Lebev Pereira for proof reading the first chapter and for his suggestions for third chapter of this thesis.
- Prof. Dr. Rainer Haag, Dr. Zhenhui Qi, and Mr. Benjamin Ziem for their extensive efforts to make a close collaboration and for providing valuable graphene material. Dr. Christoph Böttcher, Ms. Andrea Schulz for transmission electron and atomic force microscopy experiments as well as Mr. Benjamin Hatting for Raman spectroscopy experiment.
- Prof. Virgil Percec, Dr. Sebastian Krauss for their extensive efforts to make a close collaboration.
- Dr. Sharavathi Parameshwarappa and Dr. Claney Lebev Pereira for their advice and moral support which was key in finishing this dissertation.
- Dr. Bopanna Monnanda Ponnappa for proof reading and for the biological experimental suggestions for second chapter of this thesis.
- Ms. Dorothee Böhme, Ms. Katharina Tebel and Ms. Lydia Alnajjar for all the back office help.
- Especially Ankita, Silvia, Maria, Zhou, Martina, and Monika for the last few months of my PhD and for helping me to recover faster.
- and my esteemed colleagues and friends of the Biomolecular Systems department Anish, Andrew, Alonso, Annette, Andreas, Anika, Andreia A., Ben, Bart, Chandradhish, Camille, Deborah, Eva, Fei-Fei, Felix B., Fabian, Frank, Hahm, Madhu, Maria B., Marilda, Matt, Max, Naresh, Naeem, Uwe V., Oren, Olaf, Pietro, Renee, Ramesh, Rich,

Somesh, Sahid, Sandip, Sourav, Kathir, Malte, Martín, Advik, and many others for wonderful time in Berlin.

- I also like to thank Dr. Raghavendra Kikkeri for his support, and to all my friends back home in India.

Finally, I express my deepest gratitude to my family members and *in-laws* for their love and support. And big thank you to Balaji for his unfailingly support and without him I would not have come so far!

Dedicated

To

My beloved Parents

List of Publications

A) Scientific Publication and Reviews

1. Multivalency at Interfaces: Supramolecular Carbohydrate-Functionalized Graphene Derivatives for Bacterial Capture, Release, and Disinfection. Zhenhui, Q.* Bharate, P.* Lai, C. Ziem, B. Böttcher, C. Schulz, A. Beckert, F. Hatting, B. Mülhaupt, R. Seeberger, P.H. and Haag, R. *Nano Lett.*, 2015, **15**, 6051−6057.
2. Carbohydrates in supramolecular chemistry. Delbianco, M. Bharate, P. Varela-Aramburu, S. Seeberger, P.H. *Chem. Rev. 2016*, **116**, 1693−1752.
3. Tumor-targeted drug delivery with mannose-functionalized nanoparticles self-assembled from amphiphilic β-cyclodextrins. Ye, Z. Zhang, Q. Wang, S. Bharate, P. Varela-Aramburu, S. Lu, M. Seeberger, P.H. Yin, J. *Chem. Eur. J.* 2016, **22**, 15216 – 15221.

* equal contribution

B) Scientific Conferences and Symposia

1. International Carbohydrate Symposium, New Orleans, USA (2016): "Self-Assembling Carbohydrate-functionalized Graphene for Capturing and Killing *E. coli* Bacteria" (Poster).
2. International Symposium on Macrocyclic and Supramolecular Chemistry, Strasbourg, France (2015): "Self-Assembling Carbohydrate-functionalized Graphene for Capturing and Killing *E. coli* Bacteria" (Poster).
3. COST Multiglyconano, Bangor, UK (2015): "Self-Assembling Carbohydrate-functionalized Graphene for Capturing and Killing *E. coli* Bacteria" (Oral presentation + Poster).
4. MPIKG Ringberg Conference, Rottach-Egern, Germany (2014): "Self-Assembling Carbohydrate-functionalized Graphene for Capturing and Killing *E. coli* Bacteria" (Oral presentation).

Table of Contents

Table of Contents

List of Abbreviations

Ac	Acetyl
Ac_2O	Acetic anhydride
ACN/CH_3CN	Acetonitrile
A.I	Agglutination indexes
AGA	Automated glycan assembly
Azmb	2-(azidomethyl)benzoyl
$BF_3.Et_2O$	Boron trifluoride diethyl etherate
Bn	Benzyl
BnBr	Benzyl bromide
BzCl	Benzoyl chloride
$PhCH(OMe)_2$	Benzaldehyde dimethyl acetal
CAN	Ceric ammonium nitrate
$CHCl_3$	Chloroform
CsOAc	Cesium acetate
Cs_2CO_3	Cesium carbonate
CSA	Camphor sulfonic acid
CLRs	C-type lectin receptors
ConA	Concanavalin A
CFU	Colony forming units
δ	Chemical shift
d	doublet
DBU	1,8-diazabicycloundec-7-ene
Bu_2SnO	Dibutyltinoxide
DCM	Dichloromethane
DHB	2,5-dihydroxybenzoic acid
DMSO	Dimethyl Sulfoxide
DMAP	4-Dimethylaminopyridine
ER	Endoplasmic Reticulum
E.coli	*Escherichia coli*
Et_2O	Diethyl ether

List of Abbreviations

Et_3N	Triethylamine
Equiv	Equivalent
ESI	Electrospray ionization
EtOH	Ethanol
FI	Fluorescence Intensity
FITC	Fluorescein isothiocyanate
Fmoc	9-Fluorenylmethoxycarbonyl
GAG	Glycosaminoglycan
GlcNAc	*N*-acetylglucosamine
GO	Graphene oxide
HPLC	High pressure liquid chromatography
N_2H_4.AcOH	Hydrazine acetate
HRMS	High resolution mass spectroscopy
Hz	Hertz
HCOOH	Formic acid
I_2	Iodine
Lev	Levulinoyl
LM	Lipomannan
LAM	Lipoarabinomannan
Man	Mannose
MALDI	Matrix assisted laser desorption/ionization
m	Multiplet
MeOH	Methanol
MTB	*Mycobacterium tuberculosis*
Na	Sodium
NaOMe	Sodium methoxide
NaN_3	Sodium Azide
$NaBH_4$	Sodium borohydride
Nap	2-Naphthylmethyl bromide
NP	Normal phase
NIS	*N*-iodosuccinimide

NIR	Near infrared radiation
NMR	Nuclear Magnetic Resonance
PBS	Phosphate Buffer Saline
Pd/C	Palladium on activated charcoal
Ph_3P	Triphenylphosphine
TBAI	Tertabutylammonium iodide
PhMe	Toluene
PhSH	Thiophenol
PI	Phosphatidylinositol
PIMs	Phosphatidylinositol mannosides
Ppm	Parts per Million
Py	Pyridine
KSCN	Potassium thiocyanate
quant	Quantitative
r.t.	Room Temperature
s	Singulet
AdCNa	Sodium adamantine carboxylate
THF	Tetrahydrofuran
TLC	Thin Layer Chromatography
TLRs	Toll like receptors
TMSOTf	Trimethylsilyltrifluoromethanesulfonate
TRGO	Thermally reduced graphene oxide
TRGO400	Thermally reduced graphene oxide at 400 ºC
TRGO750	Thermally reduced graphene oxide at 750 ºC
UV	Ultraviolet
$Zr(acac)_2$	Zirconium(IV) acetylacetonate
Zn	Zinc

Summary

Carbohydrates are useful building blocks for supramolecular assemblies offering the possibility of multiple hydrogen bonding. Several carbohydrate-functionalized multivalent scaffolds have been used to study weak carbohydrate-protein (CPIs) and carbohydrate-carbohydrate interactions (CCIs). Simple glycans such as mono or disaccharides have been largely in use to synthesize multivalent scaffolds since until very recently, complex glycans were rarely accessible. Complex and pure saccharides are needed in order to deeply understand the structure and function of the glycans. Chemical synthesis of linear and branched carbohydrates helps to get insights into multivalency, structure-activity relationship and to understand the role of glycans in living organisms. Automated glycan assembly (AGA) offers the possibility to achieve complex and pure structures with relatively little effort. The work presented here covers various glycans starting from the linear mannose monosaccharide construct to longer and branched mannose and arabinose oligosaccharide structures assembled using AGA.

A cyclodextrin (CD) based multivalent carbohydrate systems on a graphene surface was developed. Carbohydrate functionalized scaffolds were self-assembled on a two-dimensional (2D) surface to improve the understanding of the mechanisms of multivalent interactions (Chapter 2). Cyclodextrin supramolecular glycoclusters were chosen due to their ability to form stable host-guest complexes permitting to control the orientation, spacing, and shape of the glycoclusters. The formation of a host–guest complex on the carbon surface provides a versatile strategy, not only to increase the intrinsic water solubility of graphene-based materials, but more importantly to facilitate the binding of the desired biofunctional groups on the surface. The resulting glycosylated carbon material is an excellent platform for selectively wrapping and agglutination of *E.coli* due to the vital recognition role of carbohydrates and the unique 2D large flexible surface area of the graphene sheets. The captured bacteria were partially released by adding a competitive guest such as sodium adamantine carboxylate (AdCNa). The unique thermal IR-absorption properties of graphene derivatives were used to kill the captured bacteria in the graphene–sugar–*E.coli* complex by IR-irradiation method.

Summary

To facilitate the synthesis of longer linear and branched oligosaccharides, the automated glycan assembly of lipoglycans (lipomannan and lipoarabinomannan) from the cell wall of *Mycobacterium tuberculosis*, exploring α-(1→6) and α-(1→2)-glycosidic linkage were designed (Chapter 3). Mannose and arabinose building blocks have been used to assemble the library of lipoglycans fragments on Merrifield resin. Shorter LM structures were easily assembled and the compounds were isolated in short time and high yield, while the syntheses of larger oligosaccharides require further optimization. Assembled linear and branched cell wall fragments will be used in the future to gain molecular-level understanding of the role of lipoglycans in mycobacterial pathogenesis.

Synthesized linear mannose structures assembled with AGA are also optimal substrates for the study of structure function relationship of glycans. Moreover, to expand the knowledge on carbohydrate-lectins interaction another self-assembled system such as Janus dendrimers was studied (Chapter 4). Janus glycodendrimers were obtained using mannose oligosaccharides studied for their shape and functions in biological processes. Janus glycodendrimers functionalized with higher and branched mannose oligosaccharides containing α-(1→2)-glycosidic linkage resulted into more binding towards the ConA lectin than linear oligosaccharides containing α-(1→6)-glycosidic linkage.

Zusammenfassung

Kohlenhydrate sind nützliche Bausteine für supramolekulare Strukturen, die Möglichkeiten zur Ausbildung multipler Wasserstoffbrückenbindungen bieten. Verschiedene Kohlenhydrat-funktionalisierte multivalente Gerüste stehen zur Verfügung, um schwache Kohlenhydrat-Protein- (CPIs) und Kohlenhydrat-Kohlenhydrat-Interaktionen (CCIs) zu untersuchen. Hauptsächlich wurden dabei bis vor kurzem einfache Glykane wie Mono- oder Disaccharide für die Synthese multivalenter Gerüste verwendet; komplexe Glykane waren selten verfügbar. Komplexe und reine Saccharide sind aber vonnöten, um ein tiefes Verständnis der Struktur und Funktion der Glykane zu erlangen. Die chemische Synthese linearer und verzweigter Kohlenhydrate hilft dabei, Einblicke in die Multivalenz, Struktur-Aktivität-Beziehungen und die Rolle von Glykanen in lebenden Organismen zu erlangen. Automated Glycan Assembly (AGA) bietet die Möglichkeit, komplexe und reine Strukturen mit relativ wenig Aufwand zu erhalten. Die hier präsentierte Arbeit umfasst unterschiedliche Glykane, beginnend mit einem linearen Mannose-Monosaccharid-Konstrukt bis hin zu längeren und verzweigten Mannose- und Arabinose-Oligosaccharid-Strukturen, welche mit Hilfe von AGA erzeugt wurden.

Es wurde ein Cyclodextrin (CD)-basiertes mulitvalentes Kohlenhydrat-System auf einer Graphen-Oberfläche entwickelt. Um das Verständnis der Mechanismen multivalenter Interaktionen zu verbessern, wurden Kohlenhydrat-funktionalisierte Gerüste auf einer zwei-dimensionalen Oberfläche selbst-assembliert (Kapitel 2). Supramolekulare Cyclodextrin-Glyco-Cluster wurden wegen ihrer Fähigkeit ausgewählt, stabile Wirt-Gast-Komplexe zu bilden, die eine Kontrolle der Orientierung, des Abstandes und der Form der Glyco-Cluster erlauben. Die Bildung von Wirt-Gast-Komplexen auf der Karbon-Oberfläche bietet eine vielseitig einsetzbare Strategie, um nicht nur die intrinsische Wasserlöslichkeit Graphen-basierter Materialien zu verbessern, sondern vor allem auch um die Bindung der gewünschten biofunktionalen Gruppen an die Oberfläche zu ermöglichen. Das resultierende glykosylierte Carbon-Material ist aufgrund seiner wichtigen Rolle in der Kohlenhydrat-Erkennung und der einzigartigen großen, flexiblen 2D-Oberfläche der Graphen-Flächen eine ausgezeichnete Plattform für die selektive Ummantelung und Agglutination von *E. coli*-Zellen. Die eingefangenen Bakterien wurden durch die Zugabe eines kompetitiven Gastes wie z.B. Natrium-Adamantin-Karboxylat (AdCNa) partiell freigelassen. Die einzigartigen

thermalen IR-Absorptionseigentschaften von Graphene-Derivativen wurden genutzt, um die eingefangenen Bakterien im Graphen-Zucker-*E. coli*-Komplex mittels IR-Bestrahlung abzutöten.

Um die Synthese von längeren linearen und verzweigten Oligosacchariden zu erleichtern, wurde die Automated Glycan Assembly von Lipoglykanen (Lipomannan und Lipoarabinomannan) aus der Zellwand von Mycobacterium tuberculosis, die α- (1 → 6) und α- (1 → 2) -Glycosidische Verknüpfung untersuchte entworfen. Für die Synthese einer Bibliothek von Lipoglykan-Fragmenten auf Merrifield-Resin wurden Mannose- und Arabinose-Bausteine genutzt. Kürzere LM-Strukturen konnten leicht assembliert werden und die Verbindungen wurden in kurzer Zeit mit hoher Ausbeute isoliert, während die Synthese längerer Oligosaccharid-Fragmente weiterer Optimierung bedarf. Assemblierte lineare und verzweigte Zellwand-Fragmente werden in der Zukunft genutzt werden, um auf der molekularen Ebene Einblicke in die Rolle von Lipoglykanen in der mycobaktierellen Pathogenese zu erlangen.

Um das Wissen um Kohlenhydrat-Lektin-Interaktionen zu erweitern, wurde ein weiteres selbst-assemblierendes System wie die Janus-Dendrimere untersucht (Kapitel 4). Es wurden Janus-Glykodendrimere hergestellt und mit langen und verzweigten Mannose-Oligosacchariden funktionalisiert, welche α-(1→2) und α-(1→6)-glycosidische Bindungen enthalten. Die Wichtigkeit der α-(1→2)-glycosidischen Bindung gegenüber ihrem α-(1→6)-Analog konnte in Bindungsstudien mit dem Lektin ConA gezeigt werden.

1. Introduction

1.1 Cell surface glycans

Carbohydrates are major macromolecular building blocks of life other than nucleic acids, proteins, and lipids. They play an major role in various cellular functions like cell-cell interaction, and most importantly in immune defense mechanisms of animals and humans.[1] The carbohydrate domains (mono-, oligo-, and polysaccharide) attached to lipids and proteins are also termed as glycans, and are found as their glycoconjugate forms i.e. glycoproteins or glycolipids. Attachment of glycans to other molecules occurs through an enzymatic process called glycosylation, a complex posttranslational modification. The two most widely studied protein-linked glycan classes are the *N*-and *O*-linked glycans. They are covalently linked to specific amino acids; *N*-linked glycans to the nitrogen atom of asparagine residues *via* a *N*-glycosidic bond and *O*-linked glycans to an oxygen atom of either serine or threonine residues *via* an *O*-glycosidic bond.[2, 3] *N*-Glycosylation takes place in the endoplasmic reticulum (ER) of the cell and widely occurs in archaea and rarely in bacteria while *O*-glycosylation occurs in the Golgi complex and occurs in both archaea and bacteria.[4] As *N*-glycosylation begins in the ER, it occurs on a pre-assembled oligosaccharide core (a branched oligosaccharide containing three glucoses, nine mannoses, and two *N*-acetyl-glucosamines) and can be classified mainly into three subtypes; high mannose, complex and hybrid type *N*-linked glycans (Fig. 1).[5, 6] However, during the *O*-linked glycan synthesis there is no pre-assembled core structure whereas it involves the successive addition of monosaccharide units (Fig.1).[6] Examples of *O*-glycans include simpler structures like α-linked *O*-mannose, α-linked *O*-fucose, β-linked *O*-xylose, β-linked *O*-GlcNAc (*N*-acetylglucosamine), α-/β-linked *O*-galactose, and α-/β-linked *O*-glucose glycans and proteoglycans containing glycosaminoglycan than complex *N*-glycans (Fig. 1).

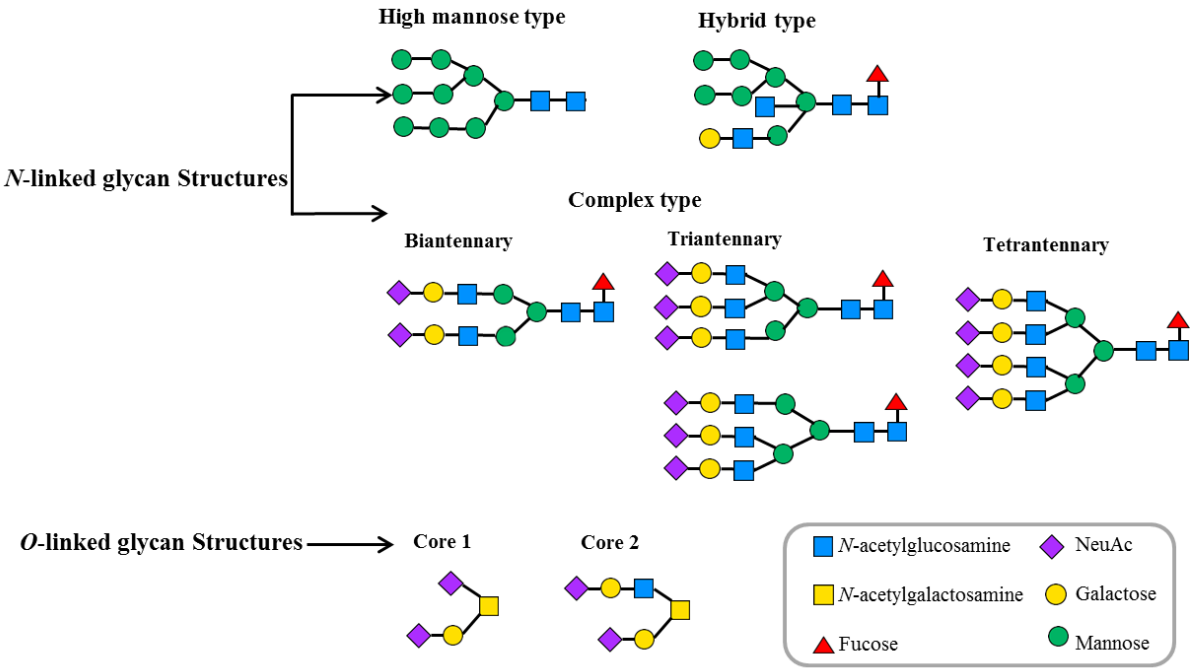

Figure 1: Schematic representation of *N*-linked and *O*-linked glycans found on glycoproteins. (Modified from ref 6)

Glycans present on the cell surface as part of the glycoprotein-polysaccharide complex are called the glycocalyx, and interact with many biological entities such as bacteria, pathogens, viruses and fungi via a number of proteins.[7-9] These cell-cell interactions are either carbohydrate-protein (CPI) or carbohydrate-carbohydrate (CCI) mediated (Fig. 2).

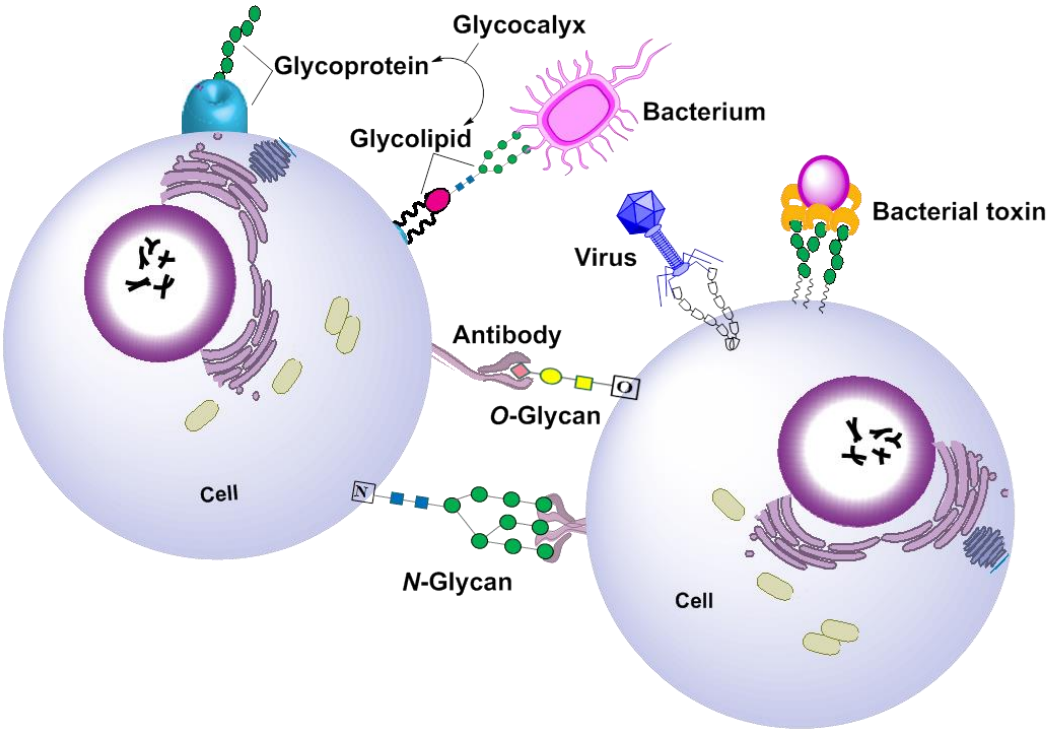

Figure 2: Schematic representation of cell surface glycan interactions with various biological entities through carbohydrate-protein and carbohydrate-carbohydrate interactions.

1.2 Gram-positive and Gram-negative Bacteria

Bacteria are one of the oldest and simplest forms of life found in nature. They can be beneficial to the organism they co-habitat (e.g. rhizobium, lactobacilli) or can be detrimental and harm the host organisms (pathogenic bacteria). In humans and other animals, large number of bacteria are present in the gut flora and on the skin;[10] some of these bacteria are beneficial and some are harmful. The pathogenic species of bacteria causes several infectious diseases including leprosy,[11] cholera,[12] syphilis[13] as well as respiratory infections such as tuberculosis, influenza, pneumonia.[14] Beneficial bacteria are used in sewage treatment (*Nitrosomonas* or *Pseudomonas* species), fermentation (*Lactobacillus*), manufacturing of antibiotics (*Streptomyces)* and many more.[15] Bacteria are few micrometers in length and exist in three shapes; spherical (coccus), rod-shape (bacilli), long and helical shaped (spirilus). The cell wall of bacteria is made of peptidoglycan layers which protect the cell from swelling and lysis.

Bacteria can be classified into two major groups namely Gram-positive or Gram-negative differentiated on the basis of Gram staining using crystal violet dye (CVS). Due to the presence of a thick peptidoglycan layer (20-80 nm) Gram-positive bacteria retain the CVS while Gram-negative bacteria do not because of the thin peptidoglycan layer (~10 nm) and stains red when observed under the light microscope. Furthermore, the cell wall of Gram-positive bacteria contains covalently bound teichoic acids and lipoteichoic acids while the outer membrane of Gram-negative bacteria comprises lipopolysaccharides, proteins and phospholipids (Fig. 3). Each bacterial cell is a reservoir of carbohydrates and proteins (discussed further in the section 1.3). The periplasm is another important and integral component of Gram-negative bacteria which contains 40% of the cell volume and the periplasmic space is rich in macromolecules which are important for nutrient binding, transport, folding and many other functions.[16-18] The peptidoglycan layer is composed of β-(1→4)-linked *N*-acetylglucosamine (GlcNAc) and *N*-acetylmuramic acid (MurNAc) and the lipopolysaccharide layer is coated with 3-deoxy-D-manno-oct-2-ulosonic acid (Kdo) and L-glycero-D-mannoheptose glycans, while mycobacteria comprises of mannose and arabinose monosaccharides.[19] *E.coli, Salmonella, Pseudomonas, Cyanobacteria* are few examples of Gram-negative bacteria while *Streptococcus pyogenes, Streptococcus pneumoniae; Staphylococcus aureus* are Gram-positive as they play important role in body defense and innate and adaptive immune system. This thesis deals with two such bacteria namely *Escherichia coli (E.coli)* and *Mycobacterium tuberculosis* (MTB). *E.coli* was used to study the CPIs using the FimH lectin and MTB to synthesize the cell wall glycan component using automated glycan assembly (AGA) respectively.

Gram Negative

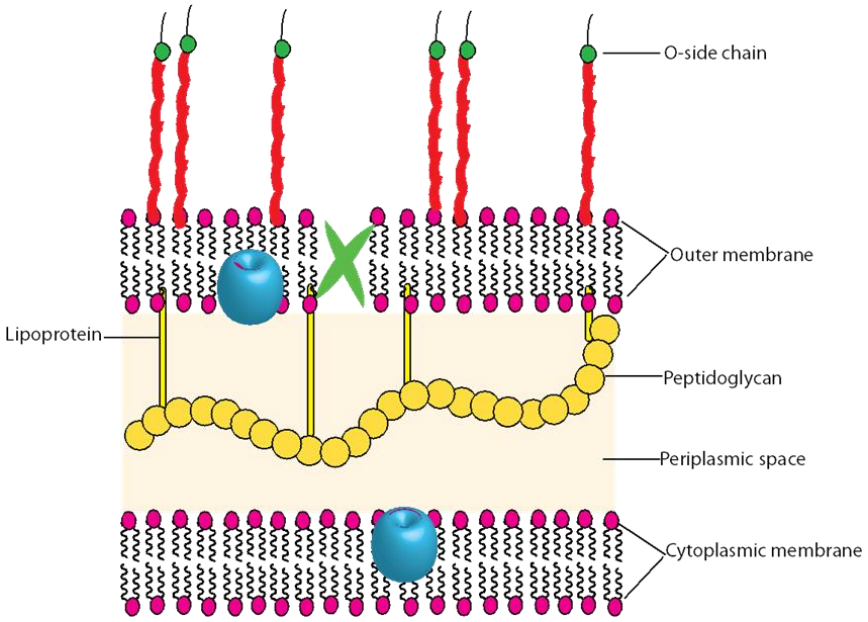

Gram Positive

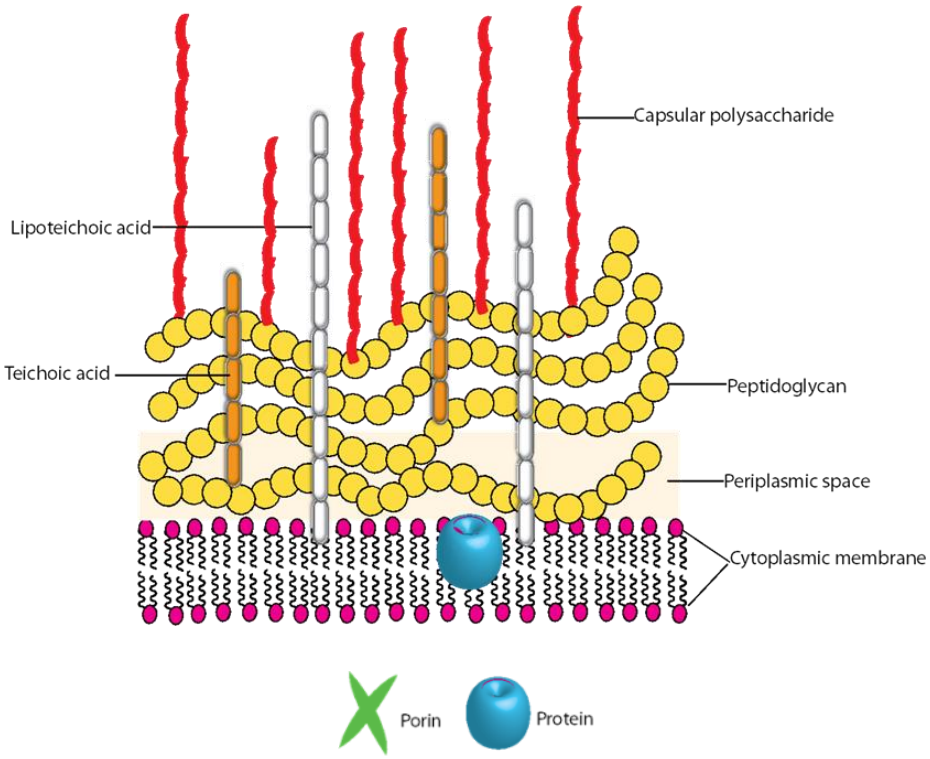

Figure 3: Schematic representation of the cell wall of Gram-negative and Gram-positive bacterium.

1.3 Carbohydrate binding lectins

Proteins are major building blocks of life and they can serve as a structural compounds as enzymes or as receptors for signal transductions.[20] Carbohydrate binding proteins are classified into two major classes: lectins and glycosaminoglycan proteins. Lectins are a special group of proteins present in plants, animals, bacteria (adhesions and toxins) and viruses (hemagglutinins).[2] The agglutinin property of lectins is based on the recognition and binding to specific sugars.[21] Animal lectins are mediators for cell recognition and are specific for monosaccharides such as fucose, galactose, mannose, *N*-acetylglucosamine, *N*-acetylgalactosamine, *N*-acetylneuraminic acid, fucose and a glycan like heparin.[22] Lectins, depending on their specificity to glycans are grouped into *C-type* lectins (selectins, collectins), *galectins*, *I-type* and *P-type* lectins (including Siglec family and mannose-6-phosphate binding ligand, respectively).[23] Lectins play an important role in innate immunity,[24] blood clearance,[25] asialoglycoprotein receptor (ASGPR) mediated endocytosis,[26] cell-specific targeting[27], apoptosis[28] etc. Another well-studied viral glycan binding protein is influenza virus hemagglutinin, which specifically binds to sialic acid containing glycans.[1] Glycosaminoglycan heparin sulfate domain is an important saccharide of cancer and these heparin-lectin interactions[29] are crucial in angiogenesis, invasion and coagulation.[30]

1.3.1 Plant lectins

Plant lectins were first discovered by Stillmark in 1882, as protein present in castor bean seeds called ricin that was found to agglutinate animal red blood cells. Plant lectins comprise of legume and ricin lectins (L- and R-type) respectively. L-type lectins are well characterized and are widely used in biomedical and analytical procedures[2] concanavalin A (ConA), soybean agglutinin, and galectin-3. ConA lectin specifically binds to mannosyl and glucosyl groups. A characteristic feature of this family is their oligomeric structure and the requirement of calcium Ca^{2+} and manganese Mn^{2+} ions for binding glycan moieties.

1.3.2 Bacterial lectins

Bacteria carry several different types of lectins on their appendages or on their surface to target glycans present on the host cells. *E.coli* carries the lectin adhesin on the top of its pili or flagella called FimH and play an important role in adherence to the epithelial cell. Each

bacteria on an average expresses 100-400 of these appendages ranging from 5-7 nm in diameter and can extend to hundreds of nm in length (Fig. 4).[31] Mannose binding type 1 pili (FimH) and globoside glycolipid (GalNAc and galactose residues) binding P pili (PapG) are two types of well-studied pilus in pathogenic *E.coli*.

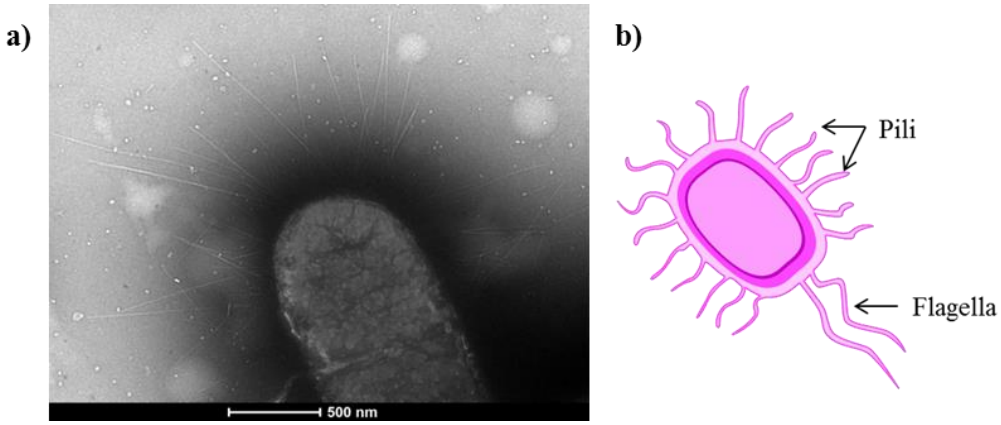

Figure 4: *E.coli* bearing several fimbriae. a) Image were taken along with an *E.coli*-agglutination studies using TEM microscope in Chapter 2 Scale bar: 500 nm, b) Cartoon interpretation of the image in a.

The FimH binding to mannose residues present on human and murine bladder cells resulting in urinary tract infections through bacterial colonization, invasion and production of biofilm-like bacterial communities.[32] The mechanical and conformational properties of the FimH-mannose binding ability have been investigated on living cell by applying external shear. As bacteria utilize a catch-bond mechanism during the mannose interaction, an induced conformation-specific immune response has been observed.[33] Bacterial toxins are another type of lectin that exploits adhesion to glycans and play an important role in intracellular trafficking. *Pseudomonas aeruginosa* (PA) is another Gram-negative bacterium present in large quantities on host epithelial surfaces and is known to produce galactose and fucose specific lectins namely PA-IL (LecA) and PA-IIL (LecB) respectively. [34] Moreover, adhesins are present on pili of *PA* and recognize mucin oligosaccharides and asialo-GM1 and GM2 glycolipids and are known to play a crucial role in bioadhesion and biofilm formation through flagellin proteins present on the surface.[35, 36]

1.3.3 Carbohydrate-protein and carbohydrate-carbohydrate interactions

In nature, CCIs and CPIs regulate a variety of biochemical processes such as cell differentiation, proliferation and adhesion, inflammation and the immune response.[2] As

described above, lectins promote a particular recognition through a lock and key model. Lectins bind to mono- or oligosaccharides without altering the structure of the bound ligand.[2]

CCIs are less explored than CPIs. CPIs on normal cells and their malignant counterparts show significant differences. These interactions occur by multiple mechanisms and incase of macromolecules can be analyzed by biophysical methods like X-ray crystallography and nuclear magnetic resonance. For smaller molecules such as chitin or GlcNAc residues, the lectin binding site can be assigned by correlating chemical shift variations of selected proton resonances. Many forces are involved during this carbohydrate:lectin or ligand:receptor bindings such as hydrogen bonding, van der Waals interaction, dipole attraction and electrostatic interaction etc. (Fig. 5).[9]

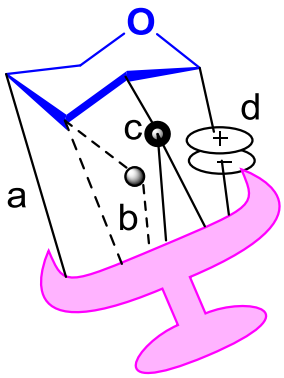

Figure 5: Carbohydrate binding to a lectin through a) hydrophobic interactions, b) water-mediated hydrogen bonding, c) metal coordination d) electrostatic interactions. (Modified from ref 37)

These interactions can be studied using different techniques. Both kinetic and near-equilibrium as well as non-equilibrium methods such as enzyme linked immunosorbent assay (ELISA), glycan microarray, agglutination, precipitation and electrophoresis.[2]. The dissociation constant, specificity and kinetics of binding between the glycans and lectins can be measured using near-equilibrium methods such as affinity chromatography, isothermal titration calorimetry (ITC) or surface plasmon resonance (SPR). In near-equilibrium method a defined equilibrium binding constant can be obtained using ITC, between the glycan and lectin upon their interaction. ITC also has been explored to study CCIs of multivalent

glycoclusters with Ca^{++} ion. It has been observed that the sugar topology and density can tune the intra- vs. intermolecular CCIs from the obtained formation constants.[37]

Lectins are used to study CCIs or CPIs with their respective glycan using the above mentioned methods. Conversely, serious problems arise while attempting to employ these specific interactions for constructing an artificial recognition interface. For example, the binding constants (K_a) for mono- and oligosaccharides to most lectins are between 10^2 and 10^5 M^{-1}.[38, 39] which are too small for assembling recognition interface. Improved CCIs and CPIs can be obtained by carbohydrate clusters. Many naturally occurring carbohydrates and glycoconjugates are multivalent and hence they show increased affinity for lectins. Multivalent effects should be adopted to detect and utilize species with lower affinities. To increase the binding strengths of CCIs and CPIs, many natural biomolecules exhibit multiple carbohydrate units that engage in multivalent interactions. Synthetic chemists have adopted Nature´s strategies and developed multivalent systems that mimic natural supramolecular interactions.[40, 41]

1.4 Supramolecular chemistry

The following section has been taken in part and modified from the article; Reprinted with permission from:

Delbianco, M., Bharate, P., Varela-Aramburu, S., and Seeberger, P. H. Carbohydrates in supramolecular chemistry *Chem. Rev.* **2016**, *116* (4), pp 1693–1752, DOI: 10.1021/acs.chemrev.5b00516.

The importance of weak, non-covalent interactions in biological systems was first appreciated at the beginning of the 20th century with an improved understanding of hydrogen bonding and ligand-receptor interactions. These weak interactions were key to “host-guest” complexes that form well-defined architectures and were recognized with the 1987 and 2016 Nobel Prize for supramolecular chemistry. Since then, a variety of supramolecular systems that respond to signals,[42] molecular machines and switches,[43, 44] well-defined networks[45, 46]

and self-assembling macroscructures[47, 48] have been created and studied. All of these new non-covalent systems are built upon weak interactions such as hydrogen bonding,[49, 50] metal coordination,[51, 52] hydrophobic or hydrophilic forces,[53, 54] π-π interactions[55-57] and van der Waals forces.[58, 59] Stable systems, that are able to mimic nature and bind analytes with great specificity, have become accessible via multiple and directional interactions.[60, 61]

Different scaffolds have been used to create supramolecular assemblies. Cyclodextrins (CDs),[40] organic macrocycles,[62, 63] dendrimers,[64] nanoparticles[65] and polymeric backbones[66] represent the most studied examples (Fig. 6). Herein the importance of carbohydrates (includes-CDs) and nanomaterials (includes-graphene) as building blocks for the synthesis and stabilization of supramolecular systems based on multiple weak interactions are emphasized.

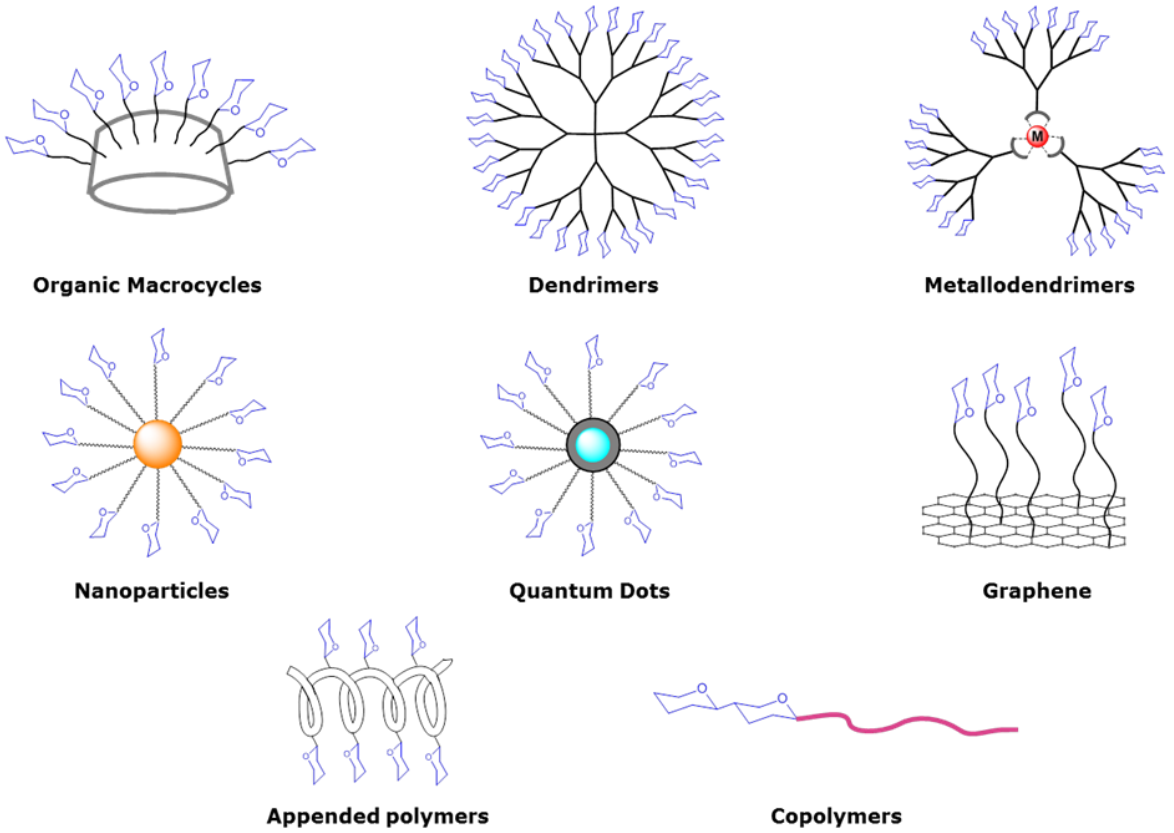

Figure 6 : Overview of the different scaffolds used for supramolecular assemblies. Adapted from Delbianco et al.[67]

1.4.1 Carbohydrate materials

Carbohydrates can form many hydrogen bonds, a feature that renders them interesting for supramolecular systems. Nanoparticles and polymers have been synthesized with various sizes using both batch and microreactor methods and functionalized with carbohydrates.[37] The resultant glycoclusters showed significant enhancements in binding affinity compared with the corresponding monovalent ligands. Other important issues regarding the preparation of multivalent carbohydrates are related to the orientation, spacing and local concentration of the sugar on the glycoclusters. General scaffolds which are facile, robust, presents tunable symmetry and exhibit optical and electrochemical properties are important to develop a direct probing system.

In this part the recent advances in use of CDs and graphene functionalized nanomaterials in supramolecular chemistry are summarized covering three main topics: 1) The use of multivalent glyco-conjugates for the formation of host-guest complexes that are used for sensing bacteria and drug delivery; 2) The combination of CCIs with other weak interactions, such as π-π interactions, for the formation of self-assembling glycoclusters; and 3) The formation of extended supramolecular networks upon binding to proteins (CPIs).

1.4.1.1 Cyclodextrins (CDs)

Cyclodextrins (CDs) are a class of cyclic oligosaccharides, with a torus-like shape, built from 1→4 linked α-D-glucopyranose units. First described in 1891, CDs were named ‘‘cellulosine”. Three types of CDs with six, seven or eight glucopyranose units are referred to as α, β and γ-CD with β-CD as the most common class.[68] CDs have a hydrophilic exterior and a hydrophobic central cavity for the non-covalent inclusion of guest molecules.[69] Different CDs can encapsulate a range of guest molecules[70] and have been employed for molecular recognition,[71] catalysis,[72] polymerization,[73] material sciences, drug delivery,[74] nanotechnology[75] and hydrolysis.[76]

The synthesis and biological applications of CDs as multivalent scaffold in carbohydrate chemistry are widely studied.[68,77,78] Cyclodextrin glycoconjugates display the glycans in a multivalent form similar to that present on the cell-surface.[79] CDs have been used for drug delivery[80] and sensing[81, 82] as well as developing saccharide (glycan)-selective systems.[83]

Within this chapter more focus is on the application of CDs in supramolecular chemistry with particular attention on CDs as glycoclusters scaffold.

Glycosylated CDs for the Study of CPIs and CCIs

C-type lectin receptors (CLRs) bind glycan structures displayed on pathogens. Multivalent carbohydrate systems with terminal sugar ligands tightly bind these lectins by glycoside clustering.[84] Straightforward access to different sugar densities *via* self-assembly helped to tune intra- to inter- molecular CCIs.[85]

Gene and Drug Delivery

CDs have been used as vehicles for drug and gene delivery. Mannose and galactose functionalized α-CDs (Man-α-CDs and Gal-α-CDs respectively) were found to have remarkable gene and drug delivery to various cells including macrophage receptor (MR) or asialoglycoprotein receptor (ASGPR)-mediated gene cells.[86] Similarly, galactose-functionalized β-CDs were designed for hepatocyte-specific drug targetting.[87] Encapsulation of rhodamine in the cyclodextrin cavity facilitated targeting of hepatocellular carcinoma cell line HepG2. A trivalent mannosylated β-CD conjugate was used to encapsulate and deliver pharmacological chaperones to macrophages *via* the macrophage mannose receptor (MMR).[88] Carbohydrate-based targeting approaches take advantage of several C-type lectin receptors (CLRs) including the ASGPR on liver cells and DC-SIGN (Dendritic Cell-Specific Intercellular adhesion molecule-3-Grabbing Non-integrin) expressed by dendritic cells.[89] A CD-based glycoconjugate was created for HIV drug delivery and bound to DC-SIGN which inhibited its interaction with HIV gp120 at nanomolar concentrations.[90]

Metal Complexes

Glycoclusters that contain a metal complex in the framework are called metalloglycoclusters.[91] Metallo-glycodendrimers bearing transition metals or lanthanide ions have been prepared by self-assembly.[92-95] The inherent physical properties of metallodendrimers, such as fluorescent emission, render them ideal for biological applications.[96] CD-based glycoclusters have been exploited for the synthesis of multivalent probes built *via* host-guest assembly around a metal core. Metallo-glycodendrimers based on

a tris(bipyridine)ruthenium ($Ru(bipy)_3$) fluorescent scaffold and appended with two, four or six adamantyl groups were adorned with mannose functionalized CD-glycoclusters by host-guest interactions.[81]

Rotaxanes

Carbohydrate-displaying (pseudo)polyrotaxanes were used to study CPIs. A variety of mechanically interlocked structures, where the CDs form inclusion complexes with the polymeric chain, were explored for macromolecular recognition.[97-99,100, 101]

Self-Assembly

Spontaneous processes forming ordered structures are key to some signaling pathways.[102, 103] Self-assembled surfaces have been used to study multivalency and stimuli responsive systems.[104] Liposome and vesicles mimic noncovalent interactions involved at the interface between cell membrane and aqueous solution phase.[105, 106]

Amphiphilic CD vesicles show enhanced host-guest interactions when different guest polymers are placed at the CD vesicle surface.[107] Host-guest assembly occurs *via* orthogonal noncovalent interactions due to metal-coordination complexes.[105] A ternary system using vesicles, carbohydrates and lectins was used to study the kinetics of the orthogonal multivalent interfacial interactions. Maltose and lactose decorated vesicles aggregate with the lectins ConA and PNA in a sugar-dependent manner.[108] The influence of multivalency and glycan surface density was explored further by amphiphilic CD vesicles involving an adamantane guest that carries mannose and CD vesicle hosts.[109]

1.4.1.2 Graphene functionalized CD's

Graphene is a one atom thick hexagonal lattice and a crystalline allotrope of carbon. Graphene based materials possess exceptional mechanical stiffness, electrical, thermal and optical properties hence due to these properties graphene have seen unprecedented development since its discovery in 2004.[110] Graphite can be chemically oxidized to graphite oxide (GO) using Hummers method and later on graphite oxide can be converted into graphene oxide by sonication. Reduction of graphene oxide yields the reduced form of graphene oxide (rGO). This rGO presents pristine graphene like properties. Chemically

modified graphene found many applications due to its large scale availability[111]. An alternative to chemical modification is thermal reduction. Chemically reduced GO yields are poor ensuing less surface area and electrical conductibility whereas thermally reduced GO have shown to bear high surface area.[112] GO, rGO, and their derivatives have received tremendous attention in the field of materials due to their conductivity, electricity and ability of surface modification possibilities.

The high surface area, strong Van der Waals forces, and л-л interactions increase the value of graphene material. However, these significant properties also limit the graphene benefits as it easily aggregates irreversibly in solvents, hence in order to overcome dispersity and solubility of graphene many new methods have been investigated to synthesize modified graphene.[113-115]

Planar two dimensional (2D) surface of GO possesses different functionalities like hydroxyl, carboxyl, phenol, lactone, carbonyl and epoxy groups either on its basal plane or on the edges.[116] These functional groups enable the modification of GO surface with reactant molecules either through covalent or non-covalent interactions. The surface of GO or rGO were covalently functionalized with amido,[117] amino,[118] PEG[119] or isocyanate[120] functionalities to produce well dispersed nanomaterials. Non-covalent interactions between the graphene nanomaterials involving the strong hydrogen bonding, hydrophobic and л-л interactions also have been investigated widely.

GO has been functionalized non-covalently using aromatic polymers, surfactants, nanoparticles, biomolecules, and nanotube.[121, 122] The resulting nanomaterials synthesized using these interactions via a supramolecular approach are reported to increase the dispersion of graphene sheets, biocompatibility, reactivity, binding properties as well as the solubility of formed material in solvents while keeping intrinsic and electrical properties of graphene intact.[121] Such modified GO with improved physico-chemical properties can be applied as sensors, photodetectors, in luminescence and in electrocatalysis, electronics, and in biological labelling (Fig. 7).[123-125] These properties of graphene/GO/rGO have been utilized in this thesis and thermally rGO functionalized CD nanomaterial has been synthesized and utilized for bacterial sensing, wrapping and killing.

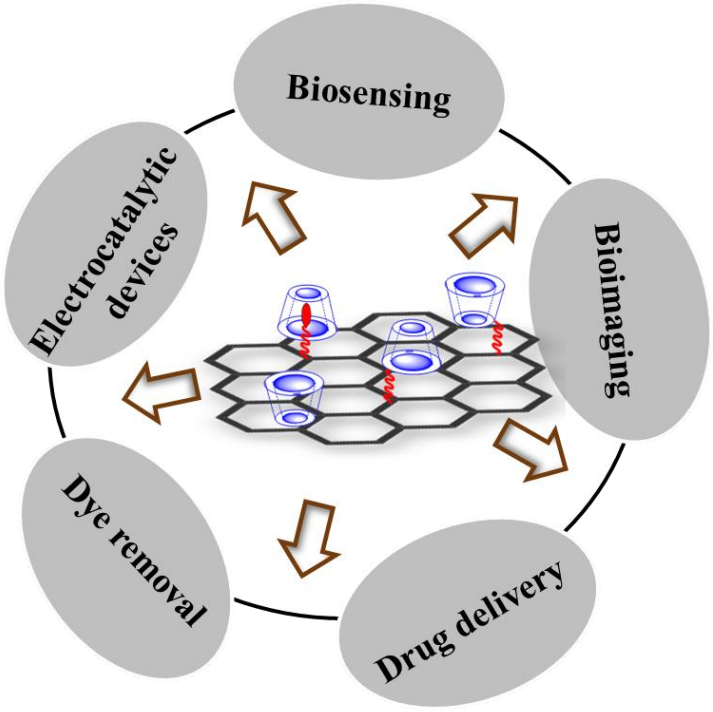

Figure 7: Schematic representation of applications of graphene-CD nanomaterials formed by either host-guest interactions, covalent or by multiple physical interactions. β-CD is represented in blue, graphene in black and linker with guest moiety in red color.

Nanomaterial formed using CD (as mentioned above in 1.4.1.1 section) through host-guest interactions can help to increase the poor dispersion, water solubility and stability of graphene functionalized material.[126]

Similarly, the supramolecular GO polymer network could form a hybrid material of GO and CD due to the ionic and host-guest interactions between them which also helps to control the colloidal size of the formed structure.[127] GO-based hybrid materials synthesized using host-guest systems and by combining multiple physical interactions has been applied in thermoresponsive bio- and electrocatalytic devices,[113] as electrochemical sensor,[128] and also as an optical sensor.[129]

CD functionalized graphene nanosheets has been synthesized, modified into glassy carbon electrode and applied in sensing of carbendazim (benzimidazole), a fungicide used in agriculture.[130] The host-guest complex formation between CDs and carbendazim on graphene nanosheets surface resulted into effective removal of fungicide. Similar glassy

carbon electrode has been synthesized using combination of GO, CD and nanoparticles and applied for detection of uric acid in human urine.[131]

Utilizing the adsorption capacity of graphene, an CD grafted GO has been used to remove dyes from the solutions such as fuchsin acid, methylene blue and methyl orange.[132] In particular, bioactive nanosupramolecular assemblies constructed from CDs through non-covalent interactions have found many applications in therapeutics and diagnostics due to their advantages of host-guest complex formations and hydrophobic cavity to encapsulate drug moieties for the specific delivery into the cells.[133] By taking advantage of the non-covalent interactions i.e. л-л interactions formed between doxorubicin and CD functionalized folic acid (FA) GO carrier could recognize the FA receptor present in cancer cells.[134]

1.5 Automated glycan assembly

One goal for glycoscientist is to correlate glycan structure with glycan function. In order to understand the physical and biological properties pure glycans are needed. Solution phase synthesis (SPS) of such glycans is laborious and time consuming (*See* Chapter 3, section 1.2), whereas automated solid phase synthesis allows for the synthesis of complex oligosaccharides in short time.

Automated solid phase synthesis of peptides,[135] and nucleic acids[136] are the milestone contributions to the field of chemistry that have substantially improved the field of biomedical research. Similarly, solid phase oligosaccharide synthesis[137] (SPOS) provided a significant contribution to carbohydrate chemistry. Eighteen years ago, the first attempt to automated glycan assembly (AGA) was undertaken, proven and further developed commercially (Glyconeer 2.1)[138] by the Seeberger group (Fig. 8).[139]

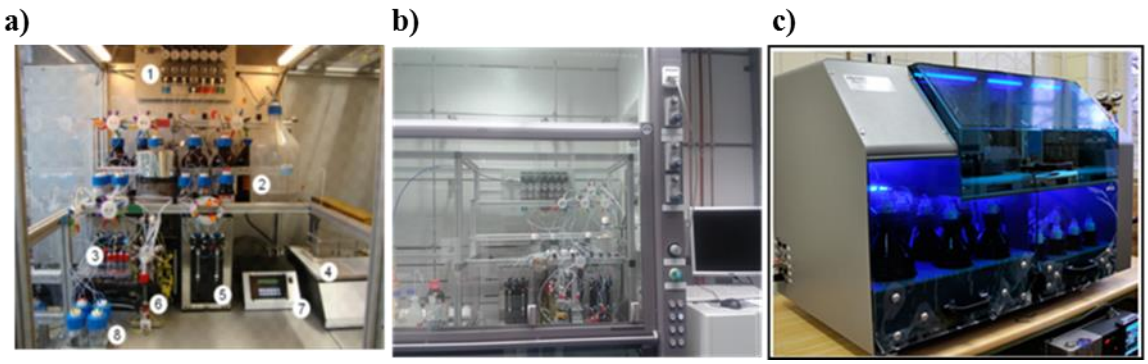

Figure 8: Development of automated glycan assembly; a) home-build synthesizer,[140] b) home-build synthesizer (Frank Schumacher thesis-under preparation) to c) Glyconeer 2.1[141].

Automated glycan assembly (AGA) makes use of Merrifield resin as a solid support, on which the oligosaccharides are assembled using monosaccharide building blocks. A set of preprogrammed modules such as glycosylation and deprotection, followed by post automated photocleavage and purification using normal phase high performance liquid chromatography (NP-HPLC), affords conjugation ready glycans (Fig. 9).[142]

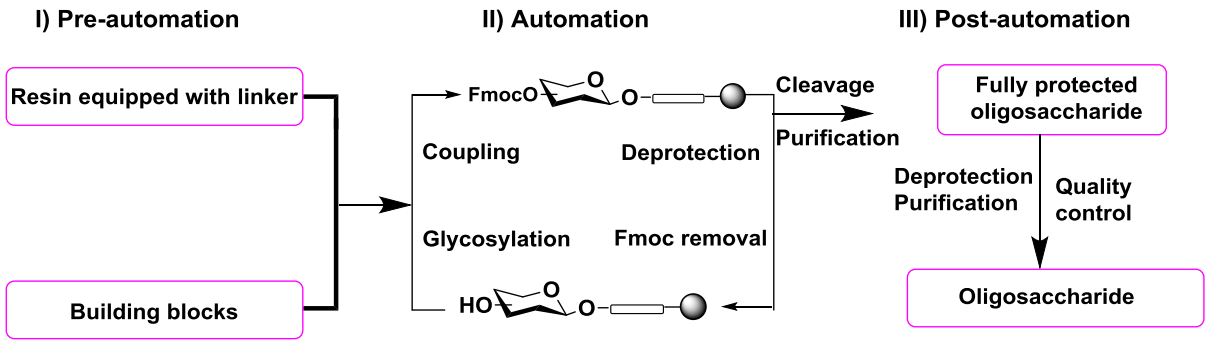

Figure 9: Schematic representation of automated glycan assembly. (Modified from ref. 152)

The monosaccharide building blocks are used for chain elongation and require careful designing of temporary, permanent protecting group patterns and anomeric leaving groups. This strategic planning is important in order to provide specific regioselctivity and stereoselctivity during the glycosidic linkage formation. The parameters such as activator solution, amount of building block donor and reaction temperature play an important role in the synthesis.[143] To date, benzyl ethers as non-participating and benzoyl ethers and pivalate esters as participating permanent protecting group have been used on AGA which can be

removed at the end. The use of an ester-protecting group at C-2 hydroxyl controls the stereochemistry of the anomeric center, as per neighboring group participation effect.[143] Also participating *N*-trichloroacetate (TCA) and a non-participating azide protecting group has been used as amine protection group for amino sugars. The main temporary protecting group used in the AGA for hydroxyls is the 9-fluorenylmethoxycarbonate (Fmoc), which is easy to remove under basic conditions and the byproduct used to quantify the loading by measuring the dibenzofulvene adduct by its UV absorption. Levulinoyl ester (Lev) and 2-naphthylmethyl ether (NAP) groups are also used as orthogonal temporary protecting groups. The obtained protected oligosaccharides are further cleaved from the solid support and deprotected affording the desired glycans.

Presented below are the solid support and linkers used in AGA with the most relevant syntheses been reported.

1.5.1 Solid support: Merrifield resin

Merrifield's peptide synthesis[144] on a resin was the start of the solid phase synthesis field and is still widely used to synthesize long peptides and proteins. The same solid support is also used for AGA. Merrifield insoluble solid beads consist of a copolymer of styrene and divinylbenzene that carry a chloromethyl functional group (Fig. 10). The porous resin exhibits very good swelling properties in solvents like dichloromethane, toluene and tetrahydrofuran allowing for the reagents to pass through. Thus, the removal of excess reagents or side products from the growing oligosaccharide chain is achieved by simple washing the resin.[145]

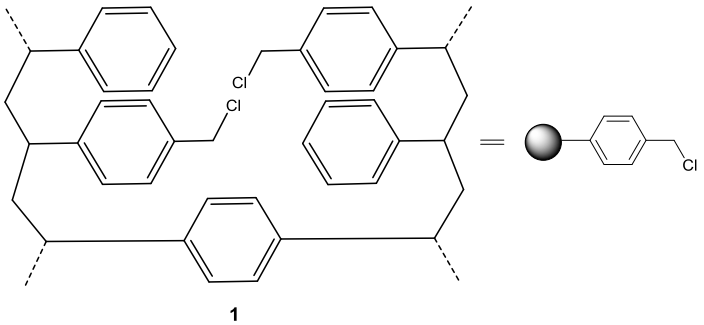

1

Figure 10: Structure of *Merrifield* resin.

1.5.2 Linkers and recent AGA syntheses

AGA follows the acceptor bound to the resin approach where the reactions between activated electrophilic glycosyl donor, and a nucleophilic glycosyl acceptor takes place. The nature of the linker is an integral part of AGA, as it has to be stable during the whole chemical synthesis and at the same time be cleavable to reveal the glycans at the end of the synthesis. To date, four different linkers have been reported for AGA bound on the resin: octanediol linker **2**, base labile linker **3,** photolabile linker **4** and traceable linker **5**, a modified version of the photolabile linker **4** that permits to liberate the product with free reducing end (Fig. 11).

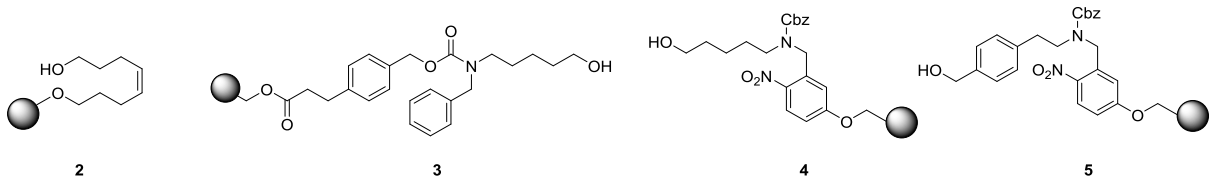

Figure 11: Different types of linkers functionalized on Merrifield resin for AGA; octanediol linker **2**, base labile linker **3**, photolabile linker **4** and traceable linker **5** respectively.

During the first attempt, Seeberger and coworkers synthesized linear α-(1→2)-polymannosides and branched oligosaccharide structures by automated synthesis. The assembly of fully protected branched phytoalexin elicitor (β-glucan) **9** was challenging as it require a carefully designed protecting group strategy The automation synthesis was carried out on solid support **2** functionalized with octanediol linker using building blocks **6** and **7** (Scheme 1). The linker was readily cleaved by olefin cross metathesis using Grubbs catalyst **8** under an atmosphere of ethylene. The levulinoyl ester was chosen as C-6 temporary protecting group and removed by hydrazine, while a pivalate ester was installed at C-2 to ensure the β-selectivity. A temperature controlled reaction vessel was introduced on the first-generation AGA synthesizer enabling lower temperatures required during glycosylation. The synthesis had some limitation such as the use of branched disaccharide building block **7** for branched structure instead of actual installing the branching. In addition the linker was not compatible with the electrophile required to activate the thioglycoside.

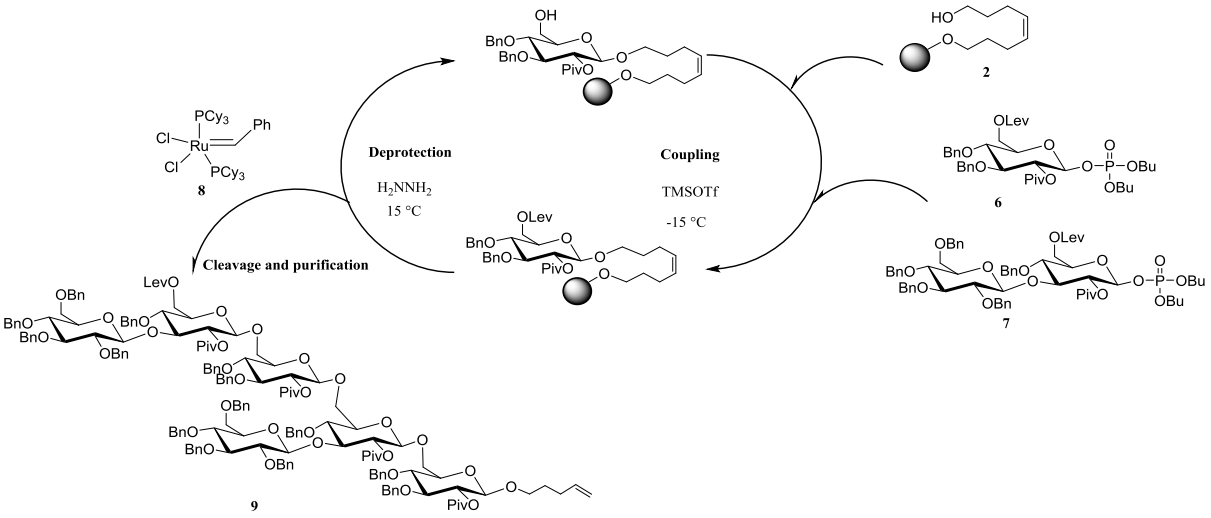

Scheme 1: Seeberger's first AGA of phytoalexin elicitor β-glucan **9** using building block **6** and **7** on solid support **2**: Reactions and conditions: Glycosylation: **6** or **7**, TMSOTf, CH_2Cl_2, -15 °C, repeated two times for 15 min; Deprotection: N_2H_4, pyridine, AcOH, 15 °C, 15 min; Cleavage: Grubbs catalyst **8**, ethylene, CH_2Cl_2, 89% overall yield.

The first example of AGA proved that linear and branched glycans can be made on solid support. However, the technique needed to overcome additional challenges related to instrument and synthetic strategies used for assembling oligosaccharides.

A new base labile linker (**3**) (Fig. 11) permitted the use of thioglycoside and temporary protecting groups like Fmoc, Lev, silyl ethers and *N*-trichloroacetate groups. With this improvement a library of oligo β-(1→6) and β-(1→4)-glucosamine structures **10, 11** and **12** were synthesized (Fig. 12).[146] The conditions used to cleave the linker possessed a dual functionality, i.e. the release of the crude product with an alkylamine linker from the solid support as well as the removal of the base labile groups present on the glycan chain.

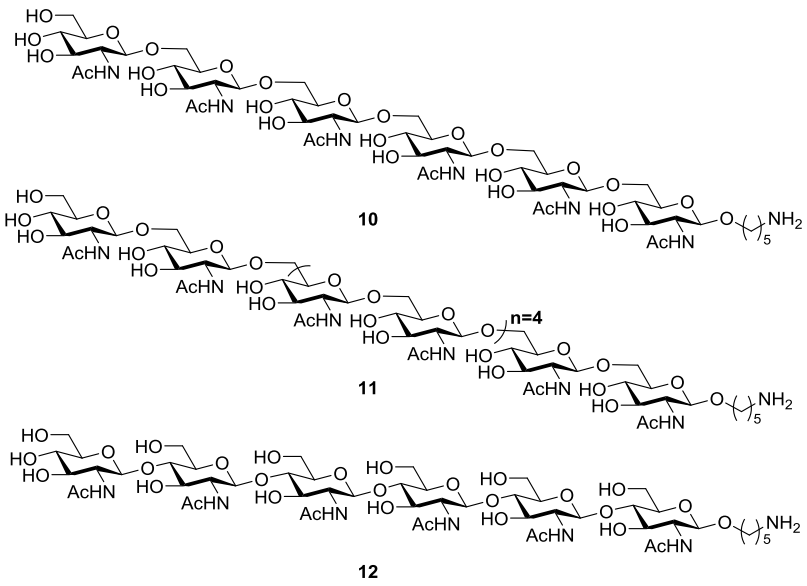

Figure 12: AGA of oligosaccharides containing **10**, **11**, and **12** β-(1→6) and β-(1→4)-glucosamine respectively.

In addition, the new base labile linker produces conjugation-ready glycans which can now use in in vitro and in vivo analysis using glycan array and in biological functions like vaccine development. However, the linker cannot be used in the presence of base labile temporarily protecting groups and was not compatible with the conditions used for activating glycosyl phosphate.[147] Hence a photolabile linker **4** (Fig. 11) was developed to overcome these limitations and was successfully applied in the assembly of linear and branched β-(1→3)-glucan oligosaccharide libraries that were used to get insights into β-glucan antibody specific epitopes using glycan array.[148]

The photolabile linker **4** is now the most used linker on AGA due its stability and compatibility with activation conditions used for glycosylation. After photocleavage it delivers the glycan with a free amine group which can easily be used for further functionalization.

The power of AGA was demonstrated by the synthesis of the linear 30-mer oligomannoside **14** (Scheme 2).[140] Furthermore, AGA has been succesfully appiled to the synthesis of α-sialylated oligosaccharides,[149] Lewis X, glycosaminoglycans[150, 151] and glycopeptides.[152]

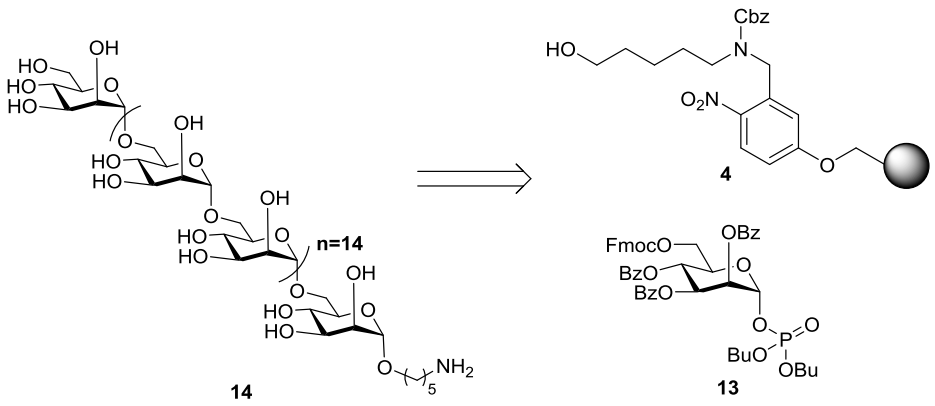

Scheme 2: AGA of linear 30mer of mannose.

S. pneumoniae is a Gram-positive bacterium, covering capsular polysaccharide as a major virulence factor and causes *pneumonia* and other types of pneumococcal infections. AGA was also applied to the production of oligosaccharide vaccine candidates; such as *S. pneumoniae* serotype 3 (ST3) **17**. The time and the low yield due to late stage oxidation step in SPS can be overcome by assembling glucuronic acid building block **16** on solid support **4** using AGA (Scheme 3). The glycosyl phosphate building blocks **15** and **16** were activated by TMSOTf (trimethylsilyl trifluoromethanesulfonate) at -30 °C to -15 °C. The Lev and Fmoc group were installed for 1,4 and 1,3 elongation respectively. The temporary Fmoc protecting group was removed with triethylamine in DMF and the Lev protecting group was removed using hydrazine monohydrate in pyridine/acetic acid (3:2 v/v). Cleavage from the solid support followed by deprotection afforded the conjugation-ready *S. pneumoniae* serotype 3 trisaccharide.

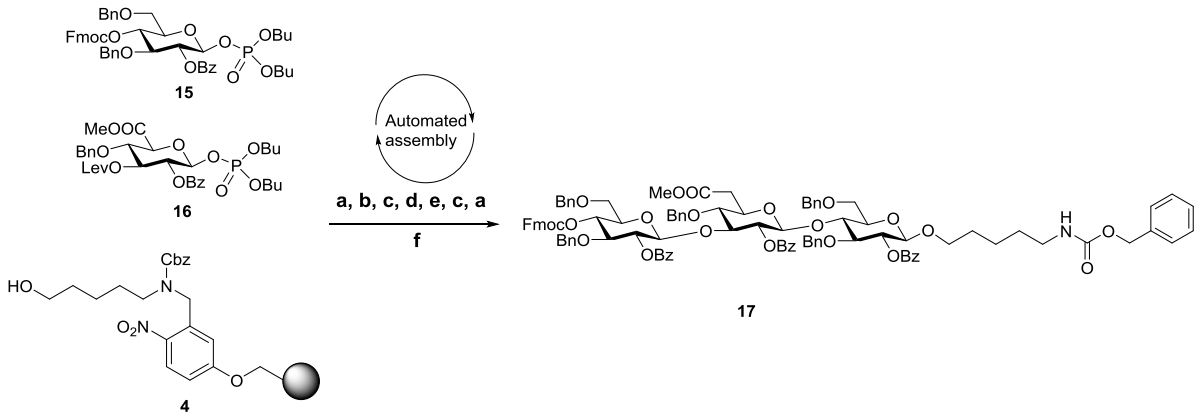

Scheme 3: Automated synthesis of ST3 trisaccharide **17** using glycosyl phosphate building blocks **15** and **16**: Reagents and conditions: a) **15**, TMSOTf, CH_2Cl_2, -30 °C to −15 °C; b) Et_3N in DMF (10% v/v), 25 °C; c) TMSOTf, CH_2Cl_2, -30 °C; d) **16**, TMSOTf, CH_2Cl_2, -30 °C to -15 °C; e) N_2H_4·OAc, pyridine/AcOH (4:1 v/v), 40 °C; f) photocleavage, 69% overall yield.

AGA has also been successively applied to the synthesis of fragments of plant cell wall polysaccharides, such as xyloglucan, arabinogalactan and arabinoxylan.[142, 153, 154] The α-(1→3) arabinofuranosyl moiety from arabinoxylan oligosaccharides were used to characterize the specific glycan-binding- antibodies of the plant cell wall.[153] A library of 19 xylan oligosaccharides was applied for active site mapping of xylan dissecting enzymes.[155] The xylan backbone **24** was constructed using four building blocks **18-21,** each equipped with phosphate leaving group (Scheme 4). Fmoc was used for chain elongation while C-2 and C-3 hydroxyls groups of xylan backbone were protected with fully orthogonal Nap and 2-(azidomethyl)benzoyl (Azmb) protecting groups for further substitution with arabinofuranose **22-23** and glucuronic acid **18-21** building blocks. The Azmb group was introduced in AGA as it was found to provide participating effect for selective β-(1→4)-glycosylation and showed potential for chemoselective removal using alkyl phosphines. Nap removal was carried out using DDQ (2,3-dichloro-5,6-dicyano-1,4-benzoquinone) solution in DCE/MeOH/H_2O (64:16:1) at 40 ºC and Azmb in tributylphosphine (PBu_3) in THF/H_2O (5:1) at 45 ºC.

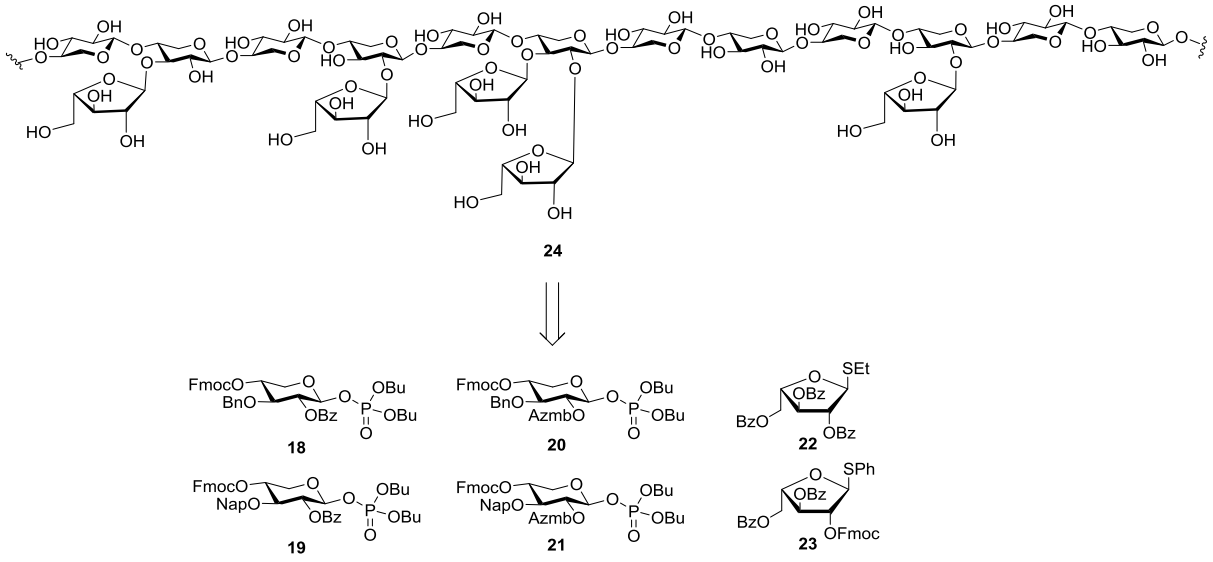

Scheme 4: Representative chemical structure of an arabinoxylan polysaccharide **24** and the building blocks required for the assembly of representative oligosaccharide fragments.

As *cis*-glycosidic bond formation does not rely on participating protecting groups and it frequently results into the formation of anomeric mixures.[156] However, such synthesis of complex oligosaccharides containg *cis*-glycosides stuctures can be efficiently performed by AGA exploiting the presence of remote protecting group partecipation.[157] Having demonstrated the feasibility of AGA, Seeberger and coworkers, further illustrated the wider applicability of this method by synthesizing a library of oligosaccharides structures containing *cis*-glucosidic and *cis*-galactosidic linkages in a rapid manner using set of different glucose and galactose building blocks (Fig. 13).[157] The importance of thiogalctoside building blocks with remote participating protecting groups such as acetyl or benzoyl esters have been highlighted in assembly of cis-glycoside formation.

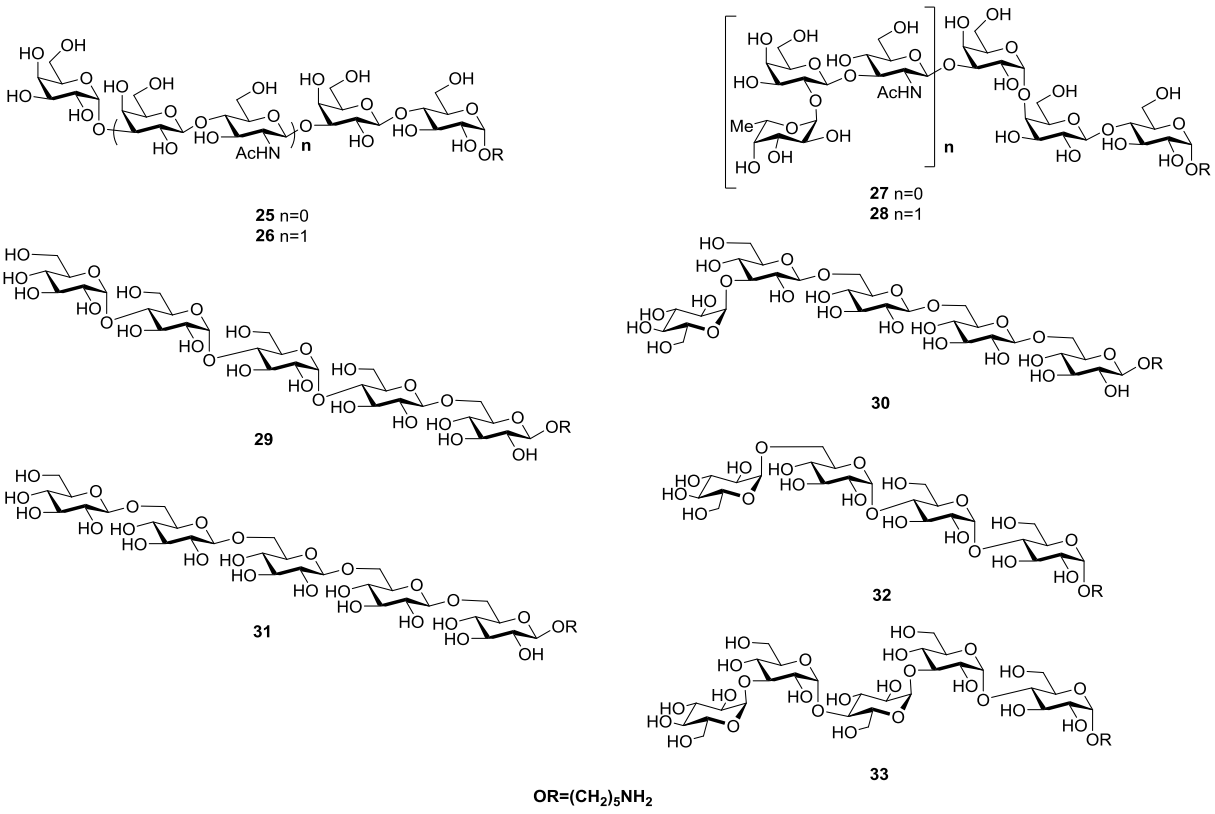

Figure 13: AGA of oligosaccharides containing different 1,2-*cis*-galactosidic linkages **25–28** and oligosaccharides contacting containing either single or multiple 1,2-cis-glucosidic linkages **29**–**33**.

1.6 Aim of the Thesis

Carbohydrates are useful building blocks for supramolecular assemblies. Linear and branched carbohydrates can help to get insights into multivalency, structure-activity relationship of glycans and to understand their role in living organisms. These longer glycans can be easily synthesized using AGA. Therefore, the overall objective of this dissertation was to synthesize a library of mannose oligosaccharides (Fig. 14) and different multivalent mannose glycoclusters. Towards this aim, this research was conducted as followed:

Firstly, oligosaccharide-based self-assembled multivalent compounds were synthesized to build a bioactive material for bacterial sensing (Chapter 2). In this part, a multivalent carbohydrate-functionalized 2D scaffold was developed by placing ManCD on adamantyl-functionalized TRGO sheets, which was found to bind, wrap and kill *E. coli* bacterium effectively.

Chapter 3 describes the synthesis of linear and branched cell wall fragments of MTB (lipomannan: LM, lipoarabinomannan: LAM) using AGA, exploring α-(1→6) and α-(1→2)-glycosidic linkages, to gain molecular-level understanding of the role of lipoglycans in mycobacterial pathogenesis. The LM and mannose capped LAM structures play an important role in host-pathogen interactions including Toll-like receptors (TLR) signaling and C-type lectins binding respectively.[158, 159] The synthesized glycans can help to identify LM and LAM substructure-specific antibodies.

In Chapter 4, linear and branched mannose oligosaccharides (from mono- to 12-mer) were synthesized using AGA for imaging studies and glycodendrimer synthesis. High-resolution imaging of a linear mannose pentasaccharide was carried out for structure elucidation. Furthermore, Janus glycodendrimers were obtained using mannose oligosaccharides to study their functions in biological processes.

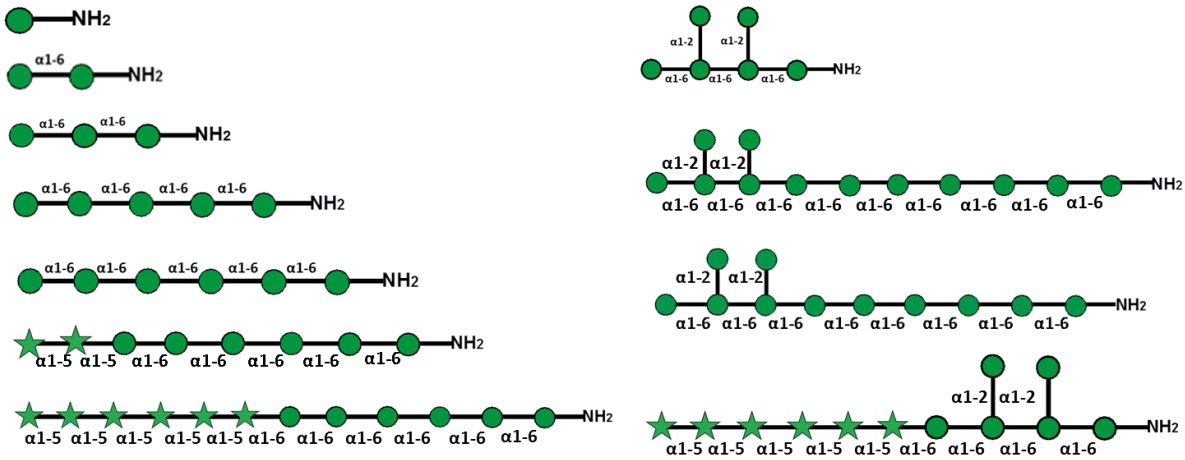

Figure 14: Library of linear and branched mannose oligosaccharides synthesized using AGA as part of my thesis work.

2. Multivalency at Interfaces: Supramolecular Carbohydrate-Functionalized Graphene Derivatives for Bacterial Capture, Release, and Disinfection

The following part has been modified from the article; Reprinted with permission from

Qi, Z.; Bharate, P.; Lai, C. H.; Ziem, B.; Bottcher, C.; Schulz, A.; Beckert, F.; Hatting, B.; Mulhaupt, R.; Seeberger, P. H.; Haag, R. Multivalency at Interfaces: Supramolecular Carbohydrate-functionalized Graphene Derivatives for Bacterial Capture, Release, and Disinfection *Nano Lett.* **2015**, *15* (9), pp 6051–6057, DOI: 10.1021/acs.nanolett.5b02256.

2.1 Introduction

Multivalency plays a pivotal role in biological processes, particularly in the adhesion of bacteria/viruses or antibodies/macrophages to the cell surface.[160-162] In contrast to weak monovalent binding, multivalent interactions result in high specificity and in thermodynamic and kinetic stability. Carbohydrates, a class of crucial biological binding units, govern huge number of life recognition processes through multivalent CCIs or CPIs.[163-166] The CCIs and CPIs occur either during the first steps of infection, for specific recognition between host and bacteria,[167-169] or at different stages of the immune response.[170] *E.coli,* a Gram-negative bacteria, and its strains are responsible for many foodborne diseases and urinary tract infections[10] which are of concern for public health, caused by drinking contaminated water. The burden is also significant from an economic point of view such as in the case of Topps meat processing company that ceased operations due to *E. coli* O157:H7 contamination of ground beef with millions of dollars loss. The quick detection of *E. coli* contamination during food processing by using specific biosensors is needed.[171]

Recent investigations have revealed that both the valency of glycoconjugates and the size of the scaffold play an important role in the effective inhibition of large particulate microorganisms and controlling their agglutination.[172, 173] Such glycoconjugtaes can be used as the antiadhesion and agglutination agents. Myongsoo *et. al*.[174] discovered that either increasing the density of exterior coated sugars or the length of nanofibers leads to enhanced

bacterial cell agglutination. Similarly Huang and coworkers synthesized nanotubes using amphiphilic pillar[5]arene coated with galactoses and hydrophobic alkyl chain and found that the increased length of sugar coated nanotubes due to self-assembly exhibit a higher binding affinity towards the pathogenic bacteria.[175] Scaffolds formed through supramolecular assembly, such as dendrimers[176, 177], nanoparticles,[178] calixarenes,[179, 180] and fullerenes[181, 182] offer zero-dimensional (0D) carrier platforms to functionalize carbohydrates. While those based on peptides,[183] carbon nanotube,[184] self-assembled fibrous nanostructures provide a one-dimensional (1D) scaffold to investigate cell targeting and anti-adhesive properties. Spontaneous processes forming ordered structures are key to signaling pathways.[102, 103] Self-assembled surfaces have been used to study multivalency and stimuli responsive systems.[104]

2.1.1 Graphene and cyclodextrin

2.1.1.1 Graphene

The discovery of graphene has fundamentally changed the field of materials science.[185] Graphene is a single-atom-thick sheet of 2D sp^2-hybridized carbon, in which atoms are arranged in a honeycomb pattern having good conductivity for heat, electricity and wide applications due to its high surface areas, low cost in nanoelectronics,[186] nanophotonics,[187] nanocomposites,[188] sensors, catalysis, batteries, and supercapacitors.[126] The thermally reduced graphite oxide (TRGO), in which some of the constituent carbon atoms of the graphene lattice bear hydroxyl groups (on the basal plane of the lattice), retains a similar structure, but holds arrays of identical reactive groups that facilitate the surface functionalization.[189] Despite the high practical value[190] of TRGO, only a few literature entries utilized these unique size and chemical characteristics for electronic, optical or sensor applications, and to conjugate multivalent carbohydrates and to implement the regulation of cell mobility.[191, 192] There are multiple possibilities for surface modification of reduced graphene oxide sheets, but functionalization with CDs has gained significant importance in recent years resulting in water-dispersion materials (*See* Chapter 1, section 1.4.1.2).[193]

2.1.1.2 Cyclodextrin

CDs have a hydrophilic exterior and a hydrophobic central cavity that enables them to form non-covalent inclusion complexes by entrapping the guest molecules into their central

cavities (*See* Chapter 1, section 1.4.1.1).[69] The enlarged sizes of the CDs greatly increases the range of guests that can be included inside the cyclodextrin cavities with efficient binding affinities with vast applications.[70] Supramolecular systems based on CDs have been explored extensively. The ability of CDs to form host-guest inclusion complexes, together with selective functionalization, led to many applications for drug delivery and chemical sensing.

Exploring larger multivalent glycoconjugate scaffolds that possess appropriate dimensions towards biological pathogens is strongly demanded. Considerable effort has been devoted to construct synthetic multivalent glycoconjugates with diverse spatial arrangement of ligands, which ideally can be used to interfere with the pathogen adhesion process and serve as antibacterial or antiviral agents.

2.1.2 Strategy

Towards this direction, a versatile platform for constructing a multivalent carbohydrate-functionalized 2D scaffold was developed by placing cyclodextrin-based sugar ligands on adamantyl-functionalized TRGO sheets (AG4) (Fig. 15). Owing to the adamantyl groups on the surface of AG4, the inclusion complex of β-cyclodextrin (β-CD) and adamantyl units reversibly connects the reduced graphene sheet and heptamannosylated β-CD (ManCD) in aqueous medium. The resulting supramolecular carbohydrate-functionalized TRGO derivative (ManCD@AG4) can agglutinate *E. coli*, and the agglutination ability of the 2D sheets is much higher than the parent water-soluble macrocyclic host (ManCD) or the TRGO itself. Taking advantage of the responsive property of the supramolecular interaction, the captured bacteria can be partially released upon addition of a competitive guest. Moreover, because of their unusual infrared absorption properties, these TRGO derivatives exhibit excellent bacteriostatic properties (99% elimination) following near-infrared (NIR) laser irradiation of the graphene-sugar- *E.coli* complexes.

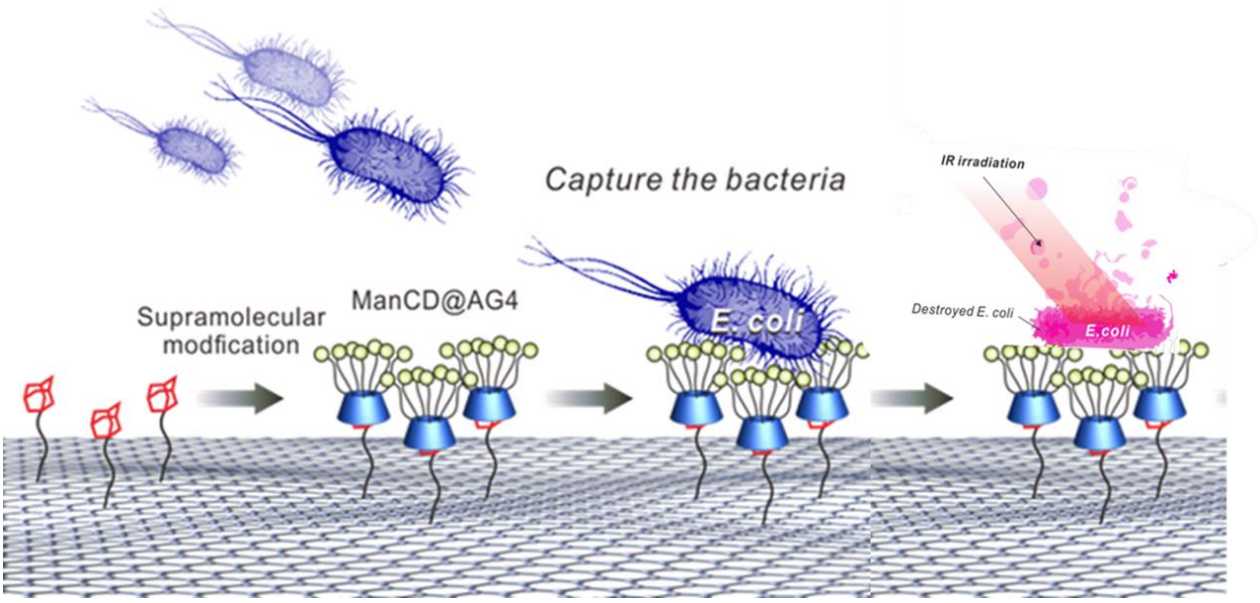

Figure 15: Schematic representation of bioactive graphene self-assembly for sensing *E. coli* bacteria using host-guest method.

2.2 Results

2.2.1 Synthesis of cyclodextrin functionalized with mannose-host moiety

The synthesis of the mannose substituted β-cyclodextrin **42** was started with known peracetylated mannose **34** (Scheme 5), glycosylated with bromoethanol in the presence of $BF_3.OEt_2$ yield **35**. Then **35** was converted to thiocyanate–mannose derivative **36** using KSCN. The thiocyanate **36** was reduced by Zn–AcOH to the corresponding thiol **37**. Cyclodextrin substrate **40** was synthesized from commercially available **38**. CD was iodinated using triphenylphosphine yields **39** which after peracetylation yields **40**. Then 6-hepta iodinated β-cyclodextrin **40** reacted with **37** in the presence of Cs_2CO_3 to yield mannose-substituted β-cyclodextrin **41**, which was finally treated with base yielding compound **42,** as previously reported.[81, 194] Mannosylated-cyclodextrin (ManCD) equipped with seven mannosyl groups at the upper rim of the cavity provided sufficient sugar density and was used for the attachment on the adamantylated TRGO surface.

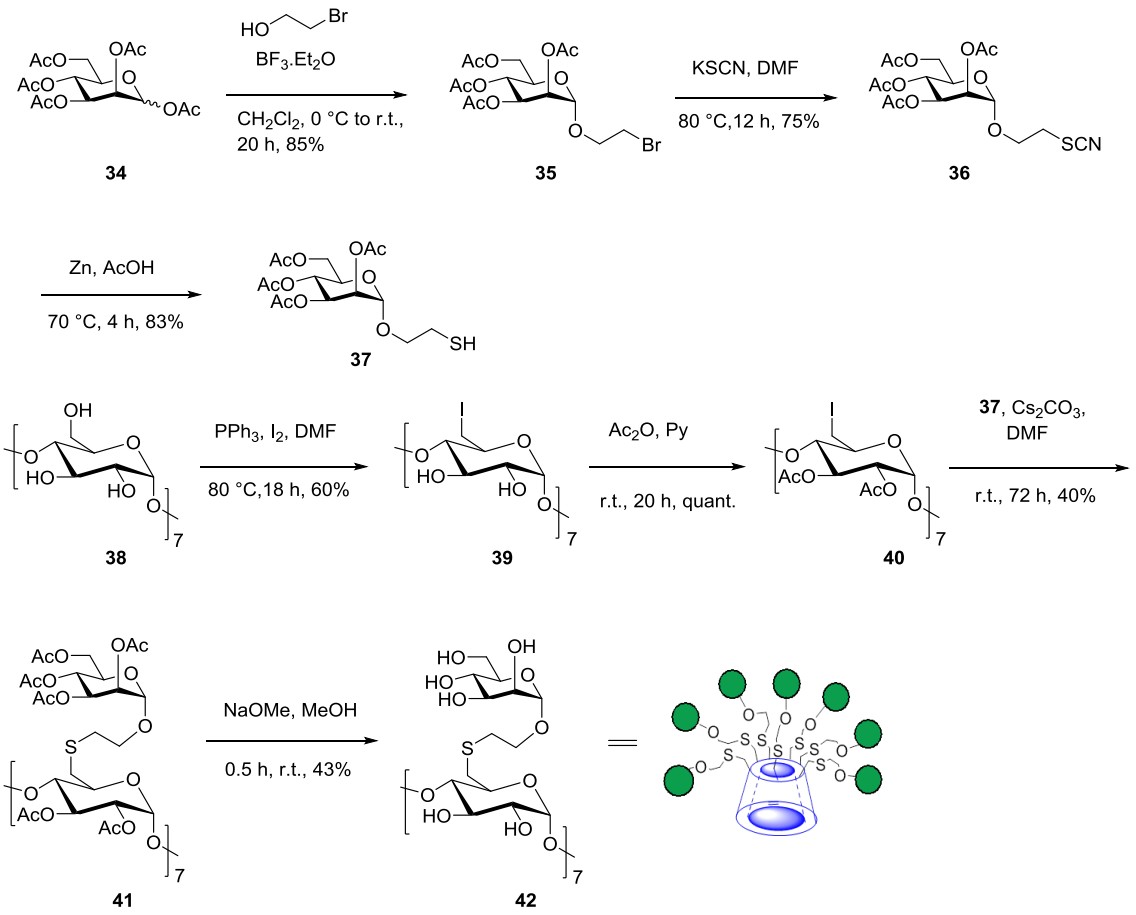

Scheme 5: Synthesis of heptamannosylated β-cyclodextrin **42**, = Man, β-CD is represented in blue color.

2.2.2 Synthesis of TRGO and adamantyl-functionalized TRGO sheets-guest moiety

The synthesis of TRGO was carried out by oxidation of graphite using known Hummers and Hoffmann method[195], followed by thermal reduction at 400 °C or 750 °C to produce TRGO400 (**46**) and TRGO750 (**47**) respectively. The degrees of adamantyl moieties covalently attached on the TRGO are readily tuned by using different TRGOs. In order to determine exactly the number of adamantyl groups that append the TRGO sheet, an elemental analysis was performed. TRGO reduced at 400 °C resulted in a higher density of adamantyl units- one adamantyl group for each of the 27 aromatic rings according to elemental analysis (Fig. 17c). The elemental analysis data shows that TRGO400 provides higher densities of hydroxyl group on the carbon surface (1.2 mol/kg), while the hydroxyl

group density in TRGO750 was lower (0.44 mol/kg). Therefore, TRGO400 were used further for the synthesis of the supramolecular scaffold.[1]

The synthesis of the adamantyl-functionalized TRGO sheets (AG4) **48** started with the reaction of 1-adamantyl isocyanate **43** and 2,2'-(ethylenedioxy)bis(ethylamine) in chloroform yielding **44**, which further reacted with di-*tert*-butyl tricarbonate[196] to give the corresponding isocyanate **45** (Scheme 6). In order to provide sufficient flexibility and better solvation to the newly formed host-guest complex, the (ethylenedioxy)bis(ethylamine)-based linker was chosen. The resulting isocyanate **45** was covalently attached to the hydroxyl groups present on **46** using catalytic amount of zirconium (IV) acetylacetonate in chloroform yielding **48**.

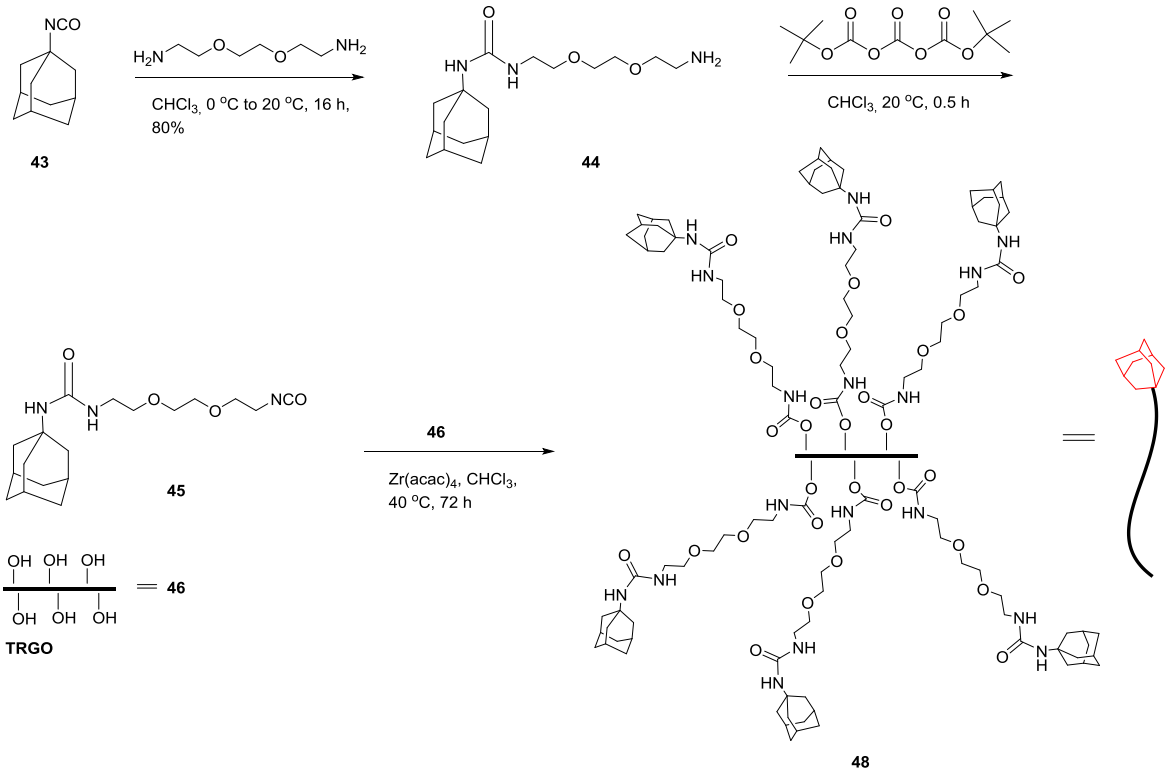

Scheme 6: Synthesis of **48**. Adamantly linker moiety represented in red color.

The dispersion of the AG4 complex has been tested using different solvents (e.g. water, chloroform, and dimethylformamide). The TRGO400 precipitates after 24 h, while AG4

[1] Synthesis and analysis of compound 48 and 49 was carried out by Benjamin Ziem and Dr. Zhenhui Qi, from Prof. Dr. Rainer Haag group (Department of Chemistry, Free University Berlin, Germany).

readily forms stable colloidal dispersions in chloroform and DMF (Fig. 16). The improved solubility of AG4 in organic solvent can be ascribed to the surface functionalization, which also correlates to the previous reported cases of functionalized TRGO systems.[197]

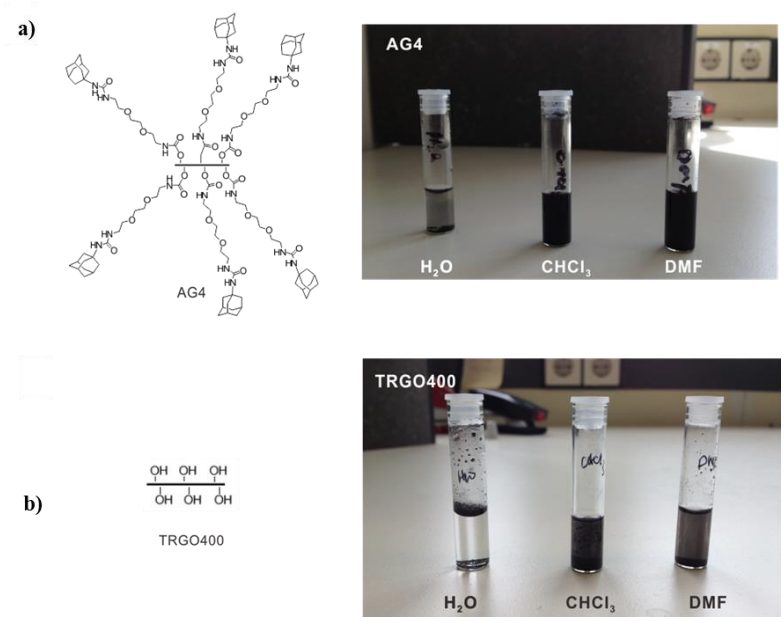

Figure 16: Solubility test: a) AG4 and b) TRGO400 dispersions in Milli-Q water, chloroform, and DMF (1 mg/mL), 24 h after ultrasonication for 10 min.

2.2.3 Physicochemical characterization of AG4

The synthesized material AG4 was characterized by FT-IR and Raman spectroscopy (Fig. 17a, b). The characteristic peaks at 1732 cm^{-1} confirms the presence of C=O group formed due to urethane linkage and the peaks at 2918 and 2850 cm^{-1} confirms the $–CH_2$ stretch of ethylenedioxy groups of TRGO surface (Fig. 17a). The Raman spectrum of AG4 displays two strong peaks at 1600 cm^{-1} and at 1350 cm^{-1}, corresponding to the G and D-bands, respectively. The G bands are related to the in-plane vibration of sp2 carbon atoms in a 2D hexagonal lattice, while D bands for the vibrations of sp3 carbon atoms of disordered graphite. The ratio of ID/IG indicates the degree of defects on the graphene sheet (Fig. 17b). The chemical composition and thermal stability and decomposition of the AG4 were determined by elemental and thermogravimetric (TGA) analysis, respectively. According to the carbon-to-nitrogen atomic ratio, the approximate functionalization degree of surface with

[2]adamantyl groups can be estimated. Approximately 55 graphene carbons per one incorporated carbamate ester unit in AG4 were calculated, which means 27 aromatic rings are surrounding one adamantyl group (Fig. 17c). The TGA curves of TRGO400 and AG4 reveal 2% and 10.2% weight loss respectively, at the temperature of 410 °C as the compound **44** undergoes most of weight loss below 410 °C (Fig. 17d). Accordingly, the amount of decorated adamantyl chains on the TRGO400 was calculated to be 8.2%. This value nicely correlates to the one obtained from elemental analysis (10%).[198]

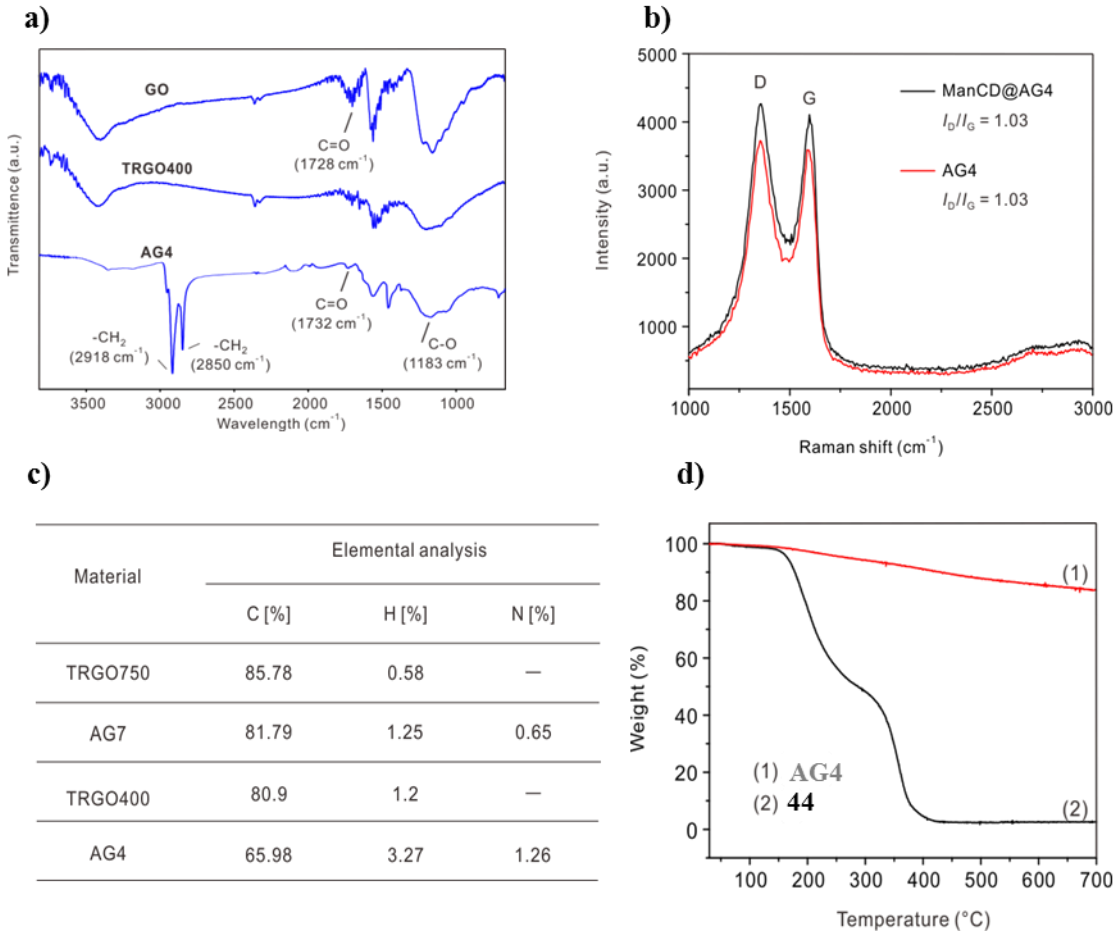

Material	Elemental analysis		
	C [%]	H [%]	N [%]
TRGO750	85.78	0.58	—
AG7	81.79	1.25	0.65
TRGO400	80.9	1.2	—
AG4	65.98	3.27	1.26

Figure 17: (a) IR spectra of GO, TRGO400, AG4- In the spectrum of AG4, the characteristic peak at 1732 cm^{-1}, 2918 and 2850 cm^{-1} are observed which are attributed to the C=O stretching of urethanes. The intensity of the peaks is associated to the -CH_2 stretching vibration. (b) Raman spectra and I_D/I_G ratio of AG4. (c)

[22] Raman spectroscopy was carried out by Benjamin Hatting (Institute of Experimental Physics, Free University Berlin, Germany).

Elemental analysis of AG4-The successful formation of the[3] carbamate esters via the reaction of the isocyanate with the surface hydroxyls can be evidenced by the increased content of nitrogen. (d) Thermogravimetric analysis of AG4 and compound **44**.

The morphological evaluation of AG4 was performed using atomic force microscopy (AFM) (Fig. 18). Well dispersed paper-like carbon sheets were observed, with size ranging from hundred nanometers (nm) to several micrometers (µm). It should be noted that in the bulk of well-dispersed AG4 sheets, many small dots can be detected on the carbon surface (indicated by yellow inverted triangle-▼). The height of these dots is observed around 2-3 nm, which could be ascribed to the adamantyl chains attached on the surface.

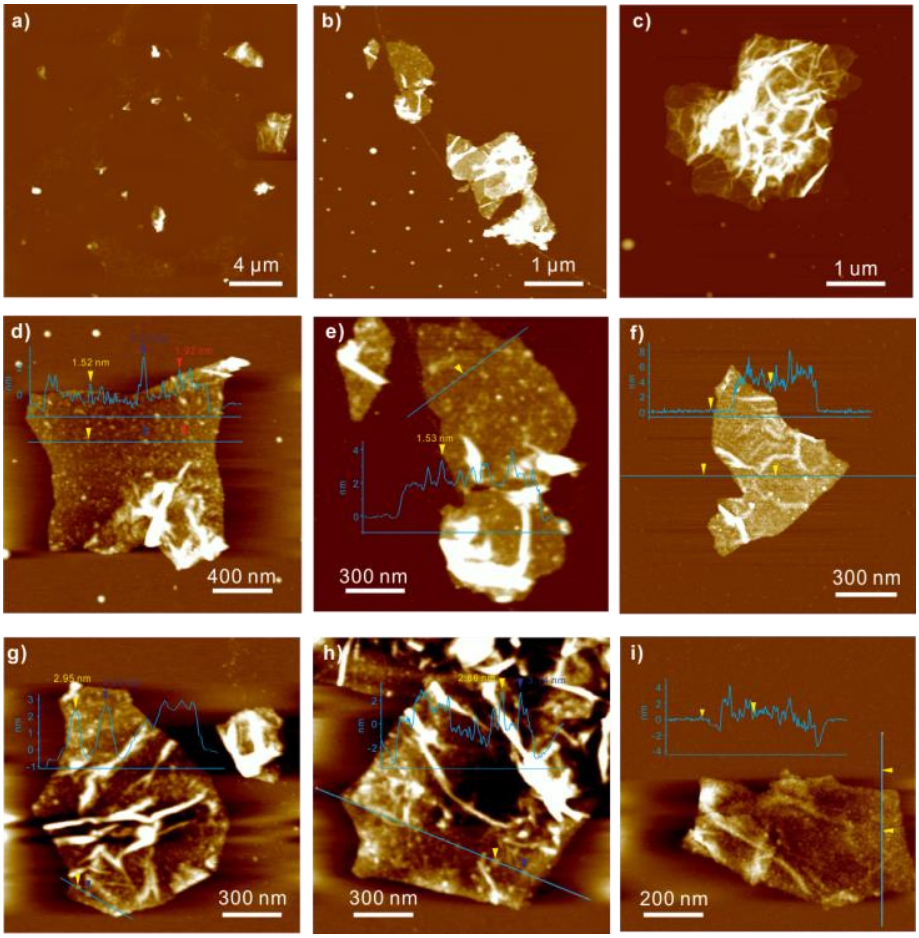

Figure 18: AFM images of AG4 at different magnifications. In order to evaluate the morphology features and height profiles of AG4 carbon sheets, several areas were randomly picked up for analysis. The

[3]AFM imaging was carried out Andrea Schulz, (Research Center for Electron Microscopy and Core Facility BioSupraMol, Free University Berlin, Germany).

functionalization [4]of adamantyl chain increase the dispersion of AG4, since many paper-like carbon sheets (d-i) can be easily observed, with diverse sizes ranging from hundreds nanometers to several micrometer while some severe aggregated sheets remain observed (c) (the error bar of height profile is ±1 nm).

Synthesized AG4 was collected at different speed of centrifugation and the morphological evaluation was carried out using transmission electron microscopy (TEM). Similar results were obtained as found in AFM studies, confirming paper like carbon surface of AG4 (Fig. 19).

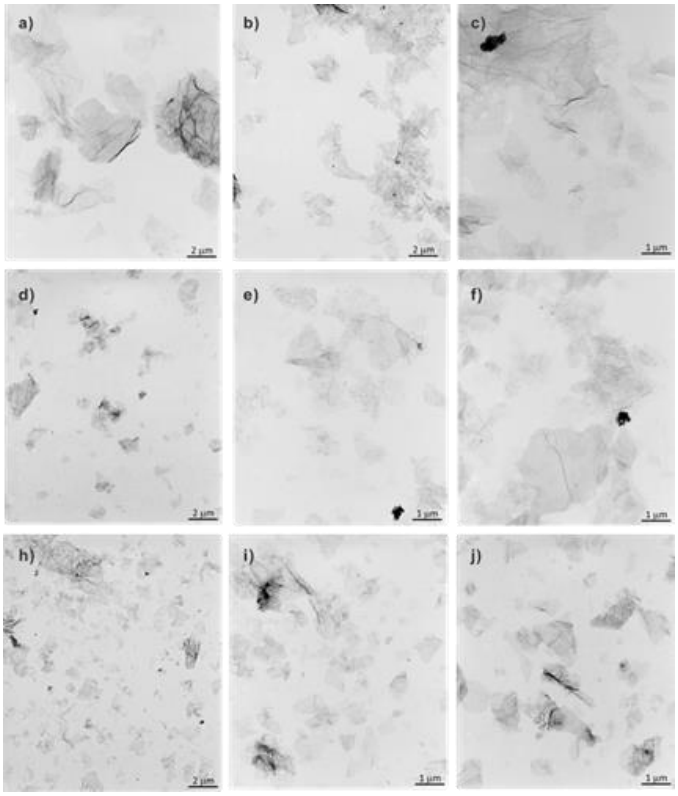

Figure 19: TEM images of sample AG4 collected by different speed of centrifugation: (a-c) the precipitated portion collected at the centrifugation cut-off of (a-c) 2000 rpm, (d-f) 4000 rpm and (h-j) 6000 rpm.

2.2.4 Assembly of the supramolecular ManCD@AG4 (49) derivative and its characterization

Supramolecular functionalization is widely recognized as a convenient strategy for constructing various glycodendrimers which are used to detect the binding events and to

[4] TEM imaging was carried out by Dr. Christoph Böttcher, (Research Center for Electron Microscopy and Core Facility BioSupraMol, Free University Berlin, Germany).

explore the aspects of fundamental multivalent CPIs.[81, 199-201] The synthesis of ManCD@AG4 **49** was carried out by mixing the guest molecule AG4 and the host ManCD in DMF as co-solvent and was subsequently transferred into water (Fig. 20a). After centrifugation at 12,000 rpm (twice), the sediment could be readily dispersed in water with considerable stability (0.83 mg/mL AG4). Under identical conditions, AG4 precipitated during the dispersion in water. The improved solubility implied the formation of host–guest complexes that had been retained at the interface due to the high binding constant (K_a) between the adamantyl and the β-CD moiety ($K_a \sim 10^5$ M^{-1}).[202] The use of ManCD increases further the water solubility of ManCD@AG4 complex resulting in homogenous complex formation as compared to limited solubility of β-CD@AG4 (**50**) (Fig. 20b, c).

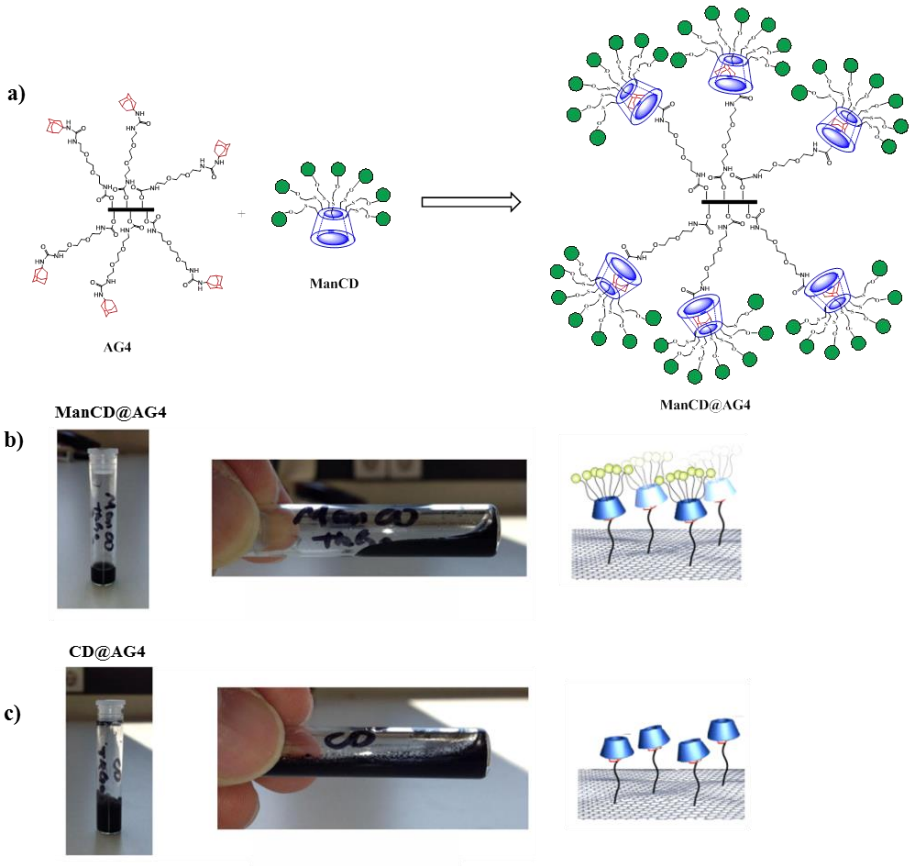

Figure 20: a) Schematic representation of host-guest self-assembly. Solubility test of ManCD@AG4 and CD@AG4: Photographs of b) ManCD@AG4 and c) CD@AG4 dispersed in Milli-Q water.

The surface morphology of scaffold ManCD@AG4 was further investigated using AFM. The AG4 height bearing the adamantyl groups was approximately 2-3 nm, where insertion

of host molecule ManCD, resulted in an increase in height of the ManCD@AG4 complex to 4-5 nm (Fig. 21a-i). Computer modeling studies also revealed that the height of ManCD was approximately 1.2 nm in support to obtained AFM data (Fig. 21j, k). Also the ratio of ID/IG for ManCD@AG4 found the same from the Raman spectra as for AG4 (Fig. 17b) even after the complexation.

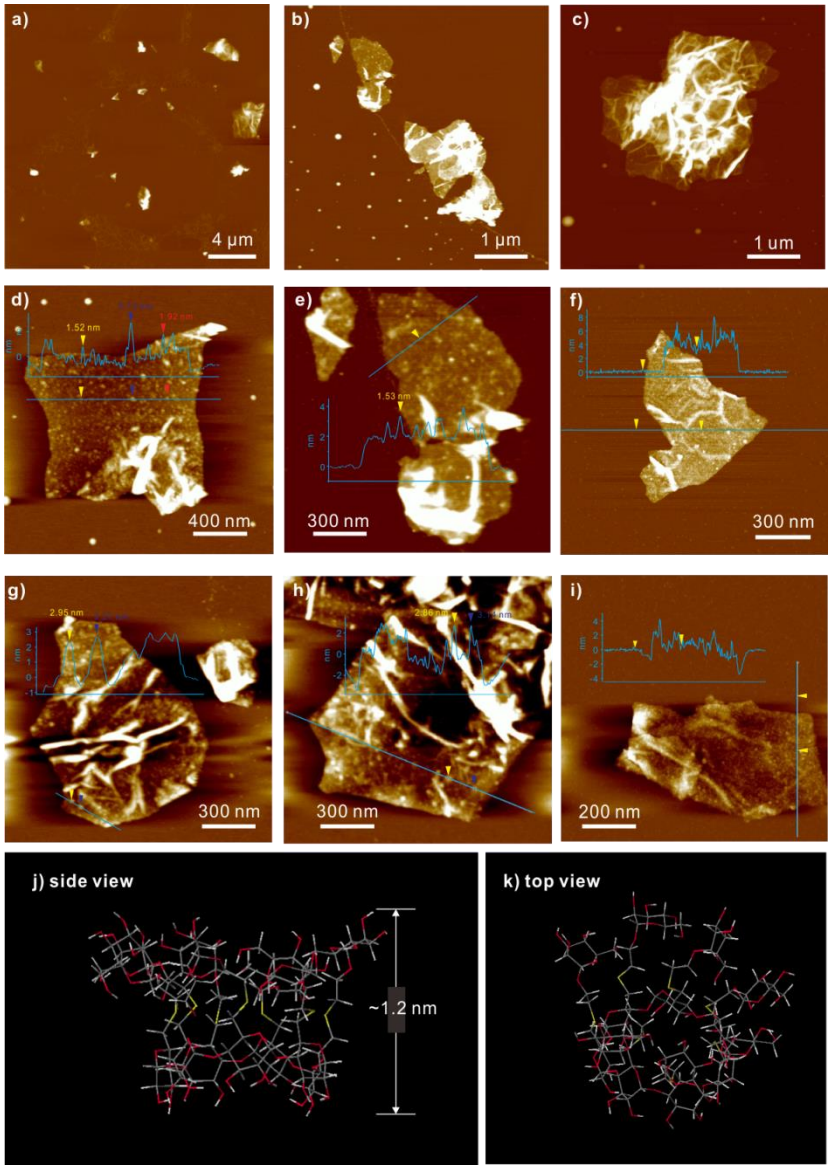

Figure 21: AFM height images (a-i) of sample ManCD@AG4 prepared by spin-coating of solution. Based on AFM data, the height of ManCD@AG4 is in the range of 4 – 5 nm. In comparison with the height of AG4 and ManCD@AG4, the increased height is around 1 nm, which is in agreement with the calculated height of ManCD (j-k) calculated by CaChe program at the AM1 MOZYME level of theory.

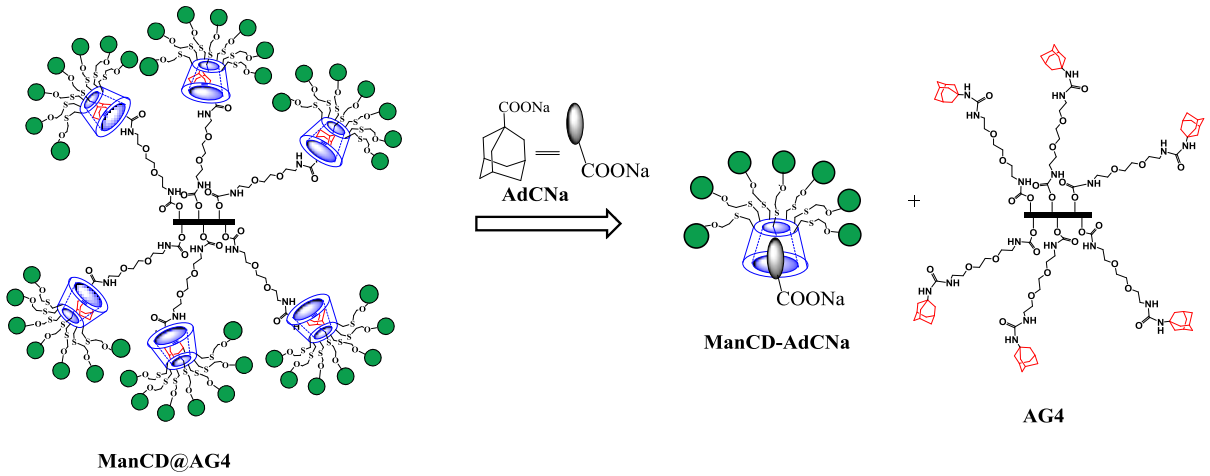

Figure 22: Schematic representation of dissociation of ManCD@AG4 upon addition of AdCNa.

Effective dissociation of ManCD@AG4 host-guest complex was achieved by addition of a competitive guest such as AdCNa to the solution that leads to the disruption of inclusion complex. As described, the host-guest inclusion complexation between ManCD and AG4 enabled the binary system to dissolve in water giving self-assembled ManCD@AG4 scaffold. The addition of competitive guest AdCNa to the self-assembled ManCD@AG4 scaffold precipitated the AG4 by complexing with ManCD groups (ManCD-AdCNa) (Fig. 22). For each batch of ManCD@AG4 scaffold, the carbohydrate loading efficiency was approx. 16% and the final concentration of ManCD in the system was determined to be 98.1 µM as determined by sugar quantification (Experimental Fig. 37).

2.2.5 Characterization of carbohydrate-lectin binding study of ManCD@AG4 using microscopic techniques

The developed multivalent 2D ManCD@AG4 scaffold was studied for its ability to bind mannose-specific *E. coli* adhesin FimH of type 1 pili. Type 1 pili are filamentous proteinaceous appendages that extend from the surface of many gram-negative organisms.[203] Two stains of *E .coli* were used; ORN 178 expressing FimH that specifically binds to mannose residues and ORN 208 which is unable to bind mannose due to a mutation in the fimH gene.[81] Multivalent binding of mannose residues in nanostructures with FimH in *E. coli* ORN178 resulted in agglutination and/or inhibition of motility of the bacteria.[204] Initially, the *E. coli* agglutination assay was carried out with Man@AG4 scaffold and the

aggregates was characterized using TEM microscopy (Fig. 23d). In disparity to previous 0D[181, 182] and 1D[184] scaffolds that induced agglutination, synthesized Man@AG4 scaffold resulted in wrapping the *E. coli* due to its 2D surface.

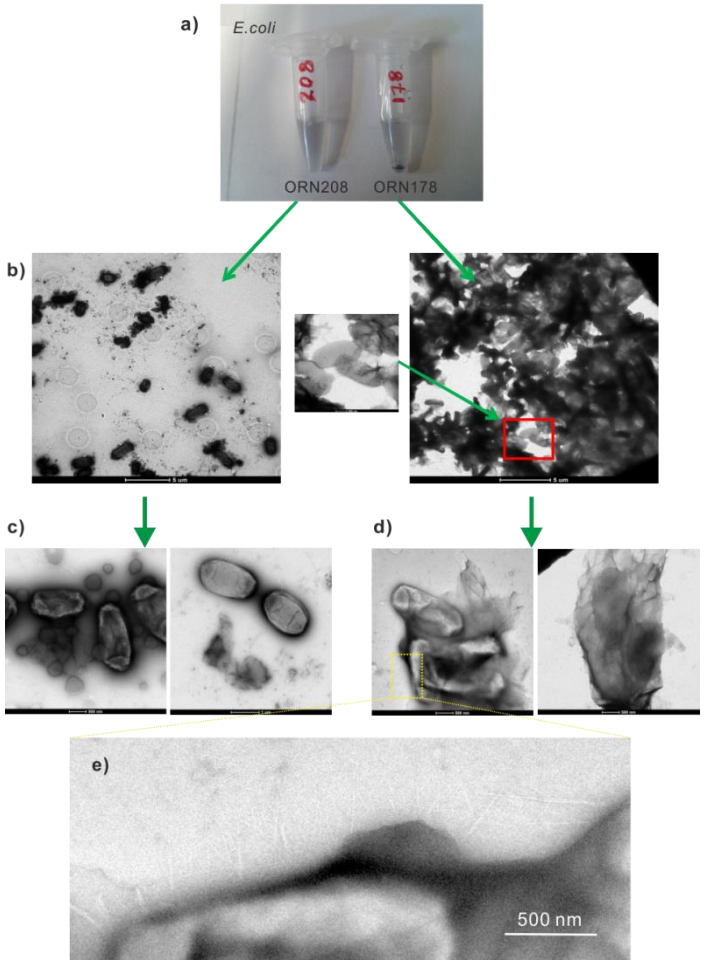

Figure 23 : (a) Visible aggregate formation after 1 h incubation of ORN208 and ORN178 with ManCD-TRGO400 at room temperature. (b) Overview TEM image at 5 µm of ORN208 and ORN178 with ManCD-TRGO400. (c) Higher magnified images at 500 nm and 1 µm of ORN208 and ORN178 with ManCD-TRGO400 respectively. (d) ORN178 with ManCD-TRGO400 respectively. (e) Enlarged domain for TEM image in d).

The TEM images clearly show that ManCD@AG4 binds the *E. coli* ORN178 strain (Fig. 24c). Several rod-shaped bacteria were tightly wrapped by these sheet-like scaffolds, which indicated strong, multivalent binding. The visible shape of the pili at the external shell of the

aggregates (Fig. 24e) provided evidence that the entrapped objects were bacteria. Also, a tilt series were recorded under low-dose conditions collecting images between −4° and +4° tilt increments having difference of 8° between two stereogenic images (Supplementary Fig.18). This finding is consistent with the surface morphology observed in a single *E. coli* (Fig. 24b) as well as with the localization pattern of FimH protein along type 1 pili.[205]

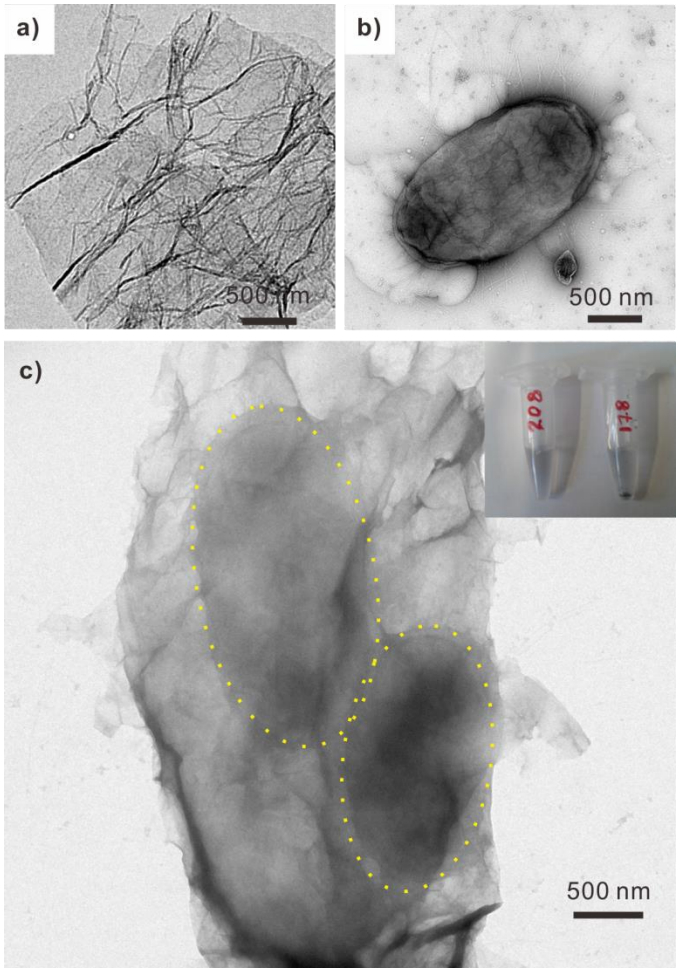

Figure 24: TEM images of the supramolecular carbohydrate-functionalized graphene derivative for bacterial capture: (a) ManCD-AG4 scaffold, (b) ORN178 *E. coli*, and (c) *E. coli* agglutination incubated with ManCD@AG4. The dashed yellow circles outline the captured bacteria. The inserted figure shows the different responses of the ManCD@AG4s after respectively adding *E. coli* strain ORN208 and *E. coli* strain ORN178. The photographs were taken an hour after incubation at room temperature. No staining agent was used in figure 24a and for figures10b-c 1% uranyl acetate solution was used as staining agent.

The specificity of the interaction and binding capacity of scaffold ManCD@AG4 was assessed with the mannose binding FimH receptor on the bacterial surface. In contrast to

ORN178, the ORN208 strain expressed abnormal type 1 pili that do not bind D-mannose. Both strains were stained by fluorescein isothiocyanate (FITC) to monitor cell agglutination by fluorescence confocal microscopy (CLSM). Incubated mixtures of ManCD@AG4 and ORN178 produced a strongly fluorescent cluster where the bacteria were bound (Fig. 25), whereas no apparent binding of ManCD@AG4 to ORN208 was detected (Fig. 25b). Due to the large interference contrast between graphene sheets and bacteria, the location of ManCD@AG4 in the cluster could be easily distinguished in the merged form of CLSM images. The merged form combines the fluorescent image and transmitted light image by software processing. The black species (assigned to ManCD@AG4) existed randomly within the agglutinated area of bacteria shown in the insert of (Fig. 25a), which indicates the agglutination of bacterial cells was due to the bilateral interaction. The macroscopic observation further supported the CLSM data that the precipitation of graphene sheets only occurred in the case of ManCD@AG4 and ORN178 (Fig. 23a), which was absent with ORN208. Agglutination experiments on a β-CD-functionalized TRGO sheet (CD@TRGO) served as a control to assign the contribution of mannose to the scaffold. Neither ORN178 nor ORN208 (Fig. 25a-d) strains aggregated in this case. Based on the TEM and CLSM, it is concluded that ManCD@AG4 selectively bound to the bacterial surface via mannose-FimH receptor interactions and that the heptamannosylated moiety played a determining role for binding and selectivity.

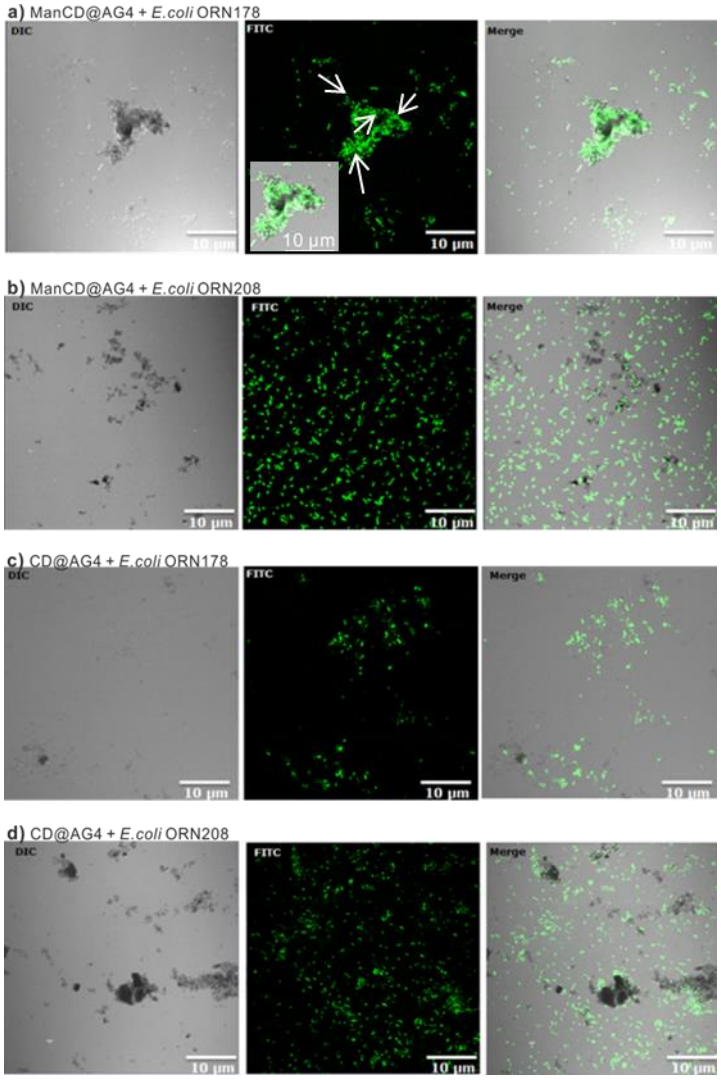

Figure 25: Confocal laser scanning microscopy images of ManCD@AG4 incubated with (a) *E. coli* strain ORN178, (b) ORN208 and incubation of CD@AG4 with (c) ORN178 and (d) ORN208, respectively. The insert in figure (a) is a software-processed merged image combining figure 11a and its transmitted light form. The location of ManCD@AG4 in the agglutination of bacteria can be easily visualized in the insert. The white arrows in figure (a) show the graphene sheet's position according to merged image.

Following as established protocol,[174, 175] the average number of *E. coli* cells was calculated contacting each other based on CLSM images as the agglutination index (A.I.) in which, the capture efficiency was quantified and the ability of ManCD@AG4, CD@AG4 and the macrocyclic host ManCD to agglutinate bacterial cells was evaluated (Fig. 26). The A.I. value of ManCD towards ORN178 at 117 was much higher than for ORN208 without mannose binding sites (14), as well as for CD@AG4 with ORN178 (18) and ORN208 (16).

Without the assistance of the graphene scaffold, the mannosyl-functionalized macrocycle ManCD only slightly induced agglutination (17), which clearly reflected the benefit of the 2D large flexible carbon surface for capturing pathogenic cells.

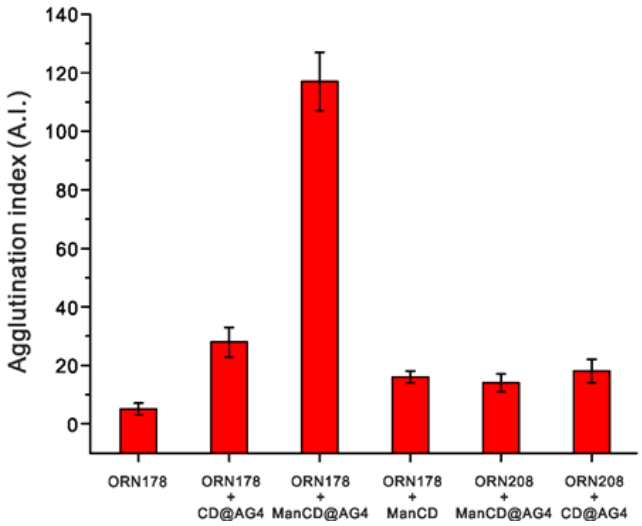

Figure 26: Agglutination ability of ManCD@AG4, CD@AG4 and ManCD with *E. coli* strain ORN178 and ORN208 respectively. The agglutination index values were determined by confocal microscopy images. Due to the insolubility of AG4 in aqueous medium, it was not included in the comparison.

Multivalent binding and the responsive release of captured bacteria by scaffold ManCD@AG4 towards *E. coli* were determined using a competition experiment: FITC-stained ORN178 *E. coli* was co-incubated with varying concentrations of the monovalent binder: methyl α-D-mannopyranoside (Me-Man) and ManCD@AG4. The competitive assay was further evaluated by a fluorescence read-out after reaching the equilibrium. Free methyl α-D-mannopyranoside at concentrations up to 2000 times of ManCD@AG4 concentration had little effect on the agglutination of ManCD@AG4 to bacteria: ~20% of captured bacteria were released. However, the competitive release of captured *E. coli* from ManCD@AG4 was induced by addition of sodium adamantane carboxylate (AdCNa) (Fig. 27). Monovalent binding between cyclodextrin and the adamantyl unit, the addition of excess AdCNa to the system was more likely to result in ~50% release of the captured *E. coli*. The competition assay clearly showed that multivalent ManCD@AG4 bound FimH at least 2000-fold better than monovalent mannose.

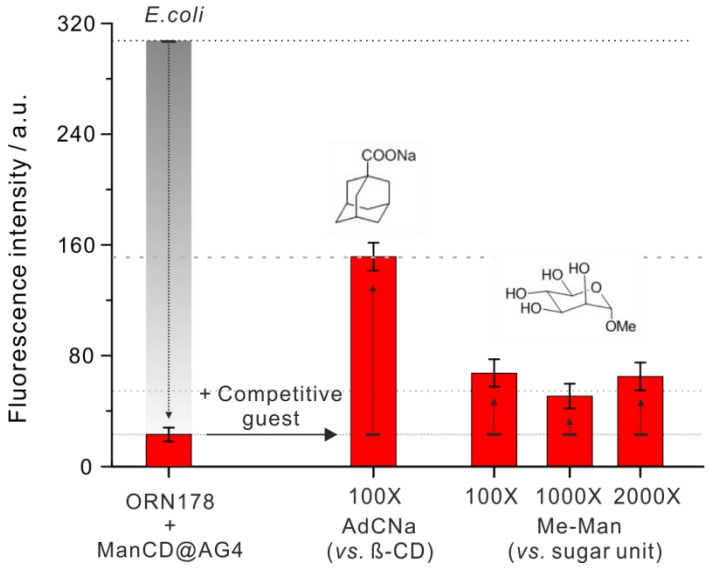

Figure 27: Release effect of the captured *E. coli* strain ORN178 upon addition of a competitive guest. The top dashed-line is the original fluorescence intensity of *E. coli* before adding the competitive guest.

Considering the potential infrared-absorption properties of TRGO[206], the scaffold was utilized to selectively destroy the captured bacteria via a photothermal effect. The captured *E. coli* in ManCD@AG4 (AG4 in 0.83 mg mL^{-1}, incubated for 1 h) were irradiated in the NIR (785 nm) range and 0.5 W cm^{-2} for 10 min (Fig. 28a). During irradiation, the sample temperature gradually increased to 70.9±1.4°C (Fig. 28b, c).

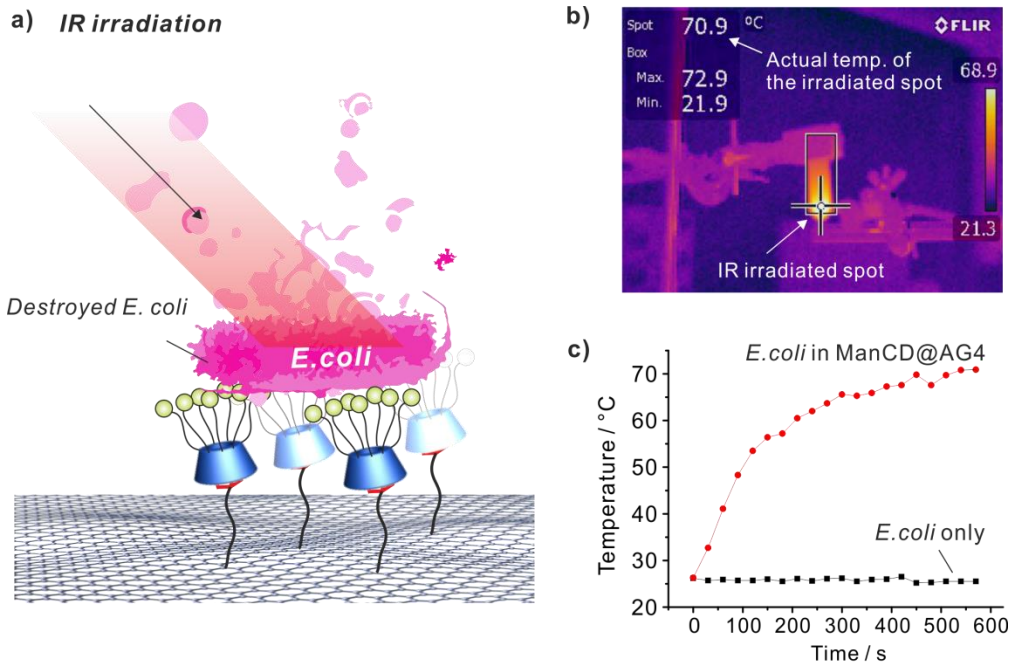

Figure 28: (a) Schematic illustration of ManCD@AG4 under NIR irradiation causing the death of captured *E. coli*. (b) Thermal image of an *E. coli* sample incubated with ManCD@AG4 under NIR laser irradiation (0.5 W/cm^2). After 10 min, the temperature of irradiated spot reached 70.9±1.4°C. (c) Temperature evolution profiles of the *E. coli* samples with and without ManCD@AG4, respectively.

After irradiation, the bacteria were spread on the agar plates to characterize the cell viability: The abundance of *E. coli* colonies on the agar plate indicated the amount of living cells. After irradiation, the agar plate contained almost no living bacteria (Fig. 29b). In a parallel experiment without IR treatment, living bacteria could be seen in large bacterial colonies (Fig. 29a).

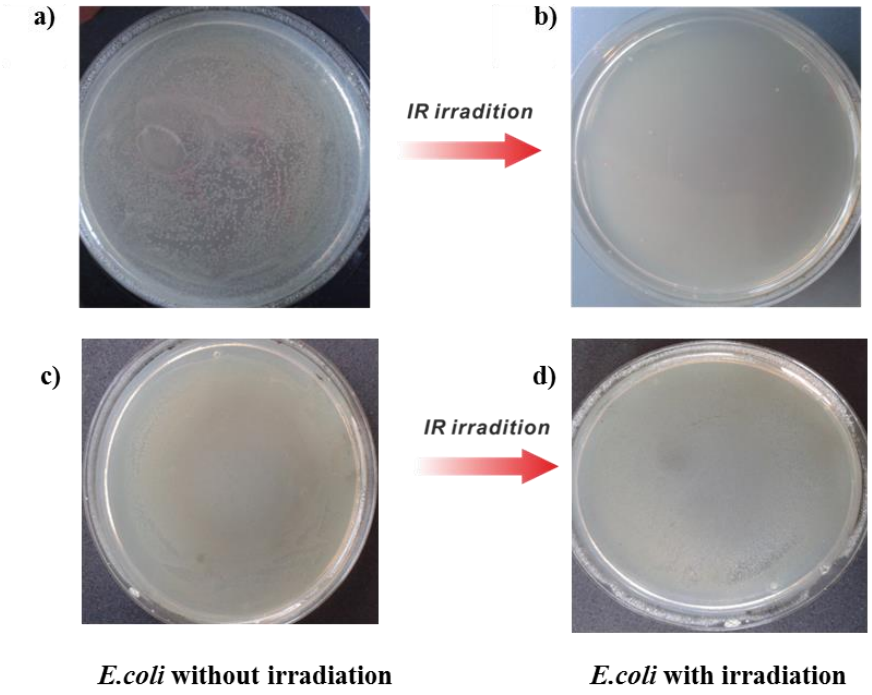

Figure 29: Images of *E. coli* colonies captured by ManCD@AG4; (a), and (b) and with control compound CD@AG4; (c) and (e) on agar plate.

According to the World Health Organization (WHO),[207] *E. coli* bacteria can be destroyed by thoroughly cooking foods until all parts reach a temperature of 70 °C or higher. Neither ManCD nor *E. coli* can expose enough IR absorption to elevate the surrounding temperature (both aqueous solution of ManCD and *E. coli* have no absorption at 785 nm). Therefore, the bacterial killing effect here can be ascribed to the unusual IR-absorption mechanism of TRGO, which leads to generate high temperature to disinfect the *E. coli*. In a diluted sample, the bacteriostatic efficiency was determined at > 99% (Supplementary Fig. 35 and 36).

2.3 Conclusion and Outlook

Novel, multivalent sugar-functionalized graphene sheets that selectively bind and kill *E. coli* were designed. A host-guest inclusion complexation between heptamannosylated β-cyclodextrin and adamantyl attached to the graphene sheets helped to enhance water solubility of carbon sheets. In this way, the synthesized cyclodextrin-graphene conjugates were optimized by performing bacterial binding assays which were characterized by

microscopic techniques (i.e. CLSM, TEM, and AFM). The addition of carbohydrate via a supramolecular binding afforded the carbon materials to agglutinate *E. coli* bacteria. The multivalent interactions were responsible for cell agglutination. The agglutination ability of graphene-based 2D sheets greatly exceeded those of pure ManCD due to a large interphase with the *E. coli* bacteria. The supramolecular linkage at the interface of graphene allowed for the controlled release of the captured bacteria through the addition of a competitive guest, such as AdCNa. Considering a number of sugar-modified cyclodextrins are available,[208] this system can be further extended to endow the graphene surface with more different functionalities which can be directly applied in the design of molecular and macromolecular biosensors. The unique thermal IR-absorption properties of TRGO enable targeted bacterial killing upon IR-laser irradiation. The integration of multivalent, supramolecular binding on graphene also provides a new strategy for the design of functional materials for filtration in healthcare and environmental protection.

2.4 Supplementary Figures

S1 AFM images of adamantyl-functionalized TRGO750 sheets (AG7)

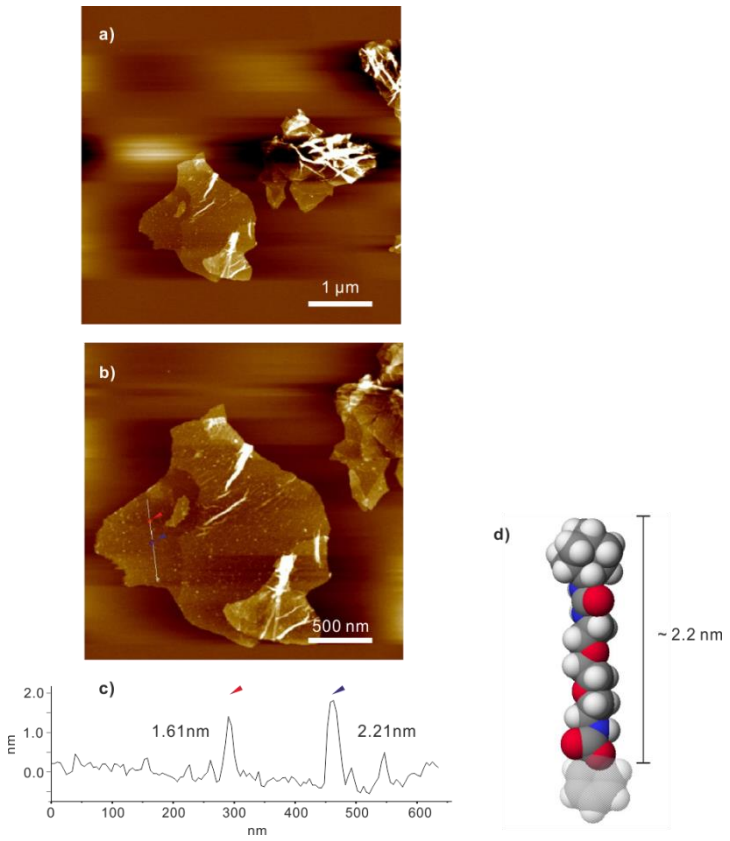

Figure 30: AFM images of AG7 prepared at different magnification.

It is much easier to find the paper-like flat carbon sheets as shown in (Fig. **18)**. Due to the fewer number of hydroxyl groups on the graphene surface; the AG7 carbon sheets have fewer defects (more sp^2 carbon) and less distortion. Accordingly, the morphology of AG7 is more flat than that of AG4. The reduced roughness of surface leads to the higher resolution of the height profiles. The derivation of surface background is less than 1 nm (± 0.5 nm). Again, many small dots were also detected on the surface of AG7. The height of these dots is determined to be ~2 nm (e.g. 1.6 nm – 2.2 nm), which is in consistent with the calculated length of fully stretched adamantyl-(ethylenedioxy)bis(ethylamine)-based linker (~2.2 nm,

calculated by CaChe program at the AM1 MOZYME level of theory, Fig. 30d). This result further confirms the small dots observed in Figure **18** are these adamantyl-linkers.

S2 Surface characterization of *ManCD@AG4* by TEM

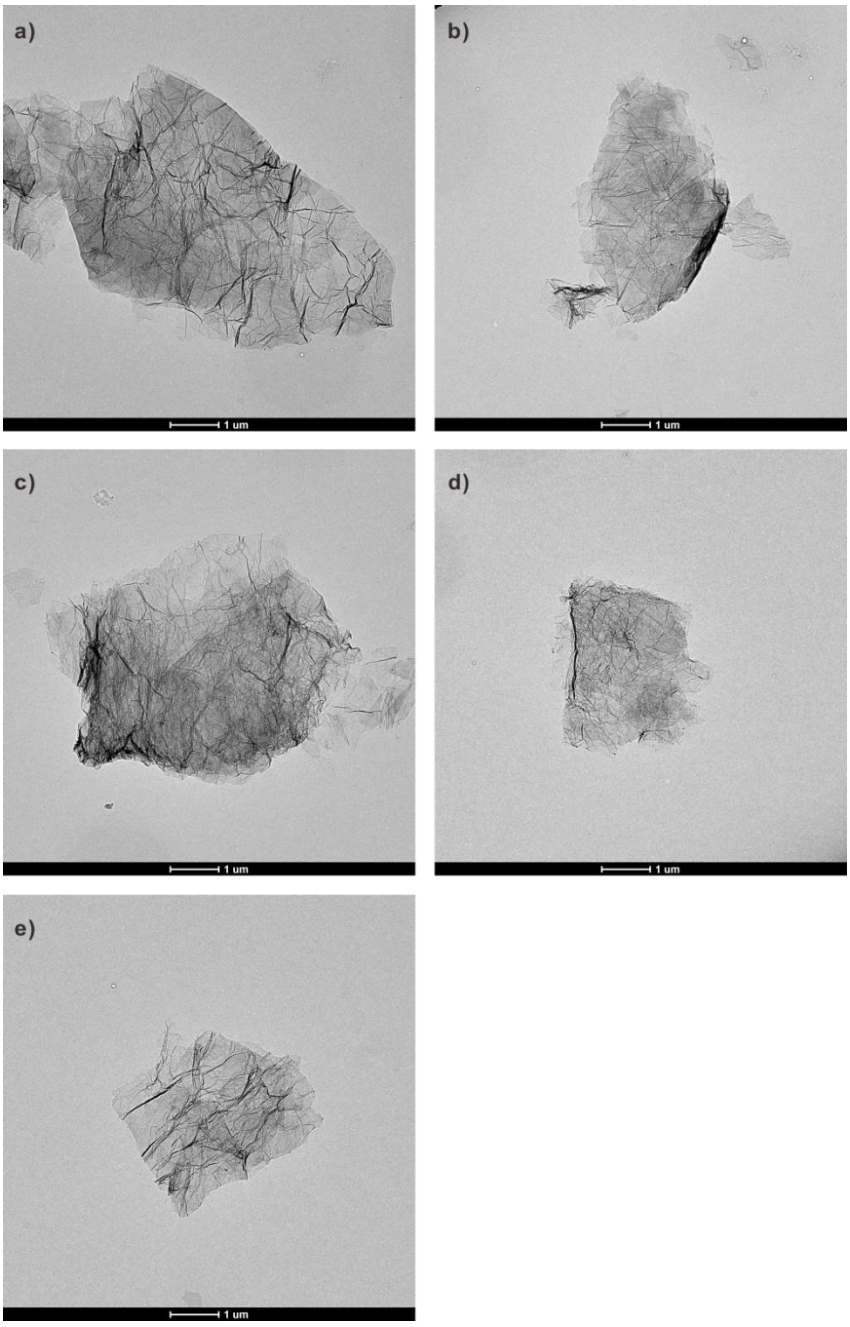

Figure 31: Morphology investigation of ManCD@AG4 by TEM.

S3 Demonstration of dissociation of ManCD@AG4 complex

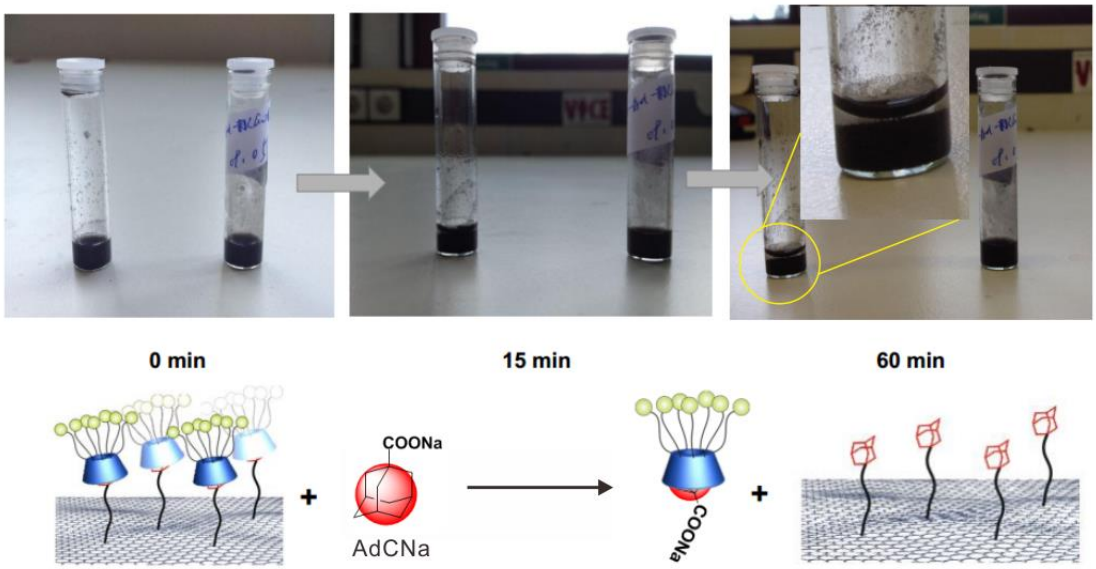

Figure 32: Control experiment demonstrating the complexation. Upon the addition of a large excess of competitive guest AdCNa (100 eq.), the ManCD is occupied by the AdCNa, and thus expelled from the AG4 surface. As expected, the dissociation of ManCD@AG4 results in the precipitation of AG4 in water. This result further confirms that the host-guest complexation occurs on the graphene surface.

***S4 E.coli* capture effect by sugar-functionalized graphene derivatives:** Visualization of *E.coli* strain ORN178 with ManCDAG4 by stereoscopic TEM

a)

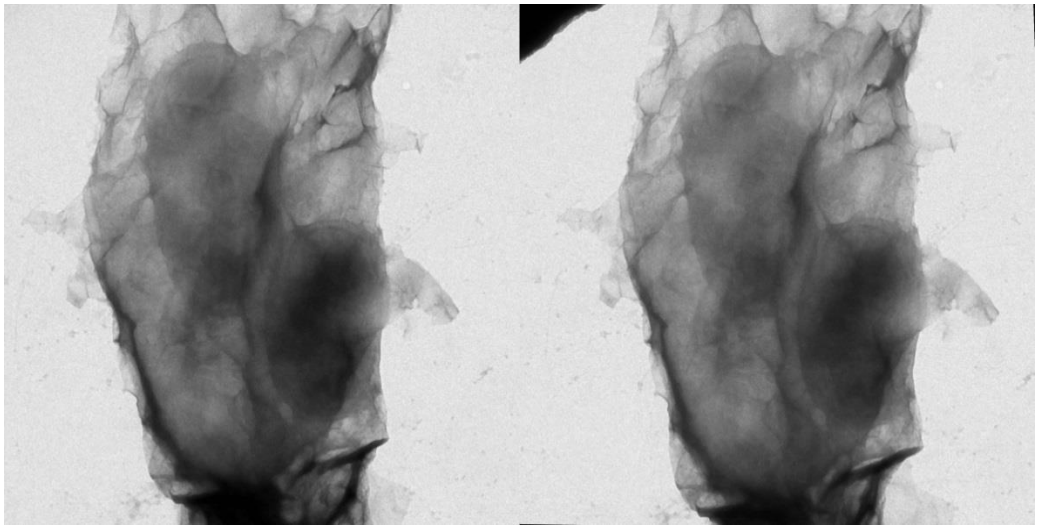

b)

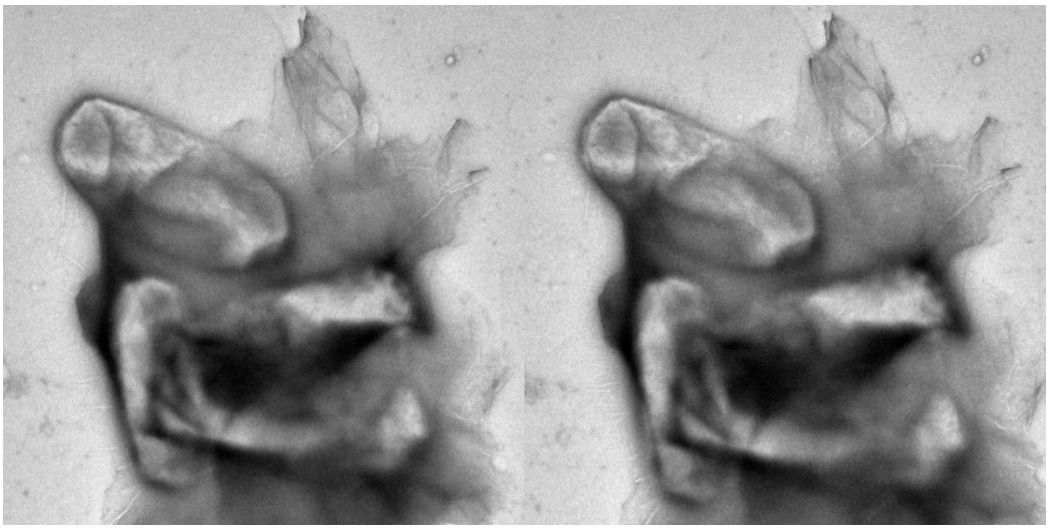

c)

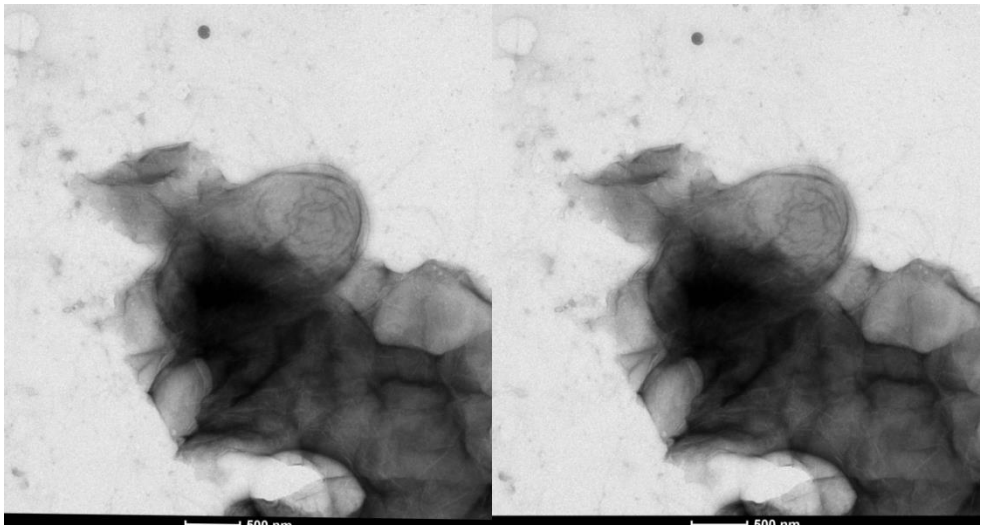

d)

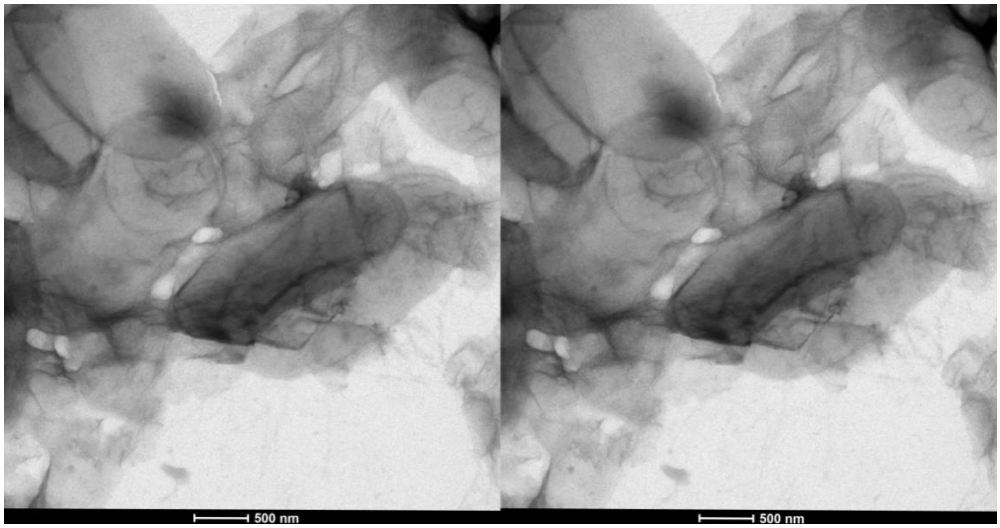

Figure 33: a) *E.coli* strain ORN178 incubated with ManCDAG4 which is in complementary to Figure 24c. TEM 3D stereoscopic images (side-by-side stereogram) at an 8º view angle. b), c) and d) Additional *E.coli* strain ORN178 incubated with ManCDAG4. The bacterium is wrapped inside ManCD@AG4 complex.

S5 Confocal laser scanning microscopy observation of *E.coli* strains with ManCD@AG4 and CD@AG4 respectively

a)

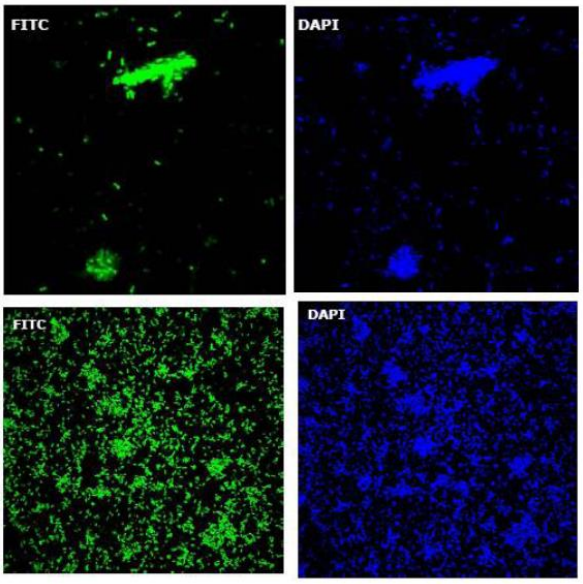

b)

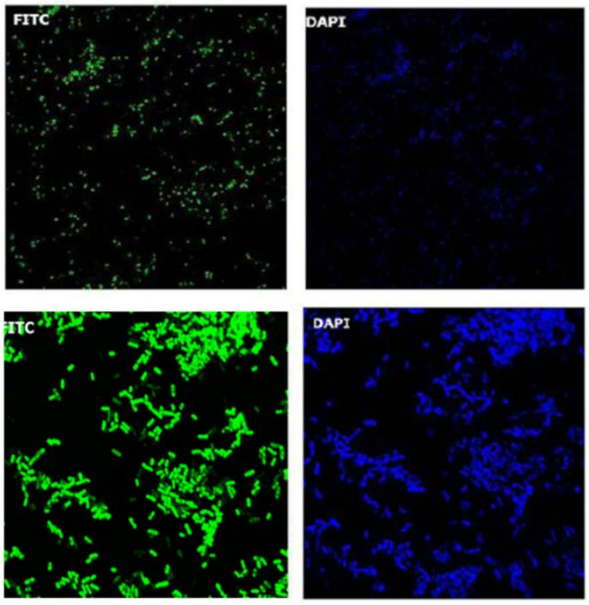

Figure 34: a) Confocal laser scanning microscopy images for the incubation of ManCD@AG4 with bacteria *E.coli* strain ORN178 (top row) and of ORN208 (bottom row). b) Confocal laser scanning microscopy images for the incubation of CD@AG4 with bacteria *E.coli* strain ORN178 (top row) and of ORN208 (bottom row). The selective capture effect is highly reproducible as demonstrated by the repeated experiment shown in (Fig. 25).

S6 E.coli killing effect by NIR laser irradiation with sugar-functionalized graphene derivatives

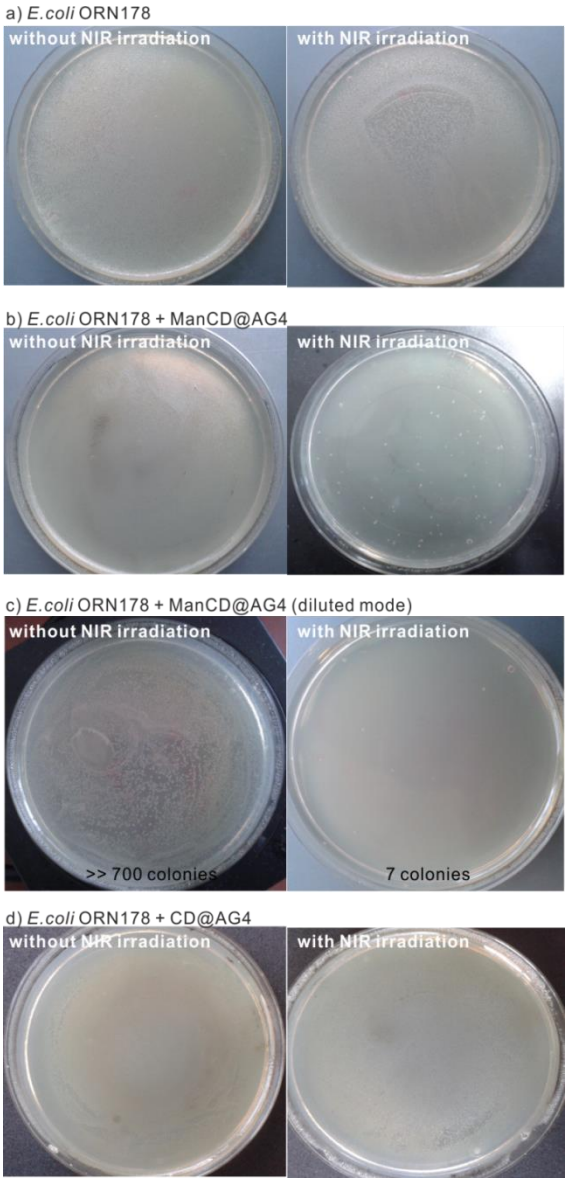

Figure 35: Comparison of photographs of *E.coli* colonies interacting with a) none; b-c) ManCD@AG4; d) CD@AG4 without (left) and with (right) NIR laser irradiation. In comparison with *E.coli* only (a), and *E.coli* incubated with CD@AG4 (d), the growth of *E.coli* with ManCD@AG4 on the agar plates (b,c) is significantly reduced due to the 10 min NIR laser irradiation (785 nm), in which very few colonies were observed. In the diluted mode, the killing efficiency number was derived from the colony counting number; the killing efficiency towards *E.coli* is > 99%.

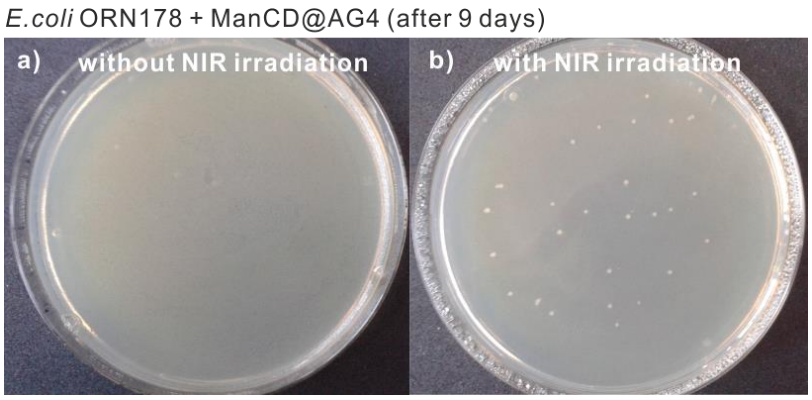

Figure 36: Evaluation of the long term inhibition of growth of bacteria on the NIR irradiation *E.coli* sample (interacting with ManCD@AG4). The photographs of *E. coli* colonies were taken from the re-cultured samples which have been kept at 4 ºC for 9 days: a) *E.coli* ORN178 incubated with ManCD@AG4 without NIR treatment; b) *E.coli* ORN178 incubated with ManCD@AG4 with NIR treatment. It is observed that NIR radiation is able to disinfect the *E.coli* and only 38 colonies were grown. However, *E.coli* grew full on the agar plate without NIR radiation.

2.5 Experimental Section

2.5.1 General methods

All reagents were procured commercially and used as supplied without further purification. Anhydrous solvents were either used from a dry solvent system (jcmeyer-solvent system) or as purchased. All glassware was oven-dried before use. Analytical thin layer chromatography (TLC) was performed on Kieselgel 60 F254 glass plates pre-coated with silica gel of 0.25 mm thickness (Macherey-Nagel, Düren, Germany). Flash chromatography was performed on Fluka Kieselgel 60 (0.04-0.063 mm). TLC chromatograms were visualized either by UV irradiation or by charring the TLC plate dipped in ammonium molybdate/ cerium (IV) sulfate solutions. NMR data were obtained on Bruker ECX 400 MHz, Jeol Eclipse 500 MHz, Varian 400 MHz, Varian 600 MHz, and Bruker AVANCE III 700 MHz NMR spectrometers, FTIR spectra recorded on a Nicolet Avatar 320 FT-IR spectrometer. UV/Vis spectra recorded on a Varian Cary 50 Bio UV/Vis spectrophotometer. Thermogravimetric analysis (TGA) of samples were performed on TGA/SDTA 851 (Mettler/Toledo, Gießen, Germany) at temperatures varied from 30 ºC to 700 ºC using a heating rate of 10 K min^{-1} (with purge gas flow of 20 mL min^{-1} nitrogen). Mass spectra were obtained using an electrospray ionization (ESI) interface on an Agilent LC/MSD TOF system. The AFM measurements have been performed using a Nanoscope Multimode V (Veeco, now Bruker AXS, Mannheim). All images were flattened previous to height analysis using algorithms contained in the software NanoScope version 1.5. Tip convolution makes lateral dimension analysis difficult. Measurements were performed in laboratory air at room temperature. The microscope was operated in the tapping mode (TM-AFM) using silicone probes, PPP-NCL-R (NanoAndMor GmbH, Wetzlar), SNL-D and SNL-A (Bruker AXS GmbH, Karlsruhe) under ambient conditions. The cantilever was forced to oscillate near its resonance frequency. The samples were prepared by spin coating (Spin Coater SCV-2) at 5.000 rpm for 300s on freshly cleaved mica.

I. Preparation of supramolecular inclusion complexes ManCD@AG4 and CD@AG4.

AG4, 0.5 mg ($n_{adamantyl\ unit}$ = 0.217 µmol) was dissolved in 200 µL DMF with the assistance of ultrasonication (10 min). After that, 1 mg ManCD ($n_{\beta\text{-cyclodextrin}}$ unit = 0.371 µmol) dissolved in 200 µL Milli-Q water was injected into the solution of AG4. The mixtures were sonicated for 30 min to aid the complexation process. The sample vial was left for 16 h at ambient condition before the addition of 500 µL water. The DMF and excess ManCD were removed by centrifugation for twice (12000 rpm, 10 min). The final centrifugal precipitation was collected and re-suspended in 600 µL water, affording the supramolecular carbohydrate functionalized graphene ManCD@AG4. The preparation of CD@AG4 was carried out under the identical protocol, except using 0.421 mg β-cyclodextrin (βCD, 0.371 µmol).

II. ***E.coli microscopy experiment and proliferation assay***.

E.coli strain bearing a mannose-binding protein (ORN178) and a mutant strain lacking the mannose binding domain (ORN208) were grown at 37 °C in Luria-Bertani (LB) medium (5 mL) to an OD_{600} of ~1.0 (1×10^8 CFU/mL). For different assays both strains were washed and appropriate dilutions made in phosphate-buffered saline (PBS, pH 7.4). LB medium was prepared dissolving 10 g Bacto-tryptone, 5 g of yeast extract and 10 g of sodium chloride up to 1 L in deionized water, autoclaved at 121 $^{\circ}$C for 15 minutes, cooled down at room temperature and used further for experiments. All the chemicals were purchased from Roth.

III. ***Confocal laser scanning microscope (CLSM) images.***

A solution of either ManCD@AG4 or CD@AG4 (10 µL, 16.33 µM) was coated on poly-l-lysine slide (Menzel-Gläser, Germany). In order to avoid dust contamination, the slide was kept in slide cover box at room temperature and further stored at 4 ºC overnight. The fluorescent dye (Fluorescein isothiocyanate -FITC)-labeled *E.coli* strains were prepared as following: 100 µL of a FITC solution (1 mg/mL) was added to the 2 mL solution of *E.coli* strain ORN178 or ORN208 (10^7 CFU mL^{-1}) in PBS. The mixture was incubated at 4 ºC for 1 h and washed three times with PBS. 10 µL FITC-labeled *E.coli* were added on coated slide and incubated at 37 ºC for 1 h. The cells were washed three times with PBS and then visualized on a confocal microscope LSM700 (Zeiss, Leipzig, Germany).

IV. ***Transmission electron microscopy (TEM) images.***

Droplets (~5 μL) of ManCD@AG4 sample solution were placed on carbon film coated copper grids (Plano GmbH, Wetzlar, Germany) and supernatant liquid was removed by blotting with a piece of filter paper. The grids were allowed to air-dry at least 40 min and were subsequently transferred into the microscope without use of a contrasting or cryo-fixation step (Note: graphene and its derivatives are known to create sufficient contrast in the TEM on their own).

V. Release the captured E.coli by competitive guests.

A 27 μL stock solution of ManCD@AG4 (98.2 μM) was diluted with 420 μL by PBS buffer, and divided into two portions (210 μL for each). Each portion was added 45 μL FITC stained *E.coli* stain ORN178 solution. The mixture was incubated at room temperature for 1 h on the orbital shaker with gentle shaking. A 40 μL solution of incubated sample was taken out and revered for recording starting fluorescent intensity (FI). After that, one portion of *E.coli* captured sample was injected by 28 μL solution of concentrated competitive guest, such as sodium adamantine carboxylate (AdCNa) or methyl α-D-mannopyranoside (Me-Man). The other portion was injected by 20 μL PBS as control. Both portions were further gently shook on the orbital shaker for another 1 h. Afterwards, both samples were left still for 10 min, and 40 μL supernatant was taken out from the upper layer of sample, and checked the FI by fluorescence reader. The amount of released *E.coli* was calculated according to the variation of FI.

VI. Near Infrared (NIR) treatment for bacteria disinfection.

The solution of *E.coli* strain ORN178 45 μL (OD_{600} = 0.3, ~10^6 CFU/mL, in PBS) was mixed with 255 μL of stock solution of ManCD@AG4 or CD@AG4 (ManCD in 98.2 μM, AG4 in 0.83 mg/mL). The mixture was incubated respectively at room temperature for 1 h on the orbital shaker with gentle shaking. Afterwards, each mixture was immediately subjected to NIR laser irradiation (785 nm, 0.5 W/cm^2) for 10 min at a distance of 1 cm. Finally, 100 μL of irradiated sample was spread on agar plate, and incubated for 24 h at 37 °C. In the diluted mode, the spreader which employed for spreading 100 μL irradiated sample was used directly without washing and spread again on agar plate. The control set

was prepared by diluting 45 µL of bacteria to 255 µL with Milli-Q water and spread on agar plates.

VII. Determination of the amount of attached carbohydrate on a graphene surface.

Anthrone is used for a popular cellulose assay and in the colorimetric determination of carbohydrates.[209] ManCD@AG4, CD@AG4 and AG4 were dispersed in deionized water (0.5 mL) in an ice bath. A freshly prepared 0.5% (w/w) solution of anthrone in sulfuric acid (1 mL) was added slowly to this solution. The resulting solution was gently mixed and heated to 80 °C for 10 min. The absorption of the solution was measured at 620 nm and compared with those that were obtained from a standard curve to determine the amount of ligand on the ManCD@AG4surface.

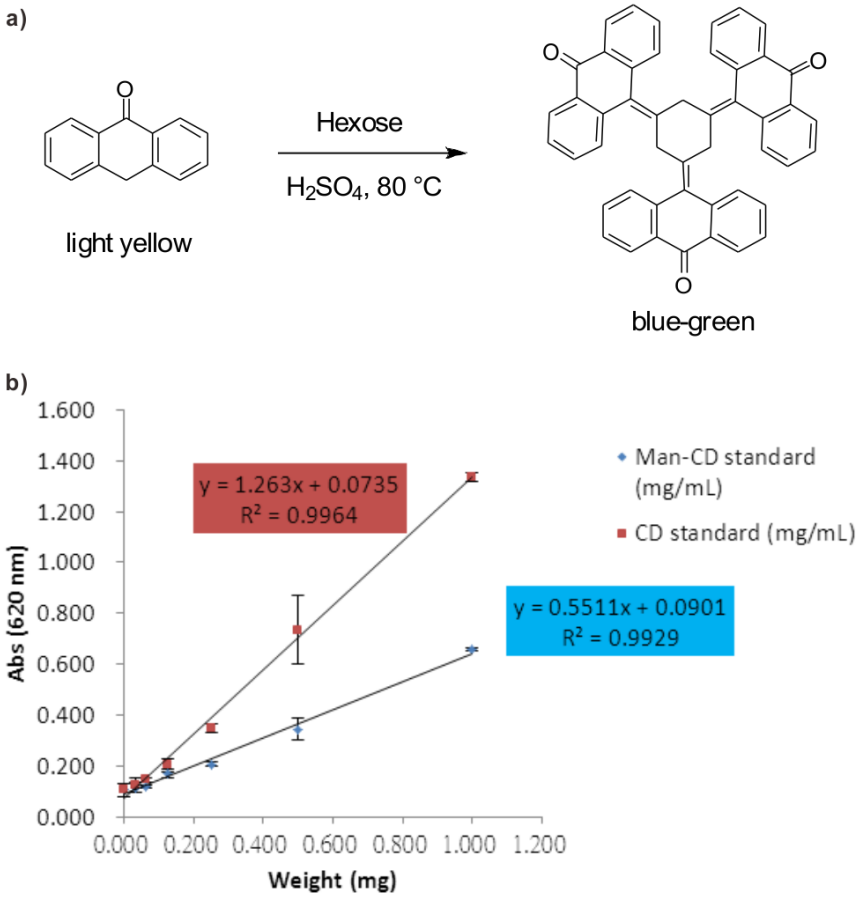

Figure 37: A standard deviation curve estimate the sugar amount (i.e. CD unit) on ManCD@AG4 is 117.8 ± 8.7 nmol/mg, and CD@AG4 is 109.2 ± 7.7 nmol/mg, according to AG4 weight.

VIII. Calculation of agglutination index (A.I.)

According to previous reported protocol,[204] the agglutination indexes (A.I.) were calculated from 10 random fields of confocal microscopic images. The number of cells in close contact was indicated by the fluorescent intensity of aggregation (FL_{agg}) which was readout by the cell counting software Image-Pro Plus (version 6.0, trail). The fluorescent intensity of non-aggregated cell was also recorded and averaged as FL_{single}. After summing of FL_{agg} from 10 random fields of confocal microscopic images ($\sum_i^{10} FL_{agg}(i)$), and then divide the FL_{single}, as:

$$\mathrm{AI} = \frac{\sum_i^{10} FL_{agg}(i)}{FL_{single}} \qquad \text{(eq.1)}$$

In accordance with the case of ManCD@AG4 and E.coli strain ORN178, other sample cases were calculated by the same method.

2.5.2 Methods of synthetic chemistry

2-Bromoethyl-2,3,4,6-tetra-*O*-acetyl-α-D-mannopyranoside (35)

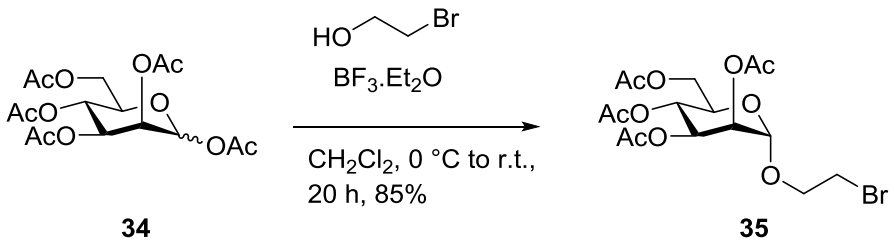

34 **35**

Compound **34** (1 g, 2. 56 mmol) was dissolved in anhydrous DCM, followed by the addition of 2-bromoethanol (0.36 mL, 5. 12 mmol) and the mixture was stirred for 1 h. Then the mixture was cooled to 0 ºC, $BF_3.OEt_2$ (1.62 mL, 12. 80 mmol) was added slowly drop by drop for 30 min and stirred for 20 h at room temperature under N_2 atmosphere. The crude mixture was diluted with DCM and water and the phases were separated. The organic layer was washed with saturated aqueous $NaHCO_3$ and brine solution. The organic layers were combined, dried over anhydrous Na_2SO_4, filtered, concentrated in vacuum and purified by silica gel flash column chromatography using hexanes: ethyl acetate (4:6) as eluted. The desired product was dried under high vacuum to afford **35** (1 g, 2.2 mmol, 85%). R_f (EtOAc/Hexanes 1:1) = 0.5; ^{1}H NMR (400 MHz, $CDCl_3$) δ 5.35 – 5.25 (m, 3H), 4.87 (s, 1H), 4.26 (ddd, J = 12.4, 5.3, 1.2 Hz, 1H), 4.12 (ddd, J = 9.6, 4.4, 2.3 Hz, 2H), 4.00 – 3.84 (m, 2H), 3.54 – 3.48 (m, 2H), 2.17 – 2.15 (m, 3H), 2.10 – 2.08 (m, 3H), 2.05 – 2.03 (m, 3H), 2.00 – 1.98 (m, 3H); LCMS m/z calculated for $C_{16}H_{27}BrNO_{10}^+$ $[M+NH_4]^+$ 473.2, found 472.0.

All spectroscopic data are in good accordance with the literature.[210]

2-Thiocyano-ethoxy-2,3,4,6-tetra-*O*-acetyl-α-D-mannopyranoside (36)

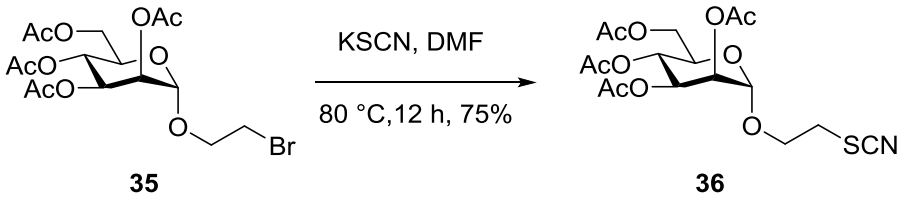

35 **36**

Compound **35** (1.2 g, 2.64 mmol) was dissolved in DMF. Then potassium thiocyanate (1.025 g, 10.54 mmol) was added and stirred at 80 °C for 12 h. The crude mixture was diluted with DCM and water and the phases were separated. The organic layer was washed with saturated aqueous $NaHCO_3$ and brine solution. The organic layers were combined, dried over Na_2SO_4, filtered and concentrated in vacuum and purified by flash column using hexanes: ethyl acetate (3.5:6.5), dried under reduced pressure and high vacuum to give the corresponding **36** (0.85 g, 1.9 mmol, 75% yield). R_f (EtOAc/Hexanes 1:1) = 0.45; ^{1}H NMR (400 MHz, $CDCl_3$) δ 5.33 – 5.30 (m, 1H), 5.28 – 5.25 (m, 2H), 4.88 (d, J = 1.5 Hz, 1H), 4.31 – 4.26 (m, 1H), 4.12 (ddd, J = 9.3, 5.2, 2.2 Hz,1H), 4.08 – 4.01 (m, 2H), 3.86 (dt, J = 10.8, 5.4 Hz, 1H), 3.24 – 3.13 (m, 2H), 2.18 – 2.14 (m, 3H), 2.12 – 2.09 (m, 3H), 2.06 – 2.04 (m, 3H), 2.00 – 1.98 (m, 3H); LCMS m/z calculated for $C_{17}H_{23}NNaO_{10}S^+$ $(M+Na)^+$ 456.4; found 456.0.
All spectroscopic data are in good accordance with the literature.[210]

2-Thioethoxy- 2,3,4,6-tetra-*O*-acetyl-α-D-mannopyranoside (37)

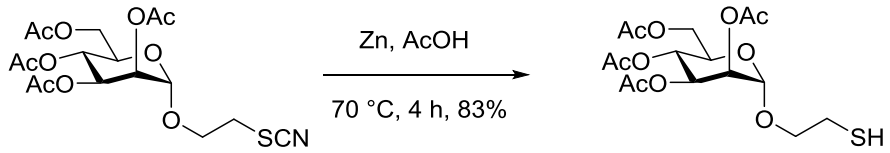

36 **37**

Compound **36** (0.5 g, 1.15 mmol) was dissolved in glacial acetic acid (75 mL). Then Zn dust (0.26 g, 3.46 mmol) was added and the mixture was refluxed at 70 °C for 4 h. The crude mixture was filtered to remove zinc dust. The organic layer was quenched with water (100 mL). Then product was extracted with EtOAc (3 X 50 mL) and dried over anhydrous Na_2SO_4. Organic layer was concentrated in vacuum to give crude product, which was further purified by flash column using hexanes: ethyl acetate (3:7) to get pure **37** (0.4 g, 0.96 mmol, 83%) yield. As the thiol is not stable, it is immediately taken to next step. LCMS m/z calculated for $C_{16}H_{24}NaO_{10}S^+$ $(M+Na)^+$ 431.4, found 431.0.

Per-acetylated 6'-Iodo- Beta-cyclodextrin (40)

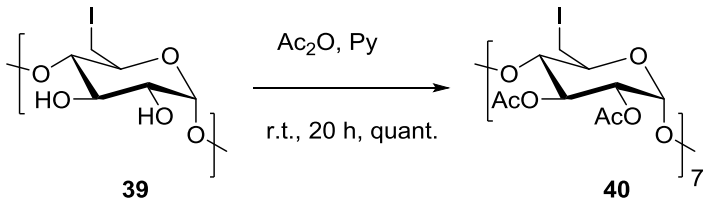

Compound **39** (1.678 g, 0.881 mmol) was dissolved in pyridine (20 mL, 247 mmol) at ambient temperature. Ac_2O (8 mL, 85 mmol) was added dropwise to this mixture and allowed to stir for 12 h with the exclusion of moisture. Pyridine was evaporated in vacuum following by co-evaporation using toluene. The crude product was purified by silica gel chromatography using DCM: MeOH (9:1), dried under reduced pressure and high vacuum to give the corresponding **40** as quantitative yield. R_f (MeOH/DCM 8:2) = 0.5; ^{1}H NMR (400 MHz, $CDCl_3$) δ 5.35 – 5.28 (m, 7H), 5.19 (d, J = 3.8 Hz, 7H), 4.82 (dd, J = 9.8, 3.7 Hz, 7H), 3.83 – 3.77 (m, 7H), 3.74 (d, J = 11.3 Hz, 7H), 3.60 (dd, J = 10.6, 6.6 Hz, 14H), 2.08 (s, 21H), 2.05 (s, 21H); ^{13}C NMR (101 MHz, cdcl$_3$) δ 170.57, 169.34, 96.46, 80.47, 70.37, 70.17, 70.03, 20.75, 7.96; HRMS m/z calculated for $C_{70}H_{91}NaI_7O_{42}$ $(M+Na)^+$ 2514.8190, found 2514.8174.

Hepta-(1-4)[2',3'-O-acetyl-6'-{2-ethoxy-(2S,3R,4S,5R,6S)-2-(acetoxymethyl)-tetrahydro-2H-pyran-3,4,5-triyl triacetate (41)

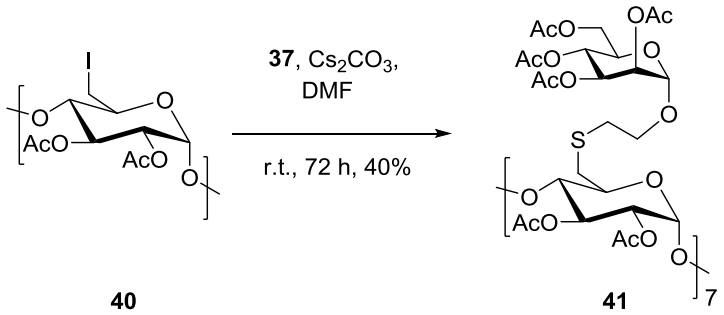

Compound **37** (0.46 g, 1.12 mmol) in DMF (10 mL) was added to compound **40** (0.20 g, 0.08 mmol) and cesium carbonate (0.36 g, 1.12 mmol) and stirred at room temperature for

72 h. The organic layer was quenched with water (50 mL). Then the product was extracted with EtOAc (3 X 50 mL) and dried over anhydrous Na_2SO_4. The organic layer was concentrated in vacuum to give crude product, which was further purified by silica gel chromatography using DCM: MeOH (8:2), dried under reduced pressure and high vacuum to give **41** (0.14 g, 0.03 mmol, 40%). R_f (MeOH/DCM 7:3) = 0.45; ^{1}H NMR (400 MHz, $CDCl_3$) δ 5.32 – 5.19 (m, 28H), 5.15 – 5.03 (m, 7H), 4.89 – 4.76 (m, 14H), 4.29 (dd, J = 12.3, 4.2 Hz, 7H), 4.17 – 4.01 (m, 21H), 3.91 – 3.65 (m, 21H), 3.35 – 2.97 (m, 14H), 2.96 – 2.76 (m, 14H), 2.12-1.95 (m, 126H); ^{13}C NMR (100 MHz, $CDCl_3$) δ 170.21, 170.16, 169.48, 169.43, 169.28, 169.03, 97.25, 96.65, 78.86, 78.54, 71.86, 70.57, 69.99, 68.98, 68.62, 68.18, 65.47, 61.80, 33.75, 32.43, 20.46, 20.37, 20.30, 20.22; MALDI-TOF m/z calculated for $C_{182}H_{252}O_{112}S_7$ $(M+K)^+$ 4495.4338, found 4495.640.

Per-mannosylated beta-cyclodextrin derivative (42)

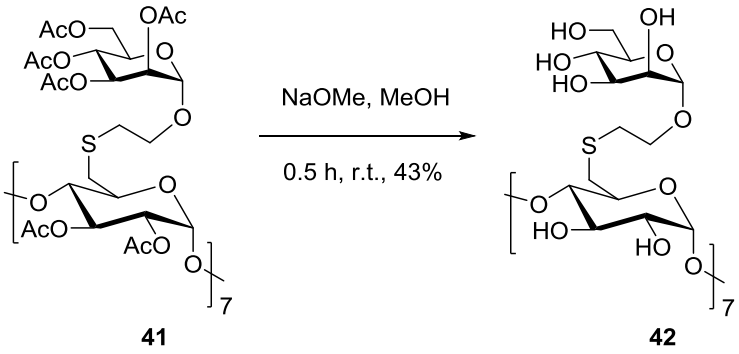

41 **42**

A solution of compound **41** (0.196 g, 0.04 mmol) in anhydrous MeOH (10 mL) was treated with sodium methoxide (55 mg, 1.02 mmol). The reaction mixture was stirred for 30 min at room temperature followed by evaporation of the solvent. The residue was dissolved in H_2O (20 mL) and the solution was neutralized with Amberlite IR-120 ion-exchange resin, filtered and concentrated in vacuum. The crude product was further purified by Sephadex™ LH-20 gel chromatography using ultra-pure water to give **42** (50 mg, 0.02 mmol, 42%) as white fluffy solid. ^{1}H NMR (600 MHz, D_2O) δ 5.15 (s, 7H), 4.92 (s, 7H), 4.10 – 3.63 (band, 70H), 3.57 (d, *J* = 8.4 Hz, 7H), 3.37 (d, *J* = 12.7 Hz, 7H), 2.99 (d, *J* = 7.0 Hz, 28H); ^{13}C NMR (100 MHz, D_2O) δ 103.80 (C-anomeric), 102.47 (C-anomeric), 86.88, 75.41, 75.12, 74.42, 73.42,

72.77, 69.74, 69.10, 63.45, 36.63, 35.04; HRMS m/z calculated for $C_{98}H_{168}O_{70}S_7$ $(M+Na)^+$ 2711.7523, found 2711.75234.

1-((3s,5s,7s)-Adamantan-1-yl)-3-(2-(2-(2-aminoethoxy)ethoxy)ethyl)urea (44)

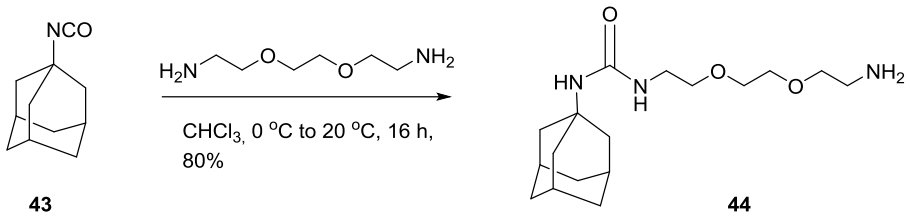

43 **44**

1-Adamantyl isocyanate **43** (886 mg, 5 mmol) was dissolved in chloroform (10 mL) and added dropwise to a solution of 2,2'-(ethylenedioxy)bis(ethylamine) (14.82 g, 100 mmol) in chloroform (15 mL) at 0 ºC. The suspension was stirred overnight at 20 °C. The reaction mixture was washed three times with water (100 mL), and the product was extracted with hydrochloric acid solution (100 mL 1 M in water). The aqueous layer was isolated, basified by addition of sodium hydroxide solution (10 mL 10 M in water), and subsequently extracted three times with dichloromethane (3×100 mL). The combined organic layers were dried with sodium sulfate and filtered, and the dichloromethane was removed under reduced pressure. Recrystallization of the product from diisopropyl ether gave the pure product **44** as colorless crystals (yield: 80%). ^{1}H NMR (500 MHz, $CDCl_3$) δ 5.36 (t, J = 5.1 Hz, 1H), 5.24 (s, 1H), 3.60 – 3.54 (m, 2H), 3.53 – 3.46 (m, 2H), 3.27 (dd, J = 10.1, 5.1 Hz, 1H), 2.86 (t, J = 5.0 Hz, 1H), 2.44 (s, 1H), 1.99 (s, 1H), 1.90 (d, J = 2.8 Hz, 3H), 1.60 (s, 3H); ^{13}C NMR (126 MHz, $CDCl_3$) δ 157.89, 77.41, 77.16, 76.91, 72.33, 70.88, 70.05, 69.95, 50.59, 42.52, 41.43, 39.73, 36.53, 29.60; HRMS m/z calculated for $[M+H]^+$ $C_{17}H_{32}N_3O_3$, 326.2438, found 326.2438.

1-((3s,5s,7s)-Adamantan-1-yl)-3-(2-(2-(2-isocyanatoethoxy)ethoxy)ethyl)urea (45)

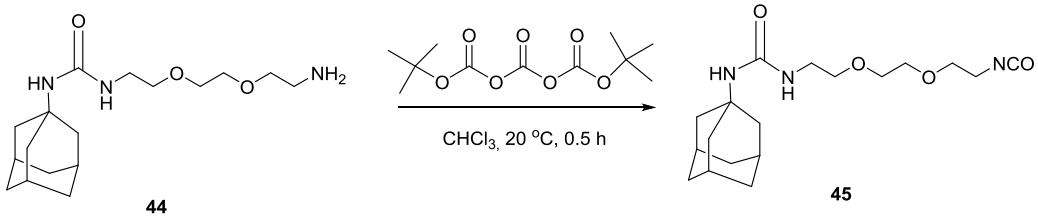

44 **45**

Di-*tert*-butyl tricarbonate[1] (103 mg, 394 µmol) was dissolved in chloroform (4 mL), and **44** (128.2 mg, 394 µmol) in chloroform (4 mL) was added at 20 ºC. The reaction mixture was stirred for 30 min to yield isocyanate **45.** The isocyanate **45** was used directly for the next reaction without any purification. ^{1}H NMR (500 MHz, $CDCl_3$) δ 3.70 – 3.61 (m, 6H), 3.55 – 3.51 (m, 2H), 3.44 – 3.40 (m, 2H), 3.35 (s, 2H), 2.05 (s, 3H), 1.95 (d, J = 3.0 Hz, 3H), 1.65 (s, 3H).

Synthesis of GO and TRGO400 (46) /750 (47)

TRGO was produced in a two-step procedure starting with graphite. At first, the graphene oxide (GO) was prepared by oxidation of graphite according to the method of Hummers and Offemann.[2] Graphite (60 g) was stirred in concentrated H_2SO_4 (1.4 L) at room temperature and $NaNO_3$ (30 g) was added. The mixture was cooled to 0 ºC and $KMnO_4$ (180 g) was added over 5 h. The reaction mixture was allowed to reach room temperature and stirred for 2 h. The reaction was quenched by pouring the reaction mixture into ice water (2 L) and adding H_2O_2 (3%, 200 mL). The GO was filtered off, washed with aqueous HCl (3%) and then with water until no AgCl precipitated when aqueous $AgNO_3$ was added to water. The purified chlorine-, sulfate- and manganese-free GO was dried in vacuum at 40 °C and powdered (60 mm mesh) by a ball mill (Retsch, Haan, Germany) using liquid nitrogen. In the second step, GO was thermally reduced at 400 ºC or 750 ºC, to produce TRGO400 (**46**) and TRGO750 (**47**) respectively. TRGO 400/750 was obtained as a black powder of very low bulk density.

Synthesis of AG4 (48)

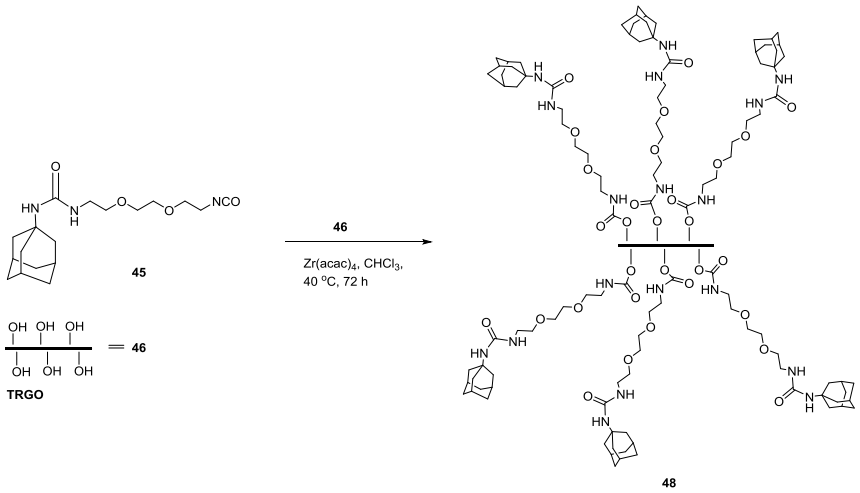

For the preparation of AG4, 40 mg TRGO400 (n_{-OH} = 64 µmol) **46** was suspended in 5 mL dry chloroform, and was consequently treated with an excess isocyanate solution **45** (15 mL) and 1 mg zirconium (IV) acetylacetonate ($Zr(acac)_2$) as catalyst in chloroform (50 mL). The mixture was stirred under argon for three days at a temperature of 40 ºC. AG4 was filtered off and washed several times with chloroform followed by drying in vacuum at 100 ºC gave **48**.

3. Automated Solid Phase Synthesis of Lipoglycans from *Mycobacterium tuberculosis*

3.1 Introduction

3.1.1 Mycobacterium tuberculosis

Tuberculosis (TB) is one of the top ten causes of death in the world. Approximately 10.4 million new cases were estimated worldwide in 2015, out of which 56% were men, 34% women and 10% children. In 2015, 480000 cases of multidrug-resistant TB (MDR-TB) and 100000 cases of newly eligible rifampicin-resistant TB (RP-TB) were registered. As estimated in 2015, 1.4 million died due to TB alone and 0.4 million people died of TB in HIV-infected people (Global tuberculosis report 2016).

Mycobacterium tuberculosis (MTB) is the causative agent of tuberculosis and was first observed and reported by Robert Koch in 1882. MTB, a highly aerobic Gram-positive bacterium, primarily colonizes the mammalian respiratory system. The bacteria are spread by cough or sneeze from a TB infected person, transformed into droplet nuclei and transmitted to healthy individuals, infecting the body's immune system. The inhaled droplet nuclei is engulfed by alveolar macrophages of the lungs by phagocytosis and expelled *via* apoptosis and autophagy, causing either latent TB, with controlled bacterial growth, or active TB, by multiplying bacteria in macrophages and infecting other parts of the body.[211] The current available vaccine against TB is an attenuated strain of *Mycobacterium bovis (M. bovis)* which was first developed and tested by Albert Calmette (1863-1933) and Camille Guerin (1872-1961), hence known as BCG.[212] Current accessible drugs for active TB are isoniazid, rifampicin, ethambutol, pyrazinamide, and streptomycin which are given either for two months or four months to an infected person (WHO 2009). If the patient does not respond to these drugs, the patients results into MDR-TB. Such highly pathogenic bacteria possesses unusual lipid rich cell wall, which is a characteristic feature of the Actinomycetaceae family including other *Corynebacterium, Mycobacterium, Nocardia* genus.[213]

3.1.2 Cell wall of MTB

The cell wall of MTB comprises the mycolyl–arabinogalactan–peptidoglycan (mAGPs) complex and other non-covalently attached lipids such as, glycolipids, glycophospholipids, glycopeptidolipids, sulfolipids, and sulfoglycolipids.[214, 215] Among these lipids, mannose-rich glycophospholids having common phosphatidyl-myo-inositol (PI) anchor are considered the most important class of glycolipids for cell wall function and for host-pathogen interactions. Some of these glycolipids are phosphatidylinositol mannosides (PIMs), lipomannan (LM), and lipoarabinomannan (LAM). The biosynthetic relationship of PI → PIMs → LM →LAM has been studied biochemically and genetically.[216-219] The PIMs are attached to the inositol moiety glycosylated with two (PIM_2) or six (PIM_6) mannoses. LM and LAM contain a long polymeric chain of α-(1→6) linked mannose (Man*p*) residues with further α-(1→2) branching and approximately 70 arabinofuranoside (Ara*f*) residues respectively (Fig. 38).[220, 221] *Mycobacterium* species including *M. tuberculosis*, *M. leprae*, *M. kansasii* and *M. smegmatis* possess a similar mannose backbone. In LAM the non-reducing end of the mannose is capped with α-(1→5)-Ara*f* residue and this arabinan chain is further branched with α-(3→5) linked Ara*f* residues.[214] LM and mannose-capped-LAM (Man-LAM) play a crucial role in host-pathogen interactions including Toll-like receptors (TLR) signaling and C-type lectins binding respectively.[158, 159]

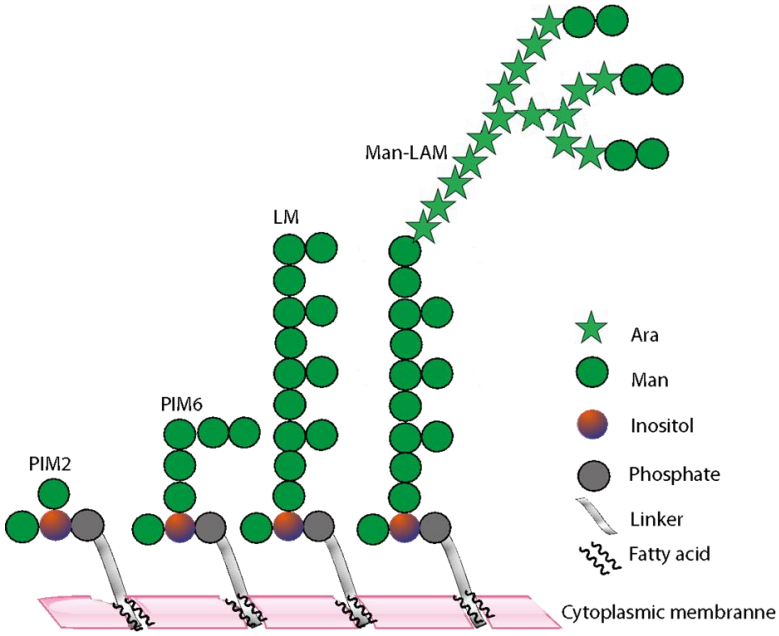

Figure 38: Schematic picture of the cell wall of *M. tuberculosis* consisting of phosphatidylinositol mannosides (PIMs); lipomannan (LM); lipoarabinomannan (LAM).

The cell wall enables the bacteria to invade, infect, survive and circulate within the human host.[213, 222] The first line drugs isoniazid and ethambutol are known to inhibit the mycolic acid and the biosynthesis of arabinan respectively, which brings attention to the mycobacterial cell wall as a potential drug target.[159, 223] Considering the pathogenicity and the increasing TB resistance properties of MTB there is an overwhelming exigency to develop desired TB vaccines.

Until now many attempts have been reported for solution phase synthesis of these cell wall components. Seebeger and co-workers[222, 224, 225] accomplished the first total synthesis of PIMs **57** together with a library of arabinomannan oligosaccharides fragments. A [6 + 6] glycosylation strategy has been employed for the synthesis of the dodecasaccharide of arabinomannan **57** (Scheme 7a). Condensation of α-(1→2)-linked fragments of hexamannoside **55** and arabinan imidate **56** was accomplished using *tert*-butyldimethylsilyl trifluoromethanesulfonate (TBSOTf) as promoter affording the target molecule **55**. The reducing end of the fragment **55** was implemented with a thiol linker for further attachment to protein carriers or microarray. The hexamannoside donor **55** was synthesized from three monosaccharide building blocks **50a**, **50b** and **51**. The mannose derivative **50b** was used for

the further α-(1→6) and for α-(1→2) side chain elongation. Building block **51** was used for α-(1→6) and α-(1→2) terminal capping. The arabinoside donor **56** was synthesized using building blocks **52-54;** the arabinoside **53** used for α-(1→3) and α-(1→5) branching and **54** for the arabinan core. In an effort to synthesize LAM fragments, the assembly of the 28-mer fragment *via* a [12 + 16] glycosylation, possessing the inositol, 15 Man*p* and 12 Ara*f* residues proved to be challenging.[226] Todd Lowary and co-workers presented the first total synthesis of β-Ara*f* containing longer arabinan fragments **57** and **56** with an aminooctyl linker (Scheme 7b).[227] This convergent fragment approach involved the use of glycosyl donors bearing 2-*O*-benzoyl protecting group for anchimeric assistance and 6-*O*-silyl group as temporary protecting group for the chain elongation. More recently Hotha and coworkers[228] employed a gold-catalyzed glycosylation strategy to synthesize *trans*- and *cis*-1,2 furanoside building blocks exploiting propargyl 1,2-ortho esters while Ito and coworkers[229] utilized 3,5-*O*-tetra-*i*-propyldisiloxanylidene (TIPDS) or NAP protected furanoside donors for intermolecular glycosylation and intramolecular aglycon delivery (IAD), respectively. The use of these new accessible building blocks was applied to the synthesis of structural motifs present in the cell wall of MTB.[230]

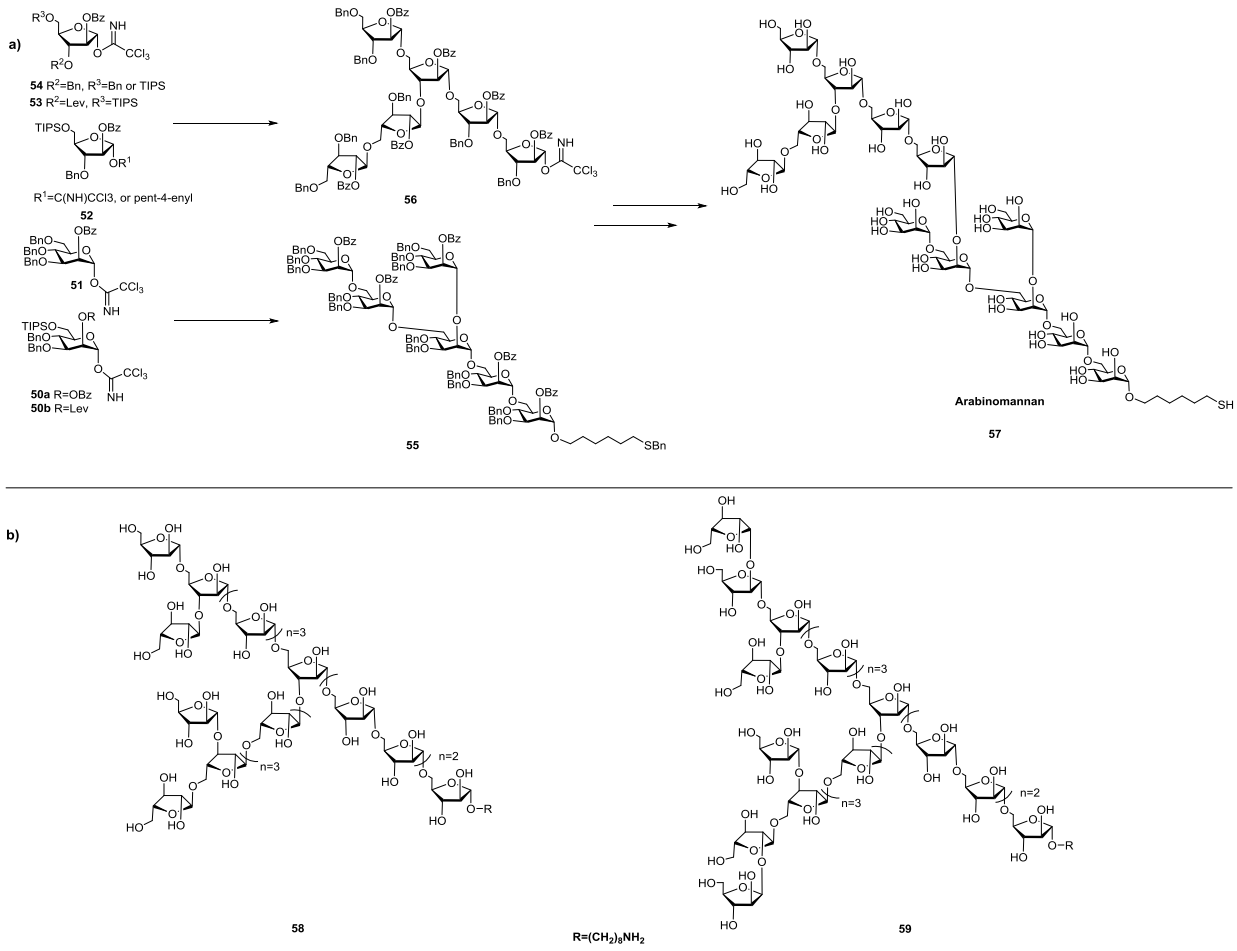

Scheme 7: Reported synthesis Arabinomannan fragments: a) Seeberger's synthesis of Arabinomannan oligosaccharides.[224] b) Lowary's synthesis of β-Ara*f* containing oligo-arabinan fragments.[227]

These are classical chemical approaches to the solution phase synthesis of large and challenging molecules; however they are tedious and include multi-steps reactions and multiple purifications of intermediate compounds. Automated solid phase synthesis is known to reduce the time and effort required to gain rapid access to complex structures.[142, 150, 157, 231] Seebeger and co-workers reported the first automated synthesis of linear and branched oligoarabinofuranosides (Scheme 8).[232] The use of two arabinose building blocks, **60** for α-(1→5) branching while **61** for α-(1→3) branching resulted into respective linear and branched target molecules **62-65**. Easy purification enabled the synthesis of conjugation ready glycans **64** and **65**, respectively isolated in a 63% and 78% yield.

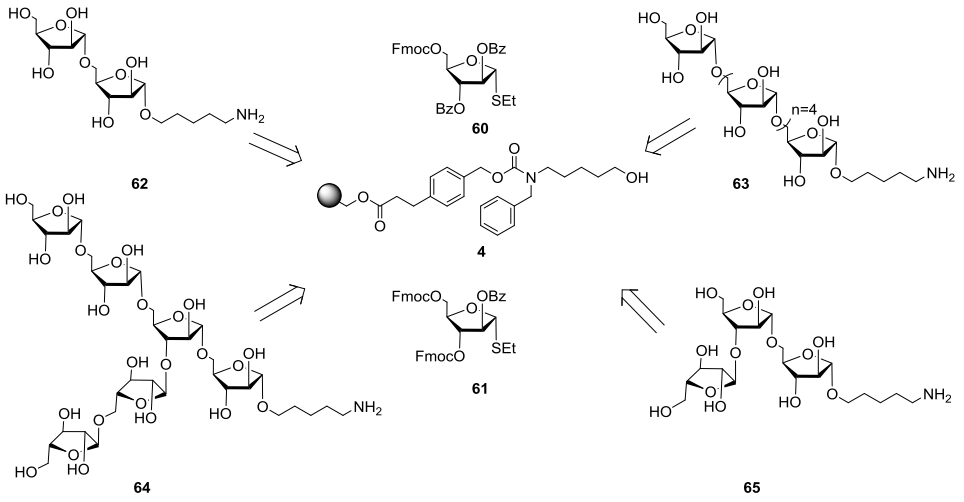

Scheme 8: Seeberger's first AGA of oilgofuranosides.

Recently, a collective effort has been taken by the members of Seeberger, Todd Lowery, Birch and Joe groups towards the synthesis of a library of 35 LAM substructures to identify LAM substructure-specific antibodies. These LAM structures were immobilized on a glycan array and incubated with human sera from 102 active TB patients, 119 healthy persons and 32 latent TB patients. As the obtained data show broad reactivity towards all LAM structures, it's difficult to differentiate between active, healthy or latent TB patients (Unpublished data[233]- Dr. Anika Reinhardt thesis).

Based on these results we decided to synthesize LM and LAM structures, as these lipoglycans (LM and LAM), with their diverse chemical structures, represents a highly challenging target for chemical synthesis. Even though some studies of the gross structural features of LM and LAMs exist, the degree of branching on the mannan and arabinan backbone and the attachment sites of the arabinan chains on the mannan core is still unknown.[215, 225] In order to gain molecular-level understanding of the role of lipoglycans in mycobacterial pathogenesis the synthesis of a library of LM and LAM compounds is pursued. The use of AGA for the synthesis of large oligosaccharides was selected. LM fragments **66-68** and LAM fragments **69-71** (Scheme 9) were chosen as targets, containing either α-(1→6)-Man*p*, α-(1→5)-Ara*f*-linked linear or α-(1→2)-α-D-Man*p*-linked branched mannose or arabinose hexasaccharide backbone. These structures will help; i) to implement the library of 35 LAM substructures previously synthesized, ii) to understand the structure-activity-relationship (SAR) of these large oligosaccharides.

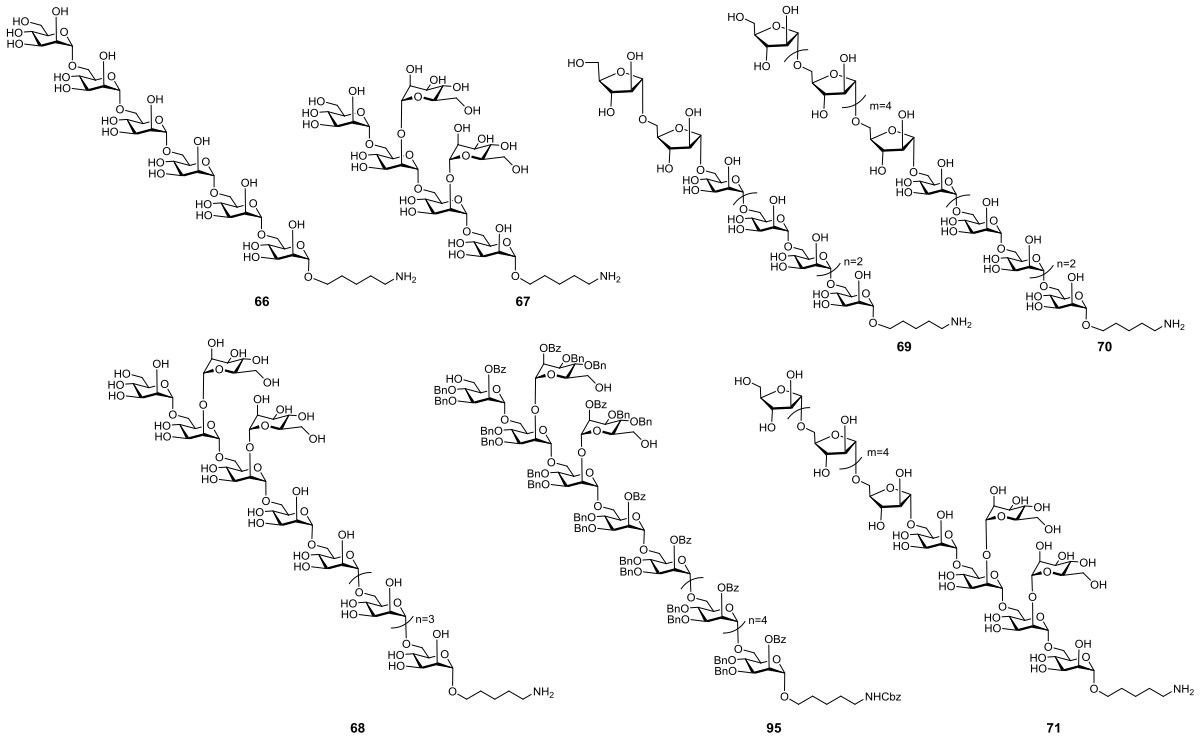

Scheme 9: Lipoglycans (**66-71** and **95**) containing different (1→6)-*trans*, (1→2)-*trans* and (1→5)-*trans*-glycosidic linkages selected as targets.

3.1.3 Strategy

The linear and branched structures of the LM and LAM were obtained from monosaccharide building blocks **72**, **73**, **74** and functionalized Merrifield solid support **4** using AGA (Fig. 39) Cleavage from the solid support, followed by purification using NP-HPLC and deprotection using *Zemplén* methanolysis and hydrogenolysis, afforded conjugation ready glycans.

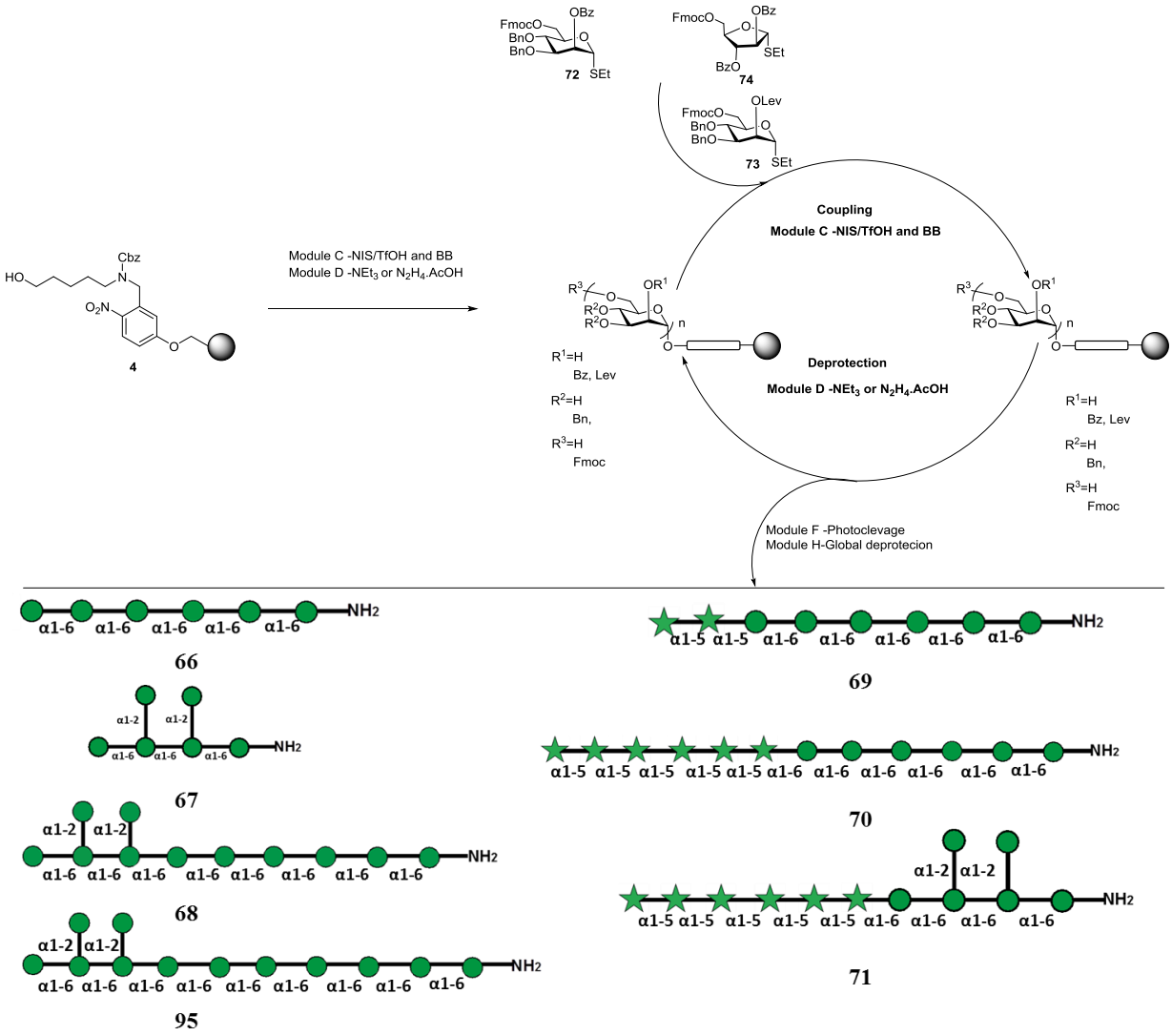

Figure 39: Schematic representation of the target LM and LAM fragment synthesis using the building blocks and the solid support on AGA followed by cleavage, deprotection and purification, ● = Man, ★ = Ara*f*.

3.2 Results

3.2.1 Synthesis of Linear LM fragment α-(1→6)-Oligomannoside by AGA

Although the synthesis of linear α-(1→6)-linked oligomers (dimer to 30mer)[140] was previously reported using the mannosyl phosphate building block **75**, the insolubility of the synthesized dodecasaccharide led to poor separation on NP-HPLC. Further purification by a magnetic bead labeling saccharide (catch–release approach) was required. This purification issue was solved by using the mannose thioglycoside **72**. Previous studies by Dr. Naresh Kottari (unpublished results) investigated the ideal building block for the synthesis. Building

blocks **76**, **77** and **72** were analyzed (Scheme 10). The use of arming protecting groups (benzyl ethers) resulted in good reactivity and better separation of obtained oligosaccharide from deletion sequences on NP-HPLC.

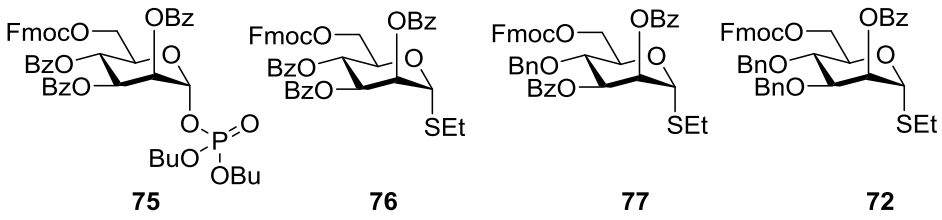

75 **76** **77** **72**

Scheme 10: Possible mannose building blocks for oligosaccharide syntheses.

Merrifield's resin[144] was selected as the solid support for the automated assembly of oligosaccharides following previously reported results.[140, 150] The Merrifield resin **1** was functionalized with a photolabile linker **78**, which acts as first glycosyl acceptor and it is stable in both acidic and basic conditions (Scheme 11).[150] The resin loading was determined by performing one glycosylation with excess building block **72** on solid support **4** followed by DBU promoted Fmoc-cleavage and determination of dibenzofulvene production by UV absorbance at 294 and 304 nm.[234] A loading of 0.37 mmol/g was obtained.

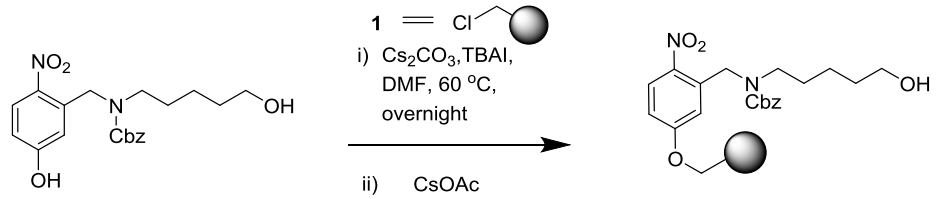

78 **4**

Scheme 11: Synthesis of functionalized Merrifield resin **4**.

Linear α-(1→6)-linked hexasaccharide (hexamer) **66** was assembled using the thiomannoside building block **72.** The C-2 hydroxyl group of glycosyl donor **72** protected with permanent benzoyl groups was installed to ensure α-selectivity. The C-3 and C-4 hydroxyl group were protected with permanent benzyl ethers. The anomeric thioglycoside leaving group allows for fast and efficient glycosylation by Lewis acid activation.[235] The C-6 hydroxyl group functionalized with the temporary protecting fluorenylmethoxycarbonyl

(Fmoc) group serves for chain elongation of α-(1→6)-Man*p* backbone (Scheme 12). The temporary Fmoc protecting group can be selectively removed *via* a basic wash (Et_3N 20% in DMF) after glycosylation during the automated synthesis.

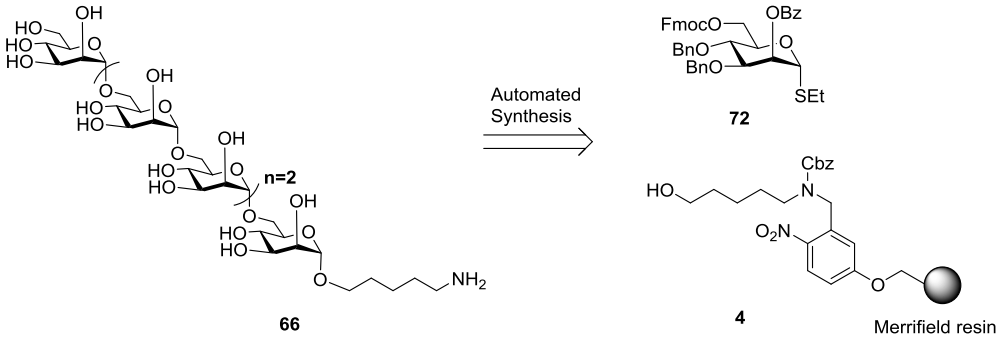

Scheme 12: Retrosynthetic analysis of linear hexasaccharide **66**.

The synthesis of the thiomannoside building block **72** started from peracetylated mannose **80** (Scheme 13). Glycosylation with ethanethiol in the presence of boron trifluoride-diethyl ether ($BF_3.OEt_2$) yielded **81**. Compound **81** was subjected to methanolysis using sodium methoxide (NaOMe) in methanol affording the α-thiomannoside **82** which, upon treatment with benzaldehyde dimethylacetal and (±)-10-camphorsulfonic acid (CSA) in acetonitrile, afforded the 4,6-*O*-benzylidene acetal protected compound **83**. The 4, 6-*O*-benzylidene thiomannoside **83** was further protected with benzyl ether using tin-mediated regioselective C-3 benzylation to give **84**.[236] Protection of C-2 hydroxyl group using benzoyl chloride in pyridine afforded compound **85** which was subjected to regioselective ring opening of 4, 6-benzylidene acetal using borane-tetrahydrofuran complex and catalytic amounts of TMSOTf to afford compound **86**. Installation of base-labile Fmoc at the C-6 hydroxyl group in the presence of pyridine gave the corresponding building block **72** in 89% yield.

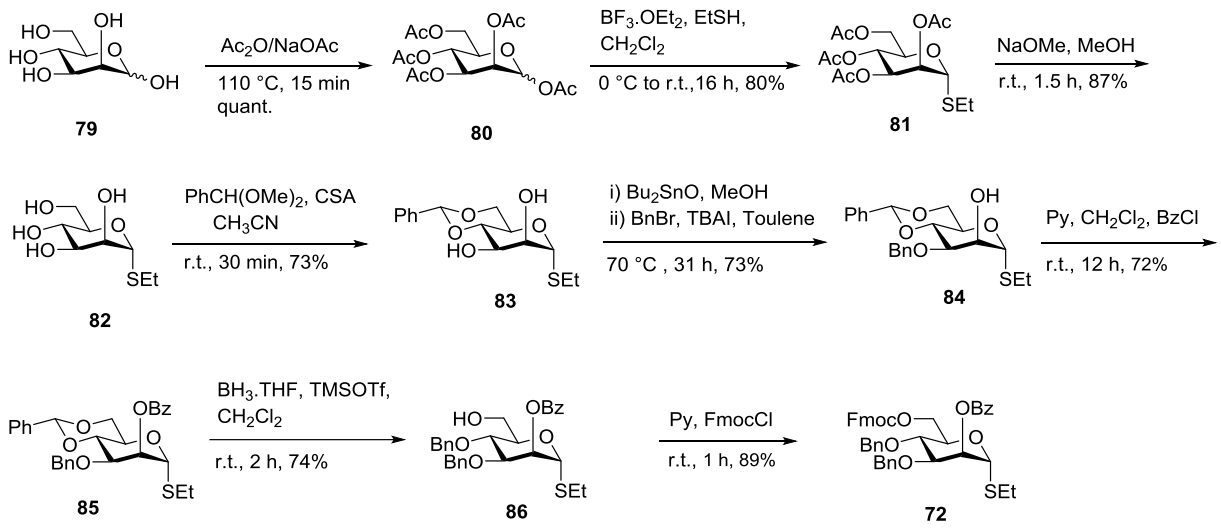

Scheme 13: Synthesis of thiomannoside **72**.

3.2.2 Optimization of automated glycosylation conditions

The syntheses of the desired oligosaccharides were carried out using a home-built automated synthesizer (Frank Schumacher thesis-under preparation). Each glycosylation step was performed in one cycle, using excess of thiomannoside building block **72,** at -40 to -20 ºC, in the presence of NIS with catalytic amount of TfOH for activation (Module C). The C-6-Fmoc group removal was carried out using Et_3N (20% solution in DMF) liberating the C-6 hydroxyl group for chain elongation (Module D). The sequence was repeated six times to achieve hexasaccharide **87**. The protected hexasaccharide **87** was cleaved from the solid support using UV light in a microfluidic photoreactor (Module F) (Scheme 14).[150]

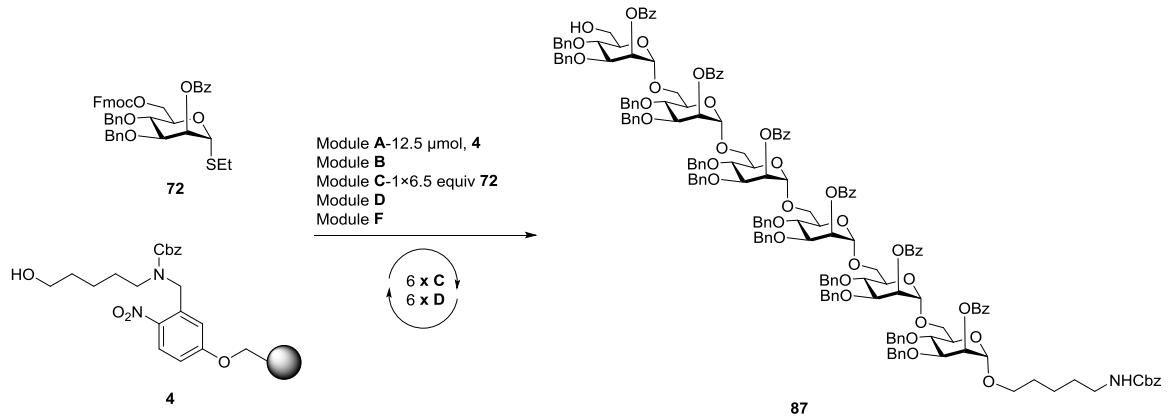

Scheme 14: Automated synthesis of linear hexasaccharide **87**: Reactions and conditions: Module **B**-Acidic wash: TMSOTf, CH_2Cl_2, -20 °C, (2 min); Module **C**-Glycosylation: **72**, NIS, TfOH, -20 °C, (30 min), CH_2Cl_2/Dioxane (5:1); Module **D**-Fmoc deprotection: 20% Et_3N in DMF, 25 °C, (3 x 5 min); Module **F**-post-automation photocleavage: hυ, CH_2Cl_2, 25 °C.

In order to optimize the glycosylation conditions disaccharide **88** was synthesized using five equivalents of building block **72** per cycle (0.37mmol resin loading). This resulted in deletion sequences as shown in Table 1, Fig. 40a. To improve the reaction outcome, the synthesis of the dimer was performed with 6.5 equiv of **72** per cycle resulting in complete conversion to the desired dimer (Table 1, Fig. 40b). Identical glycosylation conditions (6.5 equiv of **72** per cycle) were then applied to the synthesis of the desire hexasaccharide **87** (Fig. 41). The crude compound was analyzed and purified using NP-HPLC affording the hexasaccharide **87** in 55% yield over twelve steps.

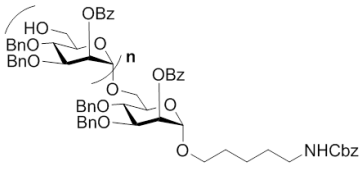

88

BB 72	Products (n=0 to n=1)
5 equiv	23 : **77**
6.5 equiv	0 : **100**

Table 1: Deletion sequence ratios were calculated from the NP-HPLC trace for **88**.

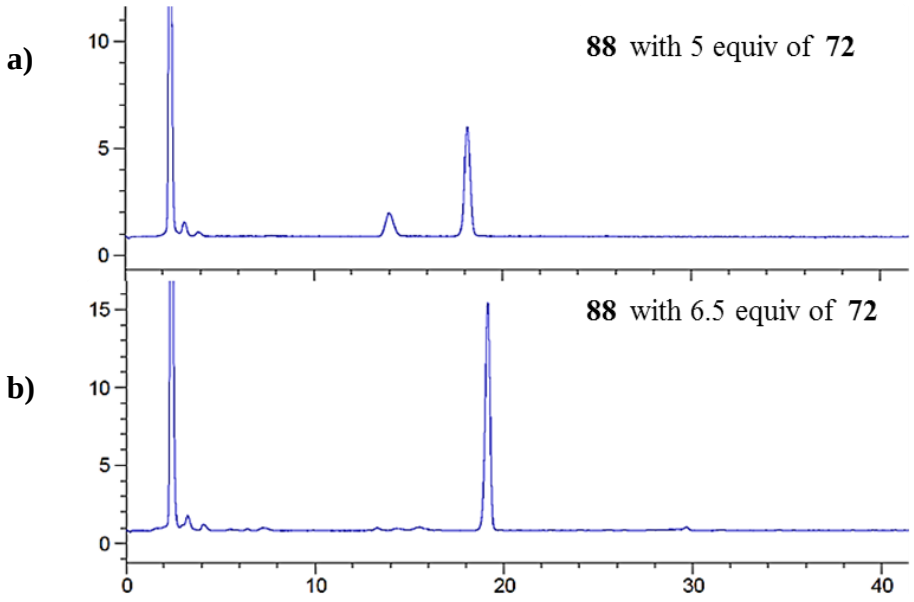

Figure 40: Crude-HPLC trace of dimer **88** with a) 5 equiv and b) 6.5 equiv of building block **72,** respectively.

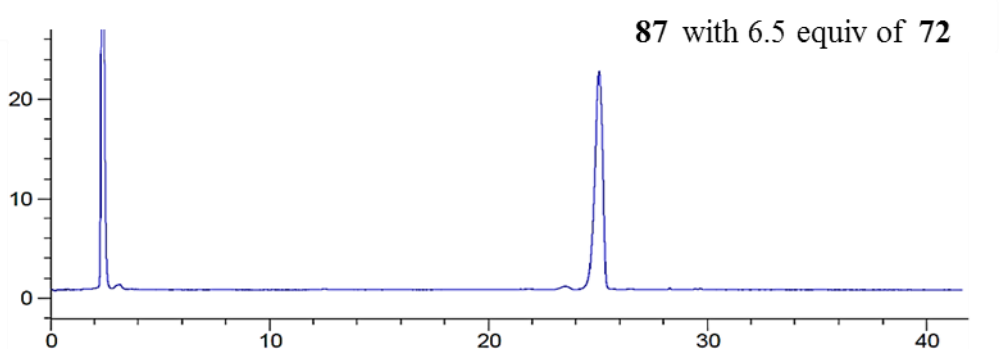

Figure 41: Crude-HPLC trace of hexamer **87** with 6.5 equiv of building block **72**.

3.2.3 Synthesis of branched hexasaccharide LM fragment 89

The introduction of α-(1→2)-branches into α-(1→6)-mannan backbone was also explored. Branched structures were assembled using two mannose building blocks **72** and **73**. The C-2 hydroxyl group of thiomannoside **73** was protected with a levulinoyl (Lev) group, for side chain elongation. In order to synthesize the target hexasaccharide **89** the following strategy was followed: first, assembly of the linear tetrasaccharide backbone **90** keeping the Lev

group intact, followed by orthogonal Lev deprotection to give **91,** and second, the last two glycosylation (branches) using donor **72** in one step followed by removal of Fmoc (Scheme 15).

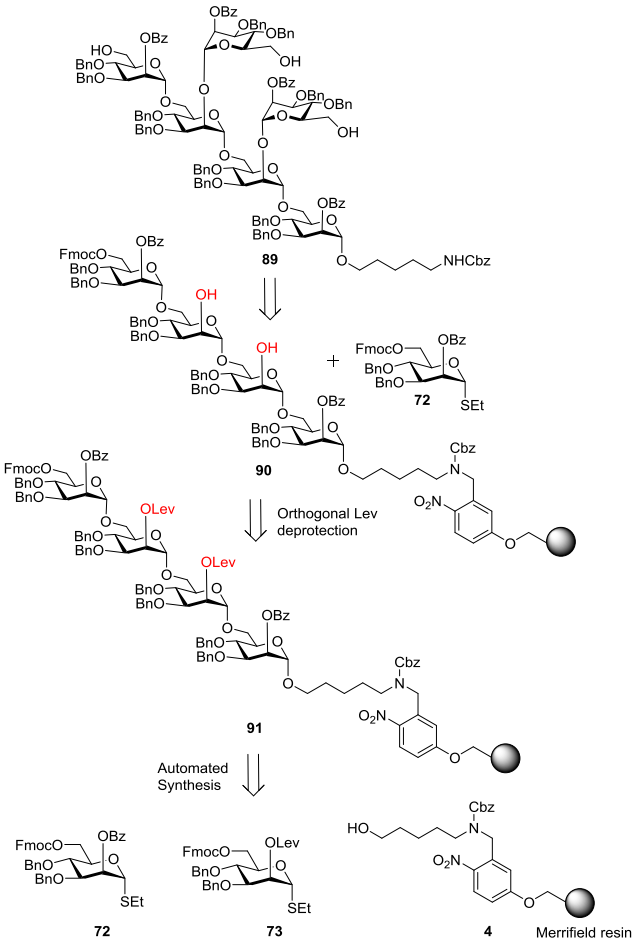

Scheme 15: Retrosynthetic analysis of branched hexasaccharide **89**.

The synthesis of the building block **73** was started with intermediate **86** as shown in scheme 11. Methanolysis yielded the 3,4-*O*-benzylated α-thiomannoside **92.** Protection of C-6 hydroxyl group using FmocCl in pyridine afforded **93** in 87% yield. Finally, the esterification of the free C-2 hydroxyl group was accomplished with levulinoyl chloride, giving building block **73** (Scheme 16).

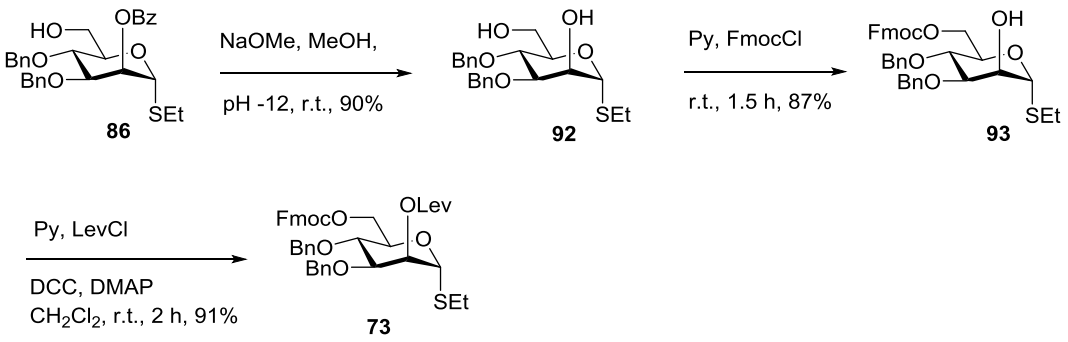

Scheme 16 : Synthesis of thiomannoside **73**.

The automated assembly of the desired hexasaccharide was performed following the strategy described above. First the linear tetrasaccharide with terminal Fmoc group intact was assembled. Following removal of the two Lev protecting groups, the two α-(1→2)-branches were simultaneously introduced using building block **72** with module **C*** in a double glycosylation (2×6.5 equiv). Removal of the three remaining Fmoc protecting groups was carried out simultaneously. Each glycosylation was performed using 6.5 equiv of thiomannoside building block **72** and **73,** at -40 to -20 ºC, in the presence of NIS with catalytic amount of TfOH for activation. Successive Fmoc and Lev group removal was carried out using Et_3N and hydrazine acetate respectively (Module D and E). Following UV cleavage from solid support and further purification from deletion sequences, the protected hexasaccharide **89** was isolated in 37 % yield over ten steps (Scheme 17).

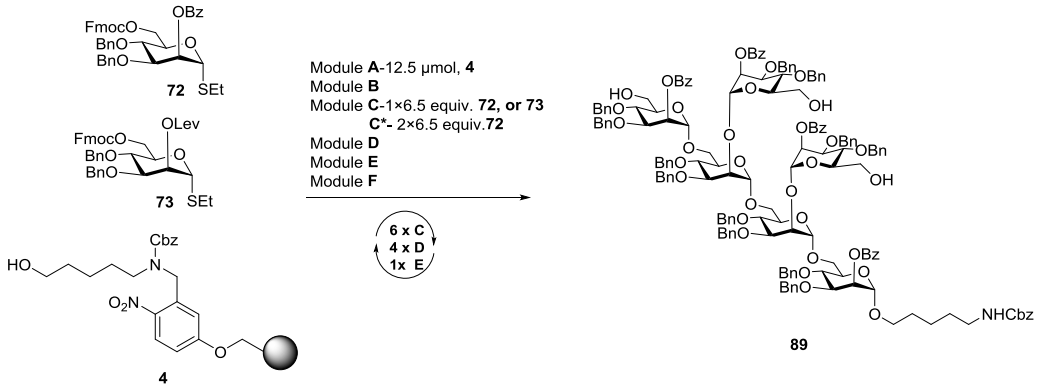

Scheme 17: Automated synthesis of linear hexasaccharide **89**: Reactions and conditions: Module **B**-Acidic wash: TMSOTf, CH_2Cl_2, -20 ºC, (2 min); Module **C**-Glycosylation: **72 or 73**, NIS, TfOH, -20 ºC, (30 min),

CH_2Cl_2/Dioxane (5:1); Module **D**-Fmoc deprotection: 20% Et_3N in DMF, 25 ºC, (3 x 5 min); Module **E**-Lev deprotection: N_2H_4.AcOH in Py/AcOH/H_2O, 25 ºC, (3 x 30 min); Module **C***- Glycosylation: **72**, NIS, TfOH, -20 ºC, (30 min), CH_2Cl_2/Dioxane (5:1); Module **F**-post-automation photocleavage: hυ, CH_2Cl_2, 25 ºC.

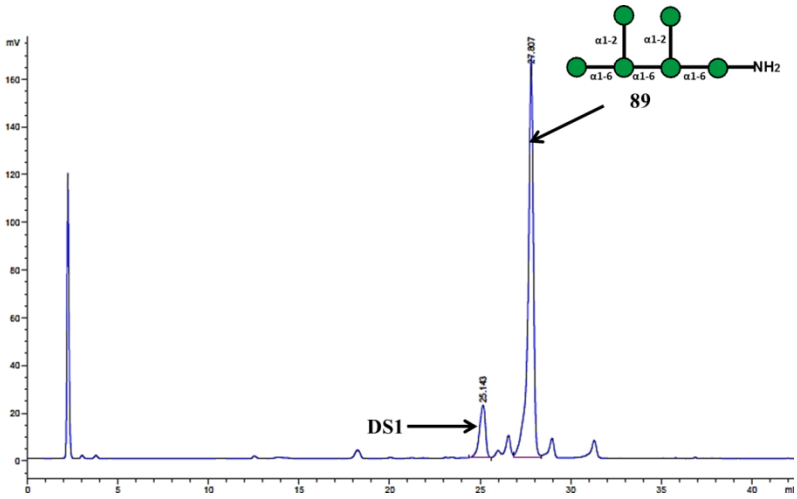

Figure 42: Crude-HPLC trace of branched hexamer **89**.

The synthesis of the linear structure **87** was achieved with full conversion without any deletion sequences observed, whereas the crude HPLC of the branched structure **89** showed the presence of a minor byproduct. Pentasaccharide (**DS1,** *See* experimental section) was identified as a deletion sequence from the last glycosylation, probably due to steric hindrance; however the major product was the desired hexamer **89** (Fig. 42, *See* **Table 2** experimental section).

The synthesis of the branched hexasaccharide **89** is confirmed by its anomeric ^{1}H, ^{13}C NMR spectral signatures. The six anomeric carbons of compound **87** are observed between δ 97.86-98.47 ppm, whereas the carbons of compound **89** were noticed in between δ 97.42-100.10 ppm.$^{1}J_{C-H}$ values for six (1→2)-*trans* linkages of compound **89** were found in the range of 173-178 Hz (Fig. 43).

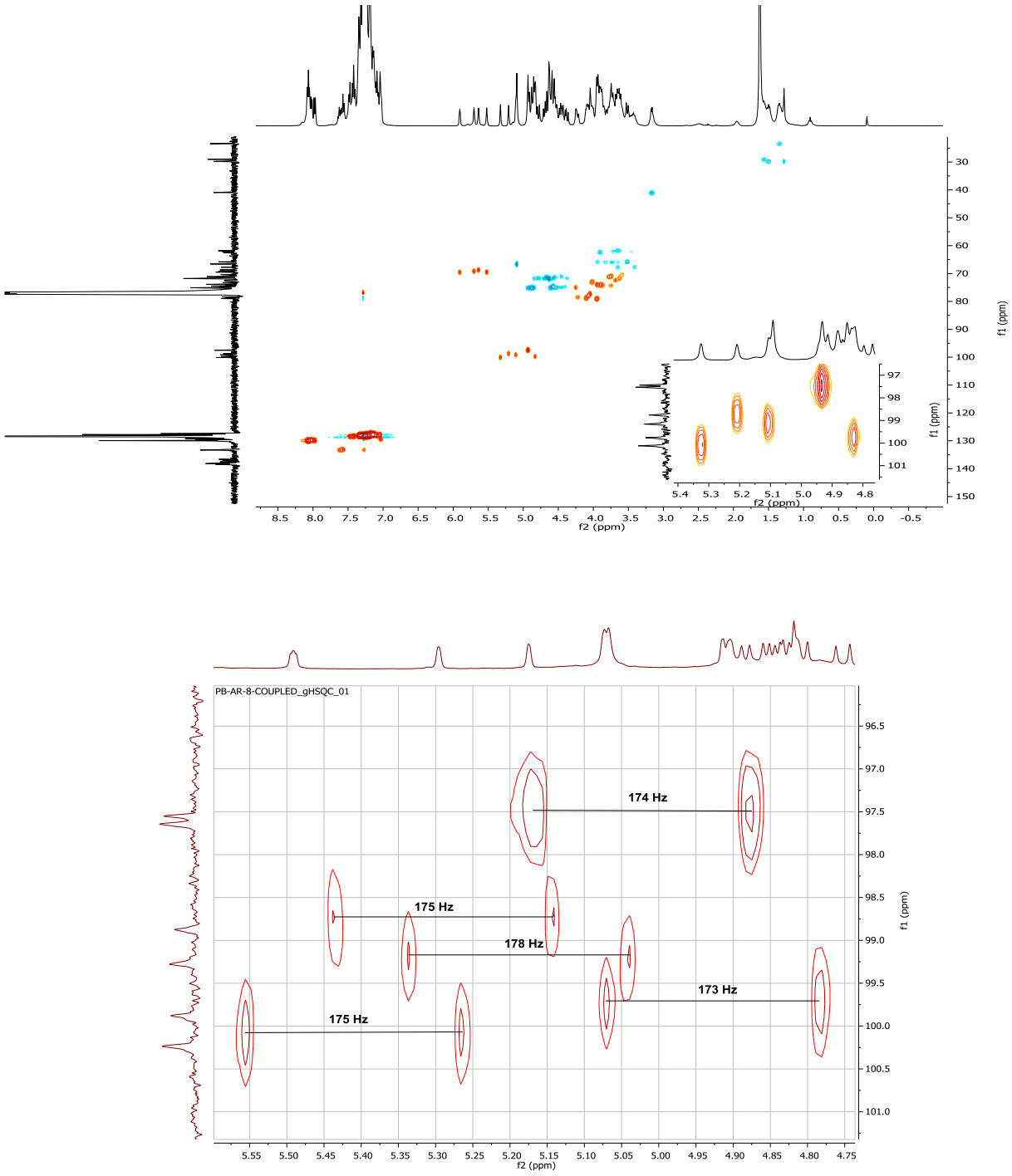

Figure 43: ^{1}H-^{13}C HSQC and coupled-HSQC NMR (600 MHz, $CDCl_3$) of **89**.

3.2.4 Synthesis of longer LM and LAM fragments

The synthesis of longer branched- oilgomannosides with length of 11 to 12 sugar units was further investigated, starting from the optimized conditions used for the synthesis of hexasaccharide **87** and **89**. Unfortunately the automated assembly of the desired undecasaccharide **94** (11mer) resulted in significant deletions sequences, likely due to the steric hindrance during the last two glycosylations. The major compound 11mer **94** was isolated in 7% yield over twenty steps (Fig. 44, Scheme 18).

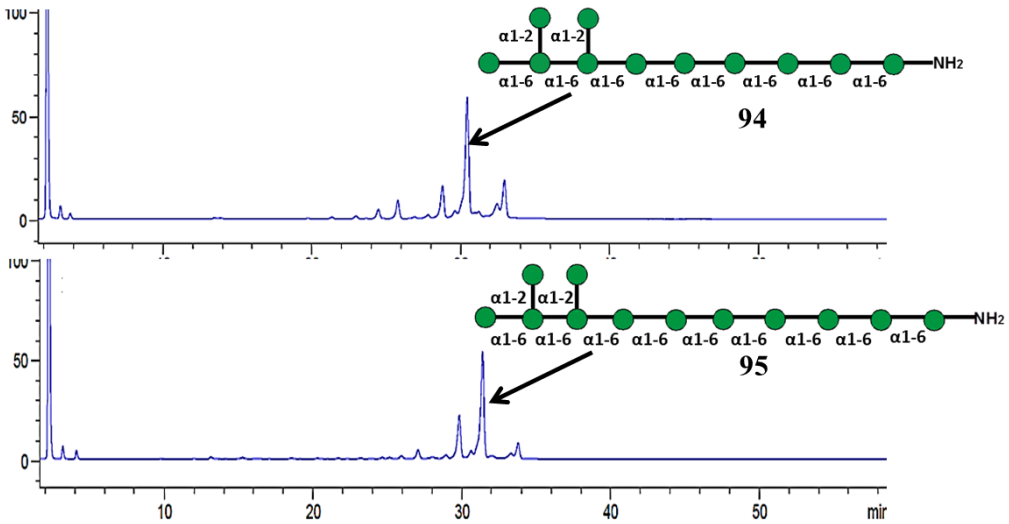

Figure 44: Crude-HPLC trace of **94** (11mer) and **95** (12mer).

To have a better outcome for the synthesis of the 12mer **95**, the synthesis was carried out with 6.5 equiv of **72** and **73** to form linear backbone and 9.75 equiv of **72** for last two cycles of glycosylation (branching). Despite the use of increased amounts of building block **72**, the synthesis resulted into a mixture of 11mer and 12mer. Nevertheless, the target compounds could be easily purified from the byproducts by NP-HPLC affording protected 12mer **95** in 6 % yields over twenty two steps (Fig. 44, Scheme 18).

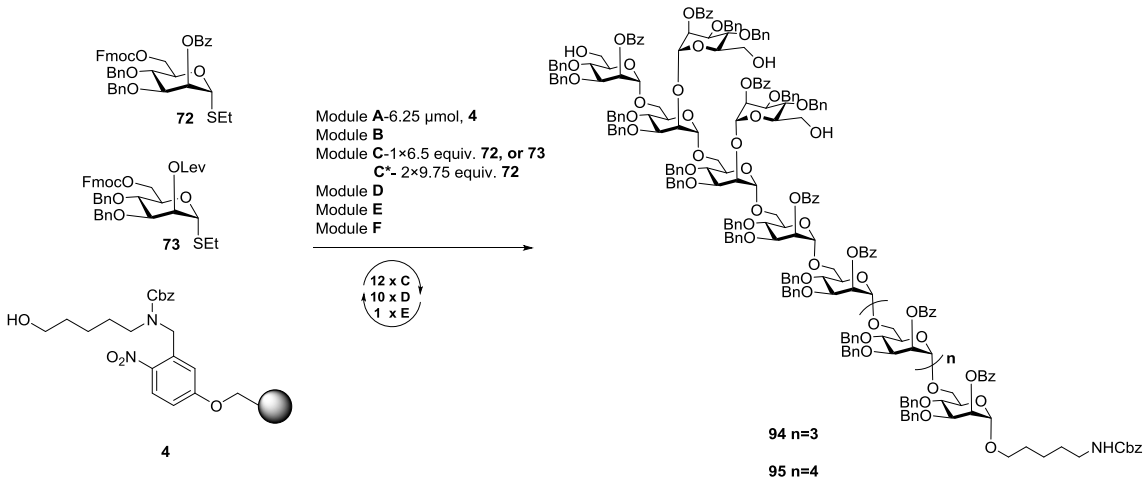

Scheme 18: Automated synthesis of branched LM oligosaccharides **94** and **95**: Reactions and conditions for 12mer: Module **B**-Acidic wash: TMSOTf, CH_2Cl_2, -20 ^oC, (2 min); Module **C**-Glycosylation: **72 or 73**, NIS, TfOH, -20 ^oC, (30 min), CH_2Cl_2/Dioxane (5:1); n=3 and n=4 for **94** and **95** mer respectively; Module **D**-Fmoc deprotection: 20% Et_3N in DMF, 25 ^oC, (3 x 5 min); Module **E**-Lev deprotection: N_2H_4.AcOH in Py/AcOH/H_2O, 25 ^oC, (3 x 30 min); Module **C***- Glycosylation: **72**, NIS, TfOH, -20 ^oC, (30 min), CH_2Cl_2/Dioxane (5:1), 9.75 equiv for **95**; Module **F**-post-automation photocleavage: hυ, CH_2Cl_2, 25 ^oC. Reactions and conditions for **94** are same as for 6mer linear **87** and branched **89**.

With these results in hand, I proceeded further to synthesize the man-LAM fragments. For this target, the synthesis of an additional arabinose building block was required. Building block **74** was prepared in three steps starting from the thioglycoside **96** following a reported procedure (Scheme 19).[232] Regioselective trityl protection of the primary hydroxyl followed by the benzoylation of the remaining hydroxyls groups and deprotection of the trityl group afforded the thioglycoside **97**. Protection of the C-5 hydroxyl group using FmocCl in pyridine gave the desired thioglycoside **74** in high yield.

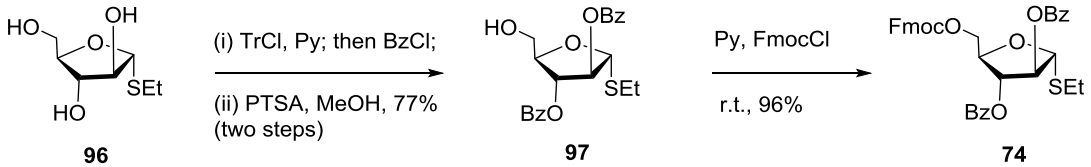

Scheme 19: Synthesis of thioarabinoside **74**.[232]

The synthesis of the 8mer **98** was first tackled using building block **72** and arabinose **74.** For the thiomannoside **72** the conditions mentioned above were used. For the arabinose **74**, each

glycosylation was carried out using two glycosylation cycles as previously reported,[232] (6.5 equiv. of building block for each cycle) at -40 to -20 ºC for 40 min, in the presence of NIS/TfOH using module **C****. The analysis of the crude product (NP-HPLC and MALDI-TOF MS) showed the presence of a deletion sequence, which was identified as a 7mer (**99**) missing one mannose unit (confirmed by MALDI-TOF MS) (Fig. 45), probably due to a technical issue during the automated assembly. Nevertheless the target compound was easily purified from the byproducts by NP-HPLC affording protected 8mer **98** in 9% yield over twelve steps (Scheme 20).

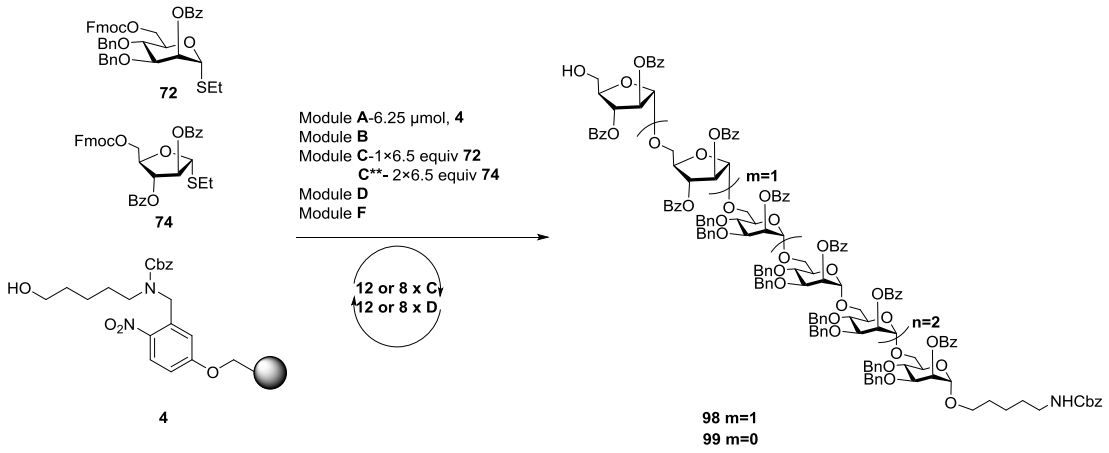

Scheme 20: Automated synthesis of linear 8mer **98**: Reactions and conditions: Module **B**-Acidic wash: TMSOTf, CH_2Cl_2, -20 ºC, (2 min); Module **C**-Glycosylation: **72**, NIS, TfOH, -20 ºC, (30 min), CH_2Cl_2/Dioxane (5:1); Module **C****-Glycosylation: **74**, NIS, TfOH, -20 ºC, (40 min), CH_2Cl_2/Dioxane (5:1); Module **D**-Fmoc deprotection: 20% Et_3N in DMF, 25 ºC, (3 x 5 min); Module **F**-post-automation photocleavage: hυ, CH_2Cl_2, 25 ºC.

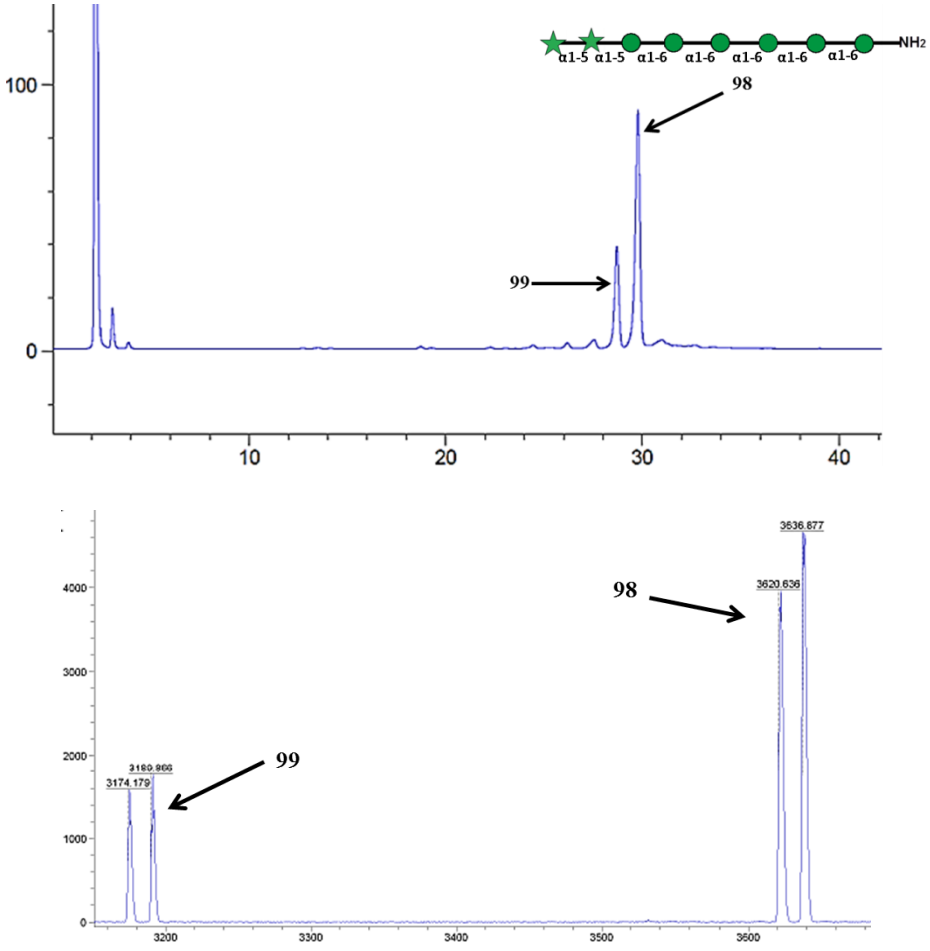

Figure 45: Crude-HPLC trace and MALDI-TOF MS of compound **98**.

For the synthesis of longer structures (**100** and **102**), a procedure using a smaller amount of building block 74 was employed; two glycosylation cycles **(**module **C**)** were used for the introduction of the first arabinose unit connected to the mannoside residue and one cycle for the following units. After the reaction, the resin has been cleaved from the solid support and the crude analyzed using NP-HPLC (Fig. 46). Similarly to the 11mer (**98**) the assembly of the LAM fragment **100** and **102** resulted in significant deletion sequences, which were anyway isolated using NP-HPLC (Scheme 21). As consequence of the several deletion sequences, the final compounds **100** and **102** were obtained in low yields such as 6% and 3% respectively.

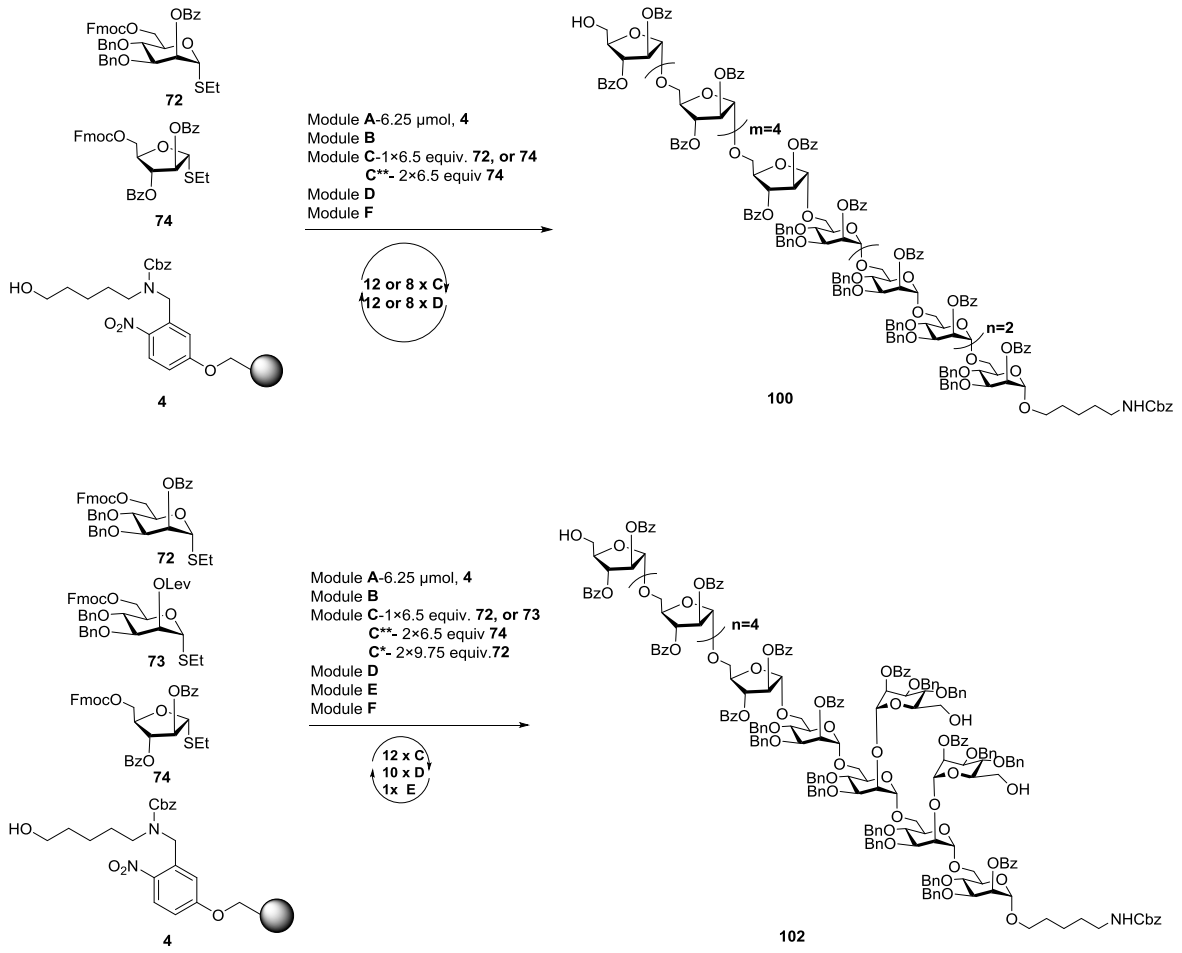

Scheme 21: Automated synthesis of linear LAM 12mer **100**: Reactions and conditions: Module **B**-Acidic wash: TMSOTf, CH_2Cl_2, -20 °C, (2 min); Module **C**-Glycosylation: **72** or **74**, NIS, TfOH, -20 °C, (30 min or 40 min respectively), CH_2Cl_2/Dioxane (5:1); Module **C****-Glycosylation: **74**, NIS, TfOH, -20 °C, (40 min), CH_2Cl_2/Dioxane (5:1); Module **D**-Fmoc deprotection: 20% Et_3N in DMF, 25 °C, (3 x 5 min); Module **F**-post-automation photocleavage: hυ, CH_2Cl_2, 25 °C and Automated synthesis of LAM 12mer **102**: Reactions and conditions: Module **B**-Acidic wash: TMSOTf, CH_2Cl_2, -20 °C, (2 min); Module **C**-Glycosylation: **72 or 73 or 74**, NIS, TfOH, -20 °C, (30 min or 40 min respectively), CH_2Cl_2/Dioxane (5:1); Module **C***- Glycosylation: **72**, NIS, TfOH, -20 °C, (30 min), CH_2Cl_2/Dioxane (5:1), 9.75 equiv; Module **C****-Glycosylation: **74**, NIS, TfOH, -20 °C, (40 min), CH_2Cl_2/Dioxane (5:1); Module **D**-Fmoc deprotection: 20% Et_3N in DMF, 25 °C, (3 x 5 min); Module **E**-Lev deprotection: N_2H_4.AcOH in Py/AcOH/H_2O, 25 °C, (3 x 30 min); Module **F**-post-automation photocleavage: hυ, CH_2Cl_2, 25 °C.

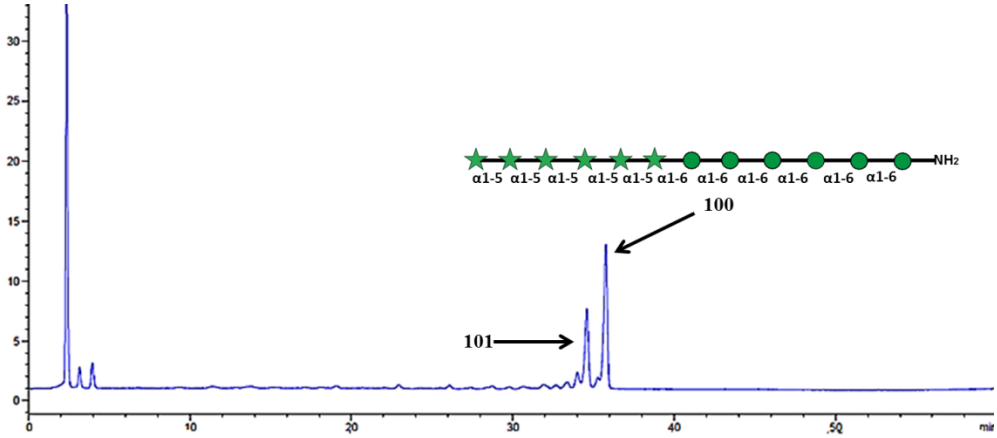

Figure 46: Crude-HPLC trace of a LAM fragment **100**.

3.2.5 Deprotection of the linear and branched LM and LAM oligosaccharides

The global deprotection of the LM and LAM compounds **87, 89, 94, 98, 100** and **102** was achieved by removal of the benzoate ester protecting group using Zemplén methanolysis followed by Pd-catalyzed hydrogenolysis of the carboxybenzyl group and the benzyl ethers (Scheme 22). For the compound **91** further deprotection was not attempted due to low amount of material.

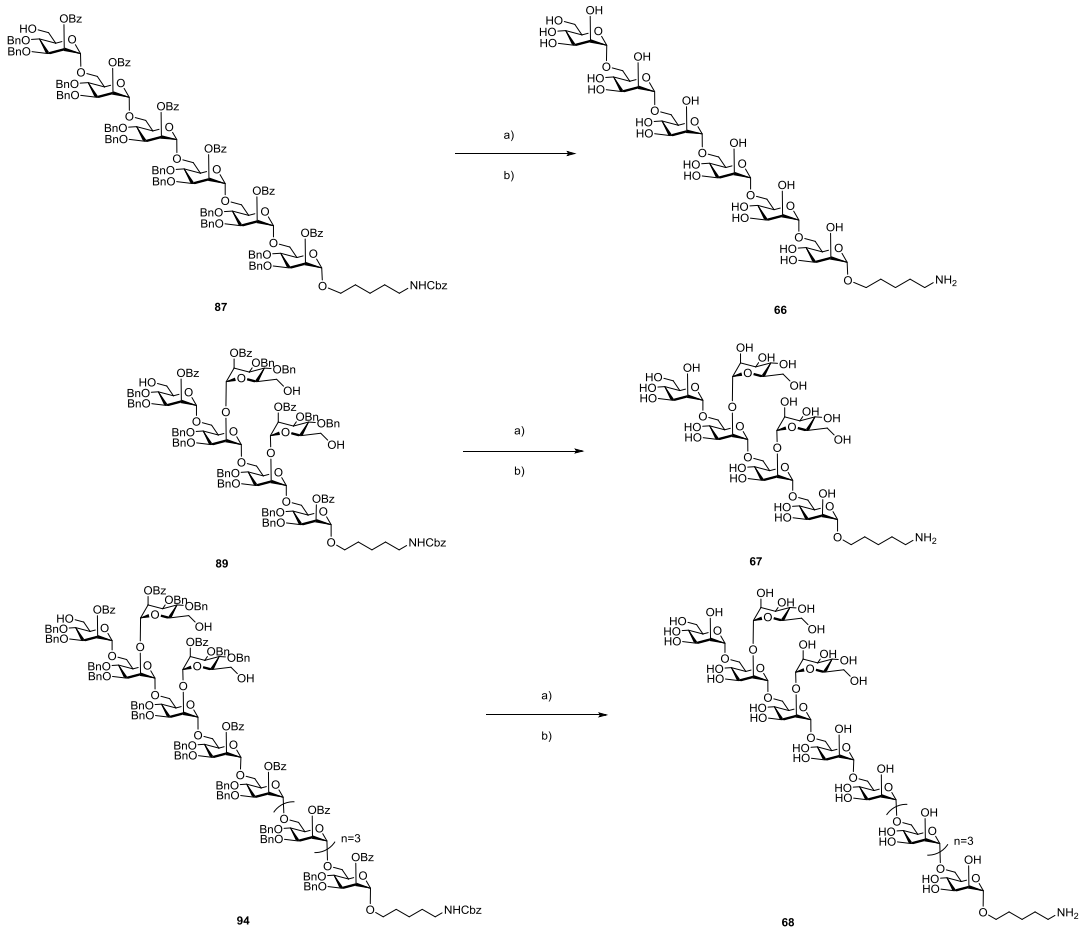

Scheme 22: Global deprotection conditions: a) NaOMe, CH_2Cl_2:MeOH, 1:1, 16 h; b) H_2, Pd/C, CH_2Cl_2:H_2O:*t*-BuOH-1:0.5:0.5, 16 h; **66**-68%, **67**-62% and **68**-50%, over two steps.

LM hexasaccharide fragments **66,** and **67** was purified using reversed phase (RP) SPE (Waters Sep-Pak®, C18) column while undecasaccharide **68** were purified using HPLC (Module G; method C) and obtained in 68%, 62% and 50% yield over two steps, equipping aminopentyl linker at the reducing end respectively (Scheme 23).

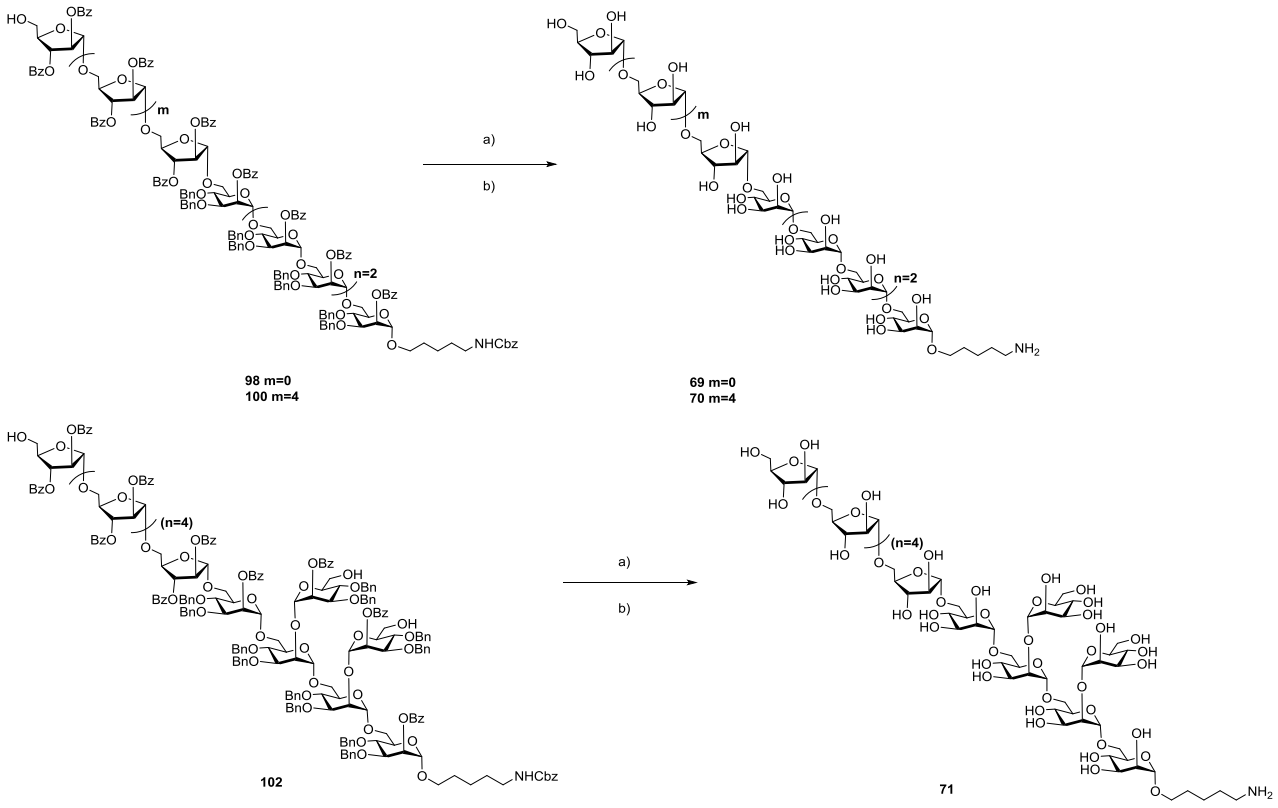

Scheme 23: Global deprotection conditions: a) NaOMe, CH_2Cl_2:MeOH, 1:1, 16 h; b) H_2, Pd/C, CH_2Cl_2:H_2O:*t*-BuOH-1:0.5:0.5, 16 h; **69-71**,40-50%, over two steps.

Similarly, LAM 12mer fragments 69-71 were purified using HPLC (Module G; method C) and obtained in 40-50% yield over two steps, equipping aminopentyl linker at the reducing end respectively (Scheme 23).

3.3 Conclusion and Outlook

A library of LM and LAM fragments has been synthesized. The AGA approach was to make use of multiple sequential glycosylation with three different sugar building blocks. Building block **72** has been synthesized and modified into **73** to enable the introduction of α-(1→2)-branches. Shorter LM structures were easily assembled and the compounds were isolated in short time and high yield (for e.g. **87** in 55% yield over twelve steps), while the synthesis of larger oligosaccharides requires further optimization. Nevertheless, it was possible to isolate these larger structures. The introduction of a capping step after each glycosylation might

improve the yield of the target compounds, as the capping step can remove the unreacted material. In addition, the introduction of a capping step will help to identify the most problematic steps during the assembly of oligosaccharides and permit the synthesis optimization. A fast and reliable capping procedure is currently under investigation at MPIKG by Mr. You Yang. The library of lipoglycans will be used to study the LM and LAM substructure-specific antibodies using glycan array and will be implemented in the library of previously synthesized 35 LAM structures in order to expand the existing database. Also these synthetic lipoglycans structures obtained by AGA will be applied for structure-activity relationship (SAR) studies.

3.4 Experimental Section

3.4.1 General methods

All reagents were commercially available and used as supplied without further purification. Anhydrous solvents were either used from a dry solvent system (jcmeyer-solvent system) or as purchased. All glasswares were oven-dried before use. Analytical thin layer chromatography (TLC) was performed on Merck silica gel 60 F254 plates (0.25 mm). Flash chromatography was performed on Fluka Kieselgel 60 (0.04-0.063 mm).TLC chromatograms were visualized either by UV irradiation or by charring the TLC plate dipped in ammonium molybdate/ cerium (IV) sulfate solutions. NMR data were obtained on Bruker Ascend 400 MHz, Varian 400 MHz, Varian 600 MHz, and Bruker AVANCE III 700 MHz NMR spectrometers. NMR chemical shifts (δ) are reported in ppm and coupling constants (*J*) in Hz. Spectra recorded in $CDCl_3$ used the solvent residual peak chemical shift as internal standard ($CDCl_3$: 7.26 ppm ^{1}H, 77.1 ppm ^{13}C). Spectra recorded in D_2O used the solvent residual peak chemical shift as internal standard as internal standard in ^{1}H NMR (D_2O: 2.08 ppm). Optical rotations were measured using a UniPol L1000 polarimeter (Schmidt&Haensch) with concentrations expressed as g/100 mL. Loading determination of functionalized resins was obtained using a Shimadzu UV-MINI-1240 UV spectrometer. High resolution mass spectra were obtained using a 6210 ESI-TOF mass spectrometer (Agilent). MALDI-TOF spectra were recorded on a Bruker Daltonics Autoflex Speed, using a 2,4,6-trihydroxyacetophenone (THAP) and 2,5-dihydroxybenzoic acid (DHB) matrix. LCMS chromatograms were recorded on an Agilent 1100 Series spectrometer. Analytical HPLC was performed on an Agilent 1200 series coupled to a quadrupole ESI LC/MS 6130 using a YMC-Pack DIOL-300-NP column (150 x 4.6 mm). Preparative HPLC was performed on an Agilent 1200 series using a preparative YMC-Pack-Diol-300-NP (150 x 20 mm).

3.4.2 Methods of synthetic chemistry

3.4.2.1 Synthesis of Photolabile Linker and Functionalization of Resin[150]

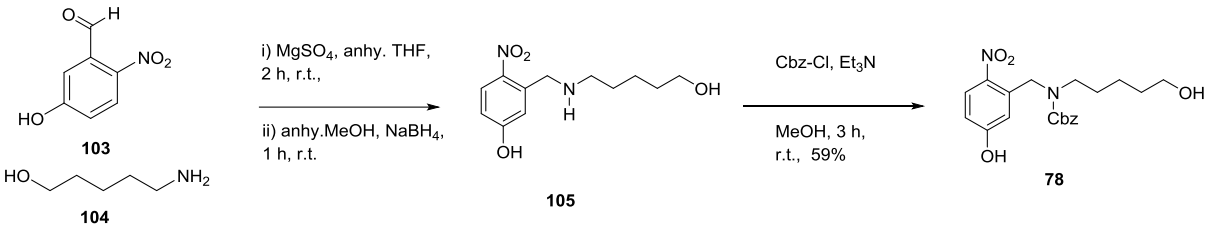

To a suspension of 5-hydroxy-2-nitrobenzaldehyde **103** (2.00 g, 12.0 mmol) and $MgSO_4$ (4.75 g, 39.5 mmol) in anhydrous THF (120 mL) at room temperature was added 5-aminopentanol **104** (1.43 mL, 13.2 mmol). After 2 hours, the solution was filtered and concentrated in vacuo. To a solution of the crude residue (imine) in anhydrous MeOH (80 mL) at room temperature was slowly added $NaBH_4$ (452 mg, 12.0 mmol). After 1 hour, acetone (30 mL) was slowly added to quench excess $NaBH_4$ and the solution concentrated in vacuo to furnish compound **105** as yellow foam. To a solution of the crude foam and triethylamine (3.32 mL, 23.9 mmol) in anhydrous MeOH (120 mL) at room temperature under Ar was added benzyl chlorocarbonate (2.05 mL, 14.4 mmol). After 3 hours, the reaction mixture was concentrated in vacuo, redissolved in DCM, washed two times with 10% aq. HCl, dried over MgSO4, filtered, and concentrated in vacuo. The crude residue was purified via flash chromatography over silica gel using hexanes:EtOAc:MeOH (1:1:0.05) to afford linker **78** as a thick yellow oil (2.75 g, 59%) over three steps. R_f in (Hexanes/EtOAc/MeOH 1:1:0.05) = 0.35; ^{1}H-NMR (400 MHz, $CDCl_3$, mixture of rotamers) δ 8.16 (d, *J* = 9.0 Hz, 1H), 7.36-7.08 (m, 5H), 6.86 – 6.68 (m, 2H), 5.05 (s, 2H), 4.90 (s, 2H), 3.64 – 3.56 (m, 2H), 3.36 (t, *J* = 6.9 Hz, 2H), 1.59 – 1.47 (m, 4H), 1.45 – 1.37 (m, 2H); ^{13}C-NMR (100 MHz, $CDCl_3$, mixture of rotamers) δ 162.81, 162.18, 157.25, 156.78, 139.79, 137.87, 135.97, 129.06, 128.67, 128.63, 128.30, 128.26, 127.64, 115.06, 114.89, 113.83, 113.16, 67.75, 66.89, 62.77, 62.37, 50.09, 49.13, 31.96, 29.81, 27.86, 22.90.

All spectroscopic data are in good accordance with the literature.[150]

Functionalization of Resin [150]

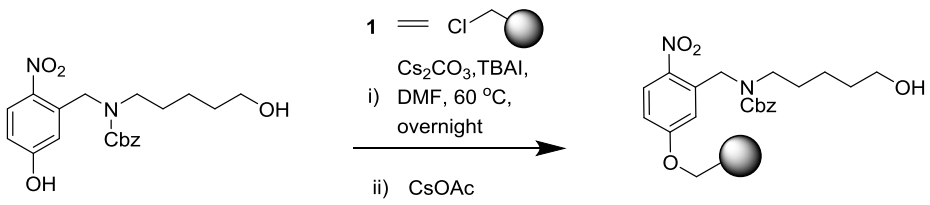

78 4

Merrifield resin **1** (~0.50 mmol/g, 3.31 g, 1.655 mmol, 1.0 eq.) and linker **78** (2.571 g, 6.62 mmol, 4.0 eq.) were taken up in a minimal amount of anhydrous DMF (~4 mL DMF/g resin) to completely swell the resin and solubilize the linker. The suspension was then degassed by placing the flask under high vaccum for a couple of minutes, followed by refilling the evacuated flask with Argon. After repeating this degassing procedure two more times, Cs_2CO_3 (2.15 g, 6.62 mmol, 4.0 eq.) and TBAI (0.611 g, 1.655 mmol, 1.0 eq.) were added to the flask and the entire suspension rotated on a rotovap at 60 °C and atmospheric pressure overnight. The next morning, water was added to the resin to dissolve all solids and the resin was subsequently washed with THF/water (1/1), THF, DMF, MeOH, DCM, MeOH, and finally DCM (six times each) to remove the yellow color. The resin was transferred again to a round bottom flask, swollen in a minimal amount of DMF (~4 mL DMF/g resin) and the flask degassed as above. Afterwards, CsOAc (0.635 g, 3.311 mmol) was added and the entire suspension rotated on a rotovap at 60 °C and atmospheric pressure overnight. The next morning, the resin was washed with THF/water (1/1), THF, DMF, MeOH, DCM, MeOH, and finally DCM (six times each) to remove the yellow color. It was then dried under high vacuum overnight affording **4** and stored in the dark.

Resin loading determination[142]

Resin loading was determined by performing one glycosylation with excess of **72** (2 cycles of Module **C**) on synthesizer followed by DBU promoted Fmoc-cleavage and determination of dibenzofulvene production by measuring its UV absorbance at 294 and 304 nm. The loading of the resin was calculated as an average of the values resulting from the formulas: $Absorption_{304\ nm} \times 16.4$/mass of resin used in mg (for 304 nm) and $Absorption_{294\ nm} \times 14.2$/mass of resin used in mg (for 294 nm). Loading of linker functionalized resin **4**: 0**.37 mmol/g.**

3.4.2.2 Synthesis of Building Block

Ethyl 1-thio-α-D-mannopyranoside (82)

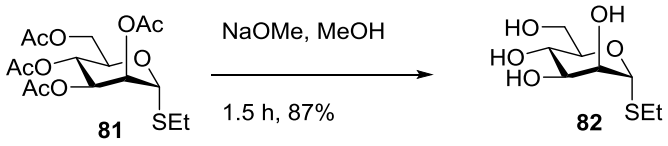

In a 500 mL of round-bottomed flask a solution of **81** (40 g, 102 mmol) in MeOH (170 mL), 0.5 M sodium methoxide solution in methanol (40 mL, 20.39 mmol) was added at room temperature and stirred for 1.5 h. After the reaction was complete as indicated by TLC, the mixture was neutralized using Amberlite IR-120 ion-exchange resin, filtered and concentrated in vacuum to yield slightly yellowish oil. The compound was further purified by a short flash column chromatography on silica gel (DCM:EtOAc:MeOH, 50:40:10) and dried under high vacuum overnight to give **82** (20 g; 89 mmol, 87%) as a solid and directly used in the next step. R_f (MeOH/DCM 1:9)= 0.16; ^{1}H NMR (400 MHz, CD_3OD) δ 5.25 (s, 1H), 3.89 (s, 2H), 3.82 (d, J = 11.8 Hz, 1H), 3.73 (dd, J = 11.7, 5.8 Hz, 1H), 3.65 (t, J = 7.5 Hz, 2H), 2.74 – 2.56 (m, 2H), 1.29 (t, J = 7.3 Hz, 3H); ^{13}C NMR (100 MHz, CD_3OD) δ 84.49, 73.40, 72.30, 71.75, 67.41, 61.38, 48.20, 47.99, 47.77, 47.56, 47.35, 47.13, 46.92, 24.25, 13.80; HRMS (ESI): calculated for $C_8H_{16}O_5S$ $[M+Na]^+$ 247.0611, found 247.0625.

Ethyl 4,6-*O*-benzylidene-1-thio-α-D-mannopyranoside (83)

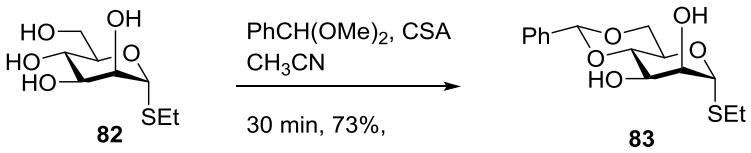

In a 500 mL of round-bottomed flask a suspension of **82** (8 g, 35.37 mmol) in acetonitrile (100 mL) was added CSA (2 g, 8.92 mmol) (try to dissolve the compound by vigorous shaking) followed by the addition of benzaldehyde dimethyl acetal (6.42 mL, 42.8 mmol) at room temperature. The reaction mixture solidifies during CSA addition, which indicates the

progress of the reaction (monitor by TLC and then only quench the reaction). After 20-40 min the reaction mixture was quenched with Et_3N (3 mL, slowly dropwise addition). The crude mixture was extracted with ethyl acetate (2 X 250 mL) and water (2 X 250 mL) and the phases were separated. The organic layer was washed with brine (2 X 150 mL) and dried over anhydrous Na_2SO_4, filtered, and concentrated in vacuum. Removal of solvents under reduced pressure gave a fluffy solid that was washed with hexane (3 X 20 mL). The desired product dried under high vacuum to give **83** (8.2 g; 26.2 mmol, 74%) as white fluffy solid. R_f (EtOAc/Hexanes 4:6) = 0.2; ^{1}H NMR (400 MHz, $CDCl_3$) δ 7.54 – 7.34 (m, 5H), 5.57 (s, 1H), 5.37 (s, 1H), 4.23 (dq, *J* = 10.7, 5.1 Hz, 2H), 4.15 (d, *J* = 3.4 Hz, 1H), 4.10 – 4.03 (m, 1H), 3.98 (d, *J* = 9.1 Hz, 1H), 3.90 – 3.81 (m, 1H), 2.72 – 2.64 (m, 2H), 1.30 (d, *J* = 7.3 Hz, 3H); ^{13}C NMR (100 MHz, $CDCl_3$) δ 129.25, 128.41, 126.29, 102.33, 84.31, 79.19, 72.35, 69.15, 68.65, 63.30, 25.09, 14.86; HRMS (ESI): calculated for $C_{15}H_{20}O_5S$ $[M+Na]^+$ 335.0924, found 335.0939.

Ethyl 4,6-*O*-benzylidene-3-*O*-benzyl-1-thio-α-D-mannopyranoside (84)

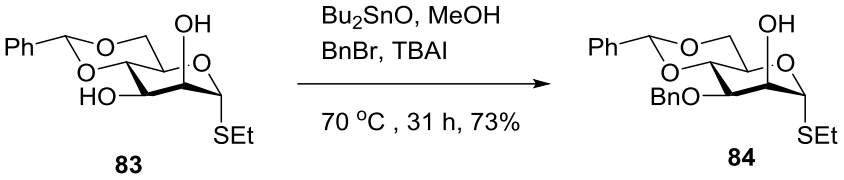

In a 500 mL round-bottomed flask, dibutylstannanone (0.274 g, 1.1 mmol) was added to a solution of **83** (6 g, 19.21 mmol) in anhydrous toluene and the reaction mixture was refluxed at 110 °C for 12 h. Removal of solvent under reduced pressure from the reaction mixture afforded stannylene acetal which was kept under high vacuum overnight. The crude acetal was dissolved in DMF and TBAI (0.851 g, 2.3 mmol), BnBr (2.74 mL, 23.05 mmol) was added to the solution under an nitrogen atmosphere. The reaction mixture was heated at 70 °C for 48 h. The crude mixture was extracted with ethyl acetate (2 X 250 mL) and water (2 X 250 mL) and the phases were separated. The organic layer was washed with brine (2 X 150 mL) and dried over anhydrous Na_2SO_4, and filtered. The organic layer concentrated in vacuum and purified by column chromatography on silica gel to give **84** (5.6 g; 14 mmol, 72%) as a white solid. R_f (EtOAc/Hexanes 4:6) = 0.5; ^{1}H NMR (400 MHz, $CDCl_3$) δ 7.52 –

7.49 (m, 2H), 7.39 – 7.34 (m, 5H), 7.35 – 7.34 (m, 3H), 5.62 (s, 1H), 5.38 (d, *J* = 1.1 Hz, 1H), 4.86 (d, *J* = 11.7 Hz, 1H), 4.71 (d, *J* = 3.7 Hz, 1H), 4.69 (d, *J* = 2.4 Hz, 1H), 4.28 – 4.21 (m, 2H), 4.13 – 4.11 (m, 1H), 3.92 – 3.88 (m, 2H), 2.70 – 2.54 (m, 2H), 1.30 (d, *J* = 7.3 Hz, 3H); ^{13}C NMR (100 MHz, $CDCl_3$) δ 137.78, 137.48, 128.99, 128.60, 128.54, 128.27, 128.04, 127.89, 127.70, 127.02, 126.09, 101.63, 84.05, 79.14, 75.86, 73.13, 71.45, 68.69, 65.44, 63.81, 24.95, 14.88; HRMS (ESI): calculated for $C_{22}H_{26}O_5S$ $[M+Na]^+$ 425.1393, found 425.1407.

Ethyl 2-*O*-benzoyl-4,6-*O*-benzylidene-3-*O*-benzyl-1-thio-α-D-mannopyranoside (85)

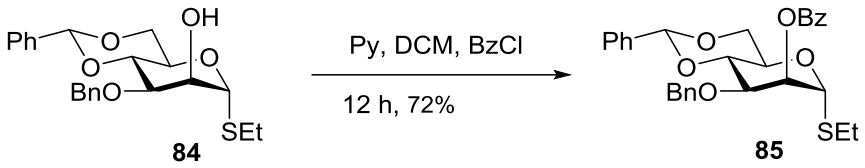

To stirred solution of **84** (5.53 g, 13.74 mmol) in anhydrous DCM and pyridine (ratio: 2:1, 92: 45.8 mL) were added at 0 °C a solution of BzCl (2.4 mL, 20.61 mmol) in DCM (3 mL) dropwise and DMAP (0.168 g, 1.4 mmol). The reaction mixture was kept stirring for 12 h. After the completion of reaction as indicated by TLC, reaction mixture was extracted with DCM and the combined organic layers were washed with 1M HCl (2 X 100 mL), saturated $NaHCO_3$ (2 X 150 mL), brine (2 X 150 mL), and dried over Na_2SO_4, filtered and concentrated in vacuum. The crude product was purified by column chromatography on silica gel (10-20% ethyl acetate / hexane) to give **85** (5 g; 9.87 mmol, 72%) as white foam. R_f (EtOAc/Hexanes 4:6) = 0.7; ^{1}H NMR (400 MHz, $CDCl_3$) δ 8.16 – 8.06 (m, 2H), 7.60 (t, *J* = 7.4 Hz, 1H), 7.54 – 7.45 (m, 5H), 7.38 (p, *J* = 4.5, 3.7 Hz, 3H), 7.33 – 7.29 (m, 2H), 5.68 (s, 1H), 5.67 – 5.64 (m, 1H), 5.42 – 5.39 (m, 1H), 4.78 – 4.64 (m, 2H), 4.33 – 4.18 (m, 3H), 4.07 (dd, *J* = 9.7, 3.4 Hz, 1H), 3.98 – 3.89 (m, 1H), 2.71 – 2.53 (m, 2H), 1.31 – 1.20 (m, 3H); ^{13}C NMR (100 MHz, $CDCl_3$) δ 165.74, 137.78, 137.41, 133.37, 129.96, 129.74, 128.98, 128.47, 128.33, 128.21, 127.68, 127.65, 126.16, 101.68, 83.57, 78.94, 74.30, 72.16, 68.67, 64.61, 25.67, 14.96; LCMS m/z calculated for $C_{29}H_{32}O_6S$ $[M+ Na]^+$: 529.6 found: 529.2.

Ethyl 2-*O*-benzoyl-3,4-di-*O*-benzyl-1-thio-α-D-mannopyranoside (86)

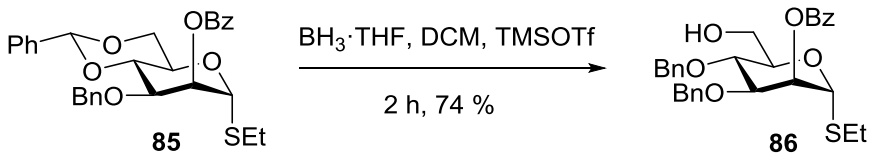

In a 250 mL round-bottomed flask, **85** (4.77 g, 9.42 mmol) was dissolved in anhydrous DCM (50 mL) followed by addition of 1M solution of BH_3·THF (47.1 mL, 47.11 mmol) and TMSOTf (0.27 ml, 1.4 mmol) at room temperature for 1 h. (check TLC for the reaction mixture every 30 min). The reaction mixture was quenched with Et_3N (5 mL), followed by the slow addition of MeOH (20 mL). The reaction mixture was concentrated under reduced pressure and co-evaporated with methanol (2 X 30 mL) twice to give crude product that was purified by column chromatography on silica gel (10-20% ethyl acetate / hexane), to afford **86** (3.55 g; 7 mmol, 74%) as colorless liquid. R_f (EtOAc/Hexanes 4:6) = 0.56; ^{1}H NMR (400 MHz, $CDCl_3$) δ 8.12 – 8.11 (m, 1H), 8.10 (dd, *J* = 1.9, 1.4 Hz, 1H), 7.63 (ddt, *J* = 8.1, 6.9, 1.3 Hz, 1H), 7.53 – 7.48 (m, 2H), 7.39 – 7.29 (m, 9H), 5.70 (dd, *J* = 2.7, 1.7 Hz, 1H), 5.40 (d, *J* = 1.6 Hz, 1H), 4.95 (d, *J* = 10.9 Hz, 1H), 4.78 (d, *J* = 11.4 Hz, 1H), 4.69 (d, *J* = 10.9 Hz, 1H), 4.59 (d, *J* = 11.4 Hz, 1H), 4.13 – 4.02 (m, 3H), 3.91 – 3.86 (m, 2H), 2.72 – 2.59 (m, 2H), 1.31 (d, *J* = 7.4 Hz, 3H); ^{13}C NMR (100 MHz, $CDCl_3$) δ 165.65, 138.18, 137.67, 133.34, 82.56, 78.54, 75.28, 74.12, 72.26, 71.60, 70.98, 62.11, 25.65, 14.91; HRMS (ESI): calculated for $C_{29}H_{32}O_6S$ $[M+Na]^+$ 531.1812, found 531.1823.

Ethyl 2-*O*-benzoyl-3,4-di-*O*-benzyl-6-*O*-fluorenylmethoxycarbonyl-1-thio-α-D-mannopyranoside (72)

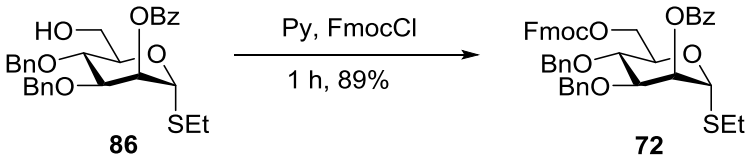

In a 250 mL round-bottomed flask, **86** (3.5 g, 6.88 mmol) was dissolved in anhydrous DCM (50 mL) and pyridine (1.63 mL, 20.64 mmol), followed by the addition of FmocCl (3.5 g, 13.76 mmol). The yellow solution is stirred at room temperature until the reaction goes to

completion (reaction monitored by TLC) for 1 h. The reaction mixture was extracted with DCM (2 X 100 mL) and the combined organic layers were washed with 1M HCl (1 X 25 mL), saturated $NaHCO_3$ (1 X 100 mL), brine (1 X 100 mL) and dried over Na_2SO_4, filtered, and concentrated in vacuum. The product is purified by column chromatography (10% ethyl acetate / hexane) to give **72** (4.5 g; 6 mmol, 89%) as a foamy white solid. R_f (EtOAc/Hexanes 3:7) = 0.75; $[\alpha]_D^{20}$ = + 42.29º (c = 1, $CHCl_3$); IR ν_{max} (film) 3067, 3033, 2930, 1749, 1722, 1603, 1498, 1479, 1452, 1395, 1318, 1257, 1178, 1096, 1028, 969, 788, 759, 741, 712, 700 cm^{-1}; ^1H NMR (400 MHz, $CDCl_3$) δ 8.12 (d, *J* = 7.7 Hz, 2H), 7.76 (d, *J* = 7.6 Hz, 2H), 7.61 (dd, *J* = 13.3, 7.7 Hz, 2H), 7.53 (t, *J* = 7.7 Hz, 1H), 7.40 (q, *J* = 7.7 Hz, 4H), 7.34 – 7.24 (m, 12H), 5.71 (s, 1H), 5.42 (s, 1H), 4.92 (d, *J* = 11.4 Hz, 1H), 4.80 – 4.75 (m, 1H), 4.59 (dd, *J* = 21.3, 11.1 Hz, 2H), 4.47 (s, 2H), 4.39 (d, *J* = 7.7 Hz, 2H), 4.35 – 4.23 (m, 2H), 4.07 – 3.94 (m, 2H), 2.65 (tp, *J* = 14.8, 8.0, 7.2 Hz, 2H), 1.33 – 1.25 (m, 3H); ^{13}C NMR (100 MHz, $CDCl_3$) δ 165.58, 155.13, 143.41, 143.25, 141.25, 137.90, 137.50, 133.27, 129.91, 128.46, 128.16, 127.88, 127.15, 125.20, 120.03, 82.55, 78.61, 75.20, 73.99, 71.59, 70.61, 70.16, 66.79, 46.75, 25.69, 14.95; HRMS (ESI): calculated for $C_{44}H_{42}O_8S$ $[M+Na]^+$ 753.2493, found 753.2421.

Ethyl 3,4-di-*O*-benzyl-1-thio-α-D-mannopyranoside (92)

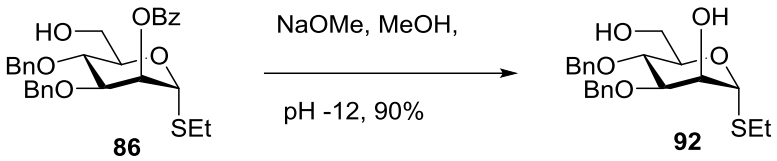

In a 100 mL of round-bottomed flask a solution of **86** (1.4 g, 2.75 mmol in MeOH (27.5 mL), 0.5 M sodium methoxide solution in methanol (pH adjusted between- 12-14) was added at room temperature and stirred for 4 h. After the reaction was complete as indicated by TLC, the mixture was neutralized using Amberlite IR-120 ion-exchange resin, filtered and concentrated in vacuum to yield clear oil. The compound was further purified by a short flash column chromatography on silica gel (DCM:EtOAc:MeOH, 50:40:10) and dried under high vacuum overnight to give **92** (1 g; 2.5 mmol, 90%) as a solid and directly used in the next step. R_f (EtOAc/Hexanes 6:4) = 0.38; ^1H NMR (400 MHz, $CDCl_3$) δ 7.28 – 7.18 (m, 10H), 5.26 (s, 1H), 4.79 (d, J = 10.9 Hz, 1H), 4.62 – 4.56 (m, 3H), 4.01 (s, 1H), 3.95 (dt, J = 9.8, 2.9 Hz, 1H), 3.88 (t, 1H), 3.75 (dd, J = 9.0, 3.1 Hz, 3H), 2.53 – 2.39 (m, 2H), 1.15 (t, J =

7.4 Hz, 3H); ^{13}C NMR (100 MHz, $CDCl_3$) δ 138.31, 137.69, 128.77, 128.62, 128.27, 128.13, 128.10, 128.00, 83.34, 80.44, 75.36, 74.46, 72.35, 71.96, 70.08, 62.23, 25.04, 14.91; LCMS m/z calculated $C_{37}H_{38}O_7S$ for $[M+ Na]^+$: 427.5, found: 427.2.

Ethyl 3,4-di-*O*-benzyl-6-*O*-fluorenylmethoxycarbonyl-1-thio-α-D-mannopyranoside (93)

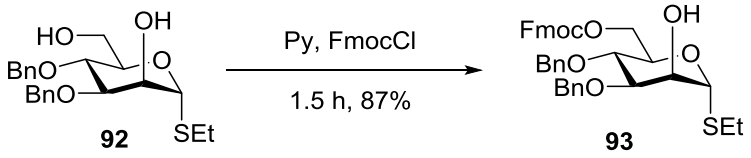

In a 100 mL round-bottomed flask, **92** (1 g, 2.47 mmol) was dissolved in anhydrous DCM (25 mL) and pyridine (0.39 mL, 4.94 mmol), followed by the addition of FmocCl (0.7 g, 2.72 mmol). The yellow solution is stirred at room temperature until the reaction goes to completion (reaction monitored by TLC) for 1.5 h. The reaction mixture was extracted with DCM (2 X 30 mL) and the combined organic layers were washed with 1M HCl (1 X 15 mL), saturated $NaHCO_3$ (1 X 50 mL), brine (1 X 30 mL) and dried over Na_2SO_4, filtered, and concentrated in vacuum. The product is purified by column chromatography (10% ethyl acetate / hexane) to give **93** (1.35 g; 2 mmol, 87%) as a white foam. R_f (EtOAc/Hexanes 4:6) = 0.56; ^{1}H NMR (400 MHz, $CDCl_3$) δ 7.77 (d, J = 7.5, 1.0 Hz, 2H), 7.62 (t, J = 7.3, 1.0 Hz, 2H), 7.43 – 7.27 (m, 14H), 5.40 (s, 1H), 4.91 (dd, J = 11.0, 1.2 Hz, 1H), 4.70 (s, 2H), 4.63 (dd, J = 10.9, 1.1 Hz, 1H), 4.47 – 4.40 (m, 2H), 4.39 – 4.34 (m, 2H), 4.32 – 4.27 (m, 1H), 4.25 (d, J = 7.4 Hz, 1H), 4.12 (dt, J = 3.7, 1.7 Hz, 1H), 3.90 – 3.86 (m, 1H), 3.85 – 3.81 (m, 1H), 2.69 – 2.65 (m, 1H), 2.63 – 2.52 (m, 1H), 1.30 (t, 3H); ^{13}C NMR (100 MHz, $CDCl_3$) δ 155.19, 143.56, 143.41, 141.37, 138.02, 137.55, 128.76, 128.61, 128.14, 128.12, 128.01, 127.97, 127.27, 125.37, 125.31, 83.40, 80.54, 75.32, 74.36, 72.22, 70.05, 69.81, 66.93, 46.80, 25.04, 14.95; LCMS m/z calculated for $C_{37}H_{38}O_7S$ $[M+ Na]^+$: 649.2 found: 649.2.

Ethyl 3,4-di-*O*-benzyl-6-*O*-fluorenylmethoxycarbonyl-2-*O*-levulinoyl-1-thio-α-D-mannopyranoside (73)

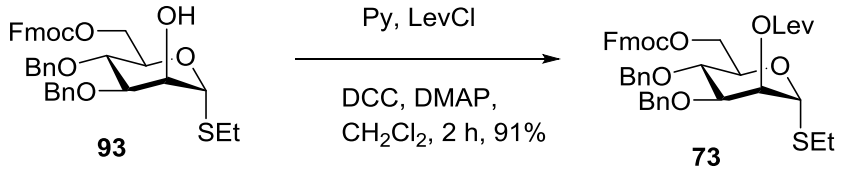

A suspension of DCC (0.19 g, 0.94 mmol) and DMAP (0.01 g, 0.09 mmol) in anhydrous DCM (3 mL) was added to a solution of **93** (0.19 g, 0.30 mmol) and 4-oxopentanoic acid (0.07 ml, 0.69 mmol) in DCM (5 mL) at 0 °C. The clear solution is stirred at room temperature (reaction monitored by TLC) for 1.5 h. The mixture was filtered over pad of celite and the filtrate concentrated in vacuum. The product is purified by column chromatography (20% ethyl acetate / hexane) to give **73** (0.2 g; 0.3 mmol, 91%) as a sticky white solid. R_f (EtOAc/Hexanes 4:6) = 0.55; $[\alpha]_D^{20}$ = + 50.30° (c = 1, $CHCl_3$); IR ν_{max} (film) 3033, 2930, 1745, 1721, 1498, 1453, 1368, 1256, 1156, 1100, 1031, 969, 851, 788, 759, 742, 700 cm^{-1}; ^1H NMR (400 MHz, $CDCl_3$) δ 7.77 (d, J = 7.6 Hz, 2H), 7.62 (t, J = 7.1 Hz, 2H), 7.40 (t, J = 7.5 Hz, 2H), 7.35 – 7.28 (m, 12H), 5.46 (s, 1H), 5.28 (s, 1H), 4.69 (d, J = 11.1 Hz, 1H), 4.58 (d, J = 10.9 Hz, 1H), 4.52 (d, J = 11.1 Hz, 1H), 4.43 (t, J = 7.0 Hz, 4H), 4.27 (q, J = 8.6, 7.8 Hz, 2H), 3.94 (dd, J = 9.3, 3.2 Hz, 1H), 3.79 (t, J = 9.5 Hz, 1H), 2.77 – 2.67 (m, 4H), 2.66 – 2.55 (m, 2H), 2.15 (s, 3H), 1.27 (t, J = 7.2 Hz, 3H); ^{13}C NMR (100 MHz, $CDCl_3$) δ 206.39, 171.99, 155.17, 143.55, 143.38, 141.41, 141.39, 138.09, 137.65, 128.55, 128.33, 128.15, 128.00, 127.95, 127.27, 127.25, 125.27, 125.22, 120.17, 82.47, 78.55, 75.33, 74.32, 71.79, 70.52, 70.17, 70.00, 66.92, 46.87, 38.06, 29.88, 28.29, 25.68; HRMS (ESI): calculated for $C_{42}H_{44}O_9S$ $[M+Na]^+$ 747.2598, found 747.2532.

3.4.2.3 Pre-Automation Steps

Preparation of Stock Solutions for Automated Synthesis:

A. **Building Block Solution:** For 0.00625 mmol scale 0.041 mmol of building block and for 0.0125 mmol scale 0.081 mmol of building block was dissolved in 1 mL of DCM.
B. **Acidic Wash Solution:** The solution prepared by adding 0.45 mL of TMSOTf to 40 mL of anhydrous DCM. The solution was kept at room temperature during the automation run.(62.5 mM TMSOTf)
C. **Activator Solution:** Recrystallized NIS (1.35 g) was dissolved in a 2:1 mixture of anhydrous DCM and anhydrous Dioxane (40.0 mL). Then Triflic Acid (55 μL) was added and the resulting solution purged with Ar for 1-2 minutes. (150 mM NIS/15 mM TfOH)
D. **Fmoc deprotection solution:** Triethylamine (20 mL) was added in anhydrous DMF (80 mL) and the solution was purged with Ar (20% Et_3N solution).
E. **Lev deprotection solution:** Hydrazine Acetate (550 mg) was dissolved in a solution of 4:1:0.25 Pyridine:AcOH:H_2O (40 mL). (150 mM $N_2H_4 \cdot AcOH$)

3.4.2.4 Modules for automated synthesis

Module A: Preparation of resin for synthesis: Automated synthesis of compound **87**, and **89** was done on 0.0125 mmol scale while of compound **94**, **95**, **98**, **100** and **102** was done on 0.00625 mmol scale (based on Fmoc loading). Resin was placed in the reaction vessel and swollen in 2 mL DCM for 30 min at room temperature prior to synthesis. The temperature of the reaction vessel was adjusted to -20 ºC. Before the first glycosylation, the resin was washed with the DMF, THF, and DCM (three times with 2 mL for 15 s each).

Module B: Acid wash: Stock solution B, 0.5 ml was delivered to the reaction vessel. After 2 min at -20 ºC, the solution was drained. The resin was swollen in 2 mL DCM for 25 s.

Module C: Glycosylation: The thioglycoside building block solution (6.5 equiv in 1.0 mL CH_2Cl_2) was delivered to the reaction vessel and the temperature was adjusted to -40 ºC. After the set temperature was reached, the reaction was started by the addition of the

activator stock solution **C**. The glycosylation was performed for 5 min at -40 ºC and for 30 min at -20 ºC. Subsequently the solution was drained and the resin was washed with Dioxane and DCM (3×).

Action	Cycles	Solvent	Reagent 1	Reagent 2	Temperature	Incubation Time
Wash	1	DCM		TMSOTf		2 min
Wash	1	DCM			25 °C	15 s
Glycosylation	1	DCM	BB (81 µmol)	NIS (150 mM), TfOH (15 mM)	-40 °C	5 min
					-20	30 min
Wash	3	Dioxane			-20 °C	15 s
Wash	3	DCM			25 °C	15 s

Module C*: Glycosylation: The thioglycoside building block solution **72** (6.5 or 9.75 equiv in 1.0 mL CH_2Cl_2) was delivered to the reaction vessel and the temperature was adjusted to -40 ºC. After the set temperature was reached, the reaction was started by the addition of the activator stock solution **C**. The glycosylation was performed for 5 min at -40 ºC and for 30 min at -20 ºC. Subsequently the solution was drained and the resin was washed with Dioxane and DCM (3×). To ensure full conversion of all –OH groups, the whole procedure was repeated once.

Action	Cycles	Solvent	Reagent 1	Reagent 2	Temperature	Incubation Time
Wash	1	DCM		TMSOTf	-20 ºC	2 min
Wash	1	DCM			-20 ºC	15 s
Glycosylation	1	DCM	BB (81	NIS (150 mM), TfOH (15 mM)	-40 ºC	5 min
					-20 ºC	30 min

			µmol)			
Wash	3	DCM			-20 ºC	15 s
Glycosylation	1	DCM	BB (81 µmol)	NIS (150 mM), TfOH (15 mM)	-40 ºC	5 min
					-20 ºC	30 min
Wash	3	DCM			-20 ºC	15 s
Wash	3	DCM			25 ºC	15 s

Module C: Glycosylation:** The thioglycoside building block solution **74** (6.5 equiv in 1.0 mL CH_2Cl_2) was delivered to the reaction vessel and the temperature was adjusted to -40 ºC. After the set temperature was reached, the reaction was started by the addition of the activator stock solution **C**. The glycosylation was performed for 5 min at -40 ºC and for 40 min at -20 ºC. Subsequently the solution was drained and the resin was washed with Dioxane and DCM (3× 15s). To ensure full conversion of all –OH groups, the whole procedure was repeated once.

Action	Cycles	Solvent	Reagent 1	Reagent 2	Temperature	Incubation Time
Wash	1	DCM		TMSOTf	-20 ºC	2 min
Wash	1	DCM			-20 ºC	15 s
Glycosylation	1	DCM	BB (81 µmol)	NIS (150 mM), TfOH (15 mM)	-40 ºC	5 min
					-20 ºC	40 min
Wash	3	DCM			-20 ºC	15 s
Glycosylation	1	DCM	BB (81 µmol)	NIS (150 mM), TfOH (15 mM)	-40 ºC	5 min
					-20 ºC	40 min
Wash	3	DCM			-20 ºC	15 s
Wash	3	DCM			25 ºC	15 s

Module D: Fmoc deprotection: The resin was washed with DMF, swollen in 2 mL DMF and the temperature of the reaction vessel was adjusted to 25 ºC. Prior to the deprotection step, the DMF was drained and the resin was washed with DMF (3×5 min). Solution **D** was delivered to the reaction vessel. After 10 min the solution was drained and the whole procedure was repeated another two times. After Fmoc deprotection, the resin was washed with DMF, THF and DCM.

Action	Cycles	Solvent	Reagent	Temperature	Incubation Time
Wash	3	DMF		25 ºC	15 s
Deprotection	3	DMF	Et_3N	25 ºC	5 min
Wash	3	DMF		25 ºC	15 s
Wash	3	THF		25 ºC	15 s
Wash	3	DCM		25 ºC	15 s

Module E: Lev deprotection: The resin was washed with DMF (3×30 min) and 1.3 mL DCM added to the reaction vessel. Solution **E** (0.8 mL) was added to the reaction vessel, and the temperature was adjusted to 25 ºC. After 30 min the reaction solution was drained and the whole procedure was repeated another two times. After Lev deprotection was complete the resin was washed with DMF, THF and DCM.

Action	Cycles	Solvent	Reagent	Temperature	Incubation Time
Wash	3	DCM		25 ºC	15 s
Deprotection	3	DMF	Pyridine:AcOH:H_2O (4:1:0.25)	25 ºC	30 min
Wash	3	DMF		25 ºC	15 s
Wash	3	THF		25 ºC	15 s
Wash	3	DCM		25 ºC	15 s

Module F: Cleavage from the solid support: The oligosaccharides were cleaved from the solid support as previously reported[150], using the Vapourtec E-Series UV-150 photoreactor, a medium pressure metal halide lamp that is filtered using a commercially available red filter. The resin suspended in DCM and transferred into a 20 mL plastic syringe using a plastic pipet. The suspension was then pumped using a syringe pump (PHD2000, Harvard Aparatus) at 0.8 mL min^{-1} through a 10 mL reactor, constructed of 1/8 inch o.d. FEP tubing. The total volume in the photoreactor was 9 mL and temperature was maintained at 20 ºC with the fixed 80% lamp power. The exiting flow outlet was deposited in a 10 mL syringe filter, with a round bottom flask below the syringe.

Module G: Purification: The crude products were analyzed and purified using analytical and preparative HPLC (Agilent 1200 Series spectrometer).

- **Method A:** (YMC-Diol-300 column, 150 x 4.6 mm) flow rate of 1.0 mL / min with Hex – 20% EtOAc as eluent [isocratic 20% EtOAc (5 min), linear gradient to 55% EtOAc (45 min), linear gradient to 100% EtOAc (5 min)].
- **Method B:** (YMC-Diol-300 column, 150 x 20 mm) flow rate of 15 mL / min with Hex – 20% EtOAc as eluents [isocratic 20% EtOAc (5 min), linear gradient to 55% EtOAc (35 min), linear gradient to 100% EtOAc (5 min)].
- **Method C:** The crude deprotected compounds **66**-**71** were purified using analytical HPLC: (Hypercarb column, 150 x 10 mm) flow rate of 1.3 mL / min with H_2O (0.1% formic acid) as eluents [isocratic (5 min), linear gradient to 30% ACN (30 min), linear gradient to 100% ACN (5 min)]. Detection: ELSD.

Module H: Global deprotection: To the solution of the purified fully protected LM and LAM fragments (**87**, **89**, **94**, **95**, **98**, **100** and **102**) in CH_2Cl_2:MeOH, 1:1 was added 0.5 M NaOMe solution (3 eq. per acetyl of benzoyl group), at room temperature. The mixture was stirred until complete conversion, neutralized by the addition of Amberlite IR 120 H^+ resin. After filtration, the filtrate was dissolved in CH_2Cl_2, water, and *t*-butanol (v/v/v =1:0.5:0.5) followed by adding 5% palladium on carbon (Pd/C), purged first with argon and then with hydrogen, and stirred overnight at room temperature under balloon pressure. The reaction mixture was filtered through a modified cellulose filter, washed with 20 mL water/methanol (9:1) and the combined solution was evaporated *in vacuo* and the crude product was further

purified using reversed phase (RP) SPE (Waters Sep-Pak®, C18) column and by analytical HPLC (Module G; method C).

3.4.2.5 Automated Synthesis

***N*-Benzyloxycarbonyl-5-amino-pentyl (2-*O*-benzoyl-3,4-di-*O*-benzyl-α-D-mannopyranosyl)-(1→6)-(2-*O*-benzoyl-3,4-di-*O*-benzyl-α-D-mannopyranosyl)-(1→6)-(2-*O*-benzoyl-3,4-di-*O*-benzyl-α-D-mannopyranosyl)-(1→6)-(2-*O*-benzoyl-3,4-di-*O*-benzyl-α-D-mannopyranosyl)-(1→6)-(2-*O*-benzoyl-3,4-di-*O*-benzyl-α-D-mannopyranosyl)-(1→6)-2-*O*-benzoyl-3,4-di-*O*-benzyl-α-D-mannopyranoside (87):** For the automated synthesis of **87,** linker-functionalized resin **4** (34 mg, 12.5 µmol) was placed in the reaction vessel and the resin was washed with DMF, THF, and DCM. Afterward the acid wash (Module **B**), the glycosylation (Module **C**) and deprotection (Module **D**) were executed according to the modules. Mixing of the components was performed by bubbling Argon (Ar) through the reaction mixture.

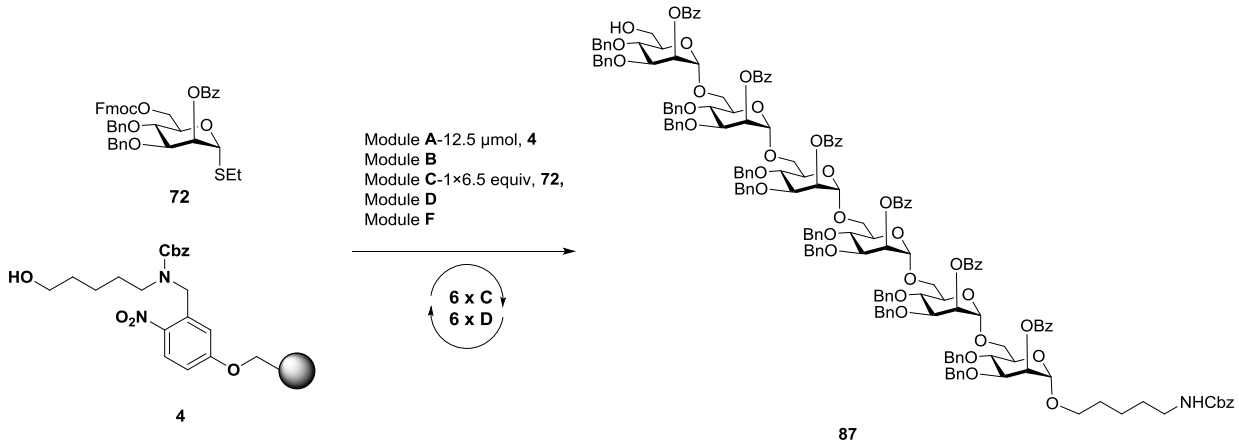

Module **B** (62.5 mM TMSOTf in DCM, 1 x 2 min, -20 ºC)

Module **C** (1 x 6.5 equiv. **72**, NIS, TfOH, DCM/Dioxane, 1 x 35 min, -40 ºC to -20 ºC)

Module **D** (20% NEt_3 in DMF, 3 x 5 min, rt)

Module **B** (62.5 mM TMSOTf in DCM, 1 x 2 min, -20 ºC)

Module **C** (1 x 6.5 equiv. **72**, NIS, TfOH, DCM/Dioxane, 1 x 35 min, -40 ºC to -20 ºC)

Module **D** (20% NEt_3 in DMF, 3 x 5 min, rt)

Module **B** (62.5 mM TMSOTf in DCM, 1 x 2 min, -20 ºC)

Module **C** (1 x 6.5 equiv. **72**, NIS, TfOH, DCM/Dioxane, 1 x 35 min, -40 ºC to -20 ºC)

Module **D** (20% NEt_3 in DMF, 3 x 5 min, rt)

Module **B** (62.5 mM TMSOTf in DCM, 1 x 2 min, -20 ºC)

Module **C** (1 x 6.5 equiv. **72**, NIS, TfOH, DCM/Dioxane, 1 x 35 min, -40 ºC to -20 ºC)

Module **D** (20% NEt_3 in DMF, 3 x 5 min, rt)

Module **B** (62.5 mM TMSOTf in DCM, 1 x 2 min, -20 ºC)

Module **C** (1 x 6.5 equiv. **72**, NIS, TfOH, DCM/Dioxane, 1 x 35 min, -40 ºC to -20 ºC)

Module **D** (20% NEt_3 in DMF, 3 x 5 min, rt)

Module **B** (62.5 mM TMSOTf in DCM, 1 x 2 min, -20 ºC)

Module **C** (1 x 6.5 equiv. **72**, NIS, TfOH, DCM/Dioxane, 1 x 35 min, -40 ºC to -20 ºC)

Module **D** (20% NEt_3 in DMF, 3 x 5 min, rt)

Module **F** Resin cleaved using UV irradiation at 305 nm in a continuous flow photoreactor.

Crude NP-HPLC of hexasaccharide 87 (ELSD trace, Method A, t_R = 25.0 min)

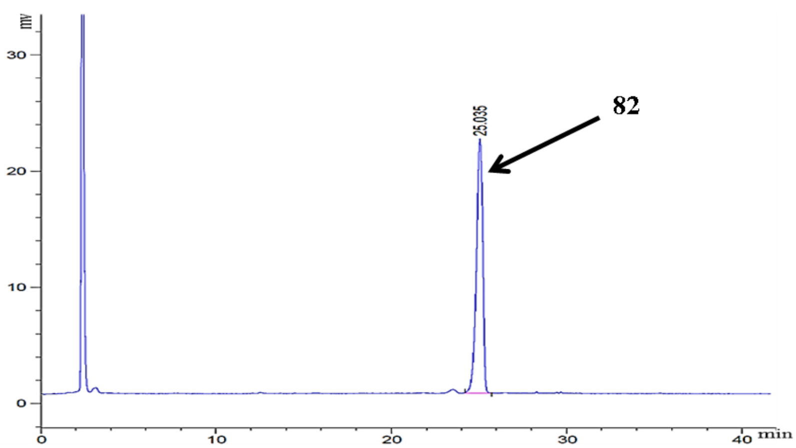

The crude product was purified using a preparative HPLC (Method B, t_R = 25.3 min), to give the fully protected linear hexasaccharide **87** **(**20 mg, 6.88 μmol, 55%, based on resin loading).

^{1}H NMR (400 MHz, $CDCl_3$) δ 8.24 – 8.09 (m, 12H), 7.64 (s, 1H), 7.56 – 7.46 (m, 17H), 7.38 – 7.30 (m, 12H), 7.29 – 7.10 (m, 56H), 5.85 (d, *J* = 9.0 Hz, 4H), 5.80 (s, 1H), 5.66 (s, 1H), 5.14 (s, 1H), 5.12 – 5.03 (m, 6H), 4.95 – 4.73 (m, 12H), 4.61 (dd, *J* = 15.6, 11.1 Hz, 2H), 4.52 – 4.41 (m, 7H), 4.37 (d, *J* = 12.4 Hz, 2H), 4.13 – 3.86 (m, 13H), 3.84 – 3.59 (m, 11H), 3.58 – 3.52 (m, 2H), 3.46 (dd, *J* = 16.9, 9.7 Hz, 4H), 3.22 – 3.16 (m, 2H), 1.64 – 1.57 (m, 2H), 1.55 – 1.47 (m, 2H), 1.41 – 1.34 (m, 2H); ^{13}C NMR (100 MHz, $CDCl_3$) δ 165.97,

165.73, 165.65, 165.54, 156.51, 138.63, 138.58, 138.41, 138.37, 138.04, 137.74, 137.67, 137.65, 137.62, 136.78, 133.45, 133.41, 130.08, 130.03, 129.99, 128.77, 128.70, 128.62, 128.47, 128.43, 128.34, 128.29, 128.26, 128.18, 128.14, 127.82, 127.78, 127.75, 127.53, 127.48, 127.44, 127.34, 127.24, 127.22, 98.58, 98.51, 98.25, 97.99, 78.72, 78.42, 78.37, 78.34, 78.28, 77.79, 76.84, 75.31, 75.22, 75.16, 75.12, 74.30, 74.01, 73.91, 73.85, 73.79, 72.20, 71.76, 71.53, 71.43, 71.30, 71.09, 71.01, 70.84, 69.16, 68.65, 68.52, 68.46, 67.89, 66.68, 66.20, 65.91, 65.82, 65.54, 61.93, 41.07, 29.90, 29.16, 23.55; HRMS (ESI): calculated for $C_{175}H_{175}NNaO_{39}$ $[M+Na]^+$ 2937.1639, found 2937.1557.

N*-Benzyloxycarbonyl-5-amino-pentyl (2-*O*-benzoyl-3,4-di-*O*-benzyl-α-D-mannopyranosyl)-(1→6)-(2-*O*-benzoyl-3,4-di-*O*-benzyl-α-D-mannopyranosyl)-(1→2)-(2-*O*-benzoyl-3,4-di-*O*-benzyl-α-D-mannopyranosyl)-(1→6)-(2-*O*-benzoyl-3,4-di-*O*-benzyl-α-D-mannopyranosyl)-(1→2)-(2-*O*-benzoyl-3,4-di-*O*-benzyl-α-D-mannopyranosyl)-(1→6)-(2-*O*-benzoyl-3,4-di-*O*-benzyl-α-D-mannopyranoside (89):** For automated synthesis of **89,** linker-functionalized resin **4** (34 mg, 12.5 μmol) was placed in the reaction vessel and the resin was washed with DMF, THF, and DCM. Afterward the acid wash (Module B), glycosylation (Module **C**) or (Module **C), and deprotection (Module **D** and **E**) executed according to the modules. Mixing of the components was performed by bubbling Argon (Ar) through the reaction mixture.

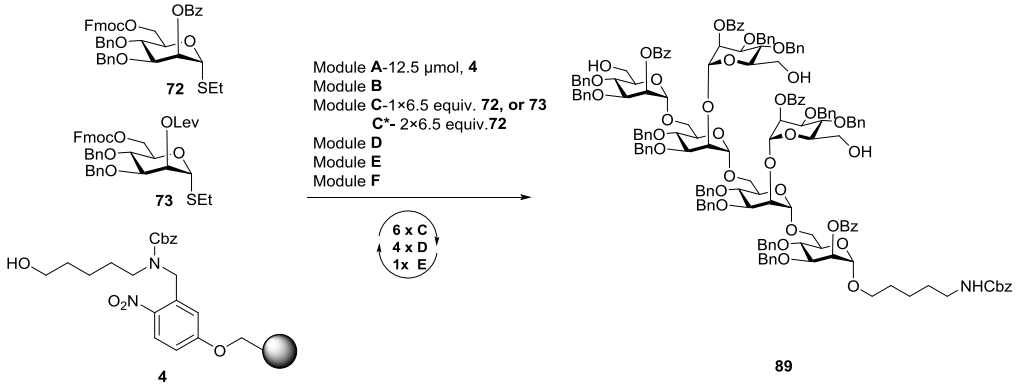

Module **B** (62.5 mM TMSOTf in DCM, 1 x 2 min, -20 ºC)

Module **C** (1 x 6.5 equiv. **72**, NIS, TfOH, DCM/Dioxane, 1 x 35 min, -40 ºC to -20 ºC)

Module **D** (20% NEt_3 in DMF, 3 x 5 min, rt)

Module **B** (62.5 mM TMSOTf in DCM, 1 x 2 min, -20 ºC)

Module **C** (1 x 6.5 equiv. **73**, NIS, TfOH, DCM/Dioxane, 1 x 35 min, -40 ºC to -20 ºC)

Module **D** (20% NEt_3 in DMF, 3 x 5 min, rt)

Module **B** (62.5 mM TMSOTf in DCM, 1 x 2 min, -20 ºC)

Module **C** (1 x 6.5 equiv. **73**, NIS, TfOH, DCM/Dioxane, 1 x 35 min, -40 ºC to -20 ºC)

Module **D** (20% NEt_3 in DMF, 3 x 5 min, rt)

Module **B** (62.5 mM TMSOTf in DCM, 1 x 2 min, -20 ºC)

Module **C** (1 x 6.5 equiv. **72**, NIS, TfOH, DCM/Dioxane, 1 x 35 min, -40 ºC to -20 ºC)

Module **E** (150 mM N_2H_4.AcOH in Py/AcOH/H_2O, 3 x 30 min, rt)

Module **B** (62.5 mM TMSOTf in DCM, 1 x 2 min, -20 ºC)

Module **C*** (2 x 6.5 equiv. **72**, NIS, TfOH, DCM/Dioxane, 2 x 35 min, -40 ºC to -20 ºC)

Module **D** (20% NEt_3 in DMF, 3 x 5 min, rt)

Module **F** Resin cleaved using UV irradiation at 305 nm in a continuous flow photoreactor.

Crude NP-HPLC of hexasaccharide 89 (ELSD trace, Method A, t_R = 27.8 min)

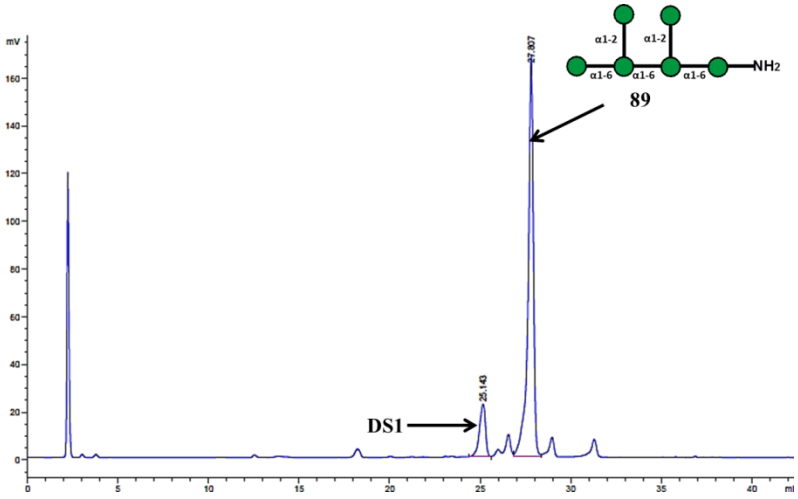

Observed deletion sequence observed (DS1)

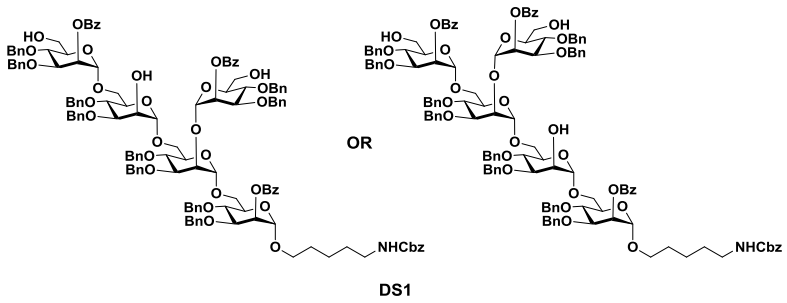

DS1

The crude product was purified using a preparative HPLC (Method B, t_R = 36.5 min), to provide the fully protected branched hexasaccharide **89** (12.5 mg, 4.62 μmol, 37%, based on resin loading).

^{1}H NMR (400 MHz, $CDCl_3$) δ 8.08 – 7.86 (m, 9H), 7.55 – 7.45 (m, 4H), 7.41 – 7.30 (m, 8H), 7.27 – 6.92 (m, 65H), 5.83 – 5.79 (m, 1H), 5.61 (t, *J* = 2.4 Hz, 1H), 5.54 (t, *J* = 2.3 Hz, 1H), 5.45 – 5.40 (m, 1H), 5.23 (s, 1H), 5.11 (s, 1H), 5.03 – 4.97 (m, 3H), 4.85 – 4.81 (m, 3H), 4.79 – 4.67 (m, 7H), 4.62 – 4.26 (m, 14H), 4.17 – 4.09 (m, 2H), 4.02 – 3.90 (m, 6H), 3.87 – 3.75 (m, 9H), 3.72 – 3.48 (m, 14H), 3.44 – 3.27 (m, 5H), 3.11 – 3.02 (m, 2H), 1.48 – 1.38 (m, 4H), 1.26 (d, *J* = 9.1 Hz, 2H); ^{13}C NMR (100 MHz, $CDCl_3$) δ 165.99, 165.52, 165.43, 165.38, 156.51, 138.66, 138.53, 138.49, 138.29, 138.21, 138.10, 138.04, 137.90, 137.81, 137.66, 137.14, 136.79, 136.76, 133.52, 133.43, 133.27, 133.22, 130.27, 130.05, 129.99, 129.90, 129.78, 129.34, 128.63, 128.55, 128.43, 128.35, 128.28, 128.16, 128.14, 128.02, 127.97, 127.88, 127.81, 127.77, 127.71, 127.56, 127.47, 127.34, 100.24 (C-anomeric), 99.88 (C-anomeric), 99.28 (C-anomeric), 98.87 (C-anomeric), 97.64 (C-anomeric), 97.55 (C-anomeric), 79.24, 79.11, 78.97, 78.61, 78.50, 75.33, 75.21, 75.12, 74.93, 74.59, 74.42, 74.10, 73.99, 73.40, 72.78, 72.49, 71.91, 71.81, 71.75, 71.39, 71.24, 71.06, 70.49, 69.62, 69.57, 69.23, 68.81, 67.84, 66.69, 66.02, 65.87, 62.59, 62.27, 61.93, 41.05, 29.86, 29.14, 23.54; HRMS (MALDI-TOF): calculated for $C_{161}H_{167}NO_{37}$ $[M+ Na]^+$ 2729.111, found 2729.650.

***N*-Benzyloxycarbonyl-5-amino-pentyl (2-*O*-benzoyl-3,4-di-*O*-benzyl-α-D-mannopyranosyl)-(1→6)-(2-*O*-benzoyl-3,4-di-*O*-benzyl-α-D-mannopyranosyl)-(1→2)-**

(2-*O*-benzoyl-3,4-di-*O*-benzyl-α-D-mannopyranosyl)-(1→6)-(2-*O*-benzoyl-3,4-di-*O*-benzyl-α-D-mannopyranosyl)-(1→2)-(2-*O*-benzoyl-3,4-di-*O*-benzyl-α-D-mannopyranosyl)-(1→6)-(2-*O*-benzoyl-3,4-di-*O*-benzyl-α-D-mannopyranosyl)-(1→6)-(2-*O*-benzoyl-3,4-di-*O*-benzyl-α-D-mannopyranosyl)-(1→6)-(2-*O*-benzoyl-3,4-di-*O*-benzyl-α-D-mannopyranosyl)-(1→6)-(2-*O*-benzoyl-3,4-di-*O*-benzyl-α-D-mannopyranosyl)-(1→6)-(2-*O*-benzoyl-3,4-di-*O*-benzyl-α-D-mannopyranosyl)-(1→6)-2-*O*-benzoyl-3,4-di-*O*-benzyl-α-D-mannopyranoside (94): For automated synthesis of **94,** linker-functionalized resin **4** (17 mg, 6.25 μmol) was placed in the reaction vessel and the resin was washed with DMF, THF, and DCM. Afterward the acid wash (Module **B**), glycosylation (Module **C**) or (Module **C***), and deprotection (Module **D** and **E**) executed according to the modules. Mixing of the components was performed by bubbling Argon (Ar) through the reaction mixture.

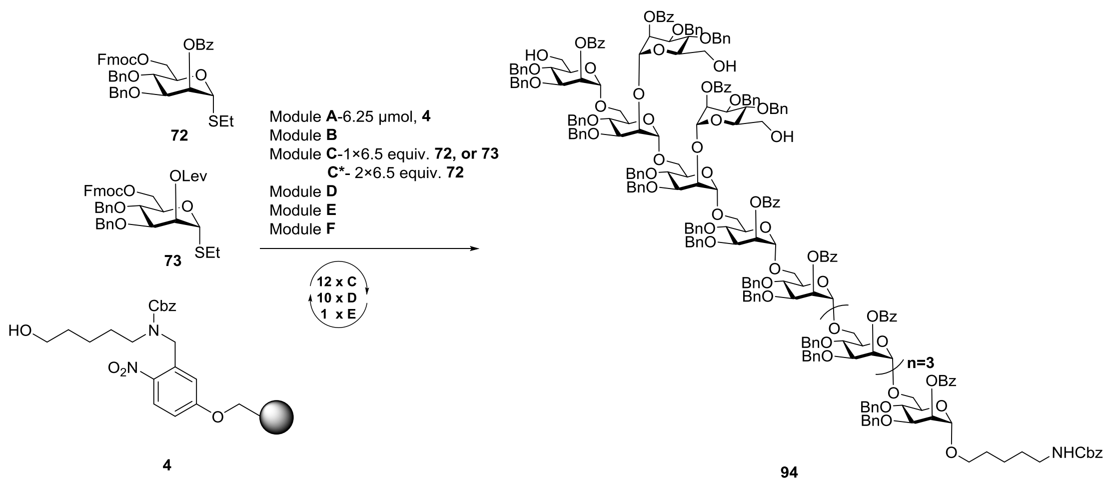

Module **B** (62.5 mM TMSOTf in DCM, 1 x 2 min, -20 ºC)

Module **C** (1 x 6.5 equiv. **72**, NIS, TfOH, DCM/Dioxane, 1 x 35 min, -40 ºC to -20 ºC)

Module **D** (20% NEt_3 in DMF, 3 x 5 min, rt)

Module **B** (62.5 mM TMSOTf in DCM, 1 x 2 min, -20 ºC)

Module **C** (1 x 6.5 equiv. **72**, NIS, TfOH, DCM/Dioxane, 1 x 35 min, -40 ºC to -20 ºC)

Module **D** (20% NEt_3 in DMF, 3 x 5 min, rt)

Module **B** (62.5 mM TMSOTf in DCM, 1 x 2 min, -20 ºC)

Module **C** (1 x 6.5 equiv. **72**, NIS, TfOH, DCM/Dioxane, 1 x 35 min, -40 ºC to -20 ºC)

Module **D** (20% NEt_3 in DMF, 3 x 5 min, rt)

Module **B** (62.5 mM TMSOTf in DCM, 1 x 2 min, -20 ºC)

Module **C** (1 x 6.5 equiv. **72**, NIS, TfOH, DCM/Dioxane, 1 x 35 min, -40 ºC to -20 ºC)

Module **D** (20% NEt_3 in DMF, 3 x 5 min, rt)

Module **B** (62.5 mM TMSOTf in DCM, 1 x 2 min, -20 ºC)

Module **C** (1 x 6.5 equiv. **72**, NIS, TfOH, DCM/Dioxane, 1 x 35 min, -40 ºC to -20 ºC)

Module **D** (20% NEt_3 in DMF, 3 x 5 min, rt)

Module **B** (62.5 mM TMSOTf in DCM, 1 x 2 min, -20 ºC)

Module **C** (1 x 6.5 equiv. **72**, NIS, TfOH, DCM/Dioxane, 1 x 35 min, -40 ºC to -20 ºC)

Module **D** (20% NEt_3 in DMF, 3 x 5 min, rt)

Module **B** (62.5 mM TMSOTf in DCM, 1 x 2 min, -20 ºC)

Module **C** (1 x 6.5 equiv. **72**, NIS, TfOH, DCM/Dioxane, 1 x 35 min, -40 ºC to -20 ºC)

Module **D** (20% NEt_3 in DMF, 3 x 5 min, rt)

Module **B** (62.5 mM TMSOTf in DCM, 1 x 2 min, -20 ºC)

Module **C** (1 x 6.5 equiv. **73**, NIS, TfOH, DCM/Dioxane, 1 x 35 min, -40 ºC to -20 ºC)

Module **D** (20% NEt_3 in DMF, 3 x 5 min, rt)

Module **B** (62.5 mM TMSOTf in DCM, 1 x 2 min, -20 ºC)

Module **C** (1 x 6.5 equiv. **73**, NIS, TfOH, DCM/Dioxane, 1 x 35 min, -40 ºC to -20 ºC)

Module **D** (20% NEt_3 in DMF, 3 x 5 min, rt)

Module **B** (62.5 mM TMSOTf in DCM, 1 x 2 min, -20 ºC)

Module **C** (1 x 6.5 equiv. **73**, NIS, TfOH, DCM/Dioxane, 1 x 35 min, -40 ºC to -20 ºC)

Module **E** (150 mM N_2H_4.AcOH in Py/AcOH/H_2O, 3 x 30 min, rt)

Module **B** (62.5 mM TMSOTf in DCM, 1 x 2 min, -20 ^oC)

Module **C*** (2 x 6.5 equiv. **72**, NIS, TfOH, DCM/Dioxane, 2 x 35 min, -40 ºC to -20 ºC)

Module **D** (20% NEt_3 in DMF, 3 x 5 min, rt)

Module **F** Resin cleaved using UV irradiation at 305 nm in a continuous flow photoreactor.

Crude NP-HPLC of hexasaccharide 94 (ELSD trace, Method A, t_R = 30.4 min)

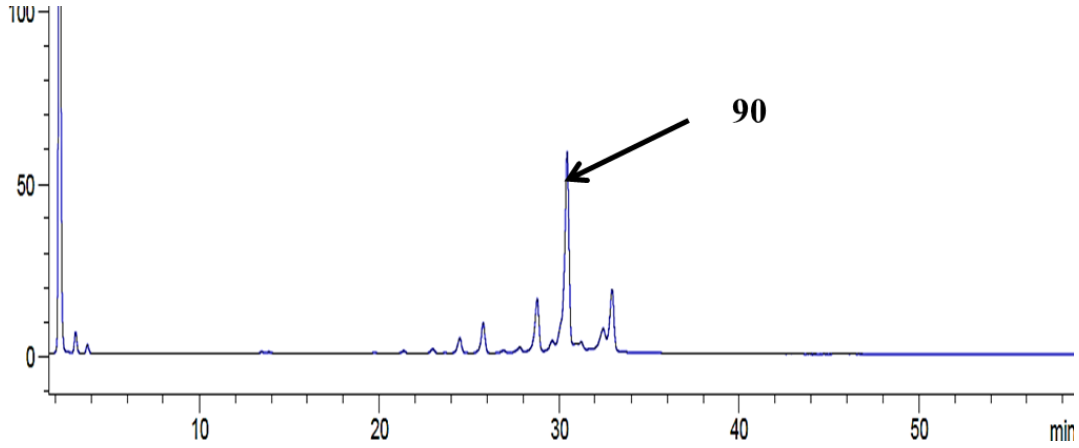

The crude product was purified using a preparative HPLC (Method B, t_R = 31.1 min), to provide the fully protected branched undecasaccharide **94** (2.3 mg, 4.66 μmol, 7%, based on resin loading).

^{1}H NMR (600 MHz, $CDCl_3$) δ 8.18 – 8.12 (m, 8H), 8.11 – 8.08 (m, 2H), 8.06 – 8.00 (m, 6H), 7.96 (d, *J* = 7.7 Hz, 2H), 7.57 (t, *J* = 7.5 Hz, 1H), 7.54 – 7.34 (m, 25H), 7.33 – 7.00 (m, 116H), 5.88 (s, 1H), 5.82 – 5.78 (m, 4H), 5.71 (s, 1H), 5.67 (s, 1H), 5.64 – 5.60 (m, 2H), 5.30 (s, 1H), 5.12 (s, 1H), 5.09 – 5.01 (m, 8H), 4.92 (s, 1H), 4.90 – 4.74 (m, 20H), 4.67 (dd, *J* = 10.9, 6.7 Hz, 2H), 4.63 – 4.29 (m, 25H), 4.26 (s, 1H), 4.22 (dd, *J* = 9.0, 3.1 Hz, 1H), 4.12 –3.98 (m, 11H), 3.95 – 3.30 (m, 45H), 3.15 (s, 2H), 1.50 – 1.45 (m, 4H), 1.35 – 1.32 (m, 2H); ^{13}C NMR (100 MHz, $CDCl_3$) δ 166.00, 165.76, 165.68, 165.54, 165.45, 165.40, 162.76, 156.53, 138.77, 138.64, 138.52, 138.42, 138.35, 138.28, 138.11, 138.04, 137.95, 137.85, 137.83, 137.78, 137.74, 137.68, 137.61, 137.25, 136.85, 133.43, 133.20, 130.18, 130.12, 130.01, 129.82, 129.33, 128.79, 128.71, 128.63, 128.47, 128.33, 127.88, 127.81, 127.79, 127.53, 127.42, 127.32, 127.15, 100.33 (C-anomeric), 99.60 (C-anomeric), 99.36 (C-anomeric), 99.08 (C-anomeric), 98.73 (C-anomeric), 98.69 (C-anomeric), 98.59 (C-anomeric), 98.45 (C-anomeric), 98.29 (C-anomeric), 98.03 (C-anomeric), 97.72 (C-anomeric), 79.23, 78.96, 78.74, 78.45, 78.39, 78.31, 78.26, 78.15, 75.32, 75.20, 75.12, 74.89, 74.76, 74.64, 74.30, 73.94, 73.84, 73.60, 73.02, 71.97, 71.87, 71.79, 71.70, 71.57, 71.49, 71.46, 71.40, 71.25, 71.17, 71.05, 71.01, 70.91, 70.61, 69.81, 69.52, 69.25, 68.93, 68.84, 68.75, 68.63, 68.59, 67.92, 66.69, 66.27, 65.97, 65.92, 62.79, 62.64, 62.51, 62.02,

41.11, 29.90, 29.18, 23.58; HRMS (ESI): calculated for $C_{296}H_{297}NO_{67}$ $[M+2Na]^{2+}$ 2491.4824, found 2491.4875.

N*-Benzyloxycarbonyl-5-amino-pentyl (2-*O*-benzoyl-3,4-di-*O*-benzyl-α-D-mannopyranosyl)-(1→6)-(2-*O*-benzoyl-3,4-di-*O*-benzyl-α-D-mannopyranosyl)-(1→2)-(2-*O*-benzoyl-3,4-di-*O*-benzyl-α-D-mannopyranosyl)-(1→6)-(2-*O*-benzoyl-3,4-di-*O*-benzyl-α-D-mannopyranosyl)-(1→2)-(2-*O*-benzoyl-3,4-di-*O*-benzyl-α-D-mannopyranosyl)-(1→6)-(2-*O*-benzoyl-3,4-di-*O*-benzyl-α-D-mannopyranosyl)-(1→6)-(2-*O*-benzoyl-3,4-di-*O*-benzyl-α-D-mannopyranosyl)-(1→6)-(2-*O*-benzoyl-3,4-di-*O*-benzyl-α-D-mannopyranosyl)-(1→6)-(2-*O*-benzoyl-3,4-di-*O*-benzyl-α-D-mannopyranosyl)-(1→6)-(2-*O*-benzoyl-3,4-di-*O*-benzyl-α-D-mannopyranosyl)-(1→6)-2-*O*-benzoyl-3,4-di-*O*-benzyl-α-D-mannopyranoside (95):** For automated synthesis of **95,** linker-functionalized resin **4** (17 mg, 6.25 μmol) was placed in the reaction vessel and the resin was washed with DMF, THF, and DCM. Afterward the acid wash (Module **B**), glycosylation (Module **C**) or (Module **C), and deprotection (Module **D** and **E**) executed according to the modules. Mixing of the components was performed by bubbling Argon (Ar) through the reaction mixture.

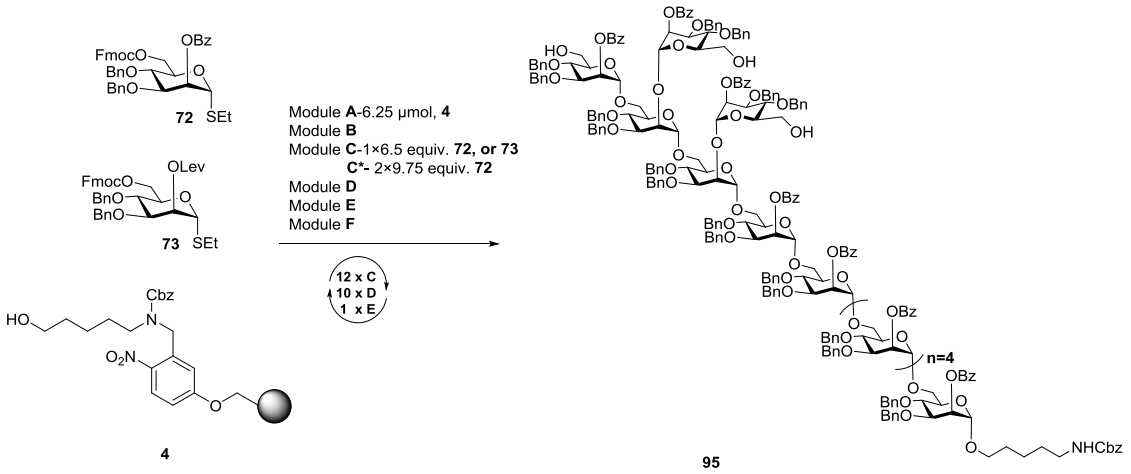

Module **B** (62.5 mM TMSOTf in DCM, 1 x 2 min, -20 ºC)

Module **C** (1 x 6.5 equiv. **72**, NIS, TfOH, DCM/Dioxane, 1 x 35 min, -40 ºC to -20 ºC)

Module **D** (20% NEt_3 in DMF, 3 x 5 min, rt)

Module **B** (62.5 mM TMSOTf in DCM, 1 x 2 min, -20 ºC)

Module **C** (1 x 6.5 equiv. **72**, NIS, TfOH, DCM/Dioxane, 1 x 35 min, -40 ºC to -20 ºC)

Module **D** (20% NEt_3 in DMF, 3 x 5 min, rt)

Module **B** (62.5 mM TMSOTf in DCM, 1 x 2 min, -20 ºC)

Module **C** (1 x 6.5 equiv. **72**, NIS, TfOH, DCM/Dioxane, 1 x 35 min, -40 ºC to -20 ºC)

Module **D** (20% NEt_3 in DMF, 3 x 5 min, rt)

Module **B** (62.5 mM TMSOTf in DCM, 1 x 2 min, -20 ºC)

Module **C** (1 x 6.5 equiv. **72**, NIS, TfOH, DCM/Dioxane, 1 x 35 min, -40 ºC to -20 ºC)

Module **D** (20% NEt_3 in DMF, 3 x 5 min, rt)

Module **B** (62.5 mM TMSOTf in DCM, 1 x 2 min, -20 ºC)

Module **C** (1 x 6.5 equiv. **72**, NIS, TfOH, DCM/Dioxane, 1 x 35 min, -40 ºC to -20 ºC)

Module **D** (20% NEt_3 in DMF, 3 x 5 min, rt)

Module **B** (62.5 mM TMSOTf in DCM, 1 x 2 min, -20 ºC)

Module **C** (1 x 6.5 equiv. **72**, NIS, TfOH, DCM/Dioxane, 1 x 35 min, -40 ºC to -20 ºC)

Module **D** (20% NEt_3 in DMF, 3 x 5 min, rt)

Module **B** (62.5 mM TMSOTf in DCM, 1 x 2 min, -20 ºC)

Module **C** (1 x 6.5 equiv. **72**, NIS, TfOH, DCM/Dioxane, 1 x 35 min, -40 ºC to -20 ºC)

Module **D** (20% NEt_3 in DMF, 3 x 5 min, rt)

Module **B** (62.5 mM TMSOTf in DCM, 1 x 2 min, -20 ºC)

Module **C** (1 x 6.5 equiv. **73**, NIS, TfOH, DCM/Dioxane, 1 x 35 min, -40 ºC to -20 ºC)

Module **D** (20% NEt_3 in DMF, 3 x 5 min, rt)

Module **B** (62.5 mM TMSOTf in DCM, 1 x 2 min, -20 ºC)

Module **C** (1 x 6.5 equiv. **73**, NIS, TfOH, DCM/Dioxane, 1 x 35 min, -40 ºC to -20 ºC)

Module **D** (20% NEt_3 in DMF, 3 x 5 min, rt)

Module **B** (62.5 mM TMSOTf in DCM, 1 x 2 min, -20 ºC)

Module **C** (1 x 6.5 equiv. **72**, NIS, TfOH, DCM/Dioxane, 1 x 35 min, -40 ºC to -20 ºC)

Module **E** (150 mM N_2H_4.AcOH in Py/AcOH/H_2O, 3 x 30 min, rt)

Module **B** (62.5 mM TMSOTf in DCM, 1 x 2 min, -20 ºC)

Module **C*** (2 x 9.75 equiv. **72**, NIS, TfOH, DCM/Dioxane, 2 x 35 min, -40 ºC to -20 ºC)

Module **D** (20% NEt_3 in DMF, 3 x 5 min, rt)

Module **F** Resin cleaved using UV irradiation at 305 nm in a continuous flow photoreactor.

Crude NP-HPLC of hexasaccharide 95 (ELSD trace, Method A, t_R = 31.3 min)

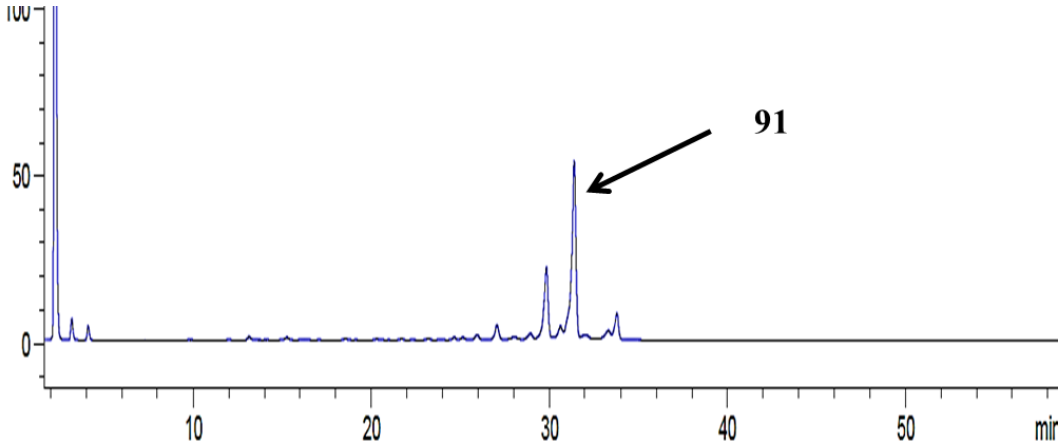

The crude product was purified using a preparative HPLC (Method B, t_R = 32.3 min), to provide the fully protected branched dodecasaccharide **95** (2.2 mg, 4.04 μmol, 6%, based on resin loading).

^{13}C NMR (152 MHz, $CDCl_3$) δ 165.99, 165.75, 165.73, 165.67, 165.53, 165.44, 165.39, 165.31, 156.52, 138.75, 138.61, 138.57, 138.49, 138.39, 138.31, 138.25, 138.08, 138.00, 137.91, 137.79, 137.73, 137.69, 137.63, 137.57, 136.82, 133.44, 133.21, 130.14, 130.06, 130.00, 129.90, 129.81, 128.78, 128.71, 128.62, 128.61, 128.47, 128.40, 128.31, 128.17, 128.11, 127.88, 127.81, 127.77, 127.56, 127.50, 127.38, 127.26, 127.11, 100.32 (C-anomeric), 99.57 (C-anomeric), 99.33 (C-anomeric), 99.04 (C-anomeric), 98.70 (C-anomeric), 98.65 (C-anomeric), 98.55 (C-anomeric), 98.43 (C-anomeric), 98.27 (C-anomeric), 98.01 (C-anomeric), 97.70 (C-anomeric), 78.73, 78.44, 78.37, 78.31, 78.24, 75.32, 75.19, 75.12, 74.34, 74.05, 73.95, 73.90, 73.59, 71.96, 71.86, 71.78, 71.68, 71.55, 71.47, 71.44, 71.38, 71.24, 71.20, 71.10, 71.01, 70.96, 70.87, 69.21, 68.89, 68.81, 68.71, 68.59, 68.54, 67.91, 66.69, 66.25, 65.95, 65.88, 41.10, 29.86, 29.18, 23.58.

HRMS (MALDI-TOF): calculated for $C_{323}H_{323}NO_{73}$ $[M+K]^+$ 5422.122, found 5426.391.

N*-Benzyloxycarbonyl-5-amino-pentyl (2,3-di-*O*-benzoyl-α-D-arabinofuranosyl)-(1→5)-(2,3-di-*O*-benzoyl-α-D-arabinofuranosyl)-(1→6)-(2-*O*-benzoyl-3,4-di-*O*-benzyl-α-D-mannopyranosyl)-(1→6)-(2-*O*-benzoyl-3,4-di-*O*-benzyl-α-D-mannopyranosyl)-(1→6)-(2-*O*-benzoyl-3,4-di-*O*-benzyl-α-D-mannopyranosyl)-(1→6)-(2-*O*-benzoyl-3,4-di-*O*-benzyl-α-D-mannopyranosyl)-(1→6)-(2-*O*-benzoyl-3,4-di-*O*-benzyl-α-D-mannopyranosyl)-(1→6)-2-*O*-benzoyl-3,4-di-*O*-benzyl-α-D-mannopyranoside (98):** For automated synthesis of **98,** linker-functionalized resin **4** (17 mg, 6.25 μmol) was placed in the reaction vessel and the resin was washed with DMF, THF, and DCM. Afterward the acid wash (Module **B**), glycosylation (Module **C**) or (Module **C*), and deprotection (Module **D**) executed according to the modules. Mixing of the components was performed by bubbling Argon (Ar) through the reaction mixture.

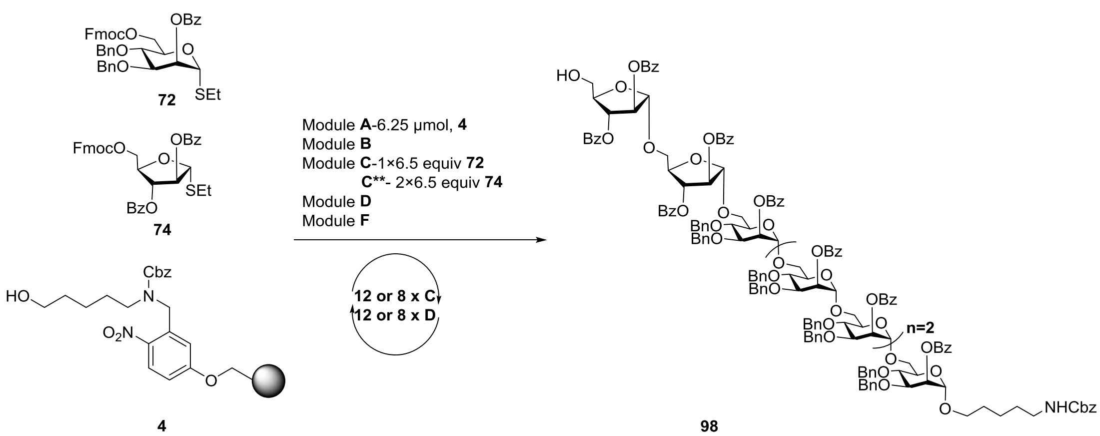

Module **B** (62.5 mM TMSOTf in DCM, 1 x 2 min, -20 ºC)

Module **C** (1 x 6.5 equiv. **72**, NIS, TfOH, DCM/Dioxane, 1 x 35 min, -40 ºC to -20 ºC)

Module **D** (20% NEt_3 in DMF, 3 x 5 min, rt)

Module **B** (62.5 mM TMSOTf in DCM, 1 x 2 min, -20 ºC)

Module **C** (1 x 6.5 equiv. **72**, NIS, TfOH, DCM/Dioxane, 1 x 35 min, -40 ºC to -20 ºC)

Module **D** (20% NEt_3 in DMF, 3 x 5 min, rt)

Module **B** (62.5 mM TMSOTf in DCM, 1 x 2 min, -20 ºC)

Module **C** (1 x 6.5 equiv. **72**, NIS, TfOH, DCM/Dioxane, 1 x 35 min, -40 ºC to -20 ºC)

Module **D** (20% NEt_3 in DMF, 3 x 5 min, rt)

Module **B** (62.5 mM TMSOTf in DCM, 1 x 2 min, -20 ^{o}C)

Module **C** (1 x 6.5 equiv. **72**, NIS, TfOH, DCM/Dioxane, 1 x 35 min, -40 °C to -20 °C)

Module **D** (20% NEt_3 in DMF, 3 x 5 min, rt)

Module **B** (62.5 mM TMSOTf in DCM, 1 x 2 min, -20 ºC)

Module **C** (1 x 6.5 equiv. **72**, NIS, TfOH, DCM/Dioxane, 1 x 35 min, -40 ºC to -20 ºC)

Module **D** (20% NEt_3 in DMF, 3 x 5 min, rt)

Module **B** (62.5 mM TMSOTf in DCM, 1 x 2 min, -20 ºC)

Module **C** (1 x 6.5 equiv. **72**, NIS, TfOH, DCM/Dioxane, 1 x 35 min, -40 ºC to -20 ºC)

Module **D** (20% NEt_3 in DMF, 3 x 5 min, rt)

Module **B** (62.5 mM TMSOTf in DCM, 1 x 2 min, -20 ºC)

Module **C**** (2 x 6.5 equiv. **74**, NIS, TfOH, DCM/Dioxane, 2 x 45 min, -40 ºC to -20 ºC)

Module **D** (20% NEt_3 in DMF, 3 x 5 min, rt)

Module **B** (62.5 mM TMSOTf in DCM, 1 x 2 min, -20 ºC)

Module **C**** (2 x 6.5 equiv. **74**, NIS, TfOH, DCM/Dioxane, 2 x 45 min, -40 ºC to -20 ºC)

Module **D** (20% NEt_3 in DMF, 3 x 5 min, rt)

Module **F** Resin cleaved using UV irradiation at 305 nm in a continuous flow photoreactor.

Crude NP-HPLC of hexasaccharide 98 (ELSD trace, Method A, t_R = 29.7 min)

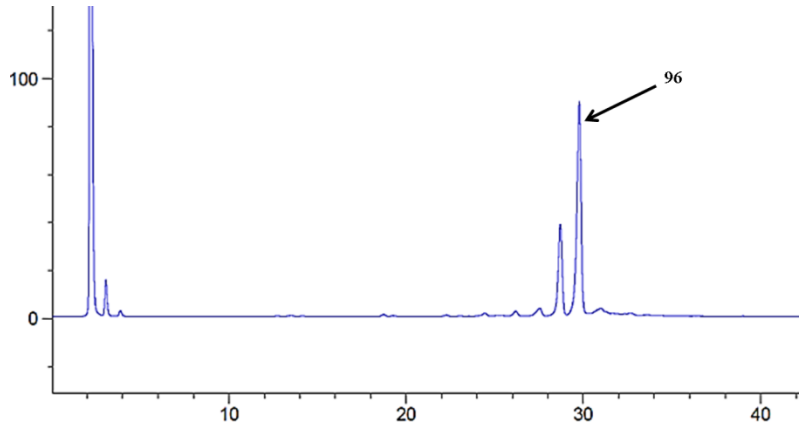

The crude product was purified using a preparative HPLC (Method B, t_R = 30 min), to provide the fully protected linear octasaccharide **98** (2 mg, 5.56 μmol, 9%, based on resin loading).

^{1}H NMR (400 MHz, $CDCl_3$) δ 8.19 – 8.08 (m, 12H), 8.06 – 8.01 (m, 4H), 7.83 – 7.76 (m, 4H), 7.62 – 7.56 (m, 1H), 7.53 – 7.05 (m, 90H), 6.98 – 6.89 (m, 4H), 5.88 – 5.74 (m, 6H),

5.62 (dd, *J* = 3.3, 1.9 Hz, 1H), 5.55 (dd, *J* = 7.9, 2.8 Hz, 2H), 5.42 (s, 1H), 5.37 – 5.30 (m, 2H), 5.10 – 5.01 (m, 6H), 4.90 – 4.75 (m, 12H), 4.66 (d, *J* = 11.4 Hz, 1H), 4.54 (d, *J* = 11.0 Hz, 1H), 4.48 – 4.31 (m, 12H), 4.26 – 4.19 (m, 1H), 4.13 (d, *J* = 3.6 Hz, 1H), 4.09 – 3.99 (m, 8H), 3.99 – 3.90 (m, 7H), 3.90 – 3.81 (m, 4H), 3.79 – 3.70 (m, 6H), 3.67 (d, *J* = 8.6 Hz, 3H), 3.58 (t, *J* = 10.4 Hz, 3H), 3.51 – 3.35 (m, 5H), 3.19 – 3.10 (m, 2H), 1.52 – 1.42 (m, 4H), 1.36 – 1.32 (m, 2H); ^{13}C NMR (150 MHz, $CDCl_3$) δ 165.95, 165.80, 165.57, 165.47, 165.29, 165.02, 138.54, 138.51, 138.47, 138.45, 138.40, 138.22, 137.90, 137.60, 137.55, 137.49, 137.26, 133.49, 133.46, 133.42, 133.25, 133.21, 133.16, 133.10, 133.06, 129.96, 129.91, 129.82, 129.73, 129.68, 129.59, 129.14, 128.90, 128.59, 128.50, 128.44, 128.38, 128.29, 128.24, 128.17, 128.15, 128.12, 127.99, 127.63, 127.59, 127.37, 127.30, 127.21, 127.07, 127.04, 126.97, 105.99 (C-anomeric), 105.78 (C-anomeric), 98.45 (C-anomeric), 98.42 (C-anomeric), 98.09 (C-anomeric), 97.83 (C-anomeric), 83.50, 83.22, 81.55, 81.44, 78.55, 78.17, 77.97, 75.13, 75.01, 74.97, 74.17, 73.99, 73.87, 73.79, 73.73, 73.69, 71.77, 71.60, 71.54, 71.38, 71.30, 71.25, 71.20, 71.15, 70.96, 70.87, 70.70, 70.04, 69.03, 68.53, 68.41, 68.36, 68.07, 67.76, 67.73, 66.51, 66.08, 65.81, 65.78, 65.75, 65.64, 65.53, 62.19, 40.92, 29.74, 29.00, 23.39; HRMS (MALDI-TOF): calculated for $C_{213}H_{207}NO_{51}$ $[M+K]^+$ 3633.327, found 3636.136.

***N*-Benzyloxycarbonyl-5-amino-pentyl (2,3-di-*O*-benzoyl-α-D-arabinofuranosyl)-(1→5)-(2,3-di-*O*-benzoyl-α-D-arabinofuranosyl)-(1→5)-(2,3-di-*O*-benzoyl-α-D-arabinofuranosyl)-(1→5)-(2,3-di-*O*-benzoyl-α-D-arabinofuranosyl)-(1→5)-(2,3-di-*O*-benzoyl-α-D-arabinofuranosyl)-(1→5)-(2,3-di-*O*-benzoyl-α-D-arabinofuranosyl)-(1→6)-(2-*O*-benzoyl-3,4-di-*O*-benzyl-α-D-mannopyranosyl)-(1→6)-(2-*O*-benzoyl-3,4-di-*O*-benzyl-α-D-mannopyranosyl)-(1→6)-(2-*O*-benzoyl-3,4-di-*O*-benzyl-α-D-mannopyranosyl)-(1→6)-(2-*O*-benzoyl-3,4-di-*O*-benzyl-α-D-mannopyranosyl)-(1→6)-(2-*O*-benzoyl-3,4-di-*O*-benzyl-α-D-mannopyranosyl)-(1→6)-2-*O*-benzoyl-3,4-di-*O*-benzyl-α-D-mannopyranoside (100):** For automated synthesis of **100,** linker-functionalized resin **4** (17 mg, 6.25 μmol) was placed in the reaction vessel and the resin was washed with DMF, THF, and DCM. Afterward the acid wash (Module **B**), glycosylation (Module **C**) or

(Module **C****), and deprotection (Module **D**) executed according to the modules. Mixing of the components was performed by bubbling Argon (Ar) through the reaction mixture.

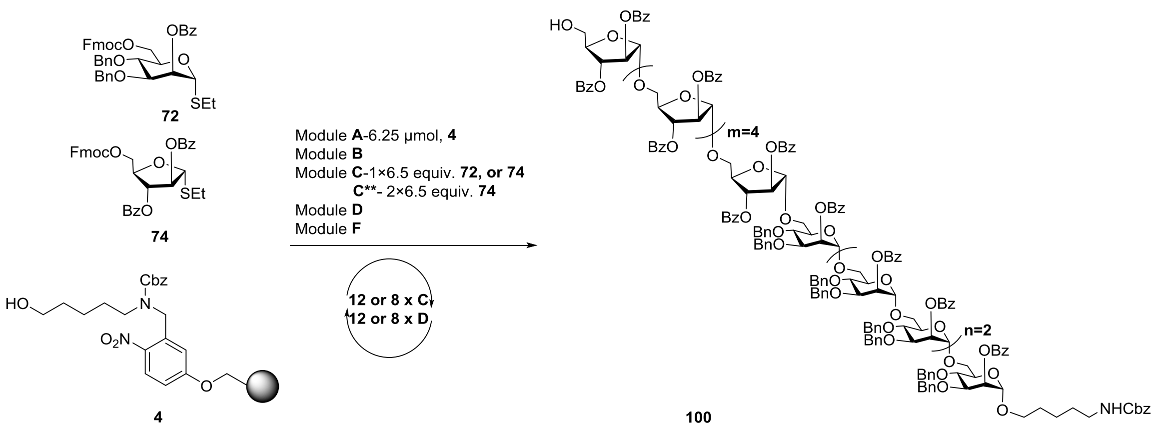

Module **B** (62.5 mM TMSOTf in DCM, 1 x 2 min, -20 ºC)

Module **C** (1 x 6.5 equiv. **72**, NIS, TfOH, DCM/Dioxane, 1 x 35 min, -40 ºC to -20 ºC)

Module **D** (20% NEt_3 in DMF, 3 x 5 min, rt)

Module **B** (62.5 mM TMSOTf in DCM, 1 x 2 min, -20 ºC)

Module **C** (1 x 6.5 equiv. **72**, NIS, TfOH, DCM/Dioxane, 1 x 35 min, -40 ºC to -20 ºC)

Module **D** (20% NEt_3 in DMF, 3 x 5 min, rt)

Module **B** (62.5 mM TMSOTf in DCM, 1 x 2 min, -20 ºC)

Module **C** (1 x 6.5 equiv. **72**, NIS, TfOH, DCM/Dioxane, 1 x 35 min, -40 ºC to -20 ºC)

Module **D** (20% NEt_3 in DMF, 3 x 5 min, rt)

Module **B** (62.5 mM TMSOTf in DCM, 1 x 2 min, -20 ºC)

Module **C** (1 x 6.5 equiv. **72**, NIS, TfOH, DCM/Dioxane, 1 x 35 min, -40 ºC to -20 ºC)

Module **D** (20% NEt_3 in DMF, 3 x 5 min, rt)

Module **B** (62.5 mM TMSOTf in DCM, 1 x 2 min, -20 ºC)

Module **C** (1 x 6.5 equiv. **72**, NIS, TfOH, DCM/Dioxane, 1 x 35 min, -40 ºC to -20 ºC)

Module **D** (20% NEt_3 in DMF, 3 x 5 min, rt)

Module **B** (62.5 mM TMSOTf in DCM, 1 x 2 min, -20 ºC)

Module **C** (1 x 6.5 equiv. **72**, NIS, TfOH, DCM/Dioxane, 1 x 35 min, -40 ºC to -20 ºC)

Module **D** (20% NEt_3 in DMF, 3 x 5 min, rt)

Module **B** (62.5 mM TMSOTf in DCM, 1 x 2 min, -20 ºC)

Module **C**** (2 x 6.5 equiv. **74**, NIS, TfOH, DCM/Dioxane, 2 x 45 min, -40 ºC to -20 ºC)

Module **D** (20% NEt_3 in DMF, 3 x 5 min, rt)

Module **B** (62.5 mM TMSOTf in DCM, 1 x 2 min, -20 ºC)

Module **C** (1 x 6.5 equiv. **74**, NIS, TfOH, DCM/Dioxane, 1 x 45 min, -40 ºC to -20 ºC)

Module **D** (20% NEt_3 in DMF, 3 x 5 min, rt)

Module **B** (62.5 mM TMSOTf in DCM, 1 x 2 min, -20 ºC)

Module **C** (1 x 6.5 equiv. **74**, NIS, TfOH, DCM/Dioxane, 1 x 45 min, -40 ºC to -20 ºC)

Module **D** (20% NEt_3 in DMF, 3 x 5 min, rt)

Module **B** (62.5 mM TMSOTf in DCM, 1 x 2 min, -20 ºC)

Module **C** (1 x 6.5 equiv. **74**, NIS, TfOH, DCM/Dioxane, 1 x 45 min, -40 ºC to -20 ºC)

Module **D** (20% NEt_3 in DMF, 3 x 5 min, rt)

Module **B** (62.5 mM TMSOTf in DCM, 1 x 2 min, -20 ºC)

Module **C** (1 x 6.5 equiv. **74**, NIS, TfOH, DCM/Dioxane, 1 x 45 min, -40 °C to -20 °C)

Module **D** (20% NEt_3 in DMF, 3 x 5 min, rt)

Module **B** (62.5 mM TMSOTf in DCM, 1 x 2 min, -20 ºC)

Module **C** (1 x 6.5 equiv. **74**, NIS, TfOH, DCM/Dioxane, 1 x 45 min, -40 ºC to -20 ºC)

Module **D** (20% NEt_3 in DMF, 3 x 5 min, rt)

Module **F** Resin cleaved using UV irradiation at 305 nm in a continuous flow photoreactor.

Crude NP-HPLC of hexasaccharide 100 (ELSD trace, Method A, t_R = 35.7 min)

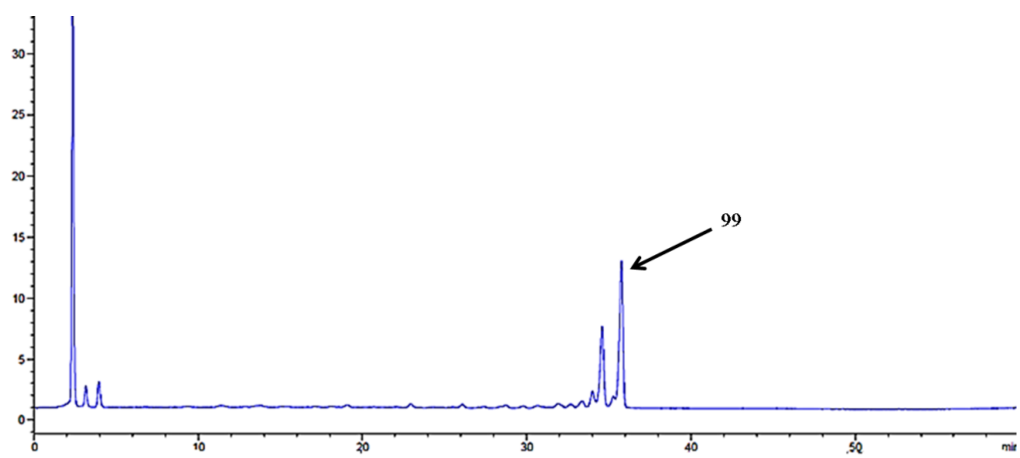

The crude product was purified using a preparative HPLC (Method B, t_R = 37.2 min), to provide the fully protected linear dodecasaccharide **100** (2 mg, 4.03 μmol, 6%, based on resin loading).

^{1}H NMR (600 MHz, $CDCl_3$) δ 8.17 – 7.98 (m, 24H), 7.90 – 7.75 (m, 12H), 7.61 – 7.05 (m, 115H), 6.98 – 6.88 (m, 4H), 5.86 – 5.74 (m, 6H), 5.63 – 5.54 (m, 11H), 5.41 – 5.34 (m, 6H), 5.31 (s, 1H), 5.15 – 4.99 (m, 7H), 4.89 – 4.74 (m, 11H), 4.66 (d, *J* = 11.4 Hz, 1H), 4.58 – 4.51 (m, 3H), 4.48 – 4.21 (m, 10H), 4.15 – 3.37 (m, 50H), 3.20 – 3.10 (m, 2H); ^{13}C NMR (100 MHz, $CDCl_3$) δ 165.76, 165.66, 165.60, 165.22, 138.64, 138.59, 137.78, 137.68, 133.64, 133.54, 133.44, 133.21, 130.15, 129.96, 129.89, 129.76, 129.26, 129.14, 128.78, 128.63, 128.47, 128.35, 127.82, 127.77, 127.37, 127.24, 127.12, 106.01 (C-anomeric), 98.64 (C-anomeric), 98.27 (C-anomeric), 83.76, 83.48, 82.19, 81.64, 81.59, 75.32, 75.20, 71.48, 71.08, 69.22, 68.61, 66.72, 66.25, 65.96, 29.86, 29.19; HRMS (MALDI-TOF): calculated for $C_{289}H_{271}NO_{75}$ $[M+K]^+$ 4993.705, found 4998.822.

N*-Benzyloxycarbonyl-5-amino-pentyl (2,3-di-*O*-benzoyl-α-D-arabinofuranosyl)-(1→5)-(2,3-di-*O*-benzoyl-α-D-arabinofuranosyl)-(1→5)-(2,3-di-*O*-benzoyl-α-D-arabinofuranosyl)-(1→5)-(2,3-di-*O*-benzoyl-α-D-arabinofuranosyl)-(1→5)-(2,3-di-*O*-benzoyl-α-D-arabinofuranosyl)-(1→5)-(2,3-di-*O*-benzoyl-α-D-arabinofuranosyl)-(1→6)-(2-*O*-benzoyl-3,4-di-*O*-benzyl-α-D-mannopyranosyl)-(1→6)-(2-*O*-benzoyl-3,4-di-*O*-benzyl-α-D-mannopyranosyl)-(1→2)-(2-*O*-benzoyl-3,4-di-*O*-benzyl-α-D-mannopyranosyl)-(1→6)-(2-*O*-benzoyl-3,4-di-*O*-benzyl-α-D-mannopyranosyl)-(1→2)-(2-*O*-benzoyl-3,4-di-*O*-benzyl-α-D-mannopyranosyl)-(1→6)-(2-*O*-benzoyl-3,4-di-*O*-benzyl-α-D-mannopyranoside (102):** For automated synthesis of **102,** linker-functionalized resin **4** (17 mg, 6.25 μmol) was placed in the reaction vessel and the resin was washed with DMF, THF, and DCM. Afterward the acid wash (Module **B**), glycosylation (Module **C**) or (Module **C) or (Module **C****), and deprotection (Module **D** and **E**) executed according to the modules. Mixing of the components was performed by bubbling Argon (Ar) through the reaction mixture.

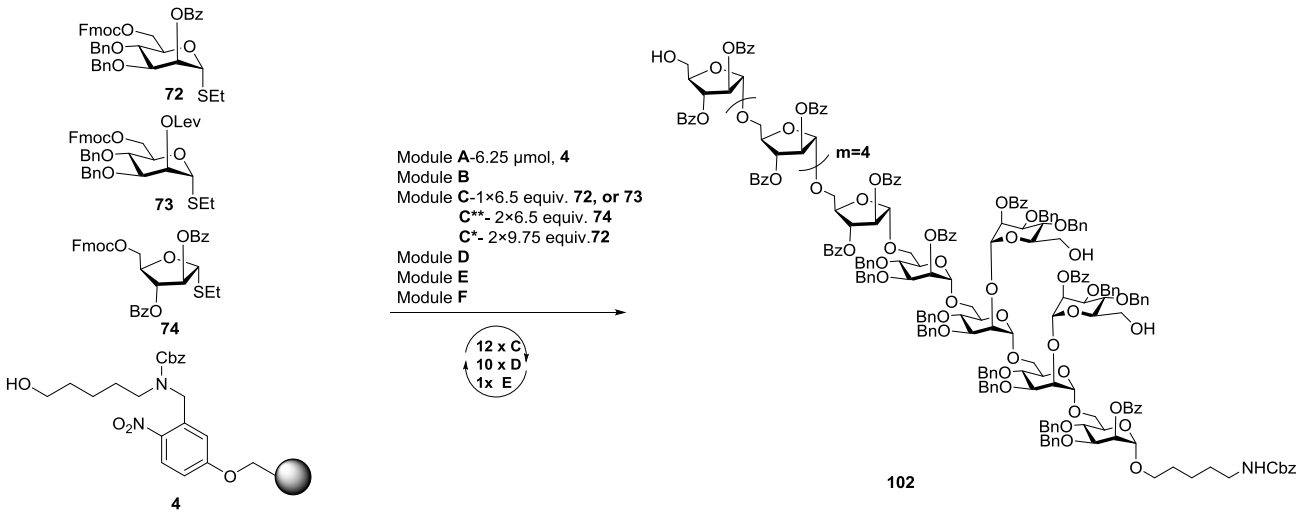

Module **B** (62.5 mM TMSOTf in DCM, 1 x 2 min, -20 ºC)

Module **C** (1 x 6.5 equiv. **72**, NIS, TfOH, DCM/Dioxane, 1 x 35 min, -40 ºC to -20 ºC)

Module **D** (20% NEt_3 in DMF, 3 x 5 min, rt)

Module **B** (62.5 mM TMSOTf in DCM, 1 x 2 min, -20 ºC)

Module **C** (1 x 6.5 equiv. **73**, NIS, TfOH, DCM/Dioxane, 1 x 35 min, -40 ºC to -20 ºC)

Module **D** (20% NEt_3 in DMF, 3 x 5 min, rt)

Module **B** (62.5 mM TMSOTf in DCM, 1 x 2 min, -20 ºC)

Module **C** (1 x 6.5 equiv. **73**, NIS, TfOH, DCM/Dioxane, 1 x 35 min, -40 ºC to -20 ºC)

Module **D** (20% NEt_3 in DMF, 3 x 5 min, rt)

Module **B** (62.5 mM TMSOTf in DCM, 1 x 2 min, -20 ºC)

Module **C** (1 x 6.5 equiv. **72**, NIS, TfOH, DCM/Dioxane, 1 x 35 min, -40 ºC to -20 ºC)

Module **D** (20% NEt_3 in DMF, 3 x 5 min, rt)

Module **B** (62.5 mM TMSOTf in DCM, 1 x 2 min, -20 ºC)

Module **C**** (2 x 6.5 equiv. **74**, NIS, TfOH, DCM/Dioxane, 2 x 45 min, -40 ºC to -20 ºC)

Module **D** (20% NEt_3 in DMF, 3 x 5 min, rt)

Module **B** (62.5 mM TMSOTf in DCM, 1 x 2 min, -20 ºC)

Module **C** (1 x 6.5 equiv. **74**, NIS, TfOH, DCM/Dioxane, 1 x 45 min, -40 ºC to -20 ºC)

Module **D** (20% NEt_3 in DMF, 3 x 5 min, rt)

Module **B** (62.5 mM TMSOTf in DCM, 1 x 2 min, -20 ºC)

Module **C** (1 x 6.5 equiv. **74**, NIS, TfOH, DCM/Dioxane, 1 x 45 min, -40 ºC to -20 ºC)

Module **D** (20% NEt_3 in DMF, 3 x 5 min, rt)

Module **B** (62.5 mM TMSOTf in DCM, 1 x 2 min, -20 ºC)

Module **C** (1 x 6.5 equiv. **74**, NIS, TfOH, DCM/Dioxane, 1 x 45 min, -40 ºC to -20 ºC)

Module **D** (20% NEt_3 in DMF, 3 x 5 min, rt)

Module **C** (1 x 6.5 equiv. **74**, NIS, TfOH, DCM/Dioxane, 1 x 45 min, -40 ºC to -20 ºC)

Module **D** (20% NEt_3 in DMF, 3 x 5 min, rt)

Module **B** (62.5 mM TMSOTf in DCM, 1 x 2 min, -20 ºC)

Module **C** (1 x 6.5 equiv. **74**, NIS, TfOH, DCM/Dioxane, 1 x 45 min, -40 ºC to -20 ºC)

Module **E** (150 mM N_2H_4.AcOH in Py/AcOH/H_2O, 3 x 30 min, rt)

Module **B** (62.5 mM TMSOTf in DCM, 1 x 2 min, -20 ºC)

Module **C*** (2 x 6.5 equiv. **72**, NIS, TfOH, DCM/Dioxane, 2 x 35 min, -40 ºC to -20 ºC)

Module **D** (20% NEt_3 in DMF, 3 x 5 min, rt)

Crude NP-HPLC of hexasaccharide 102 (ELSD trace, Method A, t_R = 37.5 min)

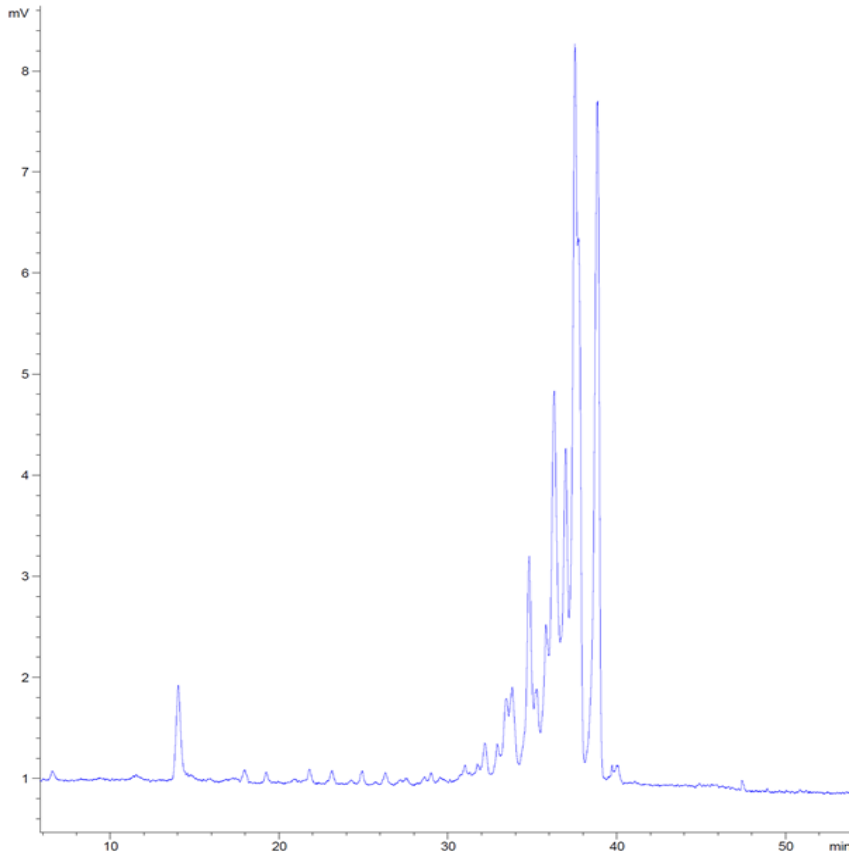

The crude product was purified using a preparative HPLC (Method B, t_R = 38.8 min), to provide the fully protected branched dodecasaccharide **102** (1 mg, 0.211 µmol, 3%, based on resin loading).

HRMS (MALDI-TOF): calculated for $C_{275}H_{263}NO_{73}$ $[M+K]^+$ 4785.653, found 4789.558.

The isolated compounds, LM fragments **87**, **89**, **94** and LAM **98**, and **100** are further characterized and subjected to the global deprotection while compound **102** analyzed by mass and directly subjected to the deprotection, without further characterization due to fewer yields.

Target Compounds	Times/Cycle	Glycosylation[a]	Reaction Time	Ratio of n:n-1:n-2	Yield[b]
87	6	1 Cycle, linear backbone with 6.5 eq of donor	16 h	100:0:0	55%
89	4 1	1 Cycle, linear backbone with 6.5 eq of donor 2 Cycle, branching with 6.5 eq of donor	16 h	87:13:0	37%

Table 2: Summary of hexasaccharide fragments of a LM linear and branched. [a]Glycosyl donor building block equivalents based on the Fmoc loading [b]Yield based on Fmoc loading (Yield in the parenthesis is based on first sugar loading on resin).

Target Compounds	Times/Cycle	Glycosylation[a]	Reaction Time	Yield[b]
91	10 1	1 Cycle, linear backbone with 6.5 eq of donor 2 Cycle, branching with 9.75 eq of donor	32 h	6%
99	6 1 5	1 Cycle, linear backbone with 6.5 eq of donor 2 Cycle, with 6.5 eq of donor 1 Cycle, linear backbone with 6.5 eq of donor	32 h	6%
100	4 1 5 1	1 Cycle, linear backbone with 6.5 eq of donor 2 Cycle, branching with 6.5 eq of donor 1 Cycle, linear backbone with 6.5 eq of donor 2 Cycle, branching with 9.75 eq of donor	32 h	3%

Table 3: Summary of dodecasaccharide fragments of a LM and LAM. [a]Glycosyl donor building block equivalents based on the Fmoc loading [b]Yield based on Fmoc loading (Yield in the parenthesis is based on first sugar loading on resin).

3.4.2.6 Deprotection of LM and LAM fragments;

5-Amino-pentanyl α-D-mannopyranosyl-(1→6)-α-D-mannopyranosyl-(1→6)-α-D-mannopyranosyl-(1→6)-α-D-mannopyranosyl-(1→6)-a-D-mannopyranosyl-(1→6)-α-D-mannopyranoside (6mer) (66)

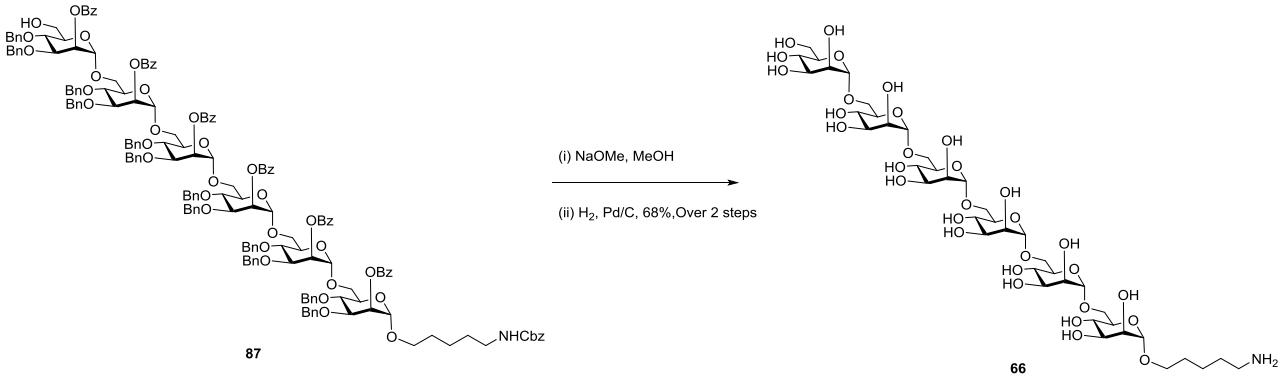

To a solution of protected hexasaccharide **87** (20 mg, 6.86 µmol) in DCM:MeOH (1:1) a solution of NaOMe (0.5 M in MeOH, 0.2 mL) was added. The mixture was stirred for 16 h, after which time was neutralized with of Amberlite IR-120 (H^+) ion exchange resin, filtered and concentrated. The crude product was dissolved in a mixture DCM: t-BuOH: H_2O (1:0.5:0.5 mL). The solution was purged with Ar, then 10% Pd/C was added and the solution purged with H_2 for 30 min, then stirred under an H_2 atmosphere for 48 h. Purification by reversed phase (RP) SPE (Waters Sep-Pak®, C18) column afforded **66** (5 mg, 4.65 µmol, 68% over two steps).^{1}H NMR (400 MHz, D_2O) δ 4.89 – 4.86 (m, 5H), 4.83 (s, 1H), 3.98 – 3.95 (m, 5H), 3.94 – 3.88 (m, 7H), 3.85 (s, 1H), 3.84 – 3.81 (m, 5H), 3.80 – 3.77 (m, 5H), 3.76 – 3.71 (m, 8H), 3.70 (d, J = 2.3 Hz, 2H), 3.69 – 3.60 (m, 4H), 3.57 – 3.51 (m, 1H), 2.98 (t, J = 7.6 Hz, 2H), 1.71 – 1.60 (m, 4H), 1.50 – 1.37 (m, 2H); ^{13}C NMR (100 MHz, D_2O) δ 99.89, 99.42, 99.30, 72.72, 70.92, 70.84, 70.80, 70.78, 70.72, 70.69, 70.55, 70.07, 69.98, 69.94, 67.63, 66.75, 66.61, 66.57, 65.61, 65.58, 65.53, 60.94, 39.38, 28.04, 26.57, 22.54; HRMS (ESI): calculated for $C_{41}H_{73}NO_{31}$ $[M+H]^+$ 1076.4239, found 1076.4244.

5-Amino-pentanyl α-D-mannopyranosyl-(1→6)-α-D-mannopyranosyl-(1→2)-α-D-mannopyranosyl-(1→6)-α-D-mannopyranosyl-(1→2)-α-D-mannopyranosyl-(1→6)-α-D-mannopyranoside (6mer) (67)

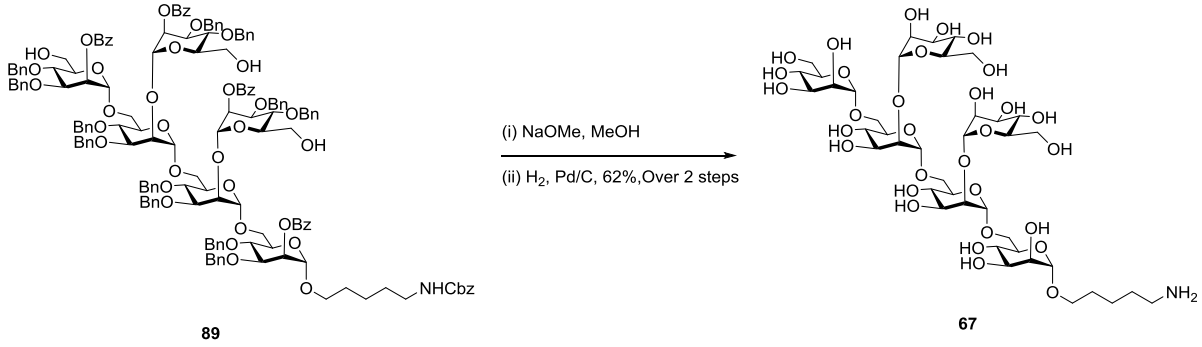

89 67

To a solution of protected hexasaccharide **89** (12.5 mg, 4.62 µmol) in DCM:MeOH (1:1) and NaOMe (0.5 M in MeOH, 0.11 mL) was added and stirred for 16 h. The reaction mixture was neutralized with of Amberlite IR-120 (H^+) ion exchange resin, filtered and concentrated. The crude product was dissolved in a mixture DCM: t-BuOH: H_2O (1:0.5:0.5 mL). The solution was purged with Ar, then 10% Pd/C was added and the solution purged with H_2 for 30 min, then stirred under an H_2 atmosphere for 48 h. Purification by reversed phase (RP) SPE (Waters Sep-Pak®, C18) column afforded **67** (3.1 mg, 2.88 µmol, 62% over two steps).^{1}H NMR (600 MHz, D_2O) δ 5.15 (s, 1H), 5.14 (s, 1H), 5.06 (s, 1H), 5.05 (s, 1H), 4.95 (s, 1H), 4.87 (s, 1H), 4.12 – 3.54 (m, 38H), 3.02 (t, J = 7.7 Hz, 2H), 1.74 – 1.64 (m, 4H), 1.52 – 1.41 (m, 2H); ^{13}C NMR (150 MHz, D_2O) δ 102.23 (2×C-anomeric), 99.85 (C-anomeric), 99.37 (C-anomeric), 98.04 (2×C-anomeric), 78.72, 73.24, 73.17, 72.73, 71.17, 71.08, 70.83, 70.57, 70.38, 69.93, 67.55, 66.64, 66.61, 66.59, 66.50, 66.42, 65.78, 65.58, 65.11, 60.99, 60.96, 60.86, 39.29, 27.95, 26.49, 22.42; HRMS (ESI): calculated for $C_{41}H_{73}NO_{31}$ $[M+H]^+$ 1076.4239, found 1076.4253.

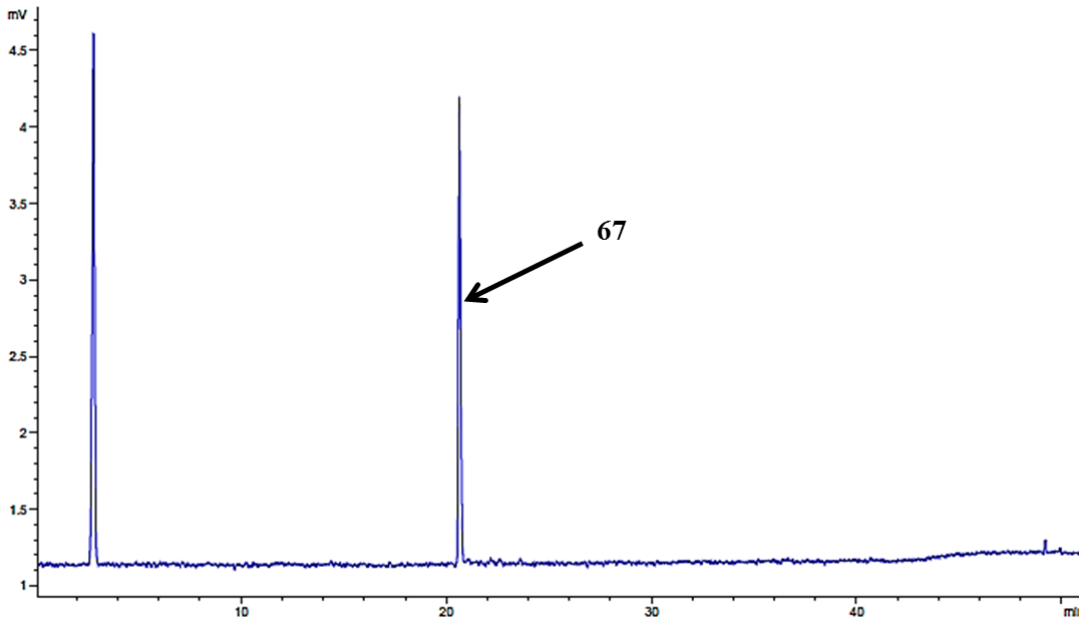

Figure 47: Purified trace of branched dodecasaccharide **67** by Hypercarb HPLC using method **C**.

5-Amino-pentanyl α-D-mannopyranosyl-(1→6)-α-D-mannopyranosyl-(1→2)-α-D-mannopyranosyl-(1→6)-α-D-mannopyranosyl-(1→2)-α-D-mannopyranosyl-(1→6)-α-D-mannopyranosyl-(1→6)-α-D-mannopyranosyl-(1→6)-α-D-mannopyranosyl-(1→6)-α-D-mannopyranosyl-(1→6)-α-D-mannopyranoside (11mer) (68)

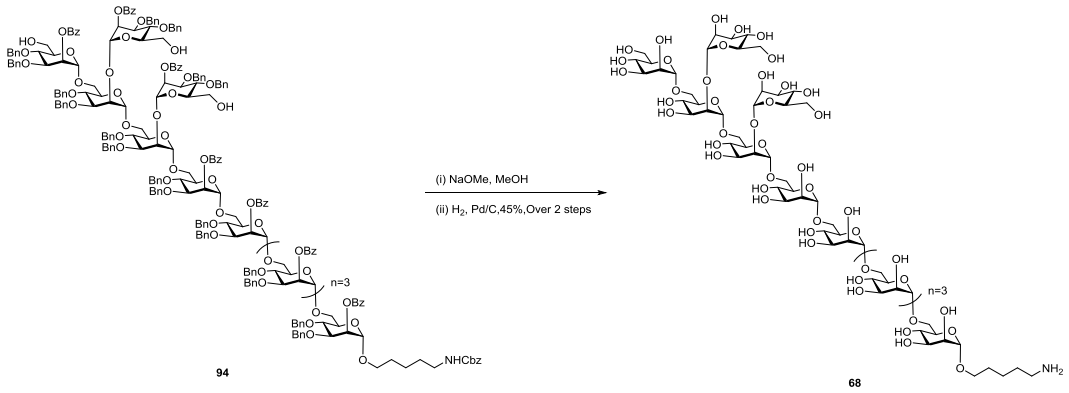

Deprotection of the compound **94** was carried out using Module H: Global deprotection.

^{1}H NMR (700 MHz, D_2O) δ 5.16 (s, 1H), 5.15 (s, 1H), 5.08 – 5.06 (m, 2H), 4.96 (s, 1H), 4.92 (d, J = 6.1 Hz, 5H), 4.89 (s, 1H), 4.12 – 4.10 (m, 2H), 4.06 (s, 2H), 4.02 (d, J = 4.6 Hz, 8H), 4.00 – 3.95 (m, 8H), 3.94 – 3.91 (m, 3H), 3.90 – 3.82 (m, 19H), 3.81 – 3.74 (m, 20H), 3.73 – 3.66 (m, 5H), 3.60 (d, J = 10.1, 6.1 Hz, 1H), 3.02 (t, J = 7.6 Hz, 2H), 1.75 – 1.67 (m, 4H), 1.53 – 1.42 (m, 2H); HRMS (ESI): calculated for $C_{71}H_{123}NO_{56}$ $[M+H]^+$ 1886.6880, found 1886.6770.

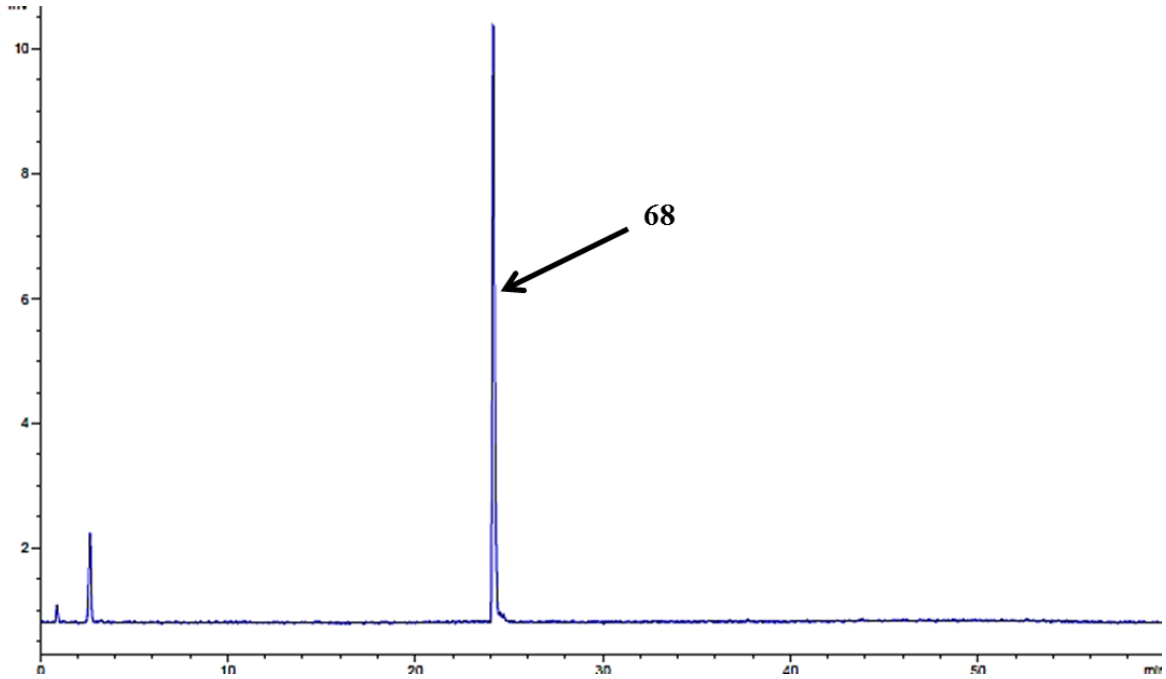

Figure 48: Purified trace of branched dodecasaccharide **102** by Hypercarb HPLC using method **C**.

5-Amino-pentanyl α-D-arabinofuranosyl-(1→5)-α-D-arabinofuranosyl-(1→6)-α-D-mannopyranosyl-(1→6)-α-D-mannopyranosyl-(1→6)-α-D-mannopyranosyl-(1→6)-α-D-mannopyranosyl-(1→6)-α-D-mannopyranosyl-(1→6)-α-D-mannopyranoside (8mer) (69)

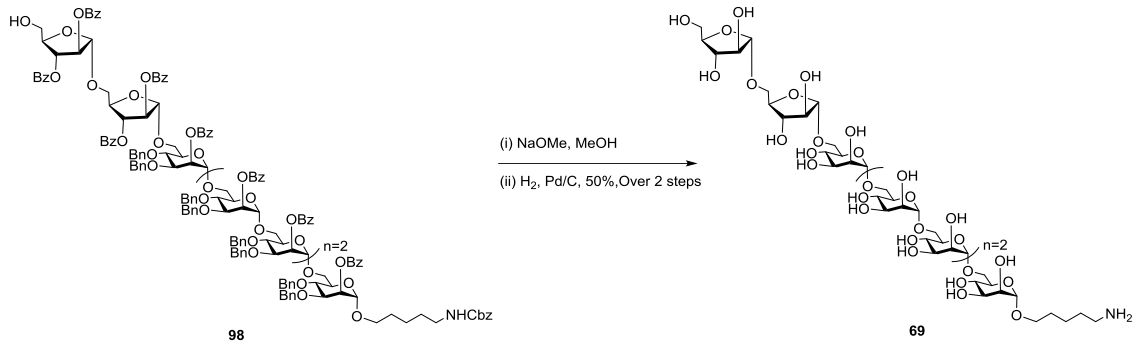

Deprotection of the compound **98** was carried out using Module H: Global deprotection. ^{1}H NMR (700 MHz, D_2O) δ 5.12 (s, 1H), 5.11 (s, 1H), 4.94 – 4.91 (m, 5H), 4.89 (s, 1H), 4.25 (s, 1H), 4.16 (d, J = 6.7 Hz, 2H), 4.12 (s, 1H), 4.04 (s, 1H), 4.01 (s, 5H), 3.97 (q, J = 11.5, 9.6 Hz, 8H), 3.93 – 3.72 (m, 28H), 3.67 (dd, J = 11.8, 4.5 Hz, 1H), 3.62 – 3.57 (m, 1H), 3.02 (t, J = 7.7 Hz, 3H), 1.74 – 1.67 (m, 3H), 1.52 – 1.43 (m, 2H); HRMS (ESI): calculated for $C_{51}H_{89}NO_{39}$ $[M+H]^+$ 1340.5084, found 1340.5016.

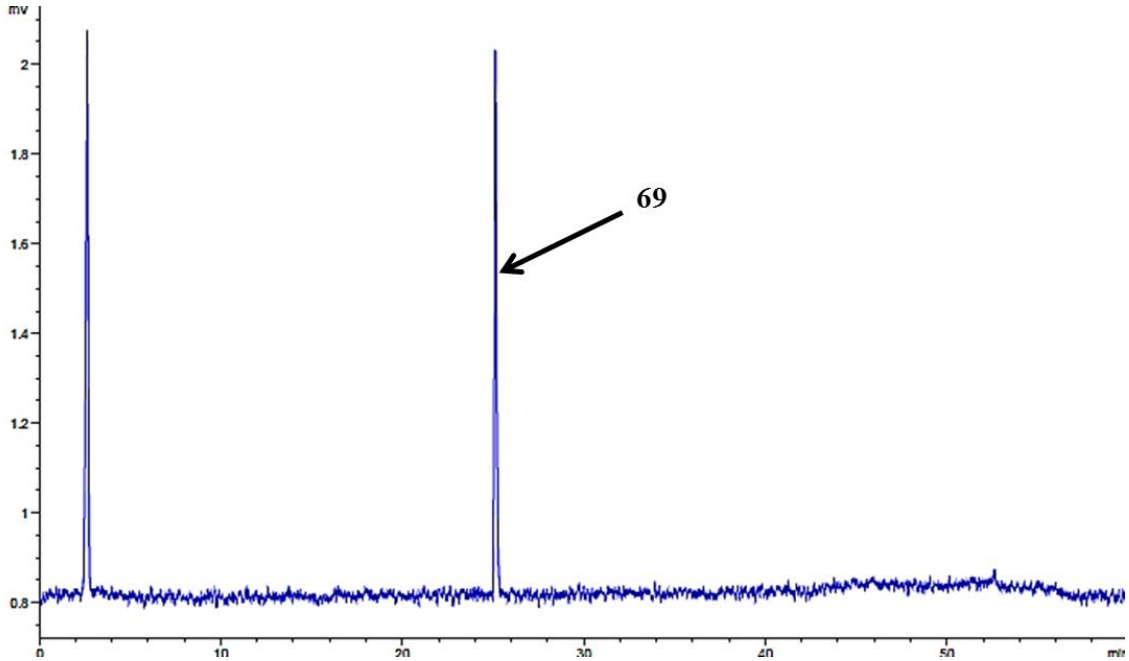

Figure 49: Purified trace of branched dodecasaccharide **69** by Hypercarb HPLC using method **C**.

5-Amino-pentanyl α-D-arabinofuranosyl-(1→5)-α-D-arabinofuranosyl-(1→5)-α-D-arabinofuranosyl-(1→5)-α-D-arabinofuranosyl-(1→5)-α-D-arabinofuranosyl-(1→5)-α-D-arabinofuranosyl-(1→6)-α-D-mannopyranosyl-(1→6)-α-D-mannopyranosyl-(1→6)-α-

D-mannopyranosyl-(1→6)-α-D-mannopyranosyl-(1→6)-α-D-mannopyranosyl-(1→6)-α-D-mannopyranoside (12mer) (70)

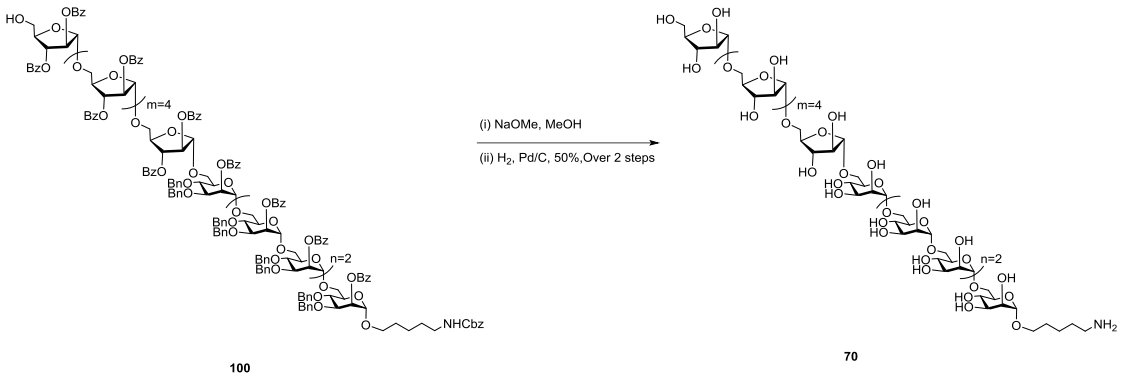

Deprotection of the compound **90** was carried out using Module H: Global deprotection. ^{1}H NMR (700 MHz, D_2O) δ 5.13 – 5.11 (m, 6H), 4.94 – 4.91 (m, 5H), 4.89 (s, 1H), 4.26 – 4.22 (m, 5H), 4.17 – 4.15 (m, 6H), 4.13 – 4.10 (m, 1H), 4.06 – 3.94 (m, 17H), 3.94 – 3.72 (m, 37H), 3.67 (dd, J = 11.6, 4.3 Hz, 1H), 3.61 – 3.57 (m, 1H), 3.02 (t, J = 7.7 Hz, 2H), 1.74 – 1.66 (m, 4H), 1.53 – 1.43 (m, 2H); HRMS (ESI): calculated for $C_{71}H_{121}NO_{55}$ $[M+H]^+$ 1868.6775, found 1868.6803.

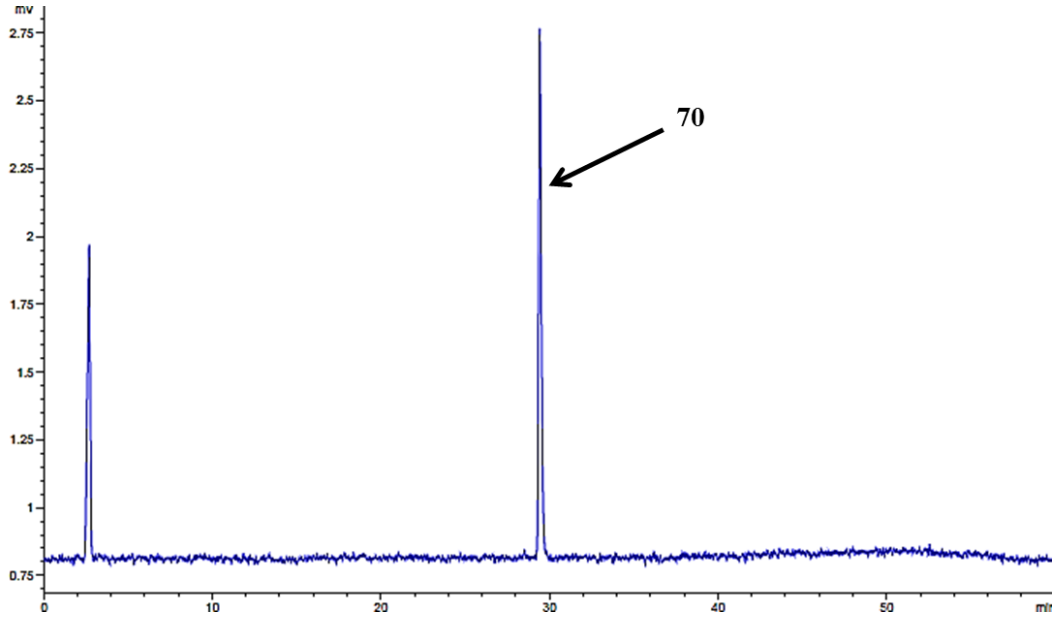

Figure 50: Purified trace of linear dodecasaccharide **70** by Hypercarb HPLC using method **C**.

5-Amino-pentanyl α-D-arabinofuranosyl-(1→5)-α-D-arabinofuranosyl-(1→5)-α-D-arabinofuranosyl-(1→5)-α-D-arabinofuranosyl-(1→5)-α-D-arabinofuranosyl-(1→5)-α-D-arabinofuranosyl-(1→6)-α-D-mannopyranosyl-(1→6)-α-D-mannopyranosyl-(1→2)-α-D-mannopyranosyl-(1→6)-α-D-mannopyranosyl-(1→2)-α-D-mannopyranosyl-(1→6)-α-D-mannopyranoside (12mer) (71)

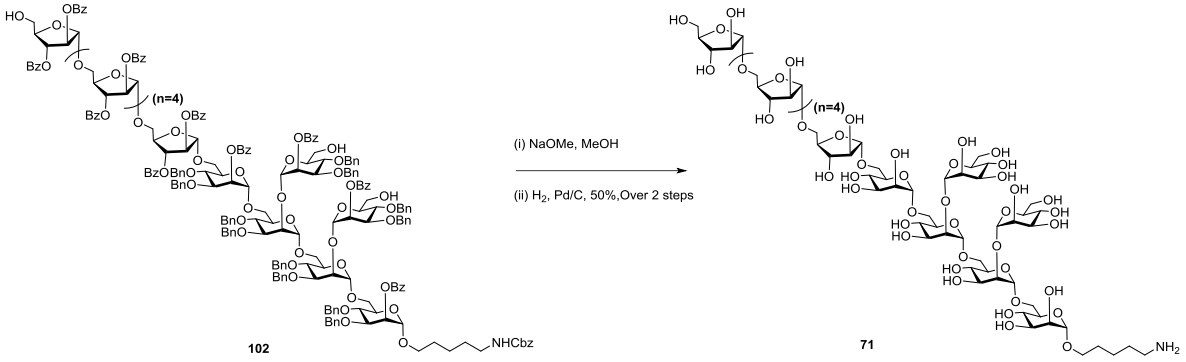

Deprotection of the compound **102** was carried out using Module H: Global deprotection. ^{1}H NMR (700 MHz, D_2O) δ 5.16 (s, 1H), 5.15 (s, 1H), 5.12 (s, 6H), 5.07 (s, 1H), 5.06 (s, 1H), 4.95 (s, 1H), 4.88 (s, 1H), 4.24 (s, 5H), 4.17 (d, J = 10.3 Hz, 6H), 4.11 (s, 3H), 4.07 – 3.94 (m, 15H), 3.94 – 3.90 (m, 7H), 3.87 – 3.81 (m, 15H), 3.80 – 3.66 (m, 16H), 3.61 – 3.57 (m, 1H), 3.03 (t, J = 7.6 Hz, 2H), 1.74 – 1.67 (m, 4H), 1.52 – 1.44 (m, 2H); HRMS (ESI): calculated for $C_{71}H_{121}NO_{55}$ $[M+H]^+$ 1868.6775, found 1868.6691.

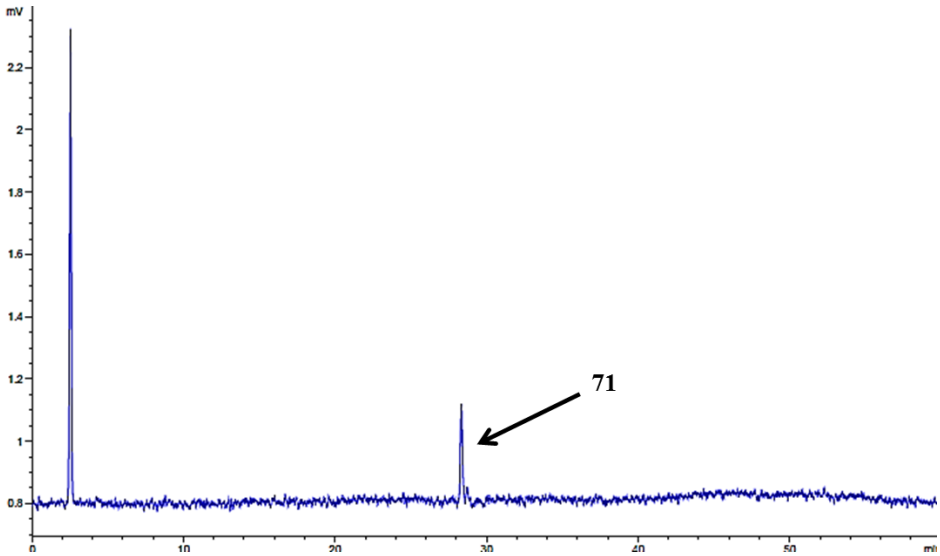

Figure 51: Purified trace of branched dodecasaccharide **71** by Hypercarb HPLC using method **C**.

The ^{13}C spectra were not recorded for the compound **68-71**, because the amount of the compounds obtained was to less.

4. Applications of Automated glycan Assembly

4.1 Introduction

The following section has been taken in part and modified from the article; Reprinted with permission from:

Delbianco, M., Bharate, P., Varela-Aramburu, S., and Seeberger, P. H. Carbohydrates in supramolecular chemistry *Chem. Rev.* **2016**, *116* (4), pp 1693–1752, DOI: 10.1021/acs.chemrev.5b00516. Copyright © 2016 American Chemical Society.

Dendrimers usually refer to a class of branched compounds with a regular and symmetric spherical shape. Terminologies such as clusters refer to small molecules with only few repeating arms, whereas the term dendrimer describes more complex and branched structures (Fig. 52). Many dendrimeric structures, presenting different cores, such as polymers, peptides, sugars, aromatic or aliphatic molecules and metal complexes have been used as a starting point to build branched structures with different geometries.[237, 238] Some of the important strategies for dendrimer synthesis are Michael reaction, click chemistry and Diels-Alder reaction to name a few.[239]

Dendrimers provide a useful platform for the creation of multivalent systems. The facile functionalization of the outer sphere permits the conjugation of different molecules on the surface while the inner sphere can be used as a depot for genes or drugs delivery.[237]

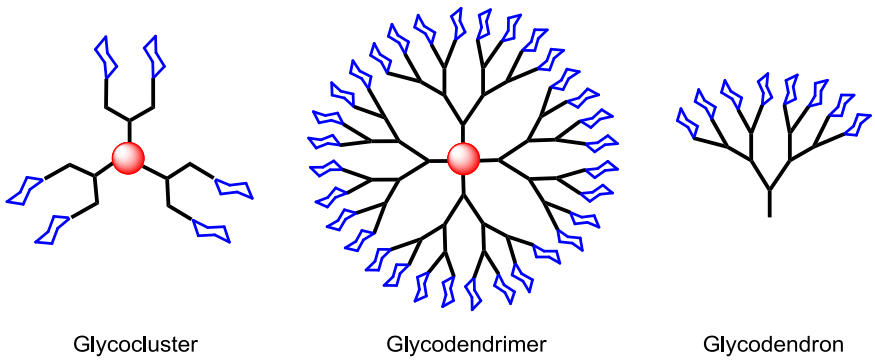

Figure 52. General structures of glycoclusters, glycodendrimers and glycodendrons. Adapted from Delbianco et al.[67]

Multivalent display enhances carbohydrate-protein interactions (CPIs) and has prompted the synthesis of a variety of synthetic glycoclusters and glycodendrimers (GDs). These glycoclusters and dendrimeric systems have found applications as vaccines, anti-bacterial agents, anti-cancer drugs, and imaging reporters.[64, 240] In addition, the hydrophilic glycodendrimers surface, makes them water soluble while the hydrophobic core can encapsulate small molecules, to enhance their solubility.

4.1.1 Self –assembling structures

Multivalent glycoclusters can be synthesized through the covalent conjugation of monomers to a branched core, through complexation around a metal or through a self-assembly process. In the case of carbohydrates, the hydrophilic sugar is generally attached to a lipophilic unit creating an amphiphilic compound. These amphiphilic units are able to self-organize in defined structures such as micelles, vesicles, wires or gels. Multiple carbohydrate-carbohydrate interactions (CCIs) can be established between single monomers to further stabilize the systems. Self-assembly offers two key advantages: multivalent scaffolds can be prepared with relatively small synthetic effort compared to covalently synthesized analogues, and well defined structures with tunable sugar distribution can be fabricated. In order to form supramolecular aggregates, CCIs and hydrophobic interactions (*e.g.* π-π interactions) are required to form simultaneously. The use of asymmetric building blocks (Janus dendrimers), which link together a lipophilic and a hydrophilic part, has been described as a strategy for the formation of self-assembling systems.[241]

Percec contributed fundamentally to the field of self-assembly and dendrimers.[242] Many sugar-substituted Janus dendrimers were prepared and shown to form different supramolecular aggregates depending on the chemical structures (Fig. 53). The supramolecular structure formed upon addition of dendrimers dissolved in THF or ethanol solution to an aqueous phase. Solid lamellae as well as solid vesicles and hard micelles were obtained depending on the monomer structures and the way of injection. Size and shape of

the aggregates were investigated by DLS and revealed that the membrane thickness was approximately equal to the length of two Janus glycodendrimers.

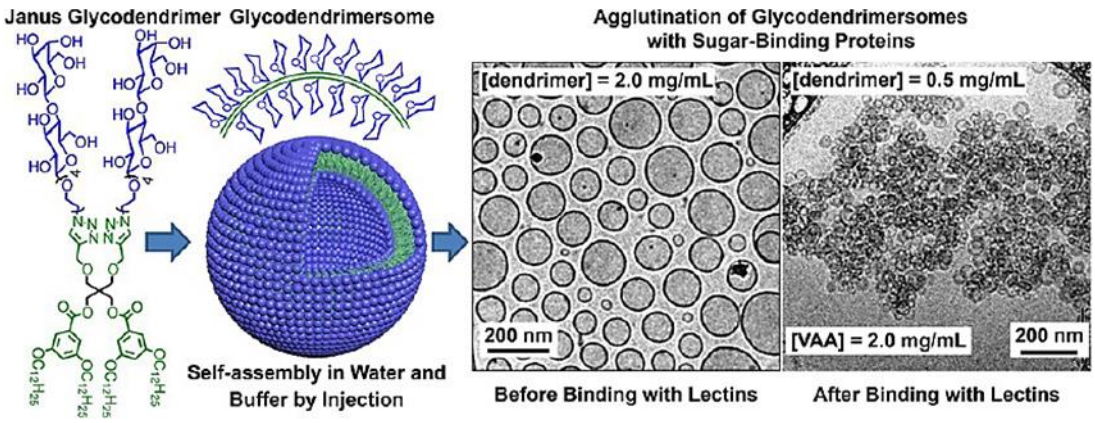

Figure 53: Percec's synthesis of Janus glycodendrimersome.[242]

The formation of aggregates or structures of different shapes and sizes has enabled many applications in the field of drug-delivery and molecular recognition.[243] The interaction with lectins was affected by the morphology of the aggregate: the smaller the glycodendrimersome (GDSs) the faster the agglutination, probably due to the higher surface/volume ratio.[244] The agglutination of these structures, in the presence of lectins, depends on the amount of sugar displayed on the surface as well as the topological conformation.[245] Furthermore, Percec and coworkers have synthesized a library of mono-Mannose-representing Janus GDs which are structurally related to multilayered vesicles. This synthetic glycolipids form after subjecting from water-miscible solvent to buffer produces, monodisperse multi-lamellar onion like GDSs (Fig. 54).[246]

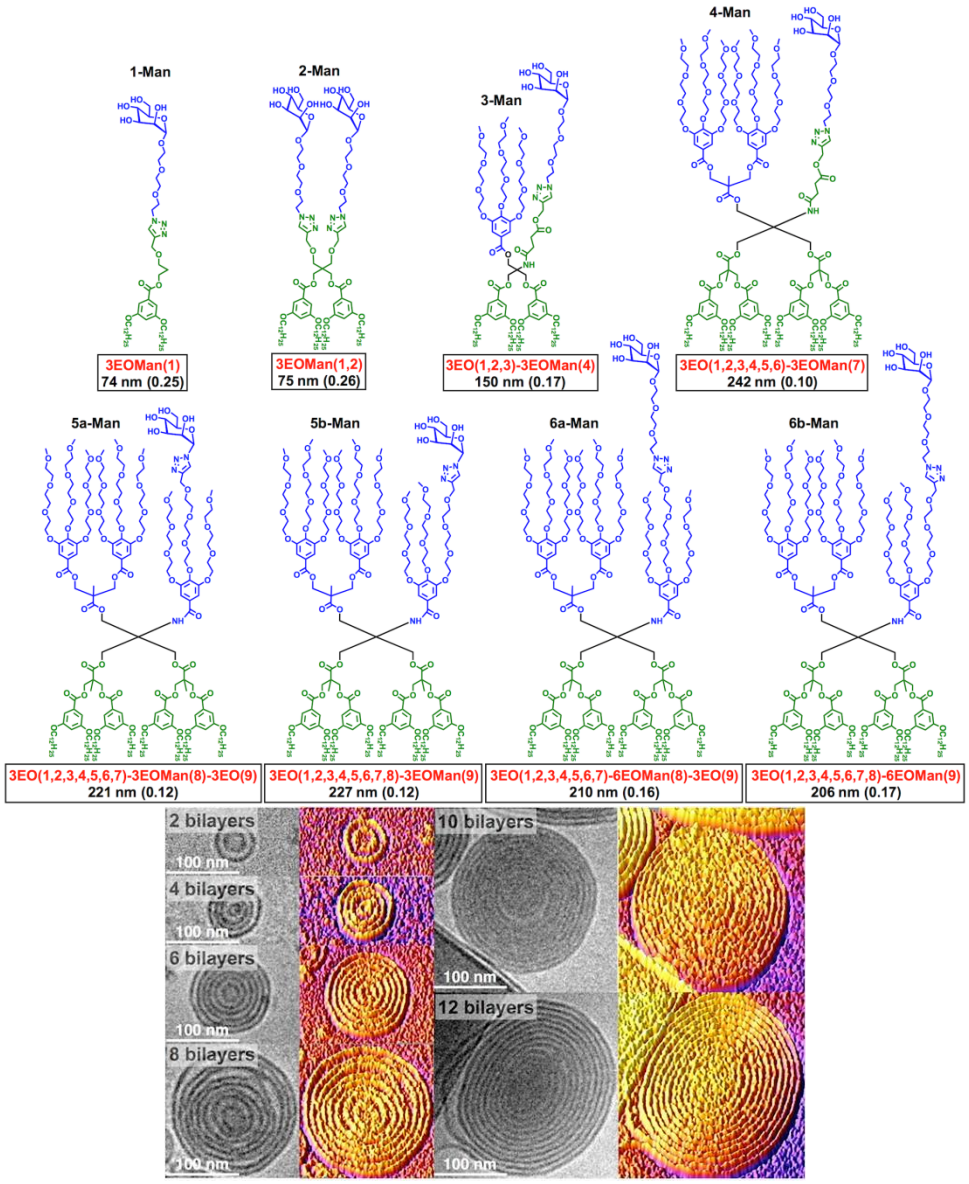

Figure 54: Percec's library of Man-presenting amphiphilic onion like Janus GDs. Adapted from Xiao et al.[246]

The main novelty and advantage of these systems is the homogeneous and controlled distribution of the sugar on the glycodendrimersome surface. This is not possible in the case of glycodendrimers forming upon covalent attachment of carbohydrate to a dendritic core, where only a statistical distribution can be obtained. Thus, these systems represent an ideal platform to study the molecular aspects of cell interactions, providing a better understanding of lectins.[247, 248]

4.1.2 Strategy

In this part of the thesis, a library of self-assembled Janus GDs functionalized with linear oilgomannosides (mono- to hexasaccharide) will be described (Fig. 55). Man-GDs will be analyzed to check their binding with ConA lectin as well as to investigate their shape and structure. As mentioned in Chapter 1 (section 1.5) and Chapter 3, AGA can afford complex oligosaccharides in short time. Those structures can be utilized to further functionalize dendrimers. This project is in collaboration with Xiao Qi, from Prof. Dr. Virgil Percec group (Department of Chemistry, University of Pennsylvania, USA), who synthesized the glycodendrimersomes. The mannose compounds (**66** and **103-106**) that were provided to Percec group were synthesized using AGA (Chapter 3, section 2.1) (Scheme 24).

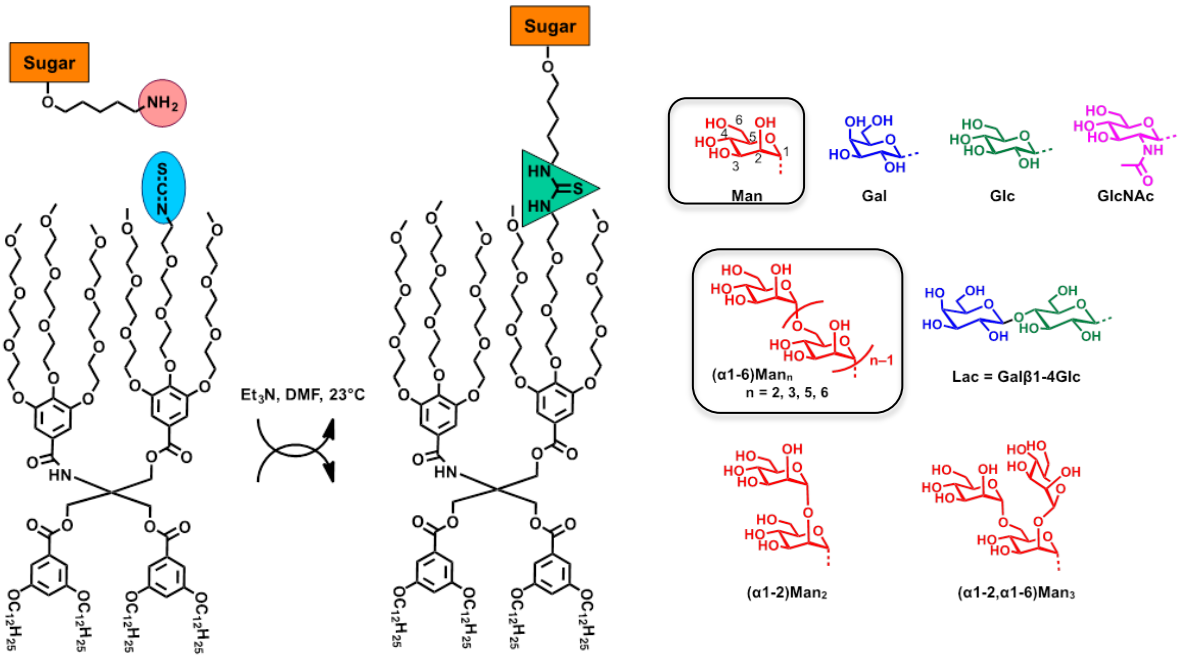

Figure 55: Synthesis of Janus glycodendrimers from automated synthesized oligosaccharides. The highlighted compounds will be discussed in this thesis.

From previous findings (Fig. 54),[246] the lectin binding is affected by the density of carbohydrate displayed on the surface of the aggregate and on the dendrimersome topology [245]. Here we present the synthesis of GDs functionalized with mannose oligosaccharides with different lengths (**103-106**) to expand the knowledge on carbohydrate-lectins interaction (Currently under investigation by Xiao Qi, from Prof. Dr. Virgil Percec group).

The required mannose oligosaccharides (**87**-**88** and **106**-**108**) were assembled following the strategy described in Chapter 3. The desired compounds (Scheme 24) were given to the collaborators for Janus dendrimer functionalization.

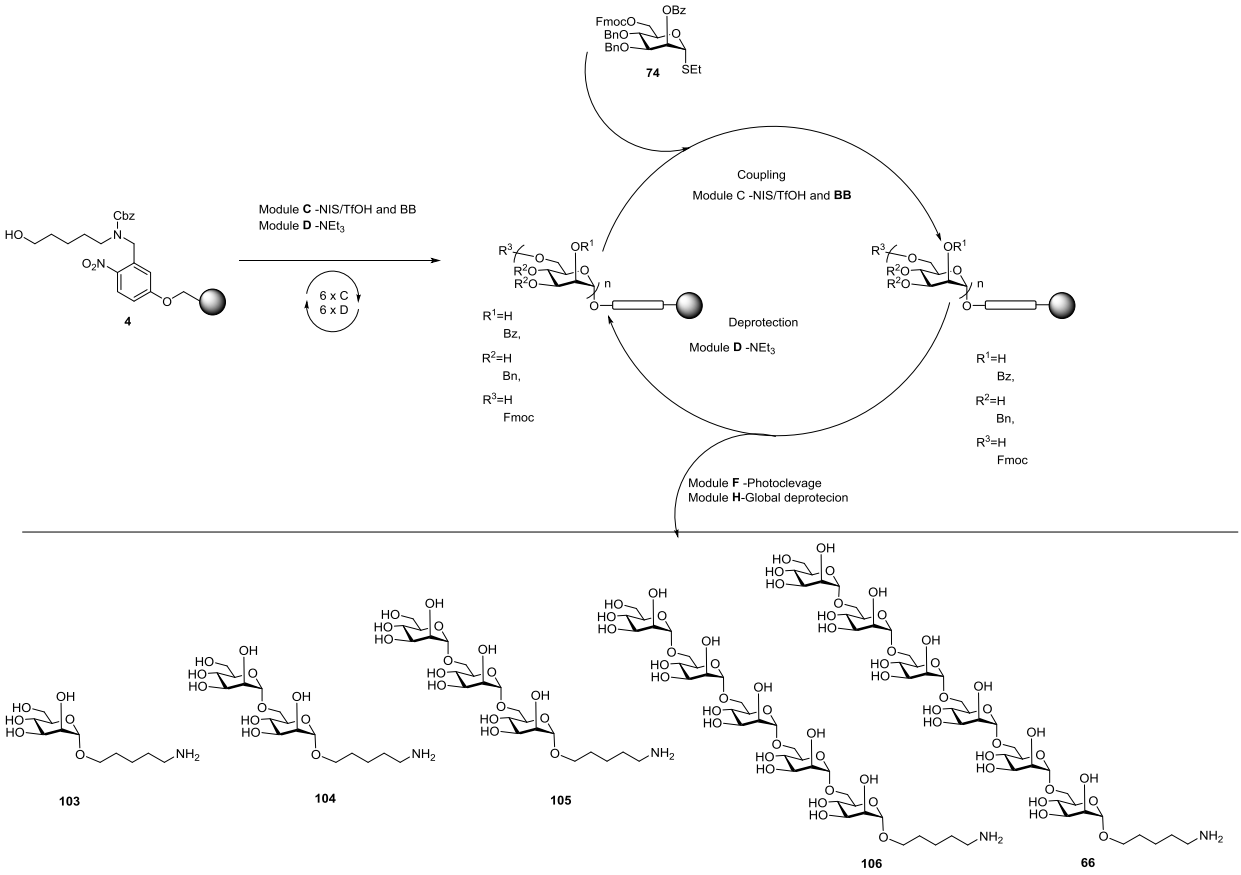

Scheme 24: Library of mannose oligosaccharides **103**-**106** assembled by AGA.

4.2 Results

4.2.1 Synthesis of a library of linear mannose fragments by AGA

A library of linear mannose oligosaccharides ranging from mono- to hexasaccharide was assembled using AGA (Scheme 1). The synthesis was carried out using 6.5 equiv of building block **74** per glycosylation cycle on solid support **4 (**12.5 µmol scale**)** (Scheme 25).

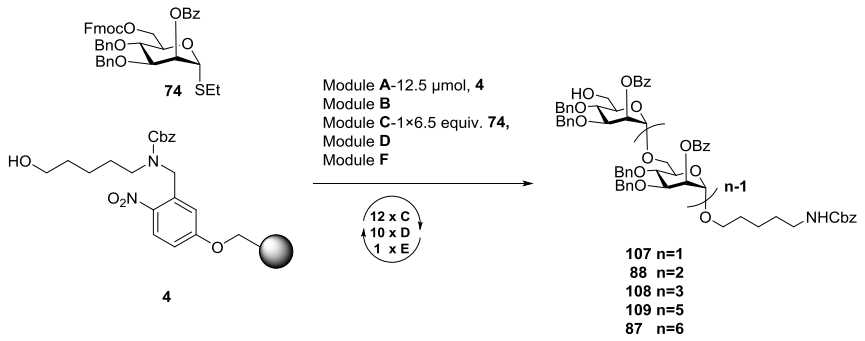

Scheme 25: Automated synthesis of linear Mannose compounds **87-88,** and **107-109**: Reactions and conditions: Module **B**-Acidic wash: TMSOTf, CH_2Cl_2, -20 ^oC, (2 min); Module **C**-Glycosylation: **74**, NIS, TfOH, -20 ^oC, (30 min), CH_2Cl_2/Dioxane (5:1); Module **D**-Fmoc deprotection: 20% Et_3N in DMF, 25 ^oC, (3 x 5 min); Module **F**-post-automation photocleavage: hυ, CH_2Cl_2, 25 ^oC.

The compounds (**87-88, 107-109**) were further purified using NP-HPLC, confirmed by ^1H, HSQC, ^{13}C NMR and MALDI-TOF and subjected to global deprotection.

4.2.3 Deprotection of the Mannose Oligosaccharides

The global deprotection of the mannose compounds **88,** and **107-109** was achieved by removal of the benzoate ester protecting group using Zemplén methanolysis followed by Pd-catalyzed hydrogenolysis of the carboxybenzyl group and the benzyl ethers.

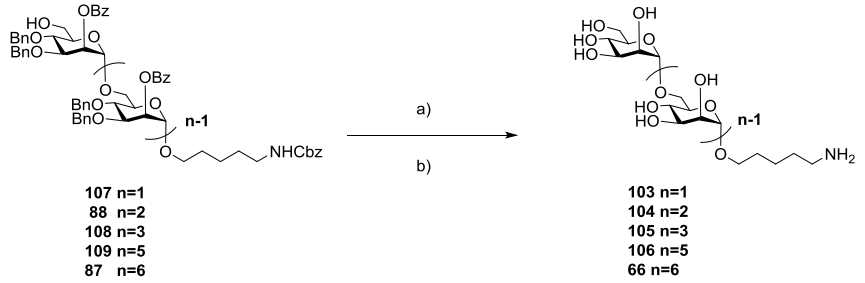

Scheme 26: Global deprotection conditions: a) NaOMe, CH_2Cl_2:MeOH, 1:1, 16 h; b) H_2, Pd/C, CH_2Cl_2:H_2O:*t*-BuOH-1:0.5:0.5, 16 h; **104**-96%, **105**-96% and **106**-98%, over two steps.

Mannose compounds **104-106** were purified using reversed phase (RP) SPE (Waters Sep-Pak®, C18) column and obtained in 96%, 96% and 98% yield over two steps, equipping aminopentyl linker at the reducing end respectively (Scheme 26).

4.2.4 Synthesis of Glycodendrimers

Mannose-glycodendrimers (Man-GDs) **111-115**[5] were synthesized by reacting the amine functionalized oilgomannosides (**103-106** and **66)** with the isothiocyanate-containing amphiphilic building block **110** in the presence of trimethylamine, affording a library of Man-GDs **111-115** (Scheme 27).

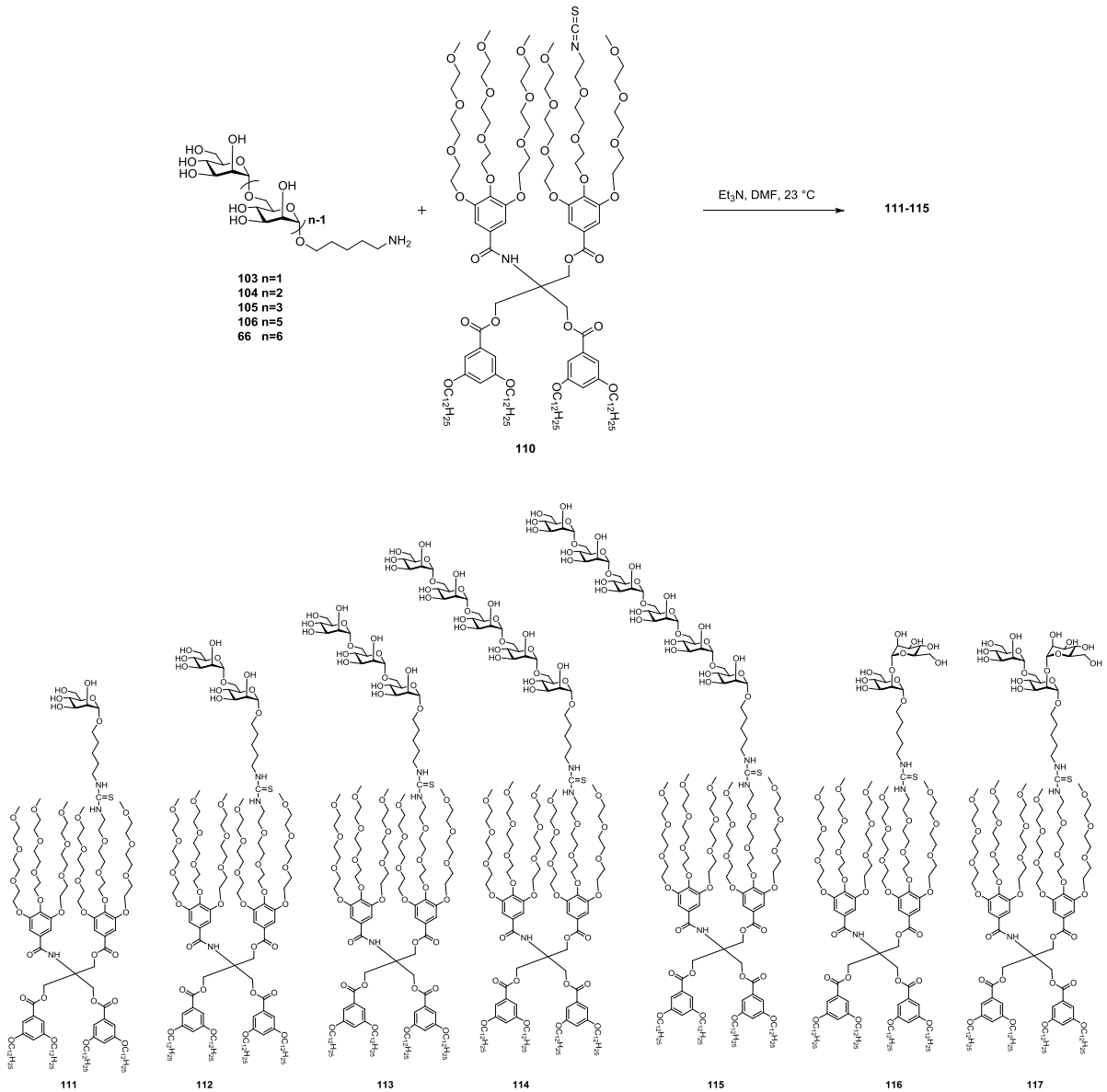

Scheme 27: Synthesis of Man-Glycodendrimers **111-117.**

[5]Synthesis and analysis of Glycodendrimers **110-115** was carried out by Xiao Qi, from Prof. Dr. Virgil Percec group (Department of Chemistry, University of Pennsylvania, USA). Branched Structures α(1→2)Man_2 and α(1→2,α1→6)Man_3 were provided by Dr. Martina Delbianco.

These Man-GDs **111-115** self-assembled into glycodendrimersomes (GDSs); **111** to **GDSs-C5-Man**, **112** to **GDSs-C5-Man$_2$**, **113** to **GDSs-C5-Man$_3$**, **114** to **GDSs-C5-Man$_5$** and **115** to **GDSs-C5-Man$_6$** respectively. The size and shape of the self-assembled **111**, and **112** was investigated by TEM imaging, which showed the formation of vesicles of 100 nm (Fig. 56a,b).

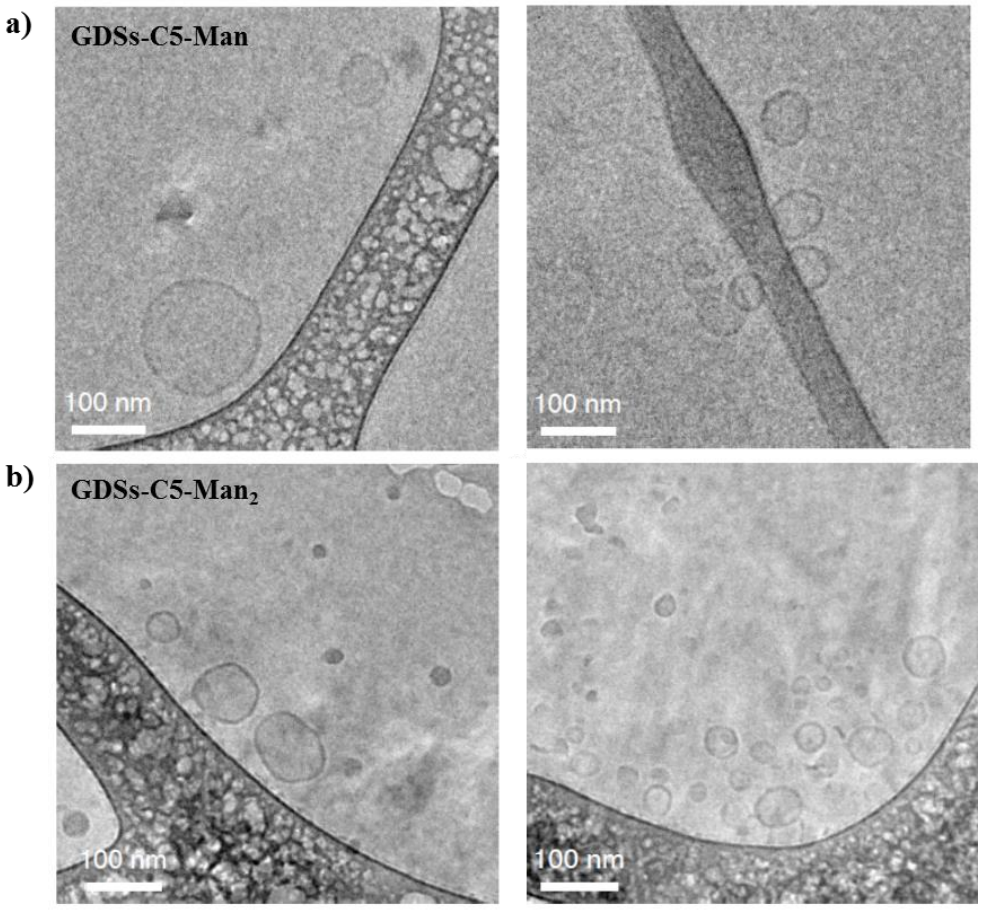

Figure 56: Analysis of JGDSs; a) TEM image of GDSs-C5-Man **111** and b) GDSs-C5-Man$_2$ **112** showing formation of vesicles.

Initially, ConA agglutination by **GDSs-C5-Man** to **GDSs-C5-Man$_6$** and **GDSs-(α1→2-Man$_2$) (116)**, **GDSs-(α1→2,α1→6-Man$_3$) (117)** was studied (Fig. 6). The results obtained from agglutination assay shows that the binding of **116** to ConA was stronger than **117** and **GDSs-C5-Man$_6$** (Fig. 57). Further studies are currently under investigation by Prof. Percec group.

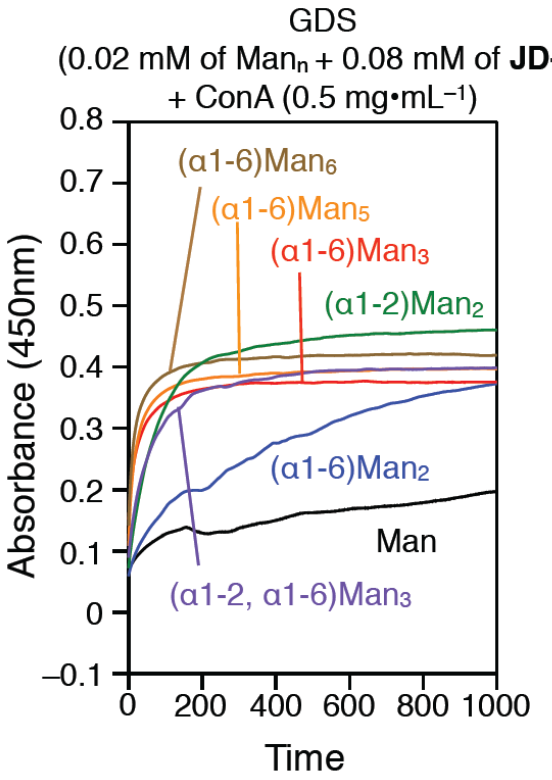

Figure 57: Agglutination assay of compounds **111-117** with ConA lectin.

4.2.5 Conclusion and Outlook

Using AGA, a library of linear mannose compounds (**87-88,** and **107-109**) has been assembled and provided to collaborators for further synthesis of Janus glycodendrimersomes. Initially, the Janus dendrimers were functionalized with mannose linear and branched structures (α1→2-Man$_2$ and α1→2, α1→6-Man$_3$) containing α-(1→6) and α-(1→2)-glycosidic linkages. Binding of self-assembled **GDSs** to ConA was observed to follow the following order,

$$\text{Man} < (\alpha1\text{-}6)\text{Man}_2 < (\alpha1\text{-}6)\text{Man}_3 < (\alpha1\text{-}6)\text{Man}_5 < (\alpha1\text{-}6)\text{Man}_6$$
$$(\alpha1\text{-}6)\text{Man}_2 < (\alpha1\text{-}2, \alpha1\text{-}6)\text{Man}_3 < (\alpha1\text{-}2)\text{Man}_2$$

Obtained results suggest that the self-assembled **GDSs** with branched α-(1→2)-glycosidic linkage have higher binding than linear α-(1→6)-linked structures. The Janus glycodendrimers **113-117** will be further analyzed for structure and shape conformation.

4.3 Experimental Section

General materials and Methods used for the synthesis of following molecules are same as mentioned in chapter 3 (*See* Experimental Section 2.1-chapter 3).

4.3.1 Automated Synthesis

***N*-Benzyloxycarbonyl-5-amino-pentyl (2-*O*-benzoyl-3,4-di-*O*-benzyl-α-D-mannopyranosyl)-(1→6)-2-*O*-benzoyl-3,4-di-*O*-benzyl-α-D-mannopyranoside (88):** For the automated synthesis of **88,** linker-functionalized resin **4** (17 mg, 6.25 μmol) was placed in the reaction vessel and the resin was washed with DMF, THF, and DCM. Afterward the acid wash (Module **B**), the glycosylation (Module **C**) and deprotection (Module **D**) were executed according to the modules. Mixing of the components was performed by bubbling Argon (Ar) through the reaction mixture.

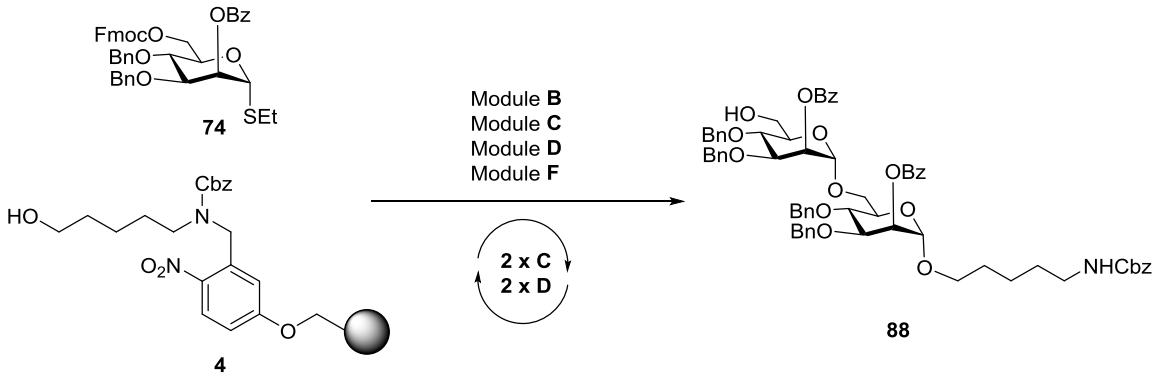

Module **B** (62.5 mM TMSOTf in DCM, 1 x 2 min, -20 ^{o}C)

Module **C** (1 x 6.5 equiv. **74**, NIS, TfOH, DCM/Dioxane, 1 x 35 min, -40 °C to -20 °C)

Module **D** (20% NEt_3 in DMF, 3 x 5 min, rt)

Module **B** (62.5 mM TMSOTf in DCM, 1 x 2 min, -20 ^{o}C)

Module **C** (1 x 6.5 equiv. **74**, NIS, TfOH, DCM/Dioxane, 1 x 35 min, -40 °C to -20 °C)

Module **D** (20% NEt_3 in DMF, 3 x 5 min, rt)

Module **F** Resin cleaved using UV irradiation at 305 nm in a continuous flow photoreactor.

Crude NP-HPLC of disaccharide 88 (ELSD trace, Method A, t_R = 19.1 min)

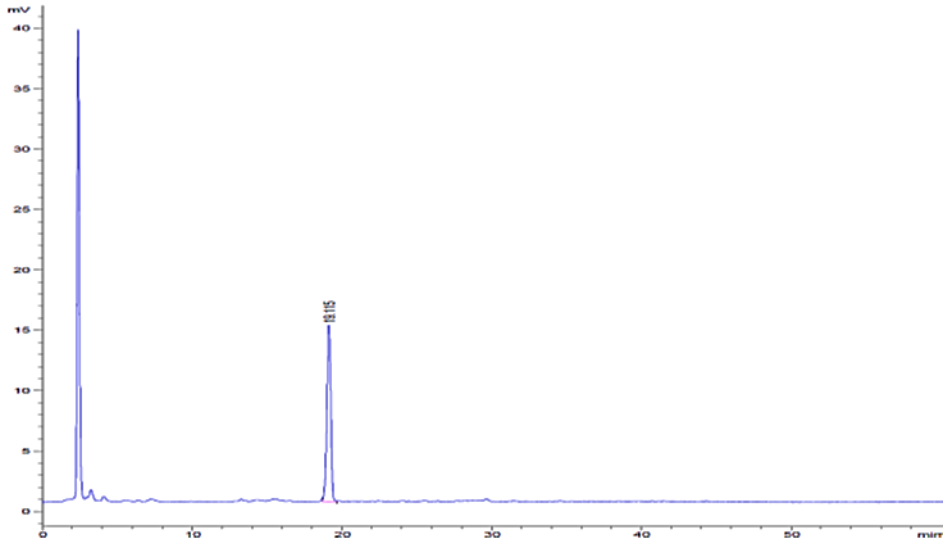

The crude product was purified using a preparative HPLC (Method B, t_R = 19.5 min), to provide the fully protected linear disaccharide **88** (3.50 mg, 3.10 μmol, 50%, based on resin loading).

^{1}H NMR (400 MHz, $CDCl_3$) δ 8.10 (dd, *J* = 19.2, 7.5 Hz, 4H), 7.59 (t, *J* = 7.6 Hz, 1H), 7.52 – 7.44 (m, 5H), 7.36 – 7.09 (m, 25H), 5.73 (s, 1H), 5.63 (s, 1H), 5.09 (s, 3H), 4.92 – 4.86 (m, 3H), 4.83 (d, *J* = 11.4 Hz, 1H), 4.74 (d, *J* = 11.7 Hz, 1H), 4.63 (d, *J* = 10.9 Hz, 1H), 4.57 (d, *J* = 11.0 Hz, 1H), 4.52 – 4.45 (m, 2H), 4.09 (d, *J* = 8.6 Hz, 2H), 4.01 – 3.92 (m, 2H), 3.87 (d, *J* = 8.7 Hz, 2H), 3.76 (q, *J* = 10.5, 10.0 Hz, 4H), 3.67 (d, *J* = 8.9 Hz, 1H), 3.43 (q, *J* = 7.4 Hz, 1H), 3.18 (q, *J* = 7.0 Hz, 2H), 1.56 (dt, *J* = 32.2, 7.5 Hz, 4H), 1.38 (q, *J* = 7.9 Hz, 2H); ^{13}C NMR (100 MHz, $CDCl_3$) δ 165.82, 165.52, 156.40, 138.28, 138.23, 137.90, 137.69, 133.26, 129.94, 129.89, 129.84, 129.80, 128.56, 128.48, 128.34, 128.30, 128.13, 128.08, 128.01, 127.94, 127.76, 127.68, 127.65, 127.61, 97.83, 78.54, 77.87, 75.18, 74.26, 73.85, 72.14, 71.62, 71.31, 70.57, 69.03, 68.78, 67.81, 66.56, 66.22, 61.96, 40.95, 29.76, 29.02, 23.42.

***N*-Benzyloxycarbonyl-5-amino-pentyl (2-*O*-benzoyl-3,4-di-*O*-benzyl-α-D-mannopyranosyl)-(1→6)-(2-*O*-benzoyl-3,4-di-*O*-benzyl-α-D-mannopyranosyl)-(1→6)-2-*O*-benzoyl-3,4-di-*O*-benzyl-α-D-mannopyranoside (108):** For the automated synthesis of **108** linker-functionalized resin **4** (34 mg, 12.5 μmol) was placed in the reaction vessel and the resin was washed with DMF, THF, and DCM. Afterward the acid wash (Module **B**), the glycosylation (Module **C**) and deprotection (Module **D**) were executed according to the modules. Mixing of the components was performed by bubbling Argon (Ar) through the reaction mixture.

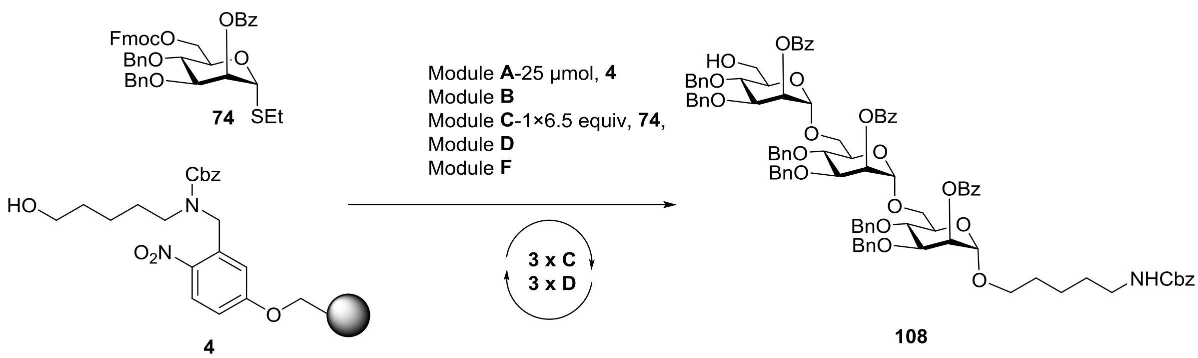

Module **B** (62.5 mM TMSOTf in DCM, 1 x 2 min, -20 °C)

Module **C** (1 x 6.5 equiv. **74**, NIS, TfOH, DCM/Dioxane, 1 x 35 min, -40 °C to -20 °C)

Module **D** (20% NEt_3 in DMF, 3 x 5 min, rt)

Module **B** (62.5 mM TMSOTf in DCM, 1 x 2 min, -20 °C)

Module **C** (1 x 6.5 equiv. **74**, NIS, TfOH, DCM/Dioxane, 1 x 35 min, -40 °C to -20 °C)

Module **D** (20% NEt_3 in DMF, 3 x 5 min, rt)

Module **B** (62.5 mM TMSOTf in DCM, 1 x 2 min, -20 °C)

Module **C** (1 x 6.5 equiv. **74**, NIS, TfOH, DCM/Dioxane, 1 x 35 min, -40 °C to -20 °C)

Module **D** (20% NEt_3 in DMF, 3 x 5 min, rt)

Module **F** Resin cleaved using UV irradiation at 305 nm in a continuous flow photoreactor.

Crude NP-HPLC of trisaccharide 108 (ELSD trace, Method A, t_R = 20.1 min)

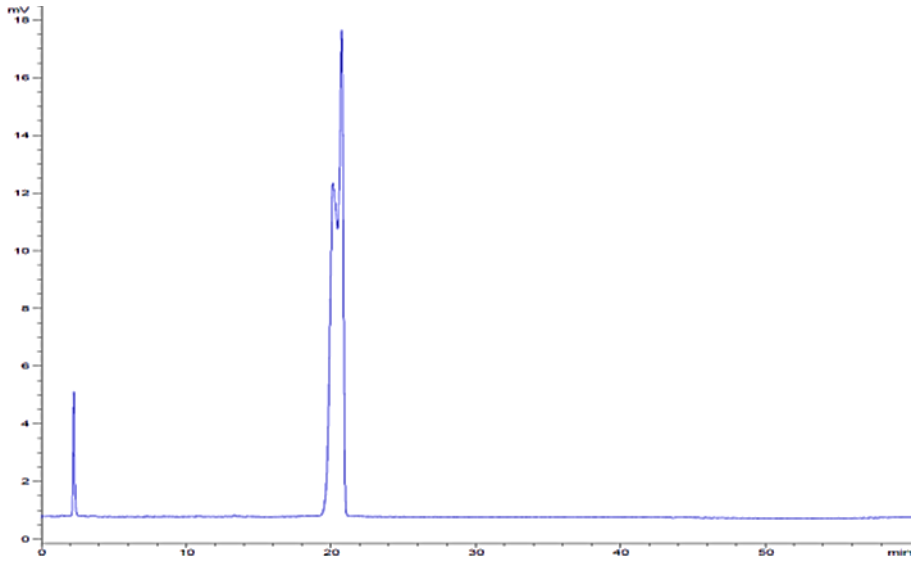

The crude product was purified using a preparative HPLC (Method B, t_R = 20 min), to provide the fully protected linear trisaccharide **108 (**20 mg, 13 μmol, 51%, based on resin loading).

^{1}H NMR (600 MHz, $CDCl_3$) δ 8.18 – 8.11 (m, 4H, Ar-H), 8.09 (d, *J* = 7.8 Hz, 2H Ar-H), 7.59 (d, *J* = 7.7 Hz, 1H, Ar-H), 7.54 – 7.07 (m, 43H, Ar-H), 5.81 (s, 1H), 5.75 (s, 1H), 5.64 (s, 1H), 5.11 (s, 1H, anomeric-H), 5.09 (s, 2H), 5.05 (s, 1H, anomeric-H), 4.92 (s, 1H, anomeric-H), 4.90 (s, 1H), 4.88 (d, *J* = 9.5 Hz, 1H), 4.83 (t, *J* = 10.6 Hz, 3H), 4.72 (d, *J* = 11.4 Hz, 1H), 4.61 (d, *J* = 11.2 Hz, 1H), 4.56 (d, *J* = 11.1 Hz, 1H), 4.49 (dd, *J* = 11.2, 5.7 Hz, 2H), 4.45 (d, *J* = 11.8 Hz, 1H), 4.41 (d, *J* = 11.5 Hz, 1H), 4.13 – 4.04 (m, 3H), 4.00 – 3.91 (m, 4H), 3.85 (d, *J* = 11.3 Hz, 2H), 3.79 (dd, *J* = 17.6, 10.6 Hz, 2H), 3.72 – 3.66 (m, 3H), 3.63 (d, *J* = 10.9 Hz, 2H), 3.46 – 3.40 (m, 1H), 3.20 – 3.14 (m, 2H), 1.63 – 1.57 (m, 2H, linker-CH_2-), 1.54 – 1.48 (m, 2H, linker-CH_2-), 1.41 – 1.34 (m, 2H, linker-CH_2-); ^{13}C NMR (100 MHz, $CDCl_3$) δ 165.96, 165.73, 165.55, 156.50, 138.55, 138.45, 138.43, 138.03, 137.76, 136.79, 133.39, 130.08, 130.06, 130.02, 130.00, 129.96, 128.74, 128.69, 128.61, 128.46, 128.42, 128.37, 128.33, 128.28, 128.22, 128.16, 128.12, 127.81, 127.78, 127.72, 127.67, 127.59, 98.22 (C-anomeric), 98.10 (C-anomeric), 98.02 (C-anomeric), 78.75, 78.37, 77.89, 75.29, 75.25, 75.23, 74.33, 74.09, 73.89, 72.22, 71.76, 71.52, 71.36, 70.94, 70.81,

69.19, 68.76, 68.65, 67.93, 66.68, 66.30, 65.86, 61.99, 41.07, 29.90, 29.17, 23.55; HRMS (MALDI-TOF): calculated for $C_{94}H_{97}NO_{21}$ $[M+Na]^+$ 1598.645, found 1599.156.

***N*-Benzyloxycarbonyl-5-amino-pentyl (2-*O*-benzoyl-3,4-di-*O*-benzyl-α-D-mannopyranosyl)-(1→6)-(2-*O*-benzoyl-3,4-di-*O*-benzyl-α-D-mannopyranosyl)-(1→6)-(2-*O*-benzoyl-3,4-di-*O*-benzyl-α-D-mannopyranosyl)-(1→6)-(2-*O*-benzoyl-3,4-di-*O*-benzyl-α-D-mannopyranosyl)-(1→6)-2-*O*-benzoyl-3,4-di-*O*-benzyl-α-D-mannopyranoside (109):** For the automated synthesis of **109,** linker-functionalized resin **4** (34 mg, 12.5 μmol) was placed in the reaction vessel and the resin was washed with DMF, THF, and DCM. Afterward the acid wash (Module **B**), the glycosylation (Module **C**) and deprotection (Module **D**) were executed according to the modules. Mixing of the components was performed by bubbling Argon (Ar) through the reaction mixture.

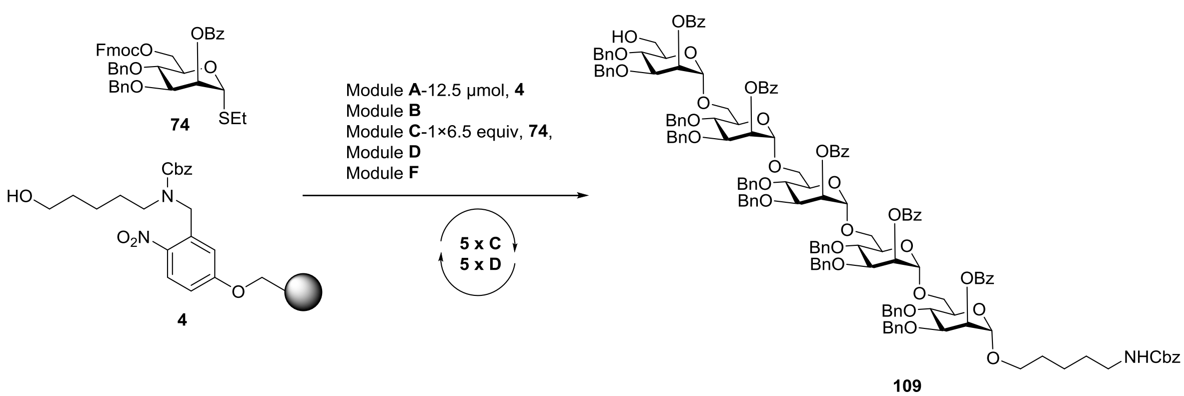

Module **B** (62.5 mM TMSOTf in DCM, 1 x 2 min, -20 °C)

Module **C** (1 x 6.5 equiv. **74**, NIS, TfOH, DCM/Dioxane, 1 x 35 min, -40 °C to -20 °C)

Module **D** (20% NEt_3 in DMF, 3 x 5 min, rt)

Module **B** (62.5 mM TMSOTf in DCM, 1 x 2 min, -20 °C)

Module **C** (1 x 6.5 equiv. **74**, NIS, TfOH, DCM/Dioxane, 1 x 35 min, -40 °C to -20 °C)

Module **D** (20% NEt_3 in DMF, 3 x 5 min, rt)

Module **B** (62.5 mM TMSOTf in DCM, 1 x 2 min, -20 °C)

Module **C** (1 x 6.5 equiv. **74**, NIS, TfOH, DCM/Dioxane, 1 x 35 min, -40 °C to -20 °C)

Module **D** (20% NEt_3 in DMF, 3 x 5 min, rt)

Module **B** (62.5 mM TMSOTf in DCM, 1 x 2 min, -20 °C)

Module **C** (1 x 6.5 equiv. **74**, NIS, TfOH, DCM/Dioxane, 1 x 35 min, -40 °C to -20 °C)

Module **D** (20% NEt_3 in DMF, 3 x 5 min, rt)

Module **B** (62.5 mM TMSOTf in DCM, 1 x 2 min, -20 ^oC)

Module **C** (1 x 6.5 equiv. **74**, NIS, TfOH, DCM/Dioxane, 1 x 35 min, -40 °C to -20 °C)

Module **D** (20% NEt_3 in DMF, 3 x 5 min, rt)

Module **F** Resin cleaved using UV irradiation at 305 nm in a continuous flow photoreactor.

Crude NP-HPLC of pentasaccharide 109 (ELSD trace, Method A, t_R = 23.2 min)

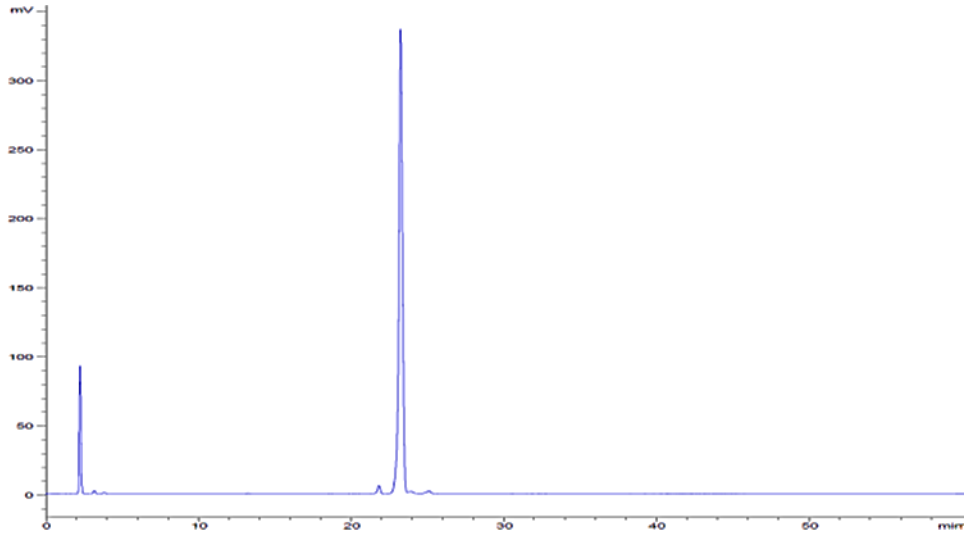

The crude product was purified using a preparative HPLC (Method B, t_R = 23.3 min), to provide the fully protected linear pentasaccharide **109 (**17 mg, 6.88 μmol, 55%, based on resin loading).

^1H NMR (400 MHz, $CDCl_3$) δ 8.23 – 8.08 (m, 10H), 7.61 (d, J = 7.5 Hz, 1H), 7.52 (q, J = 7.5, 6.5 Hz, 14H), 7.39 – 7.30 (m, 11H), 7.29 – 7.10 (m, 45H), 5.88 – 5.76 (m, 4H), 5.66 (d, J = 3.1 Hz, 1H), 5.19 – 5.04 (m, 6H), 4.94 – 4.80 (m, 10H), 4.74 (d, J = 11.4 Hz, 1H), 4.60 (dd, J = 14.6, 11.0 Hz, 2H), 4.51 – 4.34 (m, 7H), 4.13 – 3.76 (m, 18H), 3.72 – 3.60 (m, 6H), 3.58 – 3.40 (m, 4H), 3.22 – 3.13 (m, 2H), 1.63 – 1.51 (m, 4H), 1.39 – 1.35 (m, 2H); ^{13}C NMR (100 MHz, $CDCl_3$) δ 165.97, 165.72, 165.64, 165.53, 156.50, 138.62, 138.58, 138.40, 138.37, 138.03, 137.71, 137.65, 136.76, 133.46, 130.00, 128.77, 128.70, 128.62, 128.48, 128.44, 128.33, 128.31, 128.27, 128.18, 128.13, 127.83, 127.79, 127.75, 127.74, 127.48, 127.35, 127.22, 98.53, 98.50, 98.21, 97.99, 78.72, 78.42, 78.38, 78.28, 77.77, 75.31, 75.21,

75.15, 74.28, 73.98, 73.87, 73.84, 73.76, 72.17, 71.75, 71.52, 71.43, 71.29, 71.07, 70.98, 70.81, 69.12, 68.61, 68.44, 67.89, 66.68, 66.19, 65.87, 65.81, 65.52, 61.91, 41.06, 29.90, 29.16, 23.55; HRMS (MALDI-TOF): calculated for $C_{148}H_{149}NO_{33}$ $[M+K]^+$ 2506.9643, found 2508.5875.

5-Amino-pentanyl α-D-mannopyranosyl-(1→6)-α-D-mannopyranoside (104)

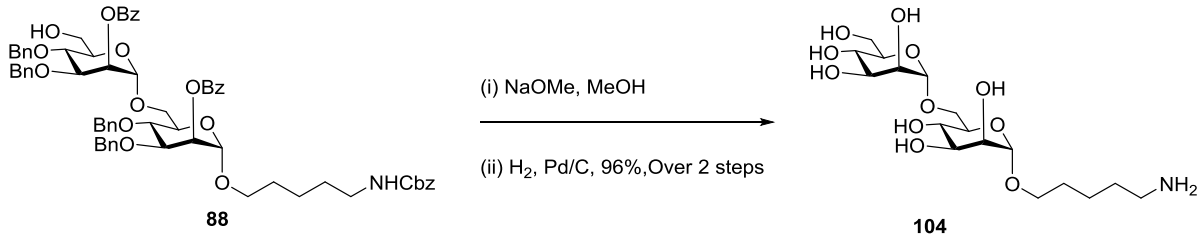

To a solution of protected disaccharide **88** (55 mg, 49 µmol) in DCM:MeOH (1:1) and NaOMe (0.5 M in MeOH, pH~13) was added and stirred for 4 h. The reaction mixture was neutralized with of Amberlite IR-120 (H^+) ion exchange resin,filtered and concentrated. The crude product was dissolved in a mixture DCM:tBuOH:H_2O (1:0.5:0.5 mL). The solution was purged with Ar, then 10% Pd/C was added and the solution purged with H_2 for 30 min, then stirred under an H_2 atmosphere for 48 h. Purification by reversed phase (RP) SPE (Waters Sep-Pak®, C18) column afforded **104** (20 mg, 47 µmol, 96%).^{1}H NMR (400 MHz, D_2O) δ 4.75 (s, 1H), 4.70 (s, 1H), 3.84 – 3.74 (m, 3H), 3.73 – 3.65 (m, 2H), 3.64 – 3.36 (m, 10H), 2.84 (d, J = 7.7 Hz, 2H), 1.58 – 1.39 (m, 4H), 1.28 (m, J = 7.1 Hz, 2H); ^{13}C NMR (100 MHz, D_2O) δ 99.78 (C-anomeric), 99.28 (C-anomeric), 72.62, 70.75, 70.51, 69.93, 69.90, 67.54, 66.62, 66.49, 65.55, 61.24, 60.83, 39.30, 27.94, 26.48, 22.45; LCMS m/z calculated for $C_{17}H_{33}NO_{11}$ $[M+H]^+$: 427.2, found: 428.2.

All spectroscopic data are in good accordance with the literature.[140]

5-Amino-pentanyl α-D-mannopyranosyl-(1→6)-α-D-mannopyranosyl-(1→6)-α-D-mannopyranoside (105)

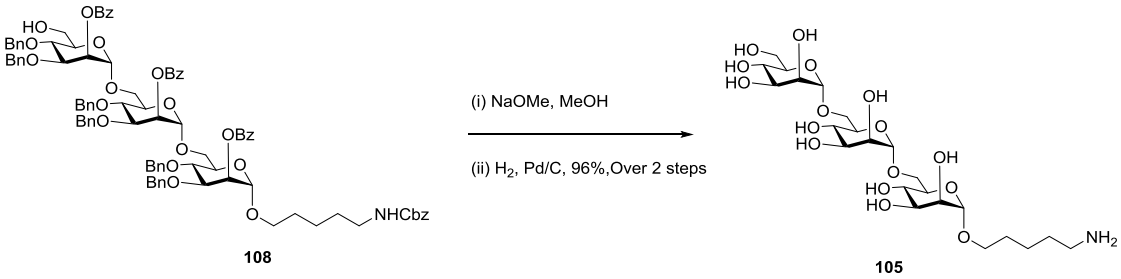

To a solution of protected trisaccharide **108** (33 mg, 21 µmol) in DCM:MeOH (1:1) and NaOMe (0.5 M in MeOH, pH~13) was added and stirred for 4 h. The reaction mixture was neutralized with of Amberlite IR-120 (H^+) ion exchange resin, filtered and concentrated. The crude product was dissolved in a mixture DCM:tBuOH:H_2O (1:0.5:0.5 mL). The solution was purged with Ar, then 10% Pd/C was added and the solution purged with H_2 for 30 min, then stirred under an H_2 atmosphere for 48 h. Purification by reversed phase (RP) SPE (Waters Sep-Pak®, C18) column afforded **105** (11.7 mg, 20 µmol, 96%). ^{1}H NMR (400 MHz, D_2O) δ 4.86 (s, 1H), 4.84 (s, 1H), 4.81 (s, 1H), 3.98 – 3.87 (m, 5H), 3.85 (d, J = 13.3 Hz, 2H), 3.81 – 3.75 (m, 3H), 3.75 – 3.67 (m, 6H), 3.67 – 3.62 (m, 2H), 3.61 – 3.48 (m, 2H), 2.96 (t, J = 7.7 Hz, 2H), 1.72 – 1.56 (m, 4H), 1.46 – 1.32 (m, 2H); ^{13}C NMR (100 MHz, D_2O) δ 99.76 (C-anomeric), 99.26 (C-anomeric), 99.12 (C-anomeric), 72.60, 70.80, 70.72, 70.67, 70.58, 70.42, 69.95, 67.51, 66.63, 66.47, 65.46, 61.22, 60.82, 39.27, 27.92, 26.46, 22.43; LCMS m/z calculated for $C_{23}H_{43}NO_{16}$ [M+ H] $^+$: 589.2, found: 590.2.

5-Amino-pentanyl α-D-mannopyranosyl-(1→6)-α-D-mannopyranosyl-(1→6)-α-D-mannopyranosyl-(1→6)-α-D-mannopyranosyl-(1→6)-α-D-mannopyranoside (106)

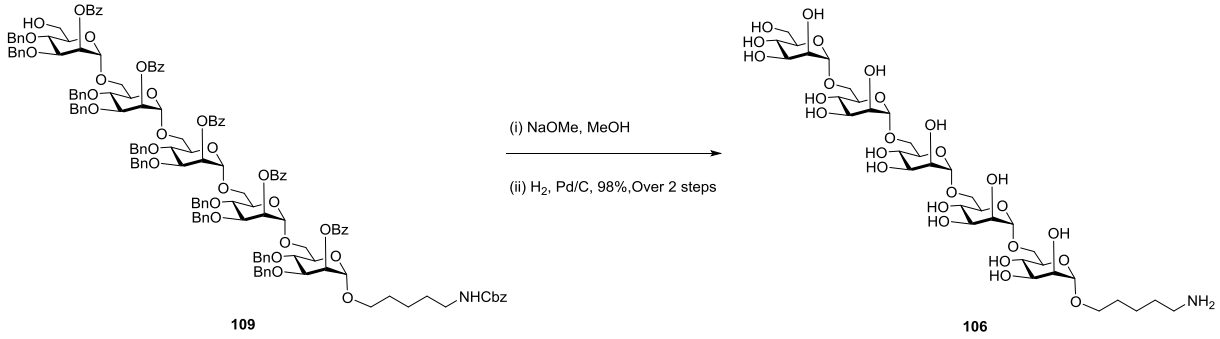

To a solution of protected pentasaccharide **109** (27.5 mg, 11 µmol) in DCM:MeOH (1:1) and NaOMe (0.5 M in MeOH, pH~13) was added and stirred for 4 h. The reaction mixture was neutralized with of Amberlite IR-120 (H^+) ion exchange resin, filtered and concentrated. The crude product was dissolved in a mixture DCM: t-BuOH: H2O (1:0.5:0.5 mL). The solution was purged with Ar, then 10% Pd/C was added and the solution purged with H_2 for 30 min, then stirred under an H_2 atmosphere for 48 h. Purification by reversed phase (RP) SPE (Waters Sep-Pak®, C18) column afforded **106** (9.99 mg, 10.93 µmol, 98%). ^{1}H NMR (400 MHz, D_2O) δ 4.88 (d, J = 6.8 Hz, 4H) (H-anomeric), 4.84 (s, 1H) (H-anomeric), 3.96 (s, 4H), 3.93 – 3.88 (m, 5H), 3.87 – 3.78 (m, 9H), 3.76 – 3.67 (m, 11H), 3.64 – 3.50 (m, 3H), 2.98 (t, J = 7.7 Hz, 2H), 1.72 – 1.60 (m, 4H), 1.43 (q, J = 7.9 Hz, 2H); ^{13}C NMR (100 MHz, D_2O) δ 99.76, 99.28, 99.13, 72.58, 70.77, 70.69, 70.63, 70.53, 70.39, 69.92, 69.84, 67.49, 66.60, 66.43, 65.44, 65.39, 60.79, 39.23, 27.91, 26.46, 22.43; HRMS (ESI): calculated for $C_{35}H_{63}NO_{26}$ $[M+H]^+$ 914.3711, found 914.3621.

5. References

1. E. M. Varki A, Cummings RD, et al. Discovery and Classification of Glycan-Binding Proteins. In: Varki A, Cummings RD, Esko JD, et al., editors. Essentials of Glycobiology. 2nd edition. Cold Spring Harbor (NY): Cold Spring Harbor Laboratory Press; 2009. Chapter 26. Available from: https://www.ncbi.nlm.nih.gov/books/NBK1923/.
2. A. C. Varki, R. D.; Esko, J. D., Freeze, H. H.; Stanley, P; Bertozzi, C. R.; Hart, G. W.; Etzler, M. E.; Eds., *Essentials of Glycobiology*, Cold Spring Harbor, NY, 2009.
3. M. E. a. D. Taylor, K. , *Introduction to glycobiology*, Oxford University Press, Oxford and New York, 2013.
4. https://en.wikipedia.org/wiki/Glycosylation.
5. A. Helenius and M. Aebi, *Annu. Rev. Biochem*, 2004, **73**, 1019-1049.
6. R. J. S. Preston, O. Rawley, E. M. Gleeson and J. S. O'Donnell, *Blood*, 2013, **121**, 3801-3810.
7. https://en.wikipedia.org/wiki/Glycocalyx.
8. A. Imberty and A. Varrot, *Current opinion in structural biology*, 2008, **18**, 567-576.
9. R. J. Pieters, in *Carbohydrate Recognition*, John Wiley & Sons, Inc., 2011, DOI: 10.1002/9781118017586.ch4, pp. 93-106.
10. C. L. Sears, *Anaerobe*, 2005, **11**, 247-251.
11. L. M. Irgens, *Tidsskr Nor Laegeforen*, 2002, **122**, 708-709.
12. *Wkly Epidemiol Rec*, 2010, **85**, 117-128.
13. L. Newman, J. Rowley, S. Vander Hoorn, N. S. Wijesooriya, M. Unemo, N. Low, G. Stevens, S. Gottlieb, J. Kiarie and M. Temmerman, *PLoS One*, 2015, **10**, e0143304.
14. T. M. Shinnick, 1996.
15. T. Ishige, K. Honda and S. Shimizu, *Curr. Opin. Chem. Biol.*, 2005, **9**, 174-180.
16. G. Seltmann and O. Holst, *The bacterial cell wall*, Springer, Berlin ; New York, 2001.
17. L. M. Prescott, J. P. Harley and D. A. Klein, *Microbiology*, McGraw-Hill Higher Education, Dubuque, IA, 6th edn., 2005.
18. T. J. Beveridge and J. L. Kadurugamuwa, *Microb Drug Resist*, 1996, **2**, 1-8.
19. V. N. Tra and D. H. Dube, *Chem Commun (Camb)*, 2014, **50**, 4659-4673.
20. B. E. c. b. N. Y. Alberts, NY: Garland Science Pub
21. W. M. Watkins and W. T. Morgan, *Nature*, 1952, **169**, 825-826.
22. G. S. Gupta, A. Gupta and R. K. Gupta, *Animal lectins : form, function and clinical applications*, Springer, Vienna ; New York, 2012.
23. D. C. Kilpatrick, *Biochim. Biophys. Acta*, 2002, **1572**, 187-197.
24. A. Cambi and C. G. Figdor, *Curr Opin Cell Biol*, 2003, **15**, 539-546.
25. G. Ashwell and A. G. Morell, *Adv. Enzymol. Relat. Areas Mol. Biol.*, 1974, **41**, 99-128.
26. E. Zacco, J. Hütter, J. L. Heier, J. Mortier, P. H. Seeberger, B. Lepenies and B. Koksch, *ACS Chemical Biology*, 2015, **10**, 2065-2072.
27. M. Maglinao, M. Eriksson, M. K. Schlegel, S. Zimmermann, T. Johannssen, S. Gotze, P. H. Seeberger and B. Lepenies, *Journal of controlled release : official journal of the Controlled Release Society*, 2014, **175**, 36-42.

28. G. J. Bernardes, R. Kikkeri, M. Maglinao, P. Laurino, M. Collot, S. Y. Hong, B. Lepenies and P. H. Seeberger, *Org Biomol Chem*, 2010, **8**, 4987-4996.
29. J. L. de Paz, C. Noti and P. H. Seeberger, *J. Am. Chem. Soc.*, 2006, **128**, 2766-2767.
30. M. Belting, *Thromb Res*, 2014, **133 Suppl 2**, S95-101.
31. S. N. M. L. H. Esko JD, Adhesins, and Toxins. In: Varki A, Cummings RD, Esko JD, et al., editors. Essentials of Glycobiology. 2nd edition. Cold Spring Harbor (NY): Cold Spring Harbor Laboratory Press; 2009. Chapter 34. Available from: https://www.ncbi.nlm.nih.gov/books/NBK1907/.
32. D. J. Schwartz, V. Kalas, J. S. Pinkner, S. L. Chen, C. N. Spaulding, K. W. Dodson and S. J. Hultgren, *Proceedings of the National Academy of Sciences of the United States of America*, 2013, **110**, 15530-15537.
33. A. Jacquot, C. Sakamoto, A. Razafitianamaharavo, C. Caillet, J. Merlin, A. Fahs, J. M. Ghigo, C. Beloin, J. F. Duval and G. Francius, *J Biomed Nanotechnol*, 2014, **10**, 3361-3372.
34. C. Sabin, E. P. Mitchell, M. Pokorna, C. Gautier, J. P. Utille, M. Wimmerova and A. Imberty, *FEBS Lett.*, 2006, **580**, 982-987.
35. H. B. Sheth, K. K. Lee, W. Y. Wong, G. Srivastava, O. Hindsgaul, R. S. Hodges, W. Paranchych and R. T. Irvin, *Mol. Microbiol.*, 1994, **11**, 715-723.
36. R. Ramphal and S. K. Arora, *Glycoconj J*, 2001, **18**, 709-713.
37. P. Laurino, R. Kikkeri and P. H. Seeberger, *Nat Protoc*, 2011, **6**, 1209-1220.
38. Y. Sato, K. Yoshioka, T. Murakami, S. Yoshimoto and O. Niwa, *Langmuir*, 2012, **28**, 1846-1851.
39. L. Wang, X. Jiang, Y. Ji, R. Bai, Y. Zhao, X. Wu and C. Chen, *Nanoscale*, 2013, **5**, 8384-8391.
40. J. L. Jimenez Blanco, C. Ortiz Mellet and J. M. Garcia Fernandez, *Chem. Soc. Rev.*, 2013, **42**, 4518-4531.
41. Y. M. Chabre and R. Roy, *Chem. Soc. Rev.*, 2013, **42**, 4657-4708.
42. L. You, D. Zha and E. V. Anslyn, *Chem. Rev.*, 2015, **115**, 7840-7892.
43. W. R. Browne and B. L. Feringa, *Nat. Nanotechnol.*, 2006, **1**, 25-35.
44. E. R. Kay, D. A. Leigh and F. Zerbetto, *Angew. Chem. Int. Ed.*, 2007, **46**, 72-191.
45. X. Yan, S. Li, T. R. Cook, X. Ji, Y. Yao, J. B. Pollock, Y. Shi, G. Yu, J. Li, F. Huang and P. J. Stang, *J. Am. Chem. Soc.*, 2013, **135**, 14036-14039.
46. S. Seiffert and J. Sprakel, *Chem. Soc. Rev.*, 2012, **41**, 909-930.
47. R. Chakrabarty, P. S. Mukherjee and P. J. Stang, *Chem. Rev.*, 2011, **111**, 6810-6918.
48. K. Petkau-Milroy and L. Brunsveld, *Org. Biomol. Chem.*, 2013, **11**, 219-232.
49. Y. Li, T. Park, J. K. Quansah and S. C. Zimmerman, *J. Am. Chem. Soc.*, 2011, **133**, 17118-17121.
50. A. G. Slater, L. M. A. Perdigão, P. H. Beton and N. R. Champness, *Acc. Chem. Res.*, 2014, **47**, 3417-3427.
51. T. R. Cook, Y.-R. Zheng and P. J. Stang, *Chem. Rev.*, 2013, **113**, 734-777.
52. L. F. Lindoy, K.-M. Park and S. S. Lee, *Chem. Soc. Rev.*, 2013, **42**, 1713-1727.
53. X. Zhang and C. Wang, *Chem. Soc. Rev.*, 2011, **40**, 94-101.
54. T. Aida, E. W. Meijer and S. I. Stupp, *Science*, 2012, **335**, 813-817.
55. M. M. Watt, M. S. Collins and D. W. Johnson, *Acc. Chem. Res.*, 2013, **46**, 955-966.
56. H. T. Chifotides and K. R. Dunbar, *Acc. Chem. Res.*, 2013, **46**, 894-906.

57. S. E. Wheeler, *Acc. Chem. Res.*, 2013, **46**, 1029-1038.
58. J. Aragó, E. Ortí and J. C. Sancho-García, *J. Chem. Theory Comput.*, 2013, **9**, 3437-3443.
59. Z. Wu, J. Liu, Y. Li, Z. Cheng, T. Li, H. Zhang, Z. Lu and B. Yang, *ACS Nano*, 2015, **9**, 6315-6323.
60. N. H. Evans and P. D. Beer, *Angew. Chem. Int. Ed.*, 2014, **53**, 11716-11754.
61. B. Zheng, F. Wang, S. Dong and F. Huang, *Chem. Soc. Rev.*, 2012, **41**, 1621-1636.
62. D. A. Fulton and J. F. Stoddart, *Bioconjugate Chem.*, 2001, **12**, 655-672.
63. F. Sansone and A. Casnati, *Chem. Soc. Rev.*, 2013, **42**, 4623-4639.
64. R. Roy, T. C. Shiao and K. Rittenhouse-Olson, *Braz. J. Pharm. Sci.*, 2013, **49**, 85-108.
65. M. Marradi, F. Chiodo, I. Garcia and S. Penades, *Chem. Soc. Rev.*, 2013, **42**, 4728-4745.
66. L. L. Kiessling and J. C. Grim, *Chem. Soc. Rev.*, 2013, **42**, 4476-4491.
67. M. Delbianco, P. Bharate, S. Varela-Aramburu and P. H. Seeberger, *Chem. Rev.*, 2016, **116**, 1693-1752.
68. J. Szejtli, *Pure Appl. Chem.*, 2004, **76**, 1825-1845.
69. T. Loftsson and D. Duchene, *Int. J. Pharm.*, 2007, **329**, 1-11.
70. L. Szente and J. Szeman, *Anal. Chem.*, 2013, **85**, 8024-8030.
71. A. Harada and Y. Takashima, *Chem. Rec.*, 2013, **13**, 420-431.
72. M. Raynal, P. Ballester, A. Vidal-Ferran and P. W. van Leeuwen, *Chem. Soc. Rev.*, 2014, **43**, 1734-1787.
73. A. Harada, Y. Takashima and M. Nakahata, *Acc. Chem. Res.*, 2014, **47**, 2128-2140.
74. M. E. Davis and M. E. Brewster, *Nat. Rev. Drug Discov.*, 2004, **3**, 1023-1035.
75. C. Y. Ang, S. Y. Tan, X. Wang, Q. Zhang, M. Khan, L. Bai, S. Tamil Selvan, X. Ma, L. Zhu, K. T. Nguyen, N. S. Tan and Y. Zhao, *J. Mater. Chem. B*, 2014, **2**, 1879-1890.
76. S. Buedenbender and G. E. Schulz, *J. Mol. Biol.*, 2009, **385**, 606-617.
77. A. Martinez, C. Ortiz Mellet and J. M. Garcia Fernandez, *Chem. Soc. Rev.*, 2013, **42**, 4746-4773.
78. G. Crini, *Chem. Rev.*, 2014, **114**, 10940-10975.
79. A. Bernardi, J. Jimenez-Barbero, A. Casnati, C. De Castro, T. Darbre, F. Fieschi, J. Finne, H. Funken, K. E. Jaeger, M. Lahmann, T. K. Lindhorst, M. Marradi, P. Messner, A. Molinaro, P. V. Murphy, C. Nativi, S. Oscarson, S. Penades, F. Peri, R. J. Pieters, O. Renaudet, J. L. Reymond, B. Richichi, J. Rojo, F. Sansone, C. Schaffer, W. B. Turnbull, T. Velasco-Torrijos, S. Vidal, S. Vincent, T. Wennekes, H. Zuilhof and A. Imberty, *Chem. Soc. Rev.*, 2013, **42**, 4709-4727.
80. S. M. N. Simoes, A. Rey-Rico, A. Concheiro and C. Alvarez-Lorenzo, *Chem. Commun.*, 2015, **51**, 6275-6289.
81. D. Grunstein, M. Maglinao, R. Kikkeri, M. Collot, K. Barylyuk, B. Lepenies, F. Kamena, R. Zenobi and P. H. Seeberger, *J. Am. Chem. Soc.*, 2011, **133**, 13957-13966.
82. H. Ikeda, Q. Li and A. Ueno, *Bioorg. Med. Chem. Lett.*, 2006, **16**, 5420-5423.
83. J. M. Benito, M. Gomez-Garcia, C. O. Mellet, I. Baussanne, J. Defaye and J. M. G. Fernandez, *J. Am. Chem. Soc.*, 2004, **126**, 10355-10363.
84. Y. C. Lee and R. T. Lee, *Acc. Chem. Res.*, 1995, **28**, 321-327.
85. H. Bavireddi and R. Kikkeri, *Analyst*, 2012, **137**, 5123-5127.
86. K. Wada, H. Arima, T. Tsutsumi, Y. Chihara, K. Hattori, F. Hirayama and K. Uekama, *J. Control. Release*, 2005, **104**, 397-413.

87. G. J. Bernardes, R. Kikkeri, M. Maglinao, P. Laurino, M. Collot, S. Y. Hong, B. Lepenies and P. H. Seeberger, *Org. Biomol. Chem.*, 2010, **8**, 4987-4996.
88. J. Rodriguez-Lavado, M. de la Mata, J. L. Jimenez-Blanco, M. I. Garcia-Moreno, J. M. Benito, A. Diaz-Quintana, J. A. Sanchez-Alcazar, K. Higaki, E. Nanba, K. Ohno, Y. Suzuki, C. Ortiz Mellet and J. M. Garcia Fernandez, *Org. Biomol. Chem.*, 2014, **12**, 2289-2301.
89. B. Lepenies, J. Lee and S. Sonkaria, *Adv. Drug Delivery Rev.*, 2013, **65**, 1271-1281.
90. Q. Zhang, L. Su, J. Collins, G. Chen, R. Wallis, D. A. Mitchell, D. M. Haddleton and C. R. Becer, *J. Am. Chem. Soc.*, 2014, **136**, 4325-4332.
91. T. Okada, *Trends Glycosci. Glycotechnol.*, 2011, **23**, 284-291.
92. S. Sakai, Y. Shigemasa and T. Sasaki, *Tetrahedron Lett.*, 1997, **38**, 8145-8148.
93. T. Hasegawa, T. Yonemura, K. Matsuura and K. Kobayashi, *Bioconjugate Chem.*, 2003, **14**, 728-737.
94. S. A. Khan, A. Adak, R. Vasudeva Murthy and R. Kikkeri, *Inorg. Chim. Acta*, 2014, **409**, 26-33.
95. P. Caravan, J. J. Ellison, T. J. McMurry and R. B. Lauffer, *Chem. Rev.*, 1999, **99**, 2293-2352.
96. G. R. Newkome, H. J. Kim, K. H. Choi and C. N. Moorefield, *Macromolecules*, 2004, **37**, 6268-6274.
97. A. Harada, M. Okada, J. Li and M. Kamachi, *Macromolecules*, 1995, **28**, 8406-8411.
98. A. Harada and M. Kamachi, *Macromolecules*, 1990, **23**, 2821-2823.
99. A. Harada, J. Li and M. Kamachi, *Macromolecules*, 1993, **26**, 5698-5703.
100. T. Nakamura, Y. Takashima, A. Hashidzume, H. Yamaguchi and A. Harada, *Nat. Commun.*, 2014, **5**, 1-9.
101. T. Kakuta, Y. Takashima, T. Sano, T. Nakamura, Y. Kobayashi, H. Yamaguchi and A. Harada, *Macromolecules*, 2015, **48**, 732-738.
102. G. M. Whitesides and M. Boncheva, *Proc. Natl. Acad. Sci. U. S. A.*, 2002, **99**, 4769-4774.
103. K. Petkau-Milroy, M. H. Sonntag and L. Brunsveld, *Chem. Eur. J.*, 2013, **19**, 10786-10793.
104. L. Yang, A. Gomez-Casado, J. F. Young, H. D. Nguyen, J. Cabanas-Danés, J. Huskens, L. Brunsveld and P. Jonkheijm, *J. Am. Chem. Soc.*, 2012, **134**, 19199-19206.
105. C. W. Lim, O. Crespo-Biel, M. C. Stuart, D. N. Reinhoudt, J. Huskens and B. J. Ravoo, *Proc. Natl. Acad. Sci. U. S. A.*, 2007, **104**, 6986-6991.
106. R. V. Vico, J. Voskuhl and B. J. Ravoo, *Langmuir*, 2011, **27**, 1391-1397.
107. B. J. Ravoo, J. C. Jacquier and G. Wenz, *Angew. Chem. Int. Ed.*, 2003, **42**, 2066-2070.
108. J. Voskuhl, M. C. A. Stuart and B. J. Ravoo, *Chem. Eur. J.*, 2010, **16**, 2790-2796.
109. U. Kauscher and B. J. Ravoo, *Beilstein J. Org. Chem.*, 2012, **8**, 1543-1551.
110. A. K. Geim and K. S. Novoselov, *Nat Mater*, 2007, **6**, 183-191.
111. J. Luo, J. Kim and J. Huang, *Acc. Chem. Res.*, 2013, **46**, 2225-2234.
112. D. Y. Lee, Z. Khatun, J.-H. Lee, Y.-k. Lee and I. In, *Biomacromolecules*, 2011, **12**, 336-341.
113. L. Q. Xu, Y. K. Yee, K.-G. Neoh, E.-T. Kang and G. D. Fu, *Polymer*, 2013, **54**, 2264-2271.
114. S. Stankovich, D. A. Dikin, G. H. Dommett, K. M. Kohlhaas, E. J. Zimney, E. A. Stach, R. D. Piner, S. T. Nguyen and R. S. Ruoff, *Nature*, 2006, **442**, 282-286.
115. M. Lotya, Y. Hernandez, P. J. King, R. J. Smith, V. Nicolosi, L. S. Karlsson, F. M. Blighe, S. De, Z. Wang, I. T. McGovern, G. S. Duesberg and J. N. Coleman, *J. Am. Chem. Soc.*, 2009, **131**, 3611-3620.

116. K. Haubner, J. Murawski, P. Olk, L. M. Eng, C. Ziegler, B. Adolphi and E. Jaehne, *ChemPhysChem*, 2010, **11**, 2131-2139.
117. L. Jianhua, A. Junwei, Z. Yecheng, M. Yuxiao, L. Mengliu, Y. Mei and L. Songmei, *ACS Appl. Mater. Interfaces*, 2012, **4**, 2870-2876.
118. A. Navaee and A. Salimi, *R. Soc. Chem. Adv.*, 2015, **5**, 59874-59880.
119. Z. Xu, S. Wang, Y. Li, M. Wang, P. Shi and X. Huang, *ACS Appl Mater Interfaces*, 2014, **6**, 17268-17276.
120. P. Lin, L. Meng, Y. Huang, L. Liu and D. Fan, *Appl. Surf. Sci.*, 2015, **324**, 784-790.
121. V. Georgakilas, J. N. Tiwari, K. C. Kemp, J. A. Perman, A. B. Bourlinos, K. S. Kim and R. Zboril, *Chem. Rev.*, 2016, **116**, 5464-5519.
122. Y. Liang, D. Wu, X. Feng and K. Müllen, *Adv. Mater.*, 2009, **21**, 1679-1683.
123. Y.-S. Ye, H.-X. Zeng, J. Wu, L.-Y. Dong, J.-T. Zhu, Z.-G. Xue, X.-P. Zhou, X.-L. Xie and Y.-W. Mai, *Green Chemistry*, 2016, **18**, 1674-1683.
124. P. Xiao, N. Qiu, J. Gu, S. Wang, J. He, C. F. Huang, J. Zhang, Y. Huang and T. Chen, *Chem Commun (Camb)*, 2017, **53**, 1949-1952.
125. A. Ciesielski and P. Samori, *Adv. Mater.*, 2016, **28**, 6030-6051.
126. Y. Guo, S. Guo, J. Ren, Y. Zhai, S. Dong and E. Wang, *ACS Nano*, 2010, **4**, 4001-4010.
127. T. Ogoshi, Y. Ichihara, T. A. Yamagishi and Y. Nakamoto, *Chem Commun (Camb)*, 2010, **46**, 6087-6089.
128. J. Liu, X. Leng, Y. Xiao, C. Hu and L. Fu, *Nanoscale*, 2015, **7**, 11922-11927.
129. A. Mondal and N. R. Jana, *Chem Commun (Camb)*, 2012, **48**, 7316-7318.
130. Y. Guo, S. Guo, J. Li, E. Wang and S. Dong, *Talanta*, 2011, **84**, 60-64.
131. X. Tian, C. Cheng, H. Yuan, J. Du, D. Xiao, S. Xie and M. M. Choi, *Talanta*, 2012, **93**, 79-85.
132. S. Wang, Y. Li, X. Fan, F. Zhang and G. Zhang, *Frontiers of Chemical Science and Engineering*, 2015, **9**, 77-83.
133. H. Dong, Y. Li, J. Yu, Y. Song, X. Cai, J. Liu, J. Zhang, R. C. Ewing and D. Shi, *Small*, 2013, **9**, 446-456.
134. Y. Yang, Y. M. Zhang, Y. Chen, D. Zhao, J. T. Chen and Y. Liu, *Chemistry*, 2012, **18**, 4208-4215.
135. R. B. Merrifield, *Science*, 1965, **150**, 178-185.
136. M. H. Caruthers, *Science*, 1985, **230**, 281-285.
137. C. Schuerch and J. M. Frechet, *J. Am. Chem. Soc.*, 1971, **93**, 492-496.
138. www.glycouniverse.de.
139. O. J. Plante, E. R. Palmacci and P. H. Seeberger, *Science*, 2001, **291**, 1523-1527.
140. O. Calin, S. Eller and P. H. Seeberger, *Angew. Chem. Int. Ed.*, 2013, **52**, 5862-5865.
141. H. S. Hahm, M. K. Schlegel, M. Hurevich, S. Eller, F. Schuhmacher, J. Hofmann, K. Pagel and P. H. Seeberger, *Proc. Natl. Acad. Sci. U. S. A.*, 2017, **114**, E3385-E3389.
142. M. P. Bartetzko, F. Schuhmacher, H. S. Hahm, P. H. Seeberger and F. Pfrengle, *Org. Lett.*, 2015, **17**, 4344-4347.
143. P. H. Seeberger, *Acc. Chem. Res.*, 2015, **48**, 1450-1463.
144. R. B. Merrifield, *J. Am. Chem. Soc.*, 1963, **85**, 2149-2154.
145. P. H. Seeberger, *Chem. Soc. Rev.*, 2008, **37**, 19-28.

146. L. Krock, D. Esposito, B. Castagner, C.-C. Wang, P. Bindschadler and P. H. Seeberger, *Chemical Science*, 2012, **3**, 1617-1622.
147. M. W. Weishaupt, S. Matthies and P. H. Seeberger, *Chemistry*, 2013, **19**, 12497-12503.
148. M. W. Weishaupt, H. S. Hahm, A. Geissner and P. H. Seeberger, *Chem Commun (Camb)*, 2017, **53**, 3591-3594.
149. C. H. Lai, H. S. Hahm, C. F. Liang and P. H. Seeberger, *Beilstein J. Org. Chem.*, 2015, **11**, 617-621.
150. S. Eller, M. Collot, J. Yin, H. S. Hahm and P. H. Seeberger, *Angew. Chem. Int. Ed.*, 2013, **52**, 5858-5861.
151. M. T. Walvoort, A. G. Volbeda, N. R. Reintjens, H. van den Elst, O. J. Plante, H. S. Overkleeft, G. A. van der Marel and J. D. Codee, *Org. Lett.*, 2012, **14**, 3776-3779.
152. M. Hurevich and P. H. Seeberger, *Chem Commun (Camb)*, 2014, **50**, 1851-1853.
153. D. Schmidt, F. Schuhmacher, A. Geissner, P. H. Seeberger and F. Pfrengle, *Chemistry*, 2015, **21**, 5709-5713.
154. P. Dallabernardina, F. Schuhmacher, P. H. Seeberger and F. Pfrengle, *Org. Biomol. Chem.*, 2016, **14**, 309-313.
155. D. Senf, C. Ruprecht, G. H. de Kruijff, S. O. Simonetti, F. Schuhmacher, P. H. Seeberger and F. Pfrengle, *Chemistry*, 2017, **23**, 3197-3205.
156. T. J. Boltje, T. Buskas and G.-J. Boons, *Nat Chem*, 2009, **1**, 611-622.
157. H. S. Hahm, M. Hurevich and P. H. Seeberger, *Nature communications*, 2016, **7**, 12482.
158. L. S. Schlesinger, T. M. Kaufman, S. Iyer, S. R. Hull and L. K. Marchiando, *The Journal of Immunology*, 1996, **157**, 4568-4575.
159. K. H. Khoo, E. Douglas, P. Azadi, J. M. Inamine, G. S. Besra, K. Mikusova, P. J. Brennan and D. Chatterjee, *J. Biol. Chem.*, 1996, **271**, 28682-28690.
160. M. Mammen, S. K. Choi and G. M. Whitesides, *Angewandte Chemie-International Edition*, 1998, **37**, 2755-2794.
161. C. Fasting, C. A. Schalley, M. Weber, O. Seitz, S. Hecht, B. Koksch, J. Dernedde, C. Graf, E. W. Knapp and R. Haag, *Angew. Chem. Int. Ed.*, 2012, **51**, 10472-10498.
162. D. Deniaud, K. Julienne and S. G. Gouin, *Org. Biomol. Chem.*, 2011, **9**, 966-979.
163. P. H. Seeberger, *Nature*, 2005, **437**, 1239.
164. R. P. Brinas, A. Sundgren, P. Sahoo, S. Morey, K. Rittenhouse-Olson, G. E. Wilding, W. Deng and J. J. Barchi, Jr., *Bioconjug Chem*, 2012, **23**, 1513-1523.
165. H. Rudiger and H. J. Gabius, *Glycoconj J*, 2001, **18**, 589-613.
166. S. M. Dimick, S. C. Powell, S. A. McMahon, D. N. Moothoo, J. H. Naismith and E. J. Toone, *J. Am. Chem. Soc.*, 1999, **121**, 10286-10296.
167. Y. C. Lee and R. T. Lee, *Acc. Chem. Res.*, 1995, **28**, 321-327.
168. T. K. Lindhorst, in *Host-Guest Chemistry: Mimetic Approaches to Study Carbohydrate Recognition*, ed. S. Penadés, Springer Berlin Heidelberg, Berlin, Heidelberg, 2002, DOI: 10.1007/3-540-45010-6_7, pp. 201-235.
169. J. E. Gestwicki, C. W. Cairo, L. E. Strong, K. A. Oetjen and L. L. Kiessling, *J. Am. Chem. Soc.*, 2002, **124**, 14922-14933.
170. P. R. Crocker, J. C. Paulson and A. Varki, *Nat Rev Immunol*, 2007, **7**, 255-266.
171. X. Guo, A. Kulkarni, A. Doepke, H. B. Halsall, S. Iyer and W. R. Heineman, *Anal. Chem.*, 2012, **84**, 241-246.

172. M. D. Disney, J. Zheng, T. M. Swager and P. H. Seeberger, *J. Am. Chem. Soc.*, 2004, **126**, 13343-13346.
173. J. Vonnemann, S. Liese, C. Kuehne, K. Ludwig, J. Dernedde, C. Bottcher, R. R. Netz and R. Haag, *J. Am. Chem. Soc.*, 2015, **137**, 2572-2579.
174. D.-W. Lee, T. Kim, I.-S. Park, Z. Huang and M. Lee, *J. Am. Chem. Soc.*, 2012, **134**, 14722-14725.
175. G. Yu, Y. Ma, C. Han, Y. Yao, G. Tang, Z. Mao, C. Gao and F. Huang, *J. Am. Chem. Soc.*, 2013, **135**, 10310-10313.
176. H. C. Siebert, K. Born, S. Andre, M. Frank, H. Kaltner, C. W. von der Lieth, A. J. Heck, J. Jimenez-Barbero, J. Kopitz and H. J. Gabius, *Chemistry*, 2005, **12**, 388-402.
177. P. M. Rendle, A. Seger, J. Rodrigues, N. J. Oldham, R. R. Bott, J. B. Jones, M. M. Cowan and B. G. Davis, *J. Am. Chem. Soc.*, 2004, **126**, 4750-4751.
178. T. D. Farr, C. H. Lai, D. Grunstein, G. Orts-Gil, C. C. Wang, P. Boehm-Sturm, P. H. Seeberger and C. Harms, *Nano Lett.*, 2014, **14**, 2130-2134.
179. L. Baldini, A. Casnati, F. Sansone and R. Ungaro, *Chem. Soc. Rev.*, 2007, **36**, 254-266.
180. S. Cecioni, R. Lalor, B. Blanchard, J. P. Praly, A. Imberty, S. E. Matthews and S. Vidal, *Chemistry*, 2009, **15**, 13232-13240.
181. P. Compain, C. Decroocq, J. Iehl, M. Holler, D. Hazelard, T. Mena Barragan, C. Ortiz Mellet and J. F. Nierengarten, *Angew. Chem. Int. Ed.*, 2010, **49**, 5753-5756.
182. M. Durka, K. Buffet, J. Iehl, M. Holler, J. F. Nierengarten and S. P. Vincent, *Chemistry*, 2012, **18**, 641-651.
183. I. van Baal, H. Malda, S. A. Synowsky, J. L. van Dongen, T. M. Hackeng, M. Merkx and E. W. Meijer, *Angew. Chem. Int. Ed.*, 2005, **44**, 5052-5057.
184. L. Gu, P. G. Luo, H. Wang, M. J. Meziani, Y. Lin, L. M. Veca, L. Cao, F. Lu, X. Wang, R. A. Quinn, W. Wang, P. Zhang, S. Lacher and Y. P. Sun, *Biomacromolecules*, 2008, **9**, 2408-2418.
185. S. Eigler and A. Hirsch, *Angew. Chem. Int. Ed.*, 2014, **53**, 7720-7738.
186. X. Li, X. Wang, L. Zhang, S. Lee and H. Dai, *Science*, 2008, **319**, 1229-1232.
187. Y. Xu, Z. Liu, X. Zhang, Y. Wang, J. Tian, Y. Huang, Y. Ma, X. Zhang and Y. Chen, *Adv. Mater.*, 2009, **21**, 1275-1279.
188. R. Pasricha, S. Gupta and A. K. Srivastava, *Small*, 2009, **5**, 2253-2259.
189. C. K. Chua and M. Pumera, *Chem. Soc. Rev.*, 2014, **43**, 291-312.
190. C. Krumm, S. Harmuth, M. Hijazi, B. Neugebauer, A. L. Kampmann, H. Geltenpoth, A. Sickmann and J. C. Tiller, *Angew. Chem. Int. Ed.*, 2014, **53**, 3830-3834.
191. S. Liu, T. H. Zeng, M. Hofmann, E. Burcombe, J. Wei, R. Jiang, J. Kong and Y. Chen, *ACS Nano*, 2011, **5**, 6971-6980.
192. M.-E. Ragoussi, S. Casado, R. Ribeiro-Viana, G. d. l. Torre, J. Rojo and T. Torres, *Chemical Science*, 2013, **4**, 4035-4041.
193. B. Konkena and S. Vasudevan, *Langmuir*, 2012, **28**, 12432-12437.
194. A. García-Barrientos, J. J. García-López, J. Isac-García, F. Ortega-Caballero, C. Uriel, A. Vargas-Berenguel and F. Santoyo-González, *Synthesis*, 2001, **2001**, 1057-1064.
195. W. S. Hummers and R. E. Offeman, *J. Am. Chem. Soc.*, 1958, **80**, 1339-1339.
196. Z. Qi, P. Malo de Molina, W. Jiang, Q. Wang, K. Nowosinski, A. Schulz, M. Gradzielski and C. A. Schalley, *Chemical Science*, 2012, **3**, 2073-2082.

197. A.-K. Appel, R. Thomann and R. Mülhaupt, *Polymer*, 2012, **53**, 4931-4939.
198. P. t. A.-K. Appel, University of Freiburg 2013, p38.
199. J. M. Lehn, *Proceedings of the National Academy of Sciences of the United States of America*, 2002, **99**, 4763-4768.
200. A. V. Ambade, S. K. Yang and M. Weck, *Angew. Chem. Int. Ed.*, 2009, **48**, 2894-2898.
201. H. Bavireddi, R. Vasudeva Murthy, M. Gade, S. Sangabathuni and R. Kikkeri, *Org Biomol Chem*, 2016, **14**, 10816-10821.
202. G. Chen and M. Jiang, *Chem. Soc. Rev.*, 2011, **40**, 2254-2266.
203. G. E. Soto and S. J. Hultgren, *J. Bacteriol.*, 1999, **181**, 1059-1071.
204. Y. B. Lim, S. Park, E. Lee, J. H. Ryu, Y. R. Yoon, T. H. Kim and M. Lee, *Chem Asian J*, 2007, **2**, 1363-1369.
205. K. A. Krogfelt, H. Bergmans and P. Klemm, *Infect Immun*, 1990, **58**, 1995-1998.
206. M. Acik, G. Lee, C. Mattevi, M. Chhowalla, K. Cho and Y. J. Chabal, *Nat Mater*, 2010, **9**, 840-845.
207. http://www.who.int/mediacentre/factsheets/fs125/en/.
208. S. Guieu and M. Sollogoub, *Angew. Chem. Int. Ed.*, 2008, **47**, 7060-7063.
209. C. H. Lai, N. C. Lai, Y. J. Chuang, F. I. Chou, C. M. Yang and C. C. Lin, *Nanoscale*, 2013, **5**, 9412-9418.
210. M. Gade, A. Paul, C. Alex, D. Choudhury, H. V. Thulasiram and R. Kikkeri, *Chem. Commun.*, 2015, **51**, 6346-6349.
211. J.-M. Yuk and E.-K. Jo, *Clin Exp Vaccine Res*, 2014, **3**, 155-167.
212. L. F. Barker, M. J. Brennan, P. K. Rosenstein and J. C. Sadoff, *Curr Opin Immunol*, 2009, **21**, 331-338.
213. P. J. Brennan and H. Nikaido, *Annu. Rev. Biochem*, 1995, **64**, 29-63.
214. A. K. Mishra, N. N. Driessen, B. J. Appelmelk and G. S. Besra, *FEMS Microbiol. Rev.*, 2011, **35**, 1126-1157.
215. B. Cao and S. J. Williams, *Natural Product Reports*, 2010, **27**, 919-947.
216. S. Berg, D. Kaur, M. Jackson and P. J. Brennan, *Glycobiology*, 2007, **17**, 35-56R.
217. P. Brennan and C. E. Ballou, *J. Biol. Chem.*, 1967, **242**, 3046-3056.
218. J. Nigou, M. Gilleron, T. Brando and G. Puzo, *Appl. Biochem. Biotechnol.*, 2004, **118**, 253-267.
219. K. J. Gibson, L. Eggeling, W. N. Maughan, K. Krumbach, S. S. Gurcha, J. Nigou, G. Puzo, H. Sahm and G. S. Besra, *J. Biol. Chem.*, 2003, **278**, 40842-40850.
220. D. Chatterjee, S. W. Hunter, M. McNeil and P. J. Brennan, *J. Biol. Chem.*, 1992, **267**, 6228-6233.
221. Y. C. Lee and C. E. Ballou, *J. Biol. Chem.*, 1964, **239**, 1316-1327.
222. X. Liu, B. L. Stocker and P. H. Seeberger, *J. Am. Chem. Soc.*, 2006, **128**, 3638-3648.
223. A. S. Lee, I. H. Lim, L. L. Tang, A. Telenti and S. Y. Wong, *Antimicrob. Agents Chemother.*, 1999, **43**, 2087-2089.
224. A. Holemann, B. L. Stocker and P. H. Seeberger, *J. Org. Chem.*, 2006, **71**, 8071-8088.
225. S. Boonyarattanakalin, X. Liu, M. Michieletti, B. Lepenies and P. H. Seeberger, *J. Am. Chem. Soc.*, 2008, **130**, 16791-16799.
226. B. Fraser-Reid, J. Lu, K. N. Jayaprakash and J. C. López, *Tetrahedron: Asymmetry*, 2006, **17**, 2449-2463.

227. M. Joe, Y. Bai, R. C. Nacario and T. L. Lowary, *J. Am. Chem. Soc.*, 2007, **129**, 9885-9901.
228. S. A. Thadke, B. Mishra and S. Hotha, *Org. Lett.*, 2013, **15**, 2466-2469.
229. A. Ishiwata and Y. Ito, *J. Am. Chem. Soc.*, 2011, **133**, 2275-2291.
230. S. A. Thadke, B. Mishra, M. Islam, S. Pasari, S. Manmode, B. V. Rao, M. Neralkar, G. P. Shinde, G. Walke and S. Hotha, *Nat. Commun.*, 2017, **8**, 14019.
231. M. W. Weishaupt, S. Matthies, M. Hurevich, C. L. Pereira, H. S. Hahm and P. H. Seeberger, *Beilstein J. Org. Chem.*, 2016, **12**, 1440-1446.
232. J. Kandasamy, M. Hurevich and P. H. Seeberger, *Chem. Commun.*, 2013, **49**, 4453-4455.
233. http://www.mpikg.mpg.de/193323/2Biomolekulare_Systeme.
234. M. Gude, J. Ryf and P. D. White, *Lett. Pept. Sci.*, 2002, **9**, 203-206.
235. T. C. Shiao and R. Roy, *Top. Curr. Chem.*, 2011, **301**, 69-108.
236. S. R. Sanapala and S. S. Kulkarni, *Chemistry*, 2014, **20**, 3578-3583.
237. S. Svenson and D. A. Tomalia, *Adv. Drug Delivery Rev.*, 2005, **57**, 2106-2129.
238. L. Crespo, G. Sanclimens, M. Pons, E. Giralt, M. Royo and F. Albericio, *Chem. Rev.*, 2005, **105**, 1663-1682.
239. M. V. Walter and M. Malkoch, *Chem. Soc. Rev.*, 2012, **41**, 4593-4609.
240. T. C. Shiao and R. Roy, *New J. Chem.*, 2012, **36**, 324-339.
241. B. M. Rosen, C. J. Wilson, D. A. Wilson, M. Peterca, M. R. Imam and V. Percec, *Chem. Rev.*, 2009, **109**, 6275-6540.
242. V. Percec, D. A. Wilson, P. Leowanawat, C. J. Wilson, A. D. Hughes, M. S. Kaucher, D. A. Hammer, D. H. Levine, A. J. Kim, F. S. Bates, K. P. Davis, T. P. Lodge, M. L. Klein, R. H. DeVane, E. Aqad, B. M. Rosen, A. O. Argintaru, M. J. Sienkowska, K. Rissanen, S. Nummelin and J. Ropponen, *Science*, 2010, **328**, 1009-1014.
243. L. Sun, X. Ma, C.-M. Dong, B. Zhu and X. Zhu, *Biomacromolecules*, 2012, **13**, 3581-3591.
244. V. Percec, P. Leowanawat, H. J. Sun, O. Kulikov, C. D. Nusbaum, T. M. Tran, A. Bertin, D. A. Wilson, M. Peterca, S. Zhang, N. P. Kamat, K. Vargo, D. Moock, E. D. Johnston, D. A. Hammer, D. J. Pochan, Y. Chen, Y. M. Chabre, T. C. Shiao, M. Bergeron-Brlek, S. Andre, R. Roy, H. J. Gabius and P. A. Heiney, *J. Am. Chem. Soc.*, 2013, **135**, 9055-9077.
245. S. Zhang, R. O. Moussodia, H. J. Sun, P. Leowanawat, A. Muncan, C. D. Nusbaum, K. M. Chelling, P. A. Heiney, M. L. Klein, S. Andre, R. Roy, H. J. Gabius and V. Percec, *Angew. Chem. Int. Ed.*, 2014, **53**, 10899-10903.
246. Q. Xiao, S. Zhang, Z. Wang, S. E. Sherman, R.-O. Moussodia, M. Peterca, A. Muncan, D. R. Williams, D. A. Hammer, S. Vértesy, S. André, H.-J. Gabius, M. L. Klein and V. Percec, *Proceedings of the National Academy of Sciences of the United States of America*, 2016, **113**, 1162-1167.
247. S. Zhang, R.-O. Moussodia, C. Murzeau, H.-J. Sun, M. L. Klein, S. Vértesy, S. André, R. Roy, H.-J. Gabius and V. Percec, *Angew. Chem. Int. Ed.*, 2015, **54**, 4036-4040.
248. S. Zhang, R.-O. Moussodia, S. Vértesy, S. André, M. L. Klein, H.-J. Gabius and V. Percec, *Proc. Natl. Acad. Sci. U. S. A.*, 2015, **112**, 5585-5590.